UNIVERSITÀ DEGLI STUDI FIRENZE

DOTTORATO DI RICERCA IN SCIENZE CHIMICHE

CICLO XXIX

COORDINATORE Prof. PIERO BAGLIONI

Synthesis, characterization and applicative study of innovative materials for the conservation of cellulosic artifacts with an artistic and architectural interest

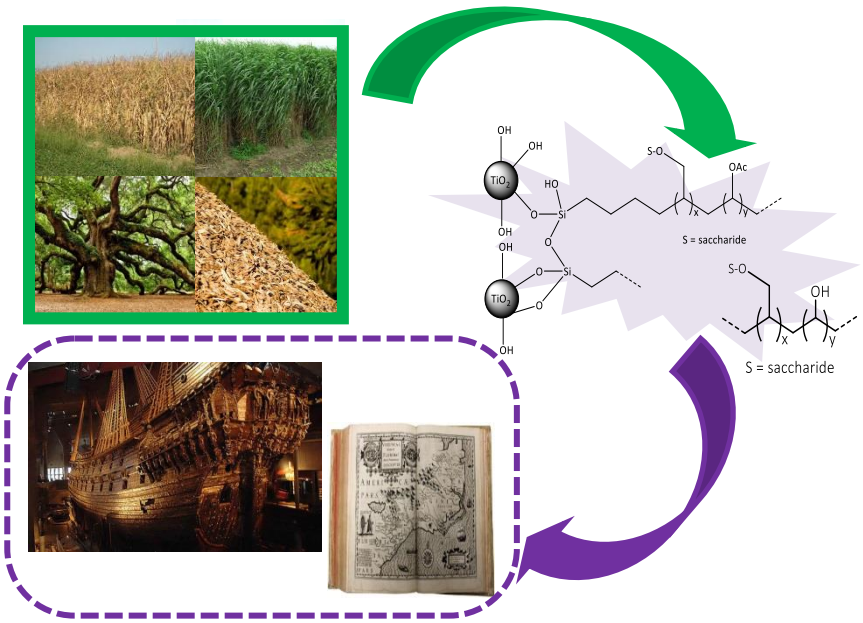

Dottorando
Dott. Alessandra Papacchini

Tutore
Prof.ssa Antonella Salvini

Co-Tutore
Prof. Luigi Dei

UNIVERSITÀ
DEGLI STUDI
FIRENZE

DOTTORATO DI RICERCA IN SCIENZE CHIMICHE

CICLO XXIX

COORDINATORE Prof. PIERO BAGLIONI

Synthesis, characterization and applicative study of innovative materials for the conservation of cellulosic artifacts with an artistic and architectural interest

Settore Scientifico Disciplinare CHIM/04 (CHIM/12)

Dottorando	**Tutore**	**Co-Tutore**
Dott. Alessandra Papacchini	Prof.ssa Antonella Salvini	Prof. Luigi Dei
_____	_____	_____
(firma)	*(firma)*	*(firma)*

Coordinatore
Prof. Piero Baglioni

_____

(firma)

Anni 2013/2016

TABLE OF CONTENTS Page

1 Introduction

1.1 Cellulosic materials in cultural heritage

The cellulosic materials are a class of materials that includes wood, paper and natural fibers and fabrics. They have the common feature of being mainly composed of cellulose, a linear homopolysaccharide of D-glucose with molecular formula $(C_6H_{10}O_5)_n$, where n is the polymerization degree, which depends on the origin of cellulose and on the treatment to which it has been subjected (**Figure 1**).

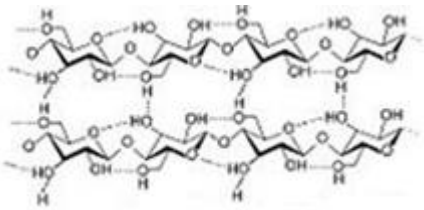

Figure 1 Structure of the cellulose

These materials have been widely used throughout human history as media for writing, raw materials for the construction of buildings, ships and tools and to manufacture clothing, ornaments (tapestries, carpets) etc. (**Figure 2**). For this reason they play a key role in the cultural heritage and a full knowledge of their characteristics and of the mechanisms of their degradation is mandatory to preserve the history and the culture of the whole humanity.

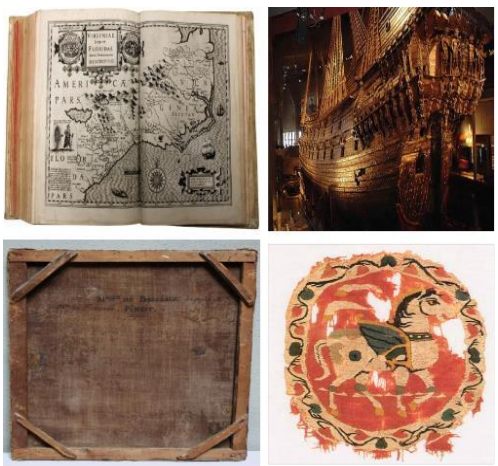

Figure 2 Cellulosic materials in cultural heritage

1.2 Wood

1.2.1 Structure and composition

The wood constitutes the tissue of the trunk, branches and roots of the trees or of the shrubs. Wood can be characterized considering the three fundamental anatomical directions (**Figure 3**):

- transverse plane (or cross-section), which is perpendicular to the axis of the trunk;
- radial plane, which is parallel to the axis of the trunk and to the medullary rays;
- tangential plane, which is parallel to the axis of the trunk but perpendicular to the medullary rays.

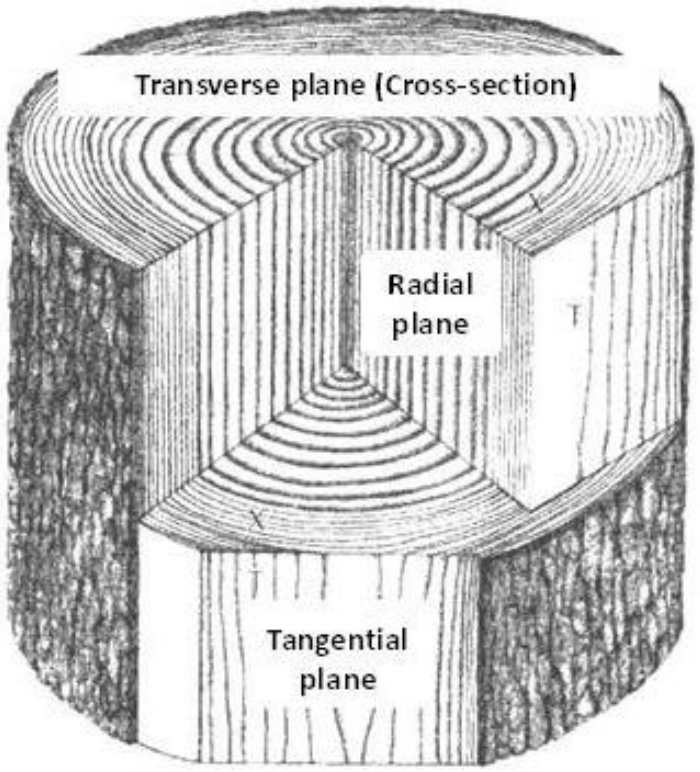

Figure 3 Wood anatomical directions

The structure of the wood can be examined at five levels (**Figure 4**).

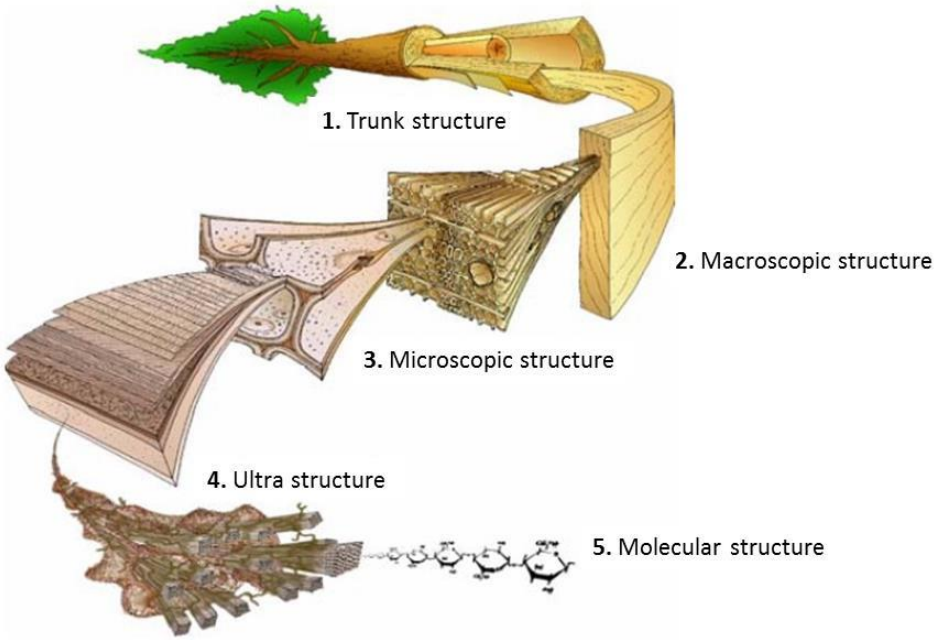

Figure 4 Structure of the wood

1th level: Trunk structure

Looking at the transverse plane of a not peeled trunk, several elements can be observed from outside to inside[1] (**Figure 5**):

- *Bark*
  The bark is divided in outer and inner bark. The outer bark is a layer of dead cells rich in suberin. This substance makes the layer impermeable to water and air so as to protect the underlying wood from the entrance of parasites and saprophytes, moisture losses and chemical, thermal or mechanical agents. The inner bark, also called phloem, is composed of a thin layer of living cells that transport the sap from the crown to the other parts of the plant.
- *Vascular cambium*
  The cambium is composed of a thin layer of living meristematic cells, which generate the xylem towards the inside and the phloem towards the outside.

- *Xylem*

  The xylem is basically the wood and it can be divided in sapwood and heartwood. The sapwood surrounds the heartwood and it is generally lighter in color. It is composed of living and physiologically active cells. The sapwood is younger and less durable compared to the heartwood and accordingly it is less resistant to the biological alterations caused by insects and fungi. The heartwood is the darker and inner part of the xylem. Its formation starts from a defined width of the sapwood when the reduction of water and oxygen leads to the death of the sapwood cells, that turn into heartwood cells. The major differences between sapwood and heartwood are not in anatomy but in physiology. The heartwood has a structural function and it is important for the stiffness and stability of the tree, while the sapwood has the function to convey water from the roots to the leaves and to store up and give back, according to the season, the reserves prepared in the leaves.

- *Pith*

  The pith is in the center of the trunk and it is surrounded by the so-called juvenile wood, which is produced by the cambium during the first year of the life of the tree. It has different characteristics compared to the mature wood, for example the juvenile wood of a conifer has wider growth rings, lower volumic mass and lower resistance and stiffness (from 50 to 70%). Starting from the twentieth year of growth, the features of the wood become that of the mature wood.

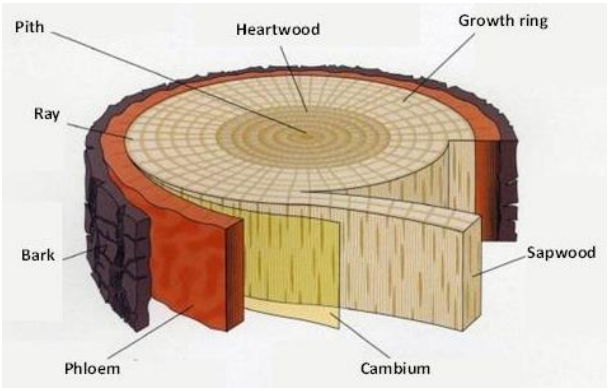

Figure 5 Structure of the trunk

2th level: Macroscopic structure

The *growth rings* are closely related to the pauses in the vegetal activity. In particular, they are generally visible because cells different in type, size, number and distribution are formed at the beginning and at the end of the vegetal activity. The early wood (or spring wood, lighter in color) ensures the rapid transportation of the lymph at the beginning of the vegetal activity, while the latewood (darker in color) has mainly structural functions. The annual rings can be used for dating archaeological wood through a dendrochronological procedure.

The *medullary rays* are radially oriented from the periphery toward the center of the trunk. They serve for the radial transport and the storage of substances, but also as a support in the radial direction.

The *resin canals* can be found in some conifers, especially in the latewood. They have a protective function because they exude resin to seal off wounds caused by mechanical damage or boring insects.

3th level: Microscopic structure

The wood is made of several cells different in type, size, shape and distribution. The majority of the cells of the wood are arranged parallel to the axis of the trunk. Contiguous cells communicate with each other through pores, which have the function of conducting the sap. Cells of the same type are grouped into tissues. There are three types of tissues in connection with the three main functions of the wood: supporting tissue, conducting tissue and storage tissue. Other types of wood tissues are the secretory tissue (for example the resin canals) and the abnormal tissue (for example damaged or abnormal fibers formed after the compression or traction of the wood).

4th level: Ultra structure

In the wood, the cells produced by the cambium develop and diversify according to their function. When they die, only the cell wall remains and it determines the features of the “wood” as raw material. The cell wall is mainly composed of cellulose micro fibrils oriented in various directions,

which constitute the main structure. In particular, in the cell wall it is possible to recognize[1] (**Figure 6**):

- The *middle lamella*
  The middle lamella is shared among multiple cells and it binds them with each other. In young tissues it is mainly composed of polysaccharides and pectic acid and consequently it is very elastic and allows the settling movements during the growth of the cell. It stiffens with the age due to lignin deposits, that can reach percentages up to 70%.
- The *primary wall*
  The primary wall is very thin and it is composed of cellulose micro fibrils immersed in an amorphous mixture of pectins, hemicelluloses and lignin.
- The *secondary wall*
  The secondary wall is thick and it is mainly composed of cellulose. It is divided in three layers in which the micro fibrils are oriented in different ways.
- The *tertiary wall*
  The tertiary wall is not always distinguishable and it is the only one which contains proteins in addition to cellulose and hemicelluloses.

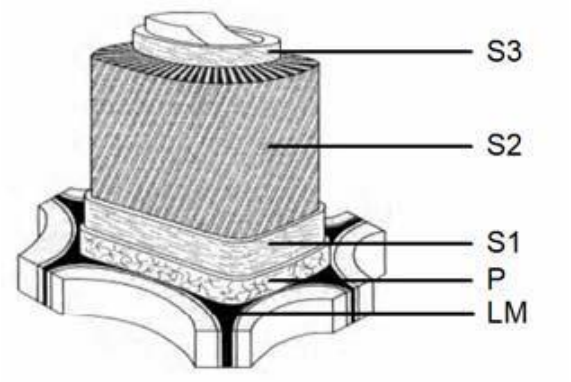

Figure 6 Cell wall model (**LM** middle lamella, **P** primary wall, **S1 S2** and **S3** three-layered secondary wall)

5th level: Molecular structure

From the elementary point of view, the chemical composition of the wood is showed in **Table 1**. However, the different properties of the wood are not

determined by the exact percentage content of the chemical elements, but by the different chemical or physical bonds between them.

Table 1 Chemical composition of the wood

Chemical element	Percentage
Carbon	49 %
Oxygen	44 %
Hydrogen	6 %
Ashes and nitrogen	1 %

The wood is a composite material consisting of macromolecular substances which form the cell walls (cellulose, hemicelluloses and lignin), but also of other secondary substances, called extractives.[1]

- *Cellulose* (40-50% of the dry weight of the wood)
  The cellulose is a linear polysaccharide formed by the polycondensation of D-cellobiose molecules, which in turns are composed of two D-glucose units linked together by a 1,4-β-glycosidic bond (**Figure 7**). The degree of polymerization ranges between 3000 and 5000 if D-cellobiose is considered as repetitive unit or between 6000 and 10000 if D-glucose is considered as repetitive unit. Higher molecular weights have been observed in the native state of cotton cellulose (15000 D-glucose residues).

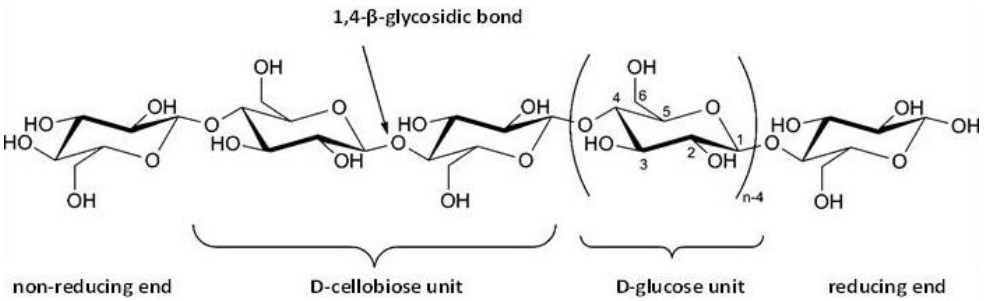

Figure 7 Structure of the cellulose

The linear structure of cellulose promotes the formation of hydrogen bonds between adjacent chains increasing the lateral cohesion. In this way, cellulose chains arranged themselves side by side so as to form

filiform bundles in which both crystalline and amorphous regions are present. Those bundles are joined together to form micro fibrils which, in turn, can aggregate themselves to form macro fibrils. Cellulose micro fibrils are connected by a homogeneous matrix composed of pectin and hemicelluloses to form the cell wall in the wood. Their presence gives to the cells high capacity of absorbing mechanical stresses, in particular tractive forces.

Concerning the chemical properties, the cellulose is insoluble in water due to the hydrogen bonds between its chains, even if it is highly hygroscopic and can swell in the transverse direction. The cellulose is quite resistant to oxidizing agents, but it is sensitive to acid hydrolysis (it can be fully hydrolyzed by strong mineral acids like H_2SO_4, HCl, H_3PO_4). Furthermore, this polysaccharide can be hydrolyzed also by specific enzymes called cellulases, cellobiases and cellulose phosphorylases.

- *Hemicelluloses* (20-35% of the dry weight of the wood)

  The hemicelluloses differ from cellulose because they are branched heteropolysaccharides, composed of different types of monosaccharide units with furanose and pyranose structures. In particular, D-glucose, D-mannose, D-xylose, L-arabinose and D-galactose are the main monomeric components (**Figure 8**), whereas L-rhamnose, D-glucuronic acid, 4-O-methyl D-glucuronic acid and galacturonic acid are present only in small quantities.

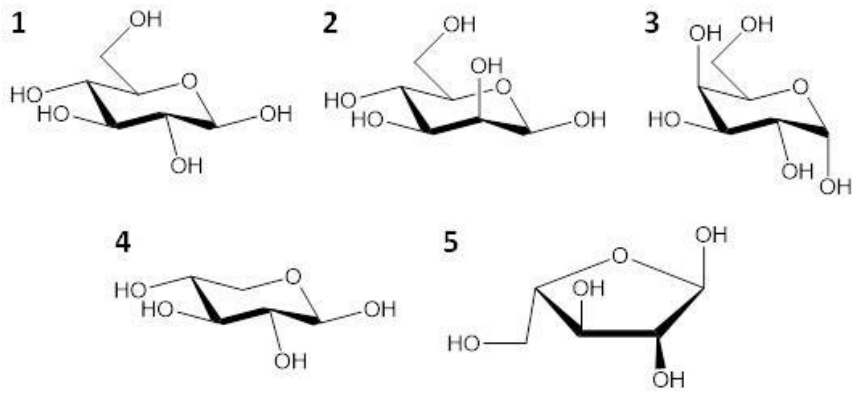

Figure 8 Structure of the principal components of the hemicelluloses (**1** D-glucose, **2** D-mannose, **3** D-galactose, **4** D-xylose, **5** L-arabinose)

The composition of the hemicelluloses depends on the tree species (softwoods or hardwoods), the climatic area, the part of the tree and the function of the vegetal tissue in which they can be found. Moreover, the hemicelluloses are amorphous polymers and their degree of polymerization is lower than that of cellulose, usually between 200 and 700.

The hemicelluloses are probably linked to lignin through covalent bonds, while they interact with cellulose by means of hydrogen bonds. They can be found in the cell walls, where they have structural functions, but also in the circulating liquids as reserve substances or exudates.

As regards the chemical properties, the hemicelluloses are soluble in alkaline and acids solutions and less resistant to the oxidant agents compared to the cellulose. Those differences are due to their lower degree of crystallinity and to the presence of different saccharide units bonded by several kind of glycosidic bonds.

- *Lignin* (15-35% of the dry weight of the wood)

  The lignin is a cross-linked aromatic polymer composed of units derived from coniferyl, coumaryl and sinapyl alcohol (**Figure 9**).

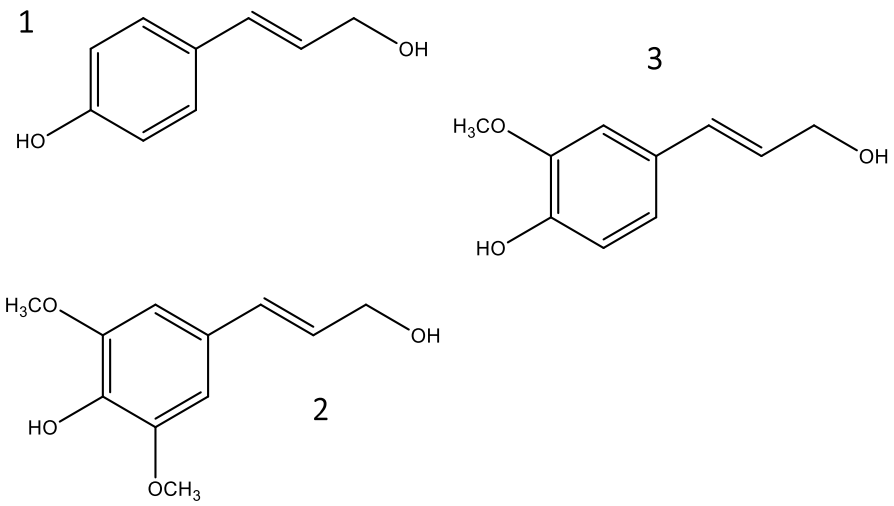

Figure 9 Structure of the principal components of the lignin (**1** coumaryl alcohol, **2** coniferyl alcohol, **3** sinapyl alcohol)

Many aspects of the lignin structure, its biosynthesis and its chemistry are still unclear. During the synthesis of the lignin, free radicals can form and polymerize with chain reactions leading to a tridimensional complex structure, which is held together by carbon-carbon and ether bonds that are more resistant to hydrolysis.[2,3] Thus, the lignin is less hygroscopic and elastic than the cellulose and its presence produces high rigidity and dimensional stability.

The lignin is not an independent constituent of the wood structure. It sediments in the middle lamella and in the primary wall during the last step of the formation of the cell wall (lignification), literally "encrusting" the micro fibrils of cellulose, the hemicelluloses and the pectins. In this way, the extensibility of the cell walls is reduced while stiffness and compressive strength are significantly increased.

- *Pectins* (1% of the dry weight of the wood)

  The pectins are amorphous polymers with high molecular weight and they are characterized by a high solubility in water. Pectins are composed of polysaccharides with different chemical composition but similar solubility. They are generally rich of galacturonic acid or of its methyl ester. During the juvenile growth of the plant, the pectins constitute the cell wall, while when the plant is fully growth they can be found in the middle lamella or in the primary wall, encrusted with lignin.

- *Extractives* (2-9% of the dry weight of the wood)

  The extractives are a heterogeneous group of substances of great importance in determining some features of the wood as the smell and the color. The name is derived from the fact that they can be extracted from the wood using solvents like ethanol, cyclohexane, acetone, toluene, dichloromethane, water etc. They can be divided in inorganic extractives, that is the ashes obtained from the calcination of the wood (soluble Ca, Mg and K salts contained in the sap) and organic extractives (lipids, waxes, oils, terpenes, tannins, flavonoids). The content and the composition of extractives are very different among different wood species and in particular between softwood and hardwood. Generally, they prevail in softwood species, which contain high amount of resin acids, fats and terpenes.

1.2.2 Main causes of degradation

The degradation can be define as any change that alters the original characteristics of the wood leading to chemical, physical, mechanical and/or morphological modifications. Wood degradation can be both biotic and abiotic and sometimes this two factors act synergistically in the alteration processes.

- *Biotic decay*[4,5]
  The biotic decay is the deterioration of wooden material caused by living organisms, mainly fungi, but also bacteria and insects. They destroy the wood to feed on its different components.
  Wood decay fungi can be classified on the base of the appearance and the overall color of the wood after the attack, which varies as a result of their preferential action on the different constituents of the wood.[6]

  – *Brown rot*
    The brown rot fungi attack the polysaccharides depolymerizing them. In an advanced state of decay, cellulose and hemicelluloses have almost disappeared, while only a fraction of lignin has been modified with a loss of methyl groups. The resulting wood has a high content of oxidized lignin, which gives it a reddish brown color (**Figure 10**) and it exhibits the characteristic cubical cracking pattern, due to the combination of the cross-grain and longitudinal cracks. The most common fungal species responsible for brown rot are some kind of basidiomycetes.

Figure 10 Brown rot

– *White rot*

The white rot fungi degrade the wood by removing lignin, hemicelluloses and cellulose more or less simultaneously. Consequently, the white rot is more dangerous and harmful than the brown rot since it affects all the components of the cell wall, thus causing accidental collapse and damage. The hyphae rapidly invade wood cells and lie along the lumen walls, where they secrete the enzymes which depolymerize cellulose and hemicelluloses and fragment the lignin.[7] Some of these fungi selectively attack the lignin and cause the bleaching of the wood, which loses strength and becomes fibrous and light in colour (**Figure 11**). However, those fungi are aerobic and they cannot survive if the cell lumens are full of water or when oxygen percentage is low. For this reason, the white rot can seldom be found in waterlogged archaeological wood, unless the attack did not happen before the immersion. The most common fungal species responsible for white rot are basidiomycetes and ascomycetes.

Figure 11 White rot

– *Soft rot*

There are two types of soft rot fungi. The most known type produces cavity of conical shape in the cell wall by attacking the cellulose. The other type is more similar to the white rot fungi, because it erodes the cell wall causing its thinning. The degraded wood is very soft as long as it remains in wet conditions, while it breaks transversely and along the grain and it acquires a brownish-gray color during the drying process (**Figure 12**). These fungi need very high humidity and very little oxygen, so they typically attack wood in permanently moist

condition such as soil or underwater. Their attack is slow because they gather the little oxygen they need from that dissolved in water. The most common fungal species responsible for soft rot are ascomycetes.

Figure 12 Soft rot

- *Bacteria* and *actinomycetes*

  The bacteria and the actinomycetes cause a degradation which generally proceeds very slowly compared to fungal attack, even if a severe decay can take place if they can act over an extended period of time. The bacteria can act both in aerobic and anaerobic conditions and so they are active also in conditions which are unfavorable for fungi. For these reason, they play a key role in the decay of waterlogged and underground wood. For example, *Erosion bacteria* are the most common degrading agents of waterlogged wood found in near-anaerobic conditions. *Tunneling bacteria* are found in aquatic or terrestrial environments, because they require a higher level of oxygen. Some bacteria are able to degrade the chemical components of the wood, causing erosions and formation of cavities in the cell walls, in particular in the secondary wall. The damage caused by bacteria to the structure of the cell walls alters their permeability and consequently can stimulate the colonization of other microorganisms. Other types of bacteria are always present on wood in association with white rot fungi and this suggest that they are not able to attack the cell wall by themselves, but they can only feed on already degraded compounds.

Finally, the insects are the more severe and frequent cause of damage of wooden objects stored indoor (e.g. museums, historical palaces, sacristies, warehouses). They exploit the wood as source of nourishment, as a refuge and for the eggs laying. Some xylophagous insects are capable of using only the compounds present inside the cells (sugars, starch), while some others are able to use the cellulose of the cell walls as carbon source. Moreover, some insects can attack the cellulose only if already partially degraded, while some others can totally depolymerize the cellulose. The main damage caused by xylophagous insects is the breakage of the wood fibers caused by the formation of exit holes and tunnels, with a consequent loss of the mechanical properties of the material. The main types of xylophagous insects are beetles (e.g. borers, long-horned beetles), termites, carpenter ants and marine wood borers (**Figure 13**).

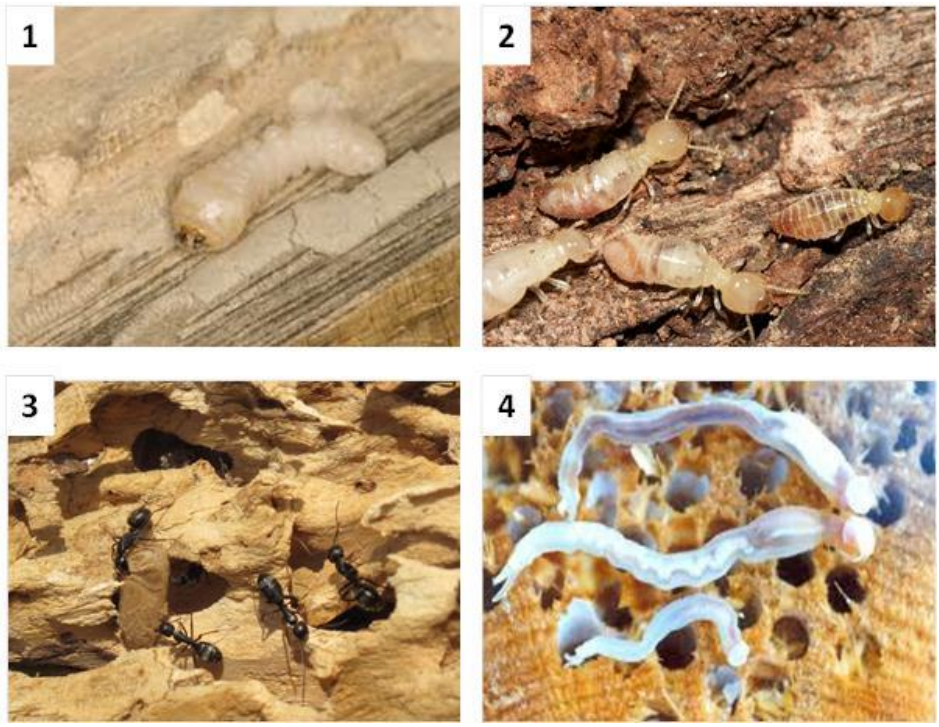

Figure 13 Xylophagous insects (**1** borers, **2** termites, **3** carpenter ants, **4** marine borers)

- *Abiotic decay*

  The abiotic decay is attributable to all those processes that are not mediated by living organisms, for example the mechanical erosion caused by the wind, the oxidation caused by electromagnetic radiation (solar radiation) and other atmospheric agents (oxygen), the action of water and heat. The oxidation of the cellulose lead to the formation of carboxyl groups on the primary alcohols and of ketones on the secondary alcohols. The former are acidic groups and can catalyze the hydrolysis of the cellulose chains, while the latter are chromophores and can cause color changes of the material.

1.2.3 Archaeological wood characteristics

The archaeological wood is a material that has escaped the natural decomposition cycle which generally leads to the transformation of this organic material in its starting inorganic components (e.g. CO_2 and H_2O) in a short time. It can be defined as "*dead wood, used by an extinct human culture, that may or may not have been modified for or by use, and that was discarded by intent or accident into a specific natural environment*".[8] Wooden findings can be unearthed in a marine, river or lake environment (waterlogged wood) or in a terrestrial environment, generally buried in soil (buried wood). The environment in which the wooden artifact is found determines the type and the extent of the decay that may take place.[9]

Focusing on waterlogged wood, the aquatic environment plays a key role in determining its state of preservation. Indeed, even if on the one hand the water slows down or prevents the action of fungi and bacteria, on the other hand it is itself a source of damage. In addition to the possible abrasive action of the sedimented materials, the water can convey inside the wood the dissolved acidic and basic substances, the salts and the oxygen. These substances can trigger and promote the degradation of the wood components. In particular, hydrolysis reactions can occur in an acidic medium, altering the chemical structure of the cellulose and the hemicelluloses and causing the formation of soluble residues. Furthermore,

the water can replace the hydrolyzed polysaccharides by creating secondary interactions with the residual components of the wood. The final results are a swelling of the fibers, an increase in the moisture content and a severe decrease in the density of the waterlogged wood if compared to the green wood, even if the structure remains apparently intact as long as the wood remains submerged. The rate of degradation depends on the burial conditions, the chemical substances dissolved in water and the wood species. As regards the biotic decay, the soft rot fungi and some types of bacteria are very harmful because they can survive in anaerobic conditions and with low oxygen.[5,10] Moreover, great damages are caused also by organisms like mollusks (shipworms) and crustaceans (gribbles), which dig tunnels deep inside the wood to feed on it (**Figure 14**).[11]

Figure 14 Shipworm (**1**) and gribbles (**2**)

1.2.4 Conservation of archaeological wood

The issues related to the conservation of wooden artifacts are extremely variable and must be analyzed in relation to the type of degradation and environment present in the recovery place. Indeed, the methodology of approach should be different whether the material was conserved in a dry or in a submerged place.

Focusing on the conservation of waterlogged archaeological wooden findings, they generally appear in quite good preservation condition as long

as they remain submerged. However, when the recovery of the findings becomes necessary, the removal of the water should be done by taking all the necessary precautions in order to prevent damage to the objects. Drying archaeological waterlogged wood often leads to its drastic shrinkage and deformation, because the water has a high surface tension and its evaporation in the extremely small pits that connect one cell to another produces a phenomenon known as collapse. The collapse occurs in a dramatic way in the degraded wood because the cell walls have lost their strength and they cannot bear the surface tension generated by the evaporation of water.[12]

For this reason, before starting a drying procedure it is necessary to assess the state of decay of the material. Firstly, the wood species should be identified and its micro-morphological characterization should be performed as reported in the Italian standard UNI 11205.[13] Then, a physico-chemical characterization should be performed. In particular, the physical characterization of the wood provides for the measurement of some parameters like the porosity, the water content, the wet and dry bulk densities and the density of the cell wall.[14] In this way it is possible to choose the proper conservation method for each type of artifact. For example, for slightly degraded objects several techniques of drying in controlled conditions have been developed, while for severely degraded objects the use of a consolidant before the drying step can become necessary to prevent shrinkage, cracks or collapses of the wood.

Some examples of drying techniques developed for waterlogged archaeological wood are:

- Controlled drying

  This procedure provides for the air-drying of the wood in a climate-controlled room, in which the temperature and the relative humidity are monitored. In some cases the controlled drying can be performed under vacuum. This easy procedure does not require expensive equipment, unless the objects to be treated are not too large. The disadvantage is that this procedure is often slow and takes a long time.

- Freeze-drying[15]

  The freeze-drying (or lyophilization) technique consist in freezing the water inside the object and transforming it directly from solid to gaseous state (sublimation) usually at reduced pressure. To prevent damages to the structure of the artifact due to the formation of ice, wood is previously impregnated with a cryoprotectant, which provides mechanical strength and elasticity (i.e. polyethylene glycol PEG 400). This method has several advantages like speed, shrinkage control and simplicity and gives a good appearance and natural weight to the treated objects. The disadvantages are related to the use of PEG 400, because it can be attacked by microorganisms and also it confers to the treated wood a waxy texture, which promotes the retention of dirt.

- Supercritical drying[16]

  A supercritical fluid is a substance at a temperature and pressure above its critical point where distinct liquid and gas phases do not exist. In addition, there is no surface tension in a supercritical fluid as there is no liquid/gas phase boundary. Therefore, by changing the pressure and the temperature of the fluid, its properties can be tuned to be more liquid or more gas-like. Thus, the method of supercritical drying allows to avoid the problems associated to phase changes inside the wood that occur in the other methods of drying. The carbon dioxide is the most commonly used supercritical fluid, with a low critical temperature and pressure (31°C and 73.8 bar). Being supercritical carbon dioxide not miscible with water, the drying method requires a pre-treatment stage in which a miscible solvent (i.e. methanol) is used to replace water inside the artifact. Then, supercritical carbon dioxide is used to replace methanol and, at the end of the process, the samples are slowly decompressed and cooled at room temperature. In principle this technique can be scaled up to cope with artifacts of any size.

The drying procedures usually require stabilization interventions, like impregnation or bulking, in order to dry but at the same time strengthen the waterlogged wooden artifact, preserving its shape and size. In these techniques the water is substituted with a solution of a consolidant that contributes to restore solidity in the degraded material after the evaporation

of the solvent. Depending on the molecular weight of the product, the viscosity and wettability of the solution and the pore size of the degraded wood, the consolidant can penetrate in the microporosity of the cell wall (bulking) or it can fill every porosity of the wood, the wall and the cell lumen (impregnation).[17,18] Diffusion and permeation processes contribute to the penetration of natural or synthetic products in the wood. In general, consolidants with low molecular weight can be applied when the wooden findings are less degraded, while the impregnation with products with high molecular weight is used when the objects are more degraded.

To evaluate the effectiveness of the treatment, in addition to the measurement of the physical properties of the wood, also other information like the penetration depth, the distribution and deposition modality of the consolidant would be useful. A common technique used to obtain information on the treatment is the optical or electron microscopy, in which cross sections at different depths from the surface of the wood are analyzed. However, the microscopy is a destructive technique. X-ray microtomography (μCT) is a promising alternative to microscopy, because it is a non-destructive technique, which does not require any specimen preparation. The degree of distribution of the consolidant in the structure of the wood and, in particular, the cavity-filling and the penetration depth can be investigated with this technique. Moreover, the use of the synchrotron radiation (SR-μCT) as the source of X-rays allows a considerable improvement of the resolution.[17] Porosity and variations in pore size distribution can be evaluated by mercury intrusion porosimetry (MIP).[18]

There are several basic requirements for a good consolidant, like:

- chemical affinity for the wood,
- physical and chemical compatibility with wood,
- good penetration ability,
- high chemical stability,
- good resistance to microbiological attacks,
- low toxicity for the operator and the environment,
- solubility in safe solvents.

Moreover, in order to ensure the maintenance of the natural permeability of the wood a good consolidant should not form continuous superficial films, which can obstruct the pores of the material. A good consolidant should also not form precipitates that can alter the appearance of wood. Finally, reversibility is a desirable aspect of any conservation process as the "Principle of Reversibility" states:

"The conservator is guided by and endeavors to apply the "principle of reversibility" in his treatments. He should avoid the use of materials which may become so intractable that their future removal could endanger the physical safety of the object. He also should avoid the use of techniques the results of which cannot be undone if that should become desirable." [19]

However, the complete reversibility of a consolidant is not easily achieved, even if the product maintains high solubility since objects that need consolidation are by definition so weak that repeated applications of solvent may cause damage. Considering this, several attempts have been made to redefine the reversibility as re-treatability as more realistic goal.[20]

Among the consolidants used for impregnation treatments, the most interesting are:

- Polyethylene glycol (PEG)
  PEG is obtained from the polymerization of the ethylene oxide and it has the generalized formula reported in **Figure 15**.

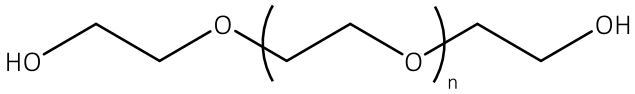

Figure 15 Generic structure of PEG

  PEG molecular weights range from 300 to 6000 g/mol and the aspect of these products change according to the molecular weight. In particular, low molecular weight PEGs (300-600 g/mol) are liquids, the intermediate ones (1000-1500 g/mol) are semi-liquids or have the consistency of very viscous oils, while the high molecular weight PEGs (3250-6000 g/mol) are wax-like materials. The characteristics that have made PEGs suitable for the impregnation of waterlogged wood are the solubility in water and

other alcoholic solvents (i.e. ethanol, methanol, 2-propanol), the low toxicity and the ability to penetrate inside the micropores of the cell wall. The PEG conservation process was the first reliable method to treat waterlogged wood.[21,22] It is also relatively easy to perform and it has the advantage of removing the excess of water while simultaneously consolidating the wood.

The treatment generally starts with a preliminary cleaning of the artifact to remove all surface dirt. Then the waterlogged object is placed in a ventilated vat containing a dilute solution of PEG in water or alcohol (usually 1-5%). Water is commonly used for the treatment of large objects because it is considerably cheaper than an equal volume of alcohol even if it requires the adding of a fungicide. The vat temperature is gradually increased until it reaches 60°C (after a period of days or weeks) and then it is kept constant until the end of the treatment. In order to have a good penetration of the product, the PEG concentration in the solution is gradually increased over a period of months (or even years) until a minimum concentration of 70% is reached. During the conservation process, the consolidant slowly permeates the wood, displacing the water. At the end of the operation, the object is removed from the vat, the excess of PEG is eliminated and the object is allowed to cool.

Even if PEG treatment is still considered one of the most efficient ones[16,23] and, thus, it is still widely used in waterlogged wood conservation, several drawbacks were unearthed after its most famous and important application, i.e. the treatment of the Vasa warship.[24] Among the main failures there are:

- hygroscopicity that increase as the molecular weight decrease;
- a not negligible conductivity even at the solid state, which allows the transportation of ions and oxygen inside the wood;
- the susceptibility of PEG to several factors, such as high temperature, proximity to metals and other substances, microbial[25], photo-chemical and oxidative degradation;
- long term creep and permanent distortion of the treated wood.[24,26]

- Sugar method

  Several saccharides have been tested as consolidants for waterlogged wood (e.g. sucrose, trehalose, lactitol)[23,27-29] as an alternative to more expensive methods. The conservation techniques include the impregnation of the object with heated sugar solution (warm conservation method) or the use of an unheated one (cold conservation method). The advantages of using sugars are:

  - sugars are easily available and not so expensive;
  - sugars are non-corrosive and their use does not involve any risk of fire and explosion or hazards to health and environment, not even during the disposal of the object after conservation;
  - their low molecular weight allows a good penetration into wood, also without heating;
  - treated wood has a natural color and can be cleaned and glued easily;
  - sugars can be removed by immersion in water;
  - sugars can be used in the treatment of composite objects (made of wood and other materials like textiles, metals …);
  - after the treatment, a good strength-increase and dimensional stabilization are achieved.[30,31]

  However, the treatment with sugars has also disadvantages that did not allow them to definitively replace the PEG. The biggest disadvantage is the risk of microbial, insect or rodent attack during and after the treatment. Biocides can be added to the solution, but they can pose some health and environmental hazards. Moreover, despite the presence of the biocide, microbial growth is still extremely difficult to control. Finally, further problems specific to each type of saccharide can be present. For example, the sucrose can easily hydrolyze, with a consequent increase in its hygroscopicity or it can form superficial crusts.

- In situ polymerization method

  The in situ polymerization method involves the absorption of monomers or oligomers that can subsequently polymerize inside the degraded wood. In this way it is possible to address the problem of the insufficient penetration of the polymers due to their molecular size.

  An in situ polymerization method developed in Germany at the end of the nineties is the so called Kauramin® method.[28] The Kauramin® is a

patented substance from BASF based on melamine and formaldehyde. This method was successfully used in the treatment of waterlogged finds from the Cantiere delle navi antiche (Pisa, Italy).[32] The treatment is usually performed by submerging the object in a solution of Kauramin® at room temperature, controlling the pH regularly. The impregnation time can take from a few weeks to one year depending upon the size (thickness) and state of preservation of the wood. At the end of the impregnation, the wood is cleaned and then the controlled polymerization is performed by keeping the object in an oven at 50°C for 7-14 days, depending on the dimension. The Kauramin® method have several advantages:

- short treatment time;
- the method is less expensive than others (e.g. PEG);
- the treated objects are light in weight thanks to the low molecular weight of the Kauramin® constituent molecules, their dimensions and surface details are preserved and they show a good mechanical resistance;
- Kauramin® stabilizes the objects containing inorganic salts like sulphur or iron;
- the impregnation solution and the treated objects are not attacked by microorganisms.

However, there are also some disadvantages like the irreversibility of the treatment, the lack of the possibility of further treatments, the requirement of a specialized equipment and a strict control to avoid uncontrolled curing of the resin and the necessity of special security precautions due to the presence of formaldehyde. Moreover, to reduce the cross linking and increase the flexibility, it was necessary to study specific formulations. Finally, as regards the aesthetic aspect of the treated objects, superficial treatments are necessary.

1.3 Paper

1.3.1 General features

Over the centuries, many different materials have been used for the production of the paper, as for example vegetable rags (cotton, hemp, linen), wood, leaves, cereals or annual plants (cotton, hemp, linen, maize) and, especially in recent years, waste paper. Depending on the material used for its preparation, the paper is called rag pulp paper, wood pulp paper and recycled paper.

- Rag pulp paper

  The use of linen, cotton or hemp rags to produce paper is the oldest technique in the West. This handmade paper has a definitely higher quality than the machine-produced paper that has begun to spread in 1798, after the invention of the first machines for the continuous production of paper. The preparation procedure involved the sizing of the sheets with vegetable (starch flour) or animal glue (bones or skins gelatin) in order to make them less permeable and more suitable to receive the ink. Starting from the 17^{th} century, the alum began to be added to the animal glue to improve the interaction between the gelatin and the paper fibers. In the early nineteenth century, a new sizing method which involves the use of alum and rosin (a mixture of organic acids obtained from plants) was introduced.
- Wood pulp paper

  The use of wood pulp for the production of the paper began to spread in the second half of the nineteenth century. Three different procedures can be used to produce wood pulp:
  - *Mechanical pulp*

    This procedure does not involve a chemical treatment of the wood but only a mechanical one. The paper produced using mechanical pulp contains all the encrusting substances present in wood together with cellulose and has a low quality.
  - *Chemical pulp*

    In this procedure the wood is treated both mechanically and chemically with acid or alkaline reagents (calcium, magnesium or

ammonium bisulfite, sodium sulfate or lime) generally at high temperature and under pressure in order to solubilize and remove the encrusting substances. Finally, processes of bleaching with chemical oxidants (chlorine, sulfur dioxide) are performed.

- *Semi-chemical pulp*
  This procedure involves a combination of mechanical and chemical processes. The wood is hulled, chopped and then treated with hot chemical reagents (sodium sulfate, sodium carbonate or lime). Finally the mechanical pulping is performed. In this way, the lignin is almost completely removed but not the hemicelluloses.

The paper is mainly composed of cellulose, but it can also contain other substances deriving from the raw materials or from the production processes (lignin, hemicelluloses, starch, animal glue, alum, rosin) or related to its use (ink). Moreover, synthetic adhesives as polyvinyl acetate are used in the paper produced in modern era or they can be used in the conservation of damaged paper. It is essential to have a full knowledge of these substances and of their properties to understand the degradation processes to which the paper is subjected.

1.3.2 Main causes of degradation

As previously mentioned, cellulose is the principal component of the paper. The degradation of cellulose is caused by hydrolysis or oxidation reactions and by biological factors.[33,34]

- Hydrolysis reactions
  The hydrolysis reactions cause the break of the 1,4-β-glycosidic bond with the consequent depolymerization of the cellulose, which results in a significant loss of the paper strength.[35] These reactions are catalyzed by both acids and bases, even if the alkaline hydrolysis is less harmful because it cannot easily occur at low temperature, unless the cellulose has not already been oxidized. In particular, if β-alkoxy carbonyl groups have formed as a result of oxidation reactions, alkaline hydrolysis takes place through the β-alkoxy elimination mechanism.[36,37]

On the contrary, acid hydrolysis deserves particular attention because the acidity may originate from intrinsic or external factors.

Some intrinsic factors are the final products of the cellulose oxidation or the residues of the industrial processing of the paper. As regards the ancient paper, other intrinsic factors are the products used in the sizing. For example, starch was generally heated together with acids to improve its film-forming properties. Moreover, when animal glues were used, the oxidation of their main component, i.e. the collagen, may have led to the formation of acidic products. Finally, alum and rosin contain acidic substances. Furthermore, from about the 5^{th} century to the 19^{th} century, the iron gall inks were widely used and they contain H_2SO_4 as byproduct (**Figure 16**).[38]

Figure 16 Degradation induced by the presence of iron gall ink

The external factors are substances produced by human or industrial processes, which come into contact with the paper through the environment. For example, the gaseous air pollutants (NO_x, SO_2, SO_3) can settle on paper and form the corresponding acids (HNO_3, H_2SO_4) in the presence of moisture and condensation. Other external factors of degradation are the restoration treatments, if not properly performed.

- <u>Oxidation reactions</u>

  The primary (C_6) and the secondary (C_2, C_3) alcoholic groups of the cellulose are involved in oxidation reactions, forming, respectively, carboxylic acids and ketones. These side groups make the molecule more easily hydrolysable[39] and contribute to raise the acidity of the paper and to change its color since they are chromophores. Moreover, they form weaker hydrogen bonds compared to the original alcoholic groups. Finally, if the oxidation is particularly severe, the carbonyl groups can be

further oxidized to carboxyl groups with a consequent breakage of the C_2-C_3 bond and opening of the ring. If this happens, the linearity of the cellulose structure is altered and a remarkable structural degradation of the fibers can be observed. The oxidative degradation of the cellulose is induced by several factors as the oxygen, the light, the air pollutants and some chemical oxidants (hypochlorite, permanganate, hydrogen peroxide,).

- Biodegradation

  Paper is highly hygroscopic and, therefore, it is very sensitive to the action of biological agents that promote processes of biodeterioration (**Figure 17**). In particular, several types of bacteria and fungi can secrete enzymes that are able to catalyze the hydrolysis of cellulose (i.e. endoglucanase, cellobiohydrolase and β-glucosidase).[40] Moreover, the metabolites produced by these microorganisms are often acidic and colored and so, in addition to the physical-mechanical damage related to the depolymerization, there is also the possibility of an optical-chromatic damage. The action of these microorganisms is promoted in certain conditions of temperature and relative humidity. For example, temperatures above 15-18°C, relative humidity greater than 50-55% and poor ventilation represent highly favorable conditions.[41] Therefore, it is very important to regularly monitor the storage conditions. Indeed, prevention is crucial because it allows to obtain even better results than those that can be achieved with the restoration of an already occurred damage.[42,43] Finally, products used in the paper production processes (e.g. sizing) as well as the pH can influence the biodeteriorating action of fungi.[44]

Figure 17 Biodeterioration of paper

1.3.3 Conservation of paper

There are several strategies available for paper conservation, which address various aspects of the deterioration. They can be classified under the following categories, which may also be considered to represent the generic steps of a paper conservation treatment:[45]

1) Preparation of the intervention
   This phase comprises several steps, including materials and decay characterization in order to help the conservator in the choice of a safe and suitable conservation treatment. Some of the usual issues investigated in this phase are the composition of inks, dyes and pigments and the composition and processing of paper. If the artifact is part of a more complex system, this phase also includes its isolation and separation from other materials. The conservator must keep permanent records of the all the examinations and conservation treatments performed on the artifacts.
2) Disinfestation and disinfection/sterilization[46]
   This step aim at protecting the artifacts from biological agents. In particular, disinfestation entails the extermination of rodents and insects, while disinfection/sterilization concerns the elimination of microorganisms, mainly of fungi. The use of modified atmosphere, which consist in substituting the oxygen of the air with nitrogen or carbon dioxide, is an effective method to perform the disinfestation and poses no threats for the health of the operators and the treated materials. As regards disinfection/sterilization, several chemicals are used as fungicide or antimicrobial and among them, especially in the past, there were some toxic products like thymol, quaternary ammonium salts, ethylene oxide and formaldehyde. Other methods, like the use of UV and γ-radiation have a very limited use due to the damage that they inflict on paper. Nevertheless, the UV radiation is exploited to activate the photocatalytic properties of TiO_2 anatase nanoparticles because, when illuminated, they produce reactive species (e.g. hydroxyl radicals and superoxide ions), which can decompose and mineralize organic compounds causing fatal damage to microorganisms. Recently, these nanoparticles have been used in the form of nanocomposites together

with deacidifying agents and/or consolidants so as to perform different conservative actions in one application.[47]

3) Surface/dry cleaning

   This procedure is used for the removal of dust, dirt, foreign materials etc. from the paper surface for aesthetic reasons and/or to facilitate the preservation of the artifact. Dry cleaning must precede aqueous treatments, because dirt can be transferred by water into the paper matrix.

4) Wet cleaning

   The immersion of the paper in water removes the water-soluble products originating from the hydrolysis and the oxidation of cellulose, the metabolism of microorganisms, the atmospheric pollution and the usage. Several precautions should be taken prior to the treatment. For example, paper must be supported and inks and media must be tested for solubility. However, although it is not a mild intervention, the immersion in water can lead to a stabilization of the paper since a part of the removed compounds is acidic.

   Another wet treatment is the bleaching, which has only an aesthetic purpose. This procedure destroys chromophore groups by oxidation or reduction depending on the type of bleaching agent, but at the same time affects the paper. Therefore, it should be carried out with the outmost care and only when it is strictly necessary.[48]

5) Chemical stabilization – Deacidification[33]

   The most important intervention concerning the long-term preservation of paper is the deacidification, since the acid hydrolysis is by far the most important degradation mechanism for this material. The goals of the deacidification are the neutralization of the acids as well as the deposition of an alkaline reserve, a substance that is able to neutralize the acidity that may be developed in the future. The final pH must be in the neutral or mildly alkaline region (7-9.5) in order to avoid alkaline degradation and autoxidation. However, it should be noticed that the deacidification cannot restore the lost mechanical strength of the aged paper.

   Mass deacidification uses advanced technical infrastructures of industrial proportions to simultaneously deacidify large quantities of books and

paper materials. These objects must be sufficiently strong to be handled and in general they come from archives and libraries and they were mostly produced between 1850 and 1970. The mass deacidification systems can be classified in three major categories: liquid solutions (Bückeburg method, Papersave, Sablé system, Vienna method), liquid suspensions (Bookkeeper, CSC Booksaver, ZBF:2 Procedure) and gas phase methods (Libertec-SOBU). Almost all of these methods are based on alkaline magnesium compounds. No mass deacidification method is suitable for all types of material. Most of these methods may cause serious damage to some paper materials, while others do not deposit an adequate alkaline reserve.

Deacidification of loose sheets of paper can be performed using aqueous or organic solvents. Calcium hydroxide and magnesium bicarbonate are two of the most common agents used to perform the aqueous deacidification because they both produce very good results. Calcium hydroxide that remains on paper after the neutralization of the acidity forms the alkaline reserve by reacting with the carbon dioxide of the air, while magnesium bicarbonate is converted to magnesium carbonate or magnesium oxide. The main drawback of using calcium hydroxide is the high pH of the deacidification bath, which can cause the yellowing of lignin-containing paper and the changing of the color of iron gall inks from black to brown. The drawbacks of using magnesium bicarbonate are a more intense yellowing of lignin-containing paper and the deposition of magnesium bicarbonate crystals on the surface of paper (gritting effect) which can be converted to foxing stains after a humid ageing.

Since the aqueous deacidification cannot be applied to artifacts with water-sensitive inks and dyes and is unsuitable for mass treatments, other methods to neutralize the acidity of paper using organic solvents have been developed. Organic solvents have the advantage of wetting the paper more rapidly than water. Moreover, they are easy to dry and they have less swelling or distorting effect on paper. Alcohols like ethanol or methanol and fluorinated solvents like perfluorocarbon or perfluoroheptane[49] are commonly used.

In recent years, the research on deacidification methods has focused on the use of hydroxide nanoparticles (calcium hydroxide, magnesium

hydroxide) dispersed in alcoholic solvents (ethanol, 2-propanol) achieving promising results.[50-53]

6) Paper repairs

This step involves the restoration of mechanical damages and the paper repairs, as lacunae filling or tears stabilization. To perform these interventions paper pulp or Japanese paper are commonly used. The Japanese paper is a thin and strong handmade paper produced using long and strong fibers extracted from the inner bark of various indigenous Japanese plants.

7) Consolidation/strengthening

Several methods are used to obtain paper strengthening. For example, the lamination consists in pasting a thin Japanese tissue[54] on one or both sides of a weak, moldy and brittle paper. More recently sheets of bacterial cellulose were studied to perform the lamination, obtaining very promising results.[55] Paper splitting entails the splitting of a paper sheet thickness-wise, the insertion of a healthy paper core, that can contain calcium and magnesium carbonate as alkaline reserve, and the reassembling of the paper sheet. However, this method poses serious risks for the paper artifacts, alters the thickness, the weight and the bending behavior of paper and its retreatability is doubtful. There are also several mass methods, like Bückeburg and Vienna methods, which combine deacidification and strengthening. Also graft copolymerization processes can be performed simultaneously to the mass deacidification. In this processes monomers, usually a mixture of ethyl acrylate and methyl acrylate, are grafted on cellulose chains and then allowed to polymerize after the exposition to γ-radiation.[56,57]

As regards consolidation, several synthetic polymers have been studied, like polymers and copolymers of alkylesters of acrylic or methacrylic acid[58] or polyvinyl acetate or vinyl acetate-acrylate copolymers. Chitosan and other natural polymers have also been studied, but they have shown low biostability and versatility. Therefore, due to the high affinity for paper and the similar physical behavior, the main choice in most paper conservation treatments are the cellulose ethers, like methyl cellulose, methyl hydroxyethyl cellulose, carboxymethyl cellulose and n-hydroxypropyl cellulose.[59-62]

1.4 Renewable materials and their role in the conservation of cellulosic artifacts

In recent years, the interest of academia and industry for the use of renewable starting materials in the synthesis of new polymers has grown worldwide and it characterizes the current industrial development.

During the second industrial revolution, the chemistry of petroleum derivatives has greatly contributed to expand the available chemicals, allowing a general spread of wealth in industrialized countries. However, in recent years various problems such as the increase in oil prices, the uncertainty about its future availability, the need to reduce greenhouse gases associated with its use and the low biodegradability of petroleum derived polymers are moving politicians and public opinion toward a new sustainable development model. In this model, renewable resources are exploited in addition to petroleum for the production of fuels and chemicals.[63]

The use of renewable feedstocks is in agreement with the 12 principles of the "Green Chemistry" developed by Anastas and Warner[64], especially if it is based on the exploitation of waste materials. Moreover, it can allow to introduce in the new sustainable products, like biopolymers, interesting properties as higher biocompatibility and biodegradability.[65] However, it is worth noting that the properties bio-based and biodegradable do not always coincide. According to the standard UNI/CEN TR 15932, the biopolymers are divided into natural biopolymers (polymers that are naturally produced by living organisms) and synthetic biopolymers, which are defined as polymers that *"are derived from renewable sources and/or are biodegradable"*. Therefore, considering the fact that bio-based products not necessarily maintain their biodegradability, in order to have synthetic biopolymers which maintain this property and also a good affinity and compatibility for artistic artifacts made of natural materials (i.e. wood or paper) it is necessary to use transformations and reactions that are capable of retaining the characteristic backbone of the starting feedstock.

In the new sustainable model that is being developed worldwide, the concept of biorefinery derives from the need to use as widely and efficiently as possible the vegetal biomasses for the production of fuels and chemicals.[66,67] The political and strategic reasons for the development and construction of biorefineries mainly consist in:

- improvement of the quality of the environment at the local level (decrease of smog), regional level (reduction of acid rains) and global level (mitigation of climate changes due to greenhouse gases);
- valorization of waste materials;
- development of rural economy.

Different kinds of biorefinery can be developed on the base of the different biomasses used as starting materials. Biomass is a generic term that includes products, byproducts, residues and wastes from agriculture, forestry and related industries, as well as the biodegradable organic fractions of industrial and municipal solid wastes (**Figure 18**).

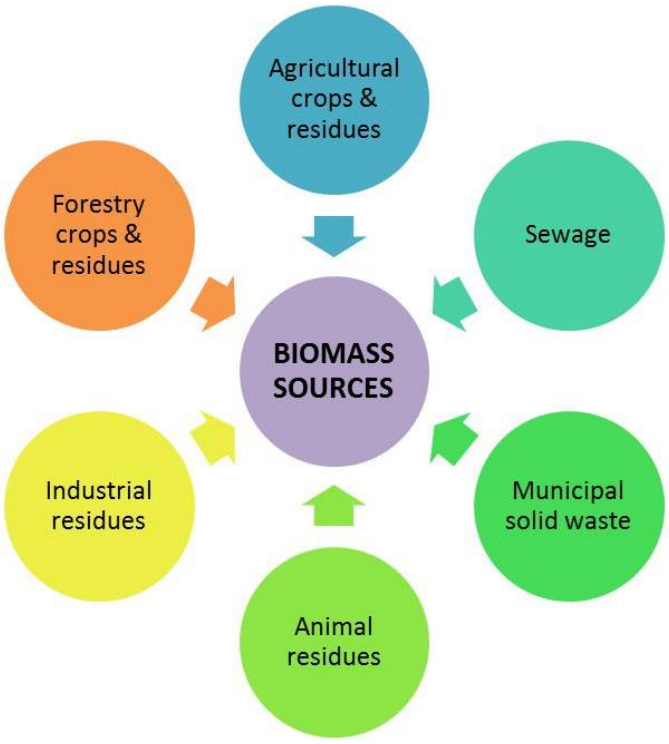

Figure 18 Biomass sources

Depending on the type of vegetal biomass used as feedstock, the different components can be recovered in different amounts. Nevertheless, those components are similar and include cellulose, hemicelluloses, lignin, extractives, lipids, proteins, simple sugars, starches, water, hydrocarbons, ash and other compounds.[68,69] The products obtained from a biorefinery can be used as such or processed to produce energy, fuels and chemicals (**Figure 19**).

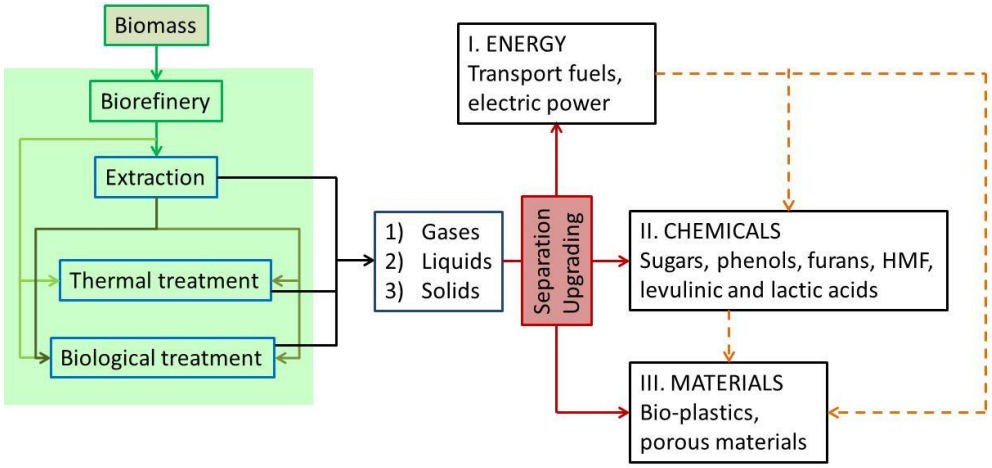

Figure 19 Products obtainable from biomass

Among the different types of biomasses, the lignocellulosic ones have great interest, because they are annually produced in large amounts (150-170x10^9 tons/year)[69] and are mostly recovered from wastes of agriculture, forestry and paper industries. Therefore, their use does not compete with the food industry, because lignocellulosic biomasses are not edible.

As one of the first step, a biorefinery based on lignocellulosic feedstock provides for a fractionation of the biomass in lignin and polysaccharides (i.e. cellulose and hemicelluloses). However, prior to the fractionation, the lignocellulosic feedstock needs a complex chemical and physical pretreatment, due to the very strong interactions between its components.[70-74] Generally, during these pretreatment procedures a selective solubilization of hemicelluloses is easily performed, while the lignin separation is realized by reductive or oxidative cleavage or by pyrolysis. The final solid residue is composed of cellulose.

Then, each component can be used as such or processed to produce energy or other derivatives. In particular, a further processing to obtain small molecules as hexoses and pentoses from polysaccharides can be performed, while phenolic compounds can be obtained from lignin (**Figure 20**). Those molecules can be used as monomers for the production of bio-based polymers.[75] For example, 5-hydroxymethyl furfural (HMF) and furfural (FF) can be obtained from the hydrolysis of polysaccharides (i.e. cellulose and hemicelluloses) and the consequent dehydration of the resulting carbohydrate monomers (i.e. glucose and xylose). Starting from HMF and FF, several furan-based monomers can be obtained and used in the synthesis of bio-based polymers.[76,77] Finally, biotechnological transformations of biomasses and their derivatives were also studied and sometimes the final products were successfully commercialized. Indeed, several monomers are enzymatically produced and then used in conventional synthetic processes to obtain polymers.[78-81]

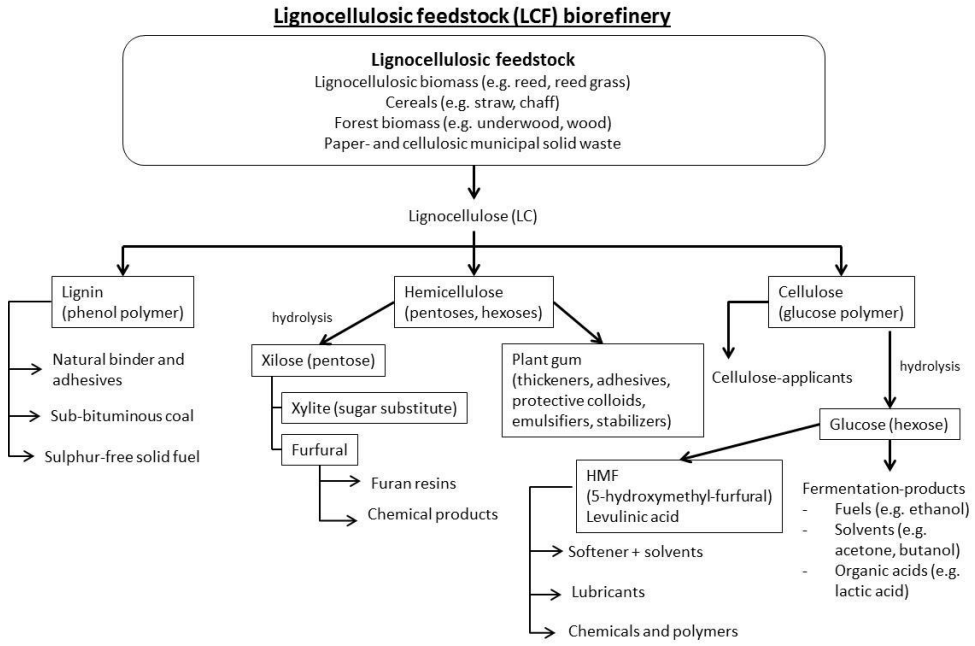

Figure 20 Scheme of a lignocellulosic feedstock biorefinery

Focusing on cellulose, one of the most studied processes which involves this polysaccharide is currently its conversion into chemicals[82] and, in particular,

into glucose which can be in turn fermented to obtain bio-ethanol for its use as fuel or as chemical product.[83-85] Essentially two methods for the hydrolysis of polysaccharides have emerged. The first is the enzymatic hydrolysis, which is specific and normally gives no byproducts. However, like all the enzymatic processes, it is slow and it might be subject to product inhibition.[86-89] The second method is the acid hydrolysis with mineral acids (i.e. H_2SO_4, HCl and HF), which is still the main established route to treat the cellulose and it is currently the reference point of most pilot-plant scale technologies. This procedure is fast and results in a complete hydrolysis, but has the disadvantage of giving toxic byproducts, which can lower the yield or reduce the conversion rate in a subsequent fermentation. Moreover, the catalyst is not easy to remove and so there is the need to purify downstream products from acidic solutions. Finally, acid hydrolysis poses corrosion hazards to the plants.

The cellulose can also be used as such and it is considered one of the most important raw material to obtain environmentally friendly and biocompatible products.[90] Many cellulose derivatives with different chemical and physical properties have been synthesized and among them, the cellulose ethers have a great industrial importance. They can be obtained with a different solubility in water or organic solvents according to the substituents used and the degree of substitution (DS) achieved at the end of the reaction.[91,92] Due to their high stability and toxicological safety, cellulose derivatives are used in several industrial applications.[93]

The central role that the renewable resources have assumed in the modern chemical industry is also reflected in the field of cultural heritage conservation, where the exploitation of these materials has further advantages in addition to the environmental and economic ones.[94] Firstly, bio-based materials has in general a low toxicity not only from the environmental point of view but also for the operator. Moreover, they are sometimes soluble in water and this allows the use of greener formulations. Finally, the natural products and their derivatives can more easily meet the requirements for compatibility and respect for the constituent materials of the work of art. This is especially true for those works of art whose supports

are made of the same chemical species that constitute the biomass, like wood and paper.

In the previous paragraphs, some techniques like the impregnation of wood with sugars and the consolidation of paper with cellulose ethers have been described and many other examples of the use of natural products or their derivatives are reported in the literature. For example, in two important case studies like the Oseberg ship from Norway[95] and the Mary Rose warship from England[96] the researchers expressed the need to find new products for the treatment of archaeological wood because the other consolidants, like PEG and Kauramin®, which had been previously tested on those ships, gave not optimal results. In particular, lignin, crystalline cellulose, 2-hydroxyethyl cellulose, guar and chitosan were tested and their use underlined some advantages like the compatibility with wood, the use of water as a solvent, the easy formation of open structures with no occlusions of the pores of the substrate.

Recently, others hydroxylated products were synthesized starting from natural resources to obtain water soluble compounds with high affinity for polar materials like wood, paper and natural fibers. Among them, some cellulose ethers[97] and hydroxylated oligoamides with different molecular weight and different hydrophilic/hydrophobic ratios[98,99] were tested as consolidants in the conservation of waterlogged wood, obtaining satisfactory results.

As a general conclusion, the examples which can be found in the literature suggest that the future of conservation technologies should lie in the use of renewable resources, which show enhanced compatibility with the natural materials present in the artifacts (i.e. wood and paper). Moreover, their use seems not to have detectable side effects and generally they are not toxic for the environment and the operator.

2 Aim of the research

The aim of the present research was the design and the development of new products and formulations to be used in the field of cultural heritage and, in particular, for the conservation of cellulosic artifacts.

As previously mentioned, the exploitation of biomasses for the production of fuels and chemicals has assumed a central role in the modern chemical industry. Therefore, one of the basic requirements for the research of new formulations and new synthetic procedures is the use of reagents and methods with reduced environmental impact, in accordance with the principles of the Green Chemistry.[64]

The use of substances of natural origin like monosaccharides, oligosaccharides or polysaccharides, either as such or after appropriate modifications, is particularly interesting not only because it matches with the growing interest towards the use of renewable resources, but also because it confers to the final products some useful properties from the point of view of the conservation of cellulosic materials. In particular, these saccharides and their derivatives (monomers or copolymers), if properly designed, have structural characteristics that make them compatible with the natural polar cellulosic materials (e.g. wood, paper, natural fibers and fabrics).

Starting from these considerations, in recent years several cellulose derivatives[97] and bio-based hydroxylated oligoamides[98,99] were synthesized in the Department of Chemistry of the University of Florence and studies on their application as consolidants for archaeological waterlogged wood were performed.

The aim of this PhD project was the expansion of this library of products by developing new bio-based vinyl copolymers using allyl derivatives of saccharides as comonomers. In particular, a more specific aim was the overcoming of some critical issues presented by the previously studied consolidants, like the poor penetration ability of cellulosic derivatives in waterlogged wood due to their high molecular weight or the need of improved *work-up* procedures for the synthesis of allyl derivatives.

Moreover, among the products suitable to expand the library of materials for cultural heritage conservation, in this research new formulations containing bio-based copolymers and nanoparticles were studied. These formulations have the advantage to join the consolidating action of the organic matrix with the specific properties of the selected nanomaterials, as for example the TiO_2 anatase nanoparticles, which show antimicrobial and antifungal properties. In particular, new core-shell nanocomposites containing allyl saccharide copolymers and TiO_2 nanoparticles were obtained.

Finally, the last aim of this research was the design of applicative procedures to evaluate and compare the performances of different products when applied in the conservation of works of art. These procedures should respond to the need for a quick comparison of the applicative properties of the new synthesized products, in order to shorten the time necessary to their development so as to arrive more quickly to materials directly applicable in the cultural heritage field. In this regard, a protocol previously used[100,101] for the study of the consolidation of the archeological wood was slightly modified in order to evaluate how the inhomogeneity of the degraded wood can affect the results. In addition, a study on new consolidants for degraded paper was started so as to compare the performances of the new synthesized copolymers with those of the previously synthesized cellulose derivatives and bio-based oligoamides, also in the presence of TiO_2 or $Ca(OH)_2$ nanoparticles.

3 Choice of the starting materials

The choice of α,α'-trehalose and D-cellobiose as starting materials was based on the affinity of their structure for the cellulosic artifacts and on the key role that the exploitation of renewable resources has taken in the modern chemical industry over the last years. As previously mentioned, the advantages of using products derived from biomass are the decrease in the consumption of fossil resources and accordingly the reduction of the pollution derived from their use, as well as the solution of the problem of waste disposal.

The chosen disaccharides occur widely in nature or can be recovered from natural resources.

The α,α'-trehalose can be found in many organisms, including bacteria, fungi, insects, plants and invertebrates where it plays different roles (e.g. carbon reserve, stabilizer and protectant of proteins and membranes, sensing compound and/or growth regulator, structural component of the bacterial cell wall).[102,103] Moreover, this disaccharide can be obtained from starch to a relatively low cost thanks to the novel enzymatic methods developed and applied to its industrial production in recent years.[104] The α,α'-trehalose is a non-reducing disaccharide with high chemical stability and thanks to this it is possible to design the synthesis of its derivatives without the need for a preventive protection of the molecule.[105-107]

The D-cellobiose is the structural component of the cellulose, the most abundant natural polymer.[90,108] It can be obtained from cellulose rich biomasses to a relatively low cost thanks to the novel enzymatic methods developed and applied to its industrial production in recent years.[109] Moreover, it is obtained together with the D-glucose from the hydrolysis of cellulose, even if the most commonly used biorefinery process actually provides for the simultaneous saccharification and fermentation (SSF) of the polysaccharide, which promotes the ethanol production and reduces the D-cellobiose concentration.[110]

In general, the interest for the D-cellobiose is due to its structure, which is similar to that of the cellulose and permits to use it as a model system to

investigate the glycosidic bond cleavage in the cellulose dissolution or hydrolysis. In this project, the initial choice of the D-cellobiose was determined by the interest of using two different disaccharides as raw materials. However, the D-cellobiose is a reducing disaccharide with a free anomeric position on one of the two D-glucose moieties that compose the molecule. For this reason, before any derivatization of the D-cellobiose, a methylation reaction was performed in methanol using an ion exchange resin with the aim of protecting the anomeric position. Unfortunately, contrary to what was expected from the literature data, the reaction conditions used in the protection step led to the hydrolysis of the disaccharide and a mixture of methyl α-D-glucopyranoside and methyl β-D-glucopyranoside was obtained. Nevertheless, the procedure and the final products were considered still interesting because it was possible to use the mixture of α and β methyl D-glucopyranoside as an alternative to the α,α'-trehalose in the synthesis of allyl monomers and their copolymers.

Even if a similar mixture can be synthesized also directly from D-glucose by performing a methylation reaction in very similar conditions[111,112], the reaction on D-cellobiose is potentially interesting for the production of these monomers directly from cellulose. Indeed, as previously mentioned the D-cellobiose is often studied as a model to evaluate the reactivity of the cellulose. The conversion of cellulosic biomass to valuable chemicals is currently one of the main topics of the modern sustainable industry. In particular, as described in paragraph 1.4, the most studied process is the hydrolysis of the cellulose to D-glucose by enzymatic or acid reactions. The acid hydrolysis with mineral acids is the main established route to treat cellulose, but it has several disadvantages, especially the difficult removal of the catalyst. Therefore, in recent years several researches have been carried out to substitute homogeneous acid catalysts with solid acid ones, which are more easily removable. These studies were performed directly from cellulose[82,113-118], but also using the D-cellobiose as a model system[119-122] in order to find the best catalyst and the best reaction conditions.

Among the various solid catalysts that have been tested, sulfonated polystyrene resins, in particular Amberlyst 15, deserves particular attention and they are used as reference in many recent research works.[113,116] The

reaction conditions commonly used in these researches involve the use of temperatures higher than 100°C, short reaction times (usually hours) and generally water as a solvent, even if also ionic liquids are reported.[114] Amberlite IR-120H, the resin used in this research, was previously tested as catalyst directly on cellulose[123] and on the D-cellobiose as a model system.[122] In both cases the hydrolysis of the D-cellobiose took place with a low conversion. In particular, after 50 hours at 80°C a conversion that not exceed the 20% was achieved for the hydrolysis of the D-cellobiose.[122] Therefore, Amberlite IR-120H was studied for the methylation of the anomeric position of the D-cellobiose at 95°C in methanol. Nevertheless, as previously said, the almost quantitative formation of α and β methyl D-glucopyranoside was obtained after 4 days, without the formation of any detectable byproduct. However, considering the D-cellobiose as a model system for the hydrolysis of cellulose, the result obtained with Amberlite IR-120H can be considered interesting as a way to directly obtain valuable chemicals from cellulose using a solid acid catalyst. This is particularly true considering that α and β methyl D-glucopyranosides are commercial products and they can be obtained as a mixture using ion exchange resins like Amberlite IR-120H in methanol starting from glucose.[111,112]

Other attempts to synthesize the methyl derivative of D-cellobiose with the methods reported in the literature were not carried out because of their complexity and low sustainability.[124,125]

In conclusion, the obtained mixture of α and β methyl D-glucopyranosides was considered interesting for this research project and used, as well as the α,α'-trehalose, in the synthesis of monomers and polymers suitable for the application in the field of cultural heritage. Indeed, these saccharides and their derivatives (monomers and copolymers) have structural characteristics that make them similar and compatible to the natural polar cellulosic materials on which they will be applied (i.e. wood, paper). The affinity and compatibility for the materials of the artwork are crucial features for an effective product for cultural heritage conservation. In particular, the compatibility guarantees the respect for the constituent materials, while the affinity increases the efficacy of the treatment (e.g. a consolidant can penetrate better or a superficial treatment can interact better with the

surface). Additionally, using disaccharides or monosaccharides as starting materials it is possible to synthesize small monomers starting from which short polymers can be obtained through a controlled growth of the chains. Low molecular weights may lead to an improvement of the ability of these new products to penetrate in the wooden matrices compared to cellulose derivatives that had been previously studied as consolidants for waterlogged wood.[97]

The allyl group was chosen as the functionalizing agent because its low reactivity can be used as a method to control the molecular weight of the final products of the radical copolymerizations with vinyl acetate. The synthesis of the monomers was designed in order to obtain a low degree of substitution (1-2 functional groups per molecule). In this way, during the polymerization, the formation of linear chains is favored increasing the penetration ability of the final product. Moreover, even if unreacted allyl groups can be present in the final polymer, their small amount ensure a low probability of long term undesired reactions, while their presence can led to cross-linking reactions inside the consolidated materials, thus decreasing the mobility of the consolidant and, accordingly, improving the efficacy of the treatment.

As regards the vinyl acetate and the vinyl alcohol, several examples of the use of vinyl acetate and vinyl alcohol polymers and copolymers in the treatment of wood, paper or natural fibers can be found in the literature.[126-128] In this research, the vinyl acetate was selected as comonomer in order to promote the polymerization of the allyl saccharides. Furthermore, allyl saccharide/vinyl alcohol copolymers can be obtained by hydrolyzing the corresponding vinyl acetate copolymers. Those products have higher affinity for cellulosic substrates and they reduce the risk of acetic acid emission after the treatment of the artifact.

Concerning the synthesis of TiO_2 nanocomposites, anatase was chosen among the three TiO_2 polymorphs because it is more stable than the other metastable form (i.e. brookite). Moreover, anatase has a high photoactivity thanks to a higher band gap (3.2 eV, 387 nm) compared to that of the stable form rutile (3.0 eV, 413 nm) and this contributes to increase its oxidation

power.[129,130] Photoactivity of TiO_2 anatase nanoparticles has been broadly studied in recent years for applications in catalysis[129,131] and in the field of paints were these nanoparticles have been used as autocleaning agents.[132] Moreover, it has been proved that TiO_2 is a strong oxidant which can decompose bacteria and fungi. The reactive oxygen species (ROS) formed as a result of the photocatalytic activity of TiO_2 react with the components of the bacterial cell membrane, causing its breakage and the death of the bacterium itself.[133] This feature is of great interest for many applications in the healthcare, food and pharmaceutical fields, but also for the cultural heritage protection against fungal and bacterial attacks on stone or wooden surfaces during excavation or outdoor exposure phases.[134-139]

In this research, nanocomposites were obtained by grafting the allyl saccharide/vinyl acetate copolymers on properly functionalized nanoparticles with an in situ polymerization. Grafting the polymers on the nanoparticles has several advantages. Firstly, the mobility of the nanoparticles and consequently the toxicity problems related to free nanoparticles are reduced thanks to the presence of the organic matrix. Secondly, the in situ polymerization leads to more homogeneous composites. Indeed, the formation of agglomerates and aggregates can take place in nanocomposites obtained by simply mixing the components and their presence can affect the mechanical properties and reduce the optical transparency of the final composites. Finally, the presence of a polar organic matrix, like the allyl saccharide/vinyl acetate copolymers, increases the interactions between the nanoparticles and the surface of the treated substrate (wood or paper). This ensures the permanence of the nanoparticles on the surface where they can be irradiated and consequently perform their antifungal activity.

In this research, $Ca(OH)_2$ nanoparticles were selected for applications on paper. In particular their mixing with biopolymers was studied in order to obtain new formulations suitable for a contemporary deacidification and consolidation of paper. Indeed, in recent years, alcoholic dispersions of those nanoparticles have been widely used in the deacidification of paper or other cellulosic materials.[51-53]

4 Results and discussion

4.1 Synthesis and characterization of the monomers

4.1.1 General considerations

In order to obtain useful monomers for subsequent polymerization reactions, allyl groups were introduced in the structure of the saccharides. The reactions were performed under nitrogen atmosphere since the allyl group could be oxidized in the presence of oxygen and high temperatures. Moreover, strongly basic conditions were used to ensure the maintenance of a basic pH during the reaction and to activate the hydroxyl groups of the saccharides, thus promoting the nucleophilic substitution on allyl bromide (**Scheme 1**).

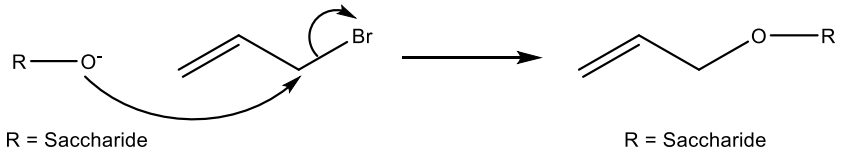

Scheme 1 Mechanism of the functionalization reaction

Initially, the α,α'-trehalose and the D-cellobiose were selected as starting materials for the synthesis of the monomers. Concerning the D-cellobiose, the presence of a highly reactive free anomeric position on the disaccharide has made a direct functionalization impossible. In particular, some attempts to obtain directly the allyl D-cellobiose were previously performed in our laboratory, but they led to unsatisfactory results.[140] Consequently the reaction on unprotected D-cellobiose was abandoned as a synthetic strategy.

Therefore, in order to protect the anomeric position of D-cellobiose, a reaction with methanol was performed using an ion exchange resin (i.e. Amberlite IR-120H) as catalyst. However, in addition to achieving the methylation of the hydroxyl anomeric group, also the alcoholysis of the 1,4-β-glycosidic bond took place and a mixture of methyl α-D-glucopyranoside and methyl β-D-glucopyranoside was obtained with quantitative yield (**Scheme 2**). The reaction was followed by thin layer chromatography (TLC, acetone/water 9:1) because the D-cellobiose (R_f 0.16) turned into the α and

β methyl D-glucopyranoside (R_f 0.59), while the formation of methyl D-cellobioside was not detected.

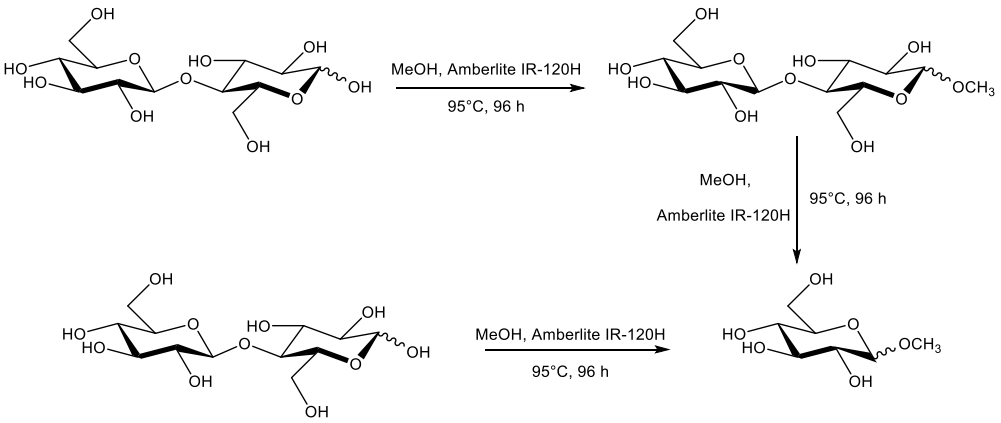

Scheme 2 Anomeric protection and alcoholysis of the D-cellobiose

The formation of the mixture of α and β methyl D-glucopyranoside was confirmed by NMR spectroscopy and mass spectrometry. **Figure 21** shows the mass spectrum (ESI-MS) recorded in negative ion mode of a water solution containing the product of the methylation reaction. The peak related to the methyl D-cellobioside at m/z 355 is visible, but its relative abundance is very low compared to the product with m/z 193, i.e. the methyl D-glucopyranoside.

Then, tandem mass spectra (MS/MS) were recorded by isolating the $[M-H]^-$ of the two molecules at m/z 193 and m/z 355 in order to analyze their fragmentation in detail. In the MS/MS spectrum of the product with m/z 193 (**Figure 22**), peaks related to typical fragmentations of sugars are visible at m/z 160, 112 and 100 in agreement with the presence of a methyl D-glucopyranoside structure. The MS/MS spectrum of the product with m/z 355 (**Figure 23**) shows a main fragmentation at m/z 193, which correspond to a loss of 162 equal to the weight of the D-glucose unit. This confirms that the peak at m/z 355 corresponds to a methyl D-cellobioside.

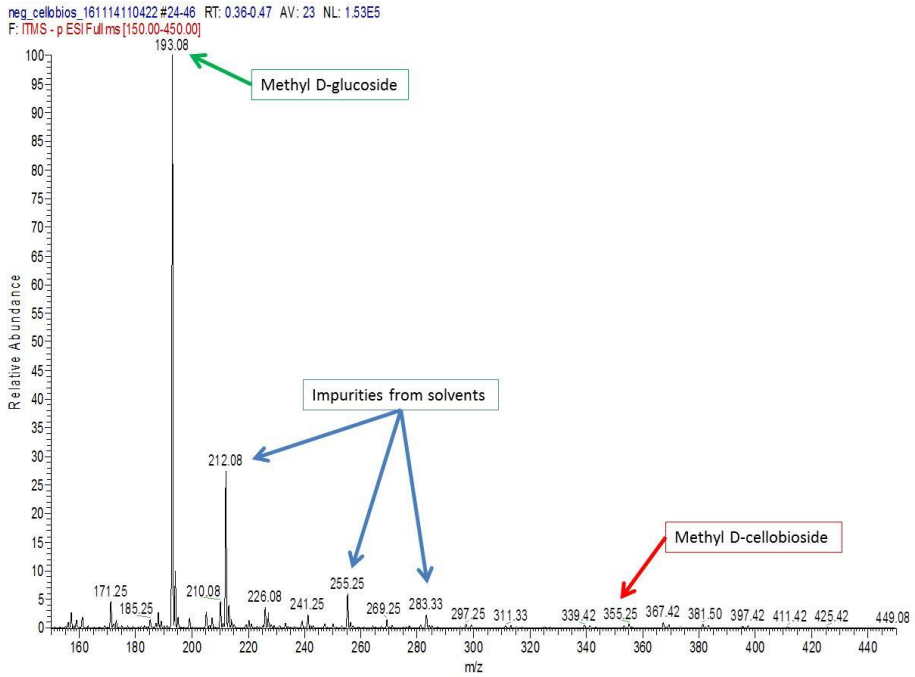

Figure 21 ESI-MS spectrum of the product obtained from the methylation reaction

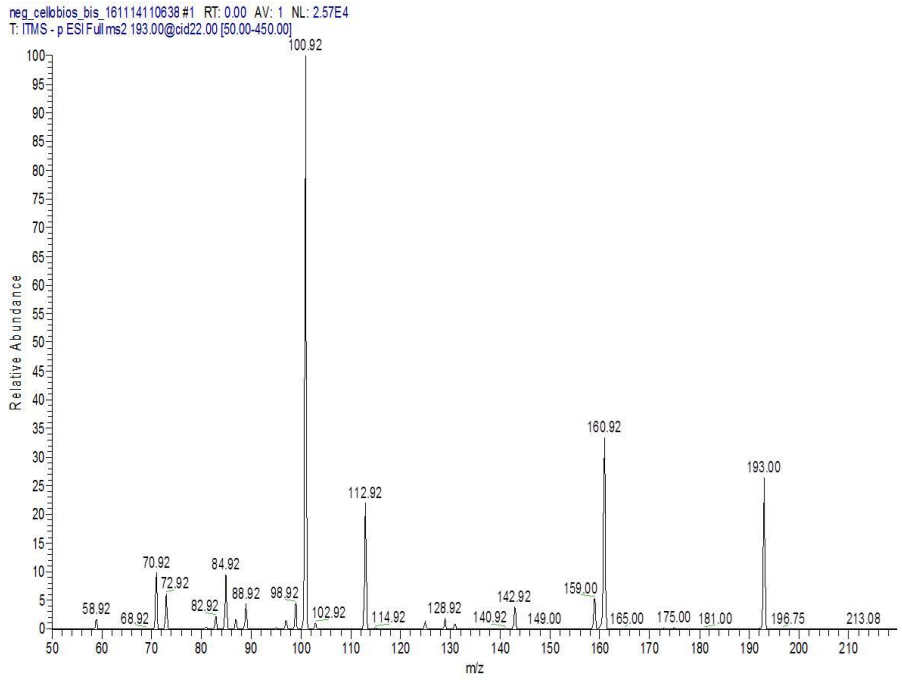

Figure 22 MS/MS spectrum of the product with m/z 193

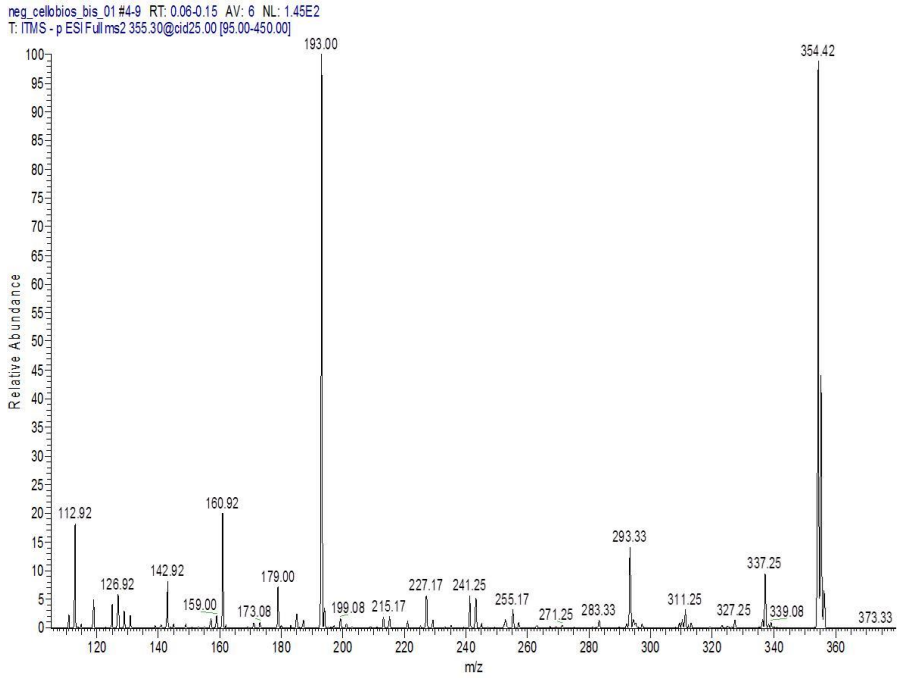

Figure 23 MS/MS spectrum of the product with m/z 355

The ^{1}H and ^{13}C-NMR spectra of the product of the methylation reaction are reported in **Figure 24**. The assignment of the spectra was performed on the basis of the data reported in the Spectral Database for Organic Compounds (SDBS) organized by the Japanese National Institute of Advanced Industrial Science and Technology.[141] The signals of the methoxy group are visible at 3.44 and 3.60 ppm in the ^{1}H-NMR spectrum and at 55.0 and 57.1 ppm in the ^{13}C-NMR spectrum, respectively for methyl α-D-glucopyranoside and methyl β-D-glucopyranoside. The higher amount of the α form compared to the β form is consistent with the *anomeric effect*[142] and can be evaluated from the intensity of the α and β methoxy signals in the ^{1}H and ^{13}C-NMR spectra.

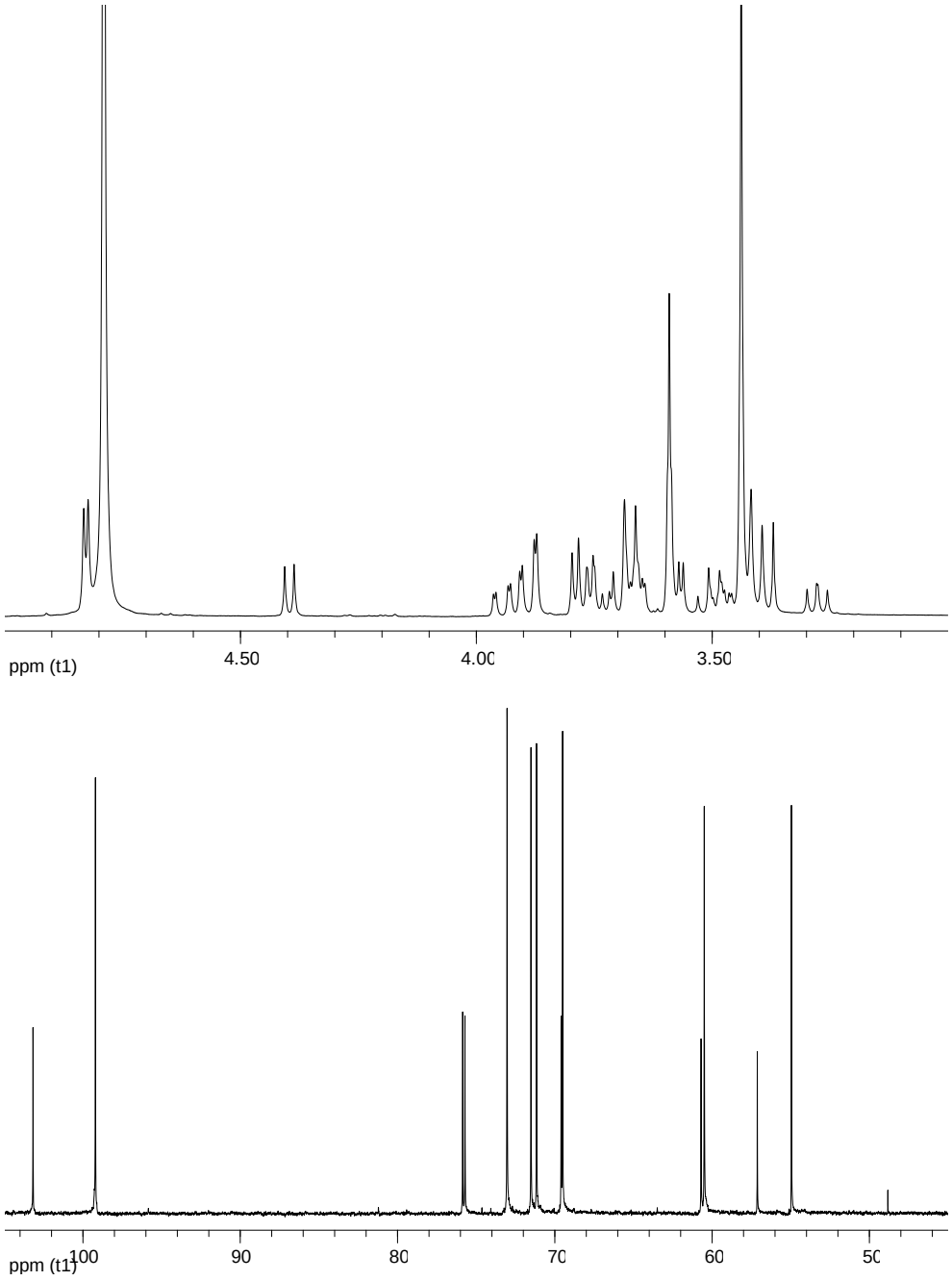

Figure 24 ^{1}H-NMR and ^{13}C-NMR spectra of the product obtained from the methylation reaction

It was possible to use the obtained mixture of α and β methyl D-glucopyranoside in the subsequent reactions without performing any further

purification, because the stereoselectivity is not required in the final derivatives and in their applications (i.e. production of adhesives or conservation of cellulosic materials in the field of cultural heritage). Moreover, the methoxy group introduced in the structure presumably does not adversely affect the performances of the final products, so it was considered as not necessary to perform a deprotection reaction.

Concerning the introduction of allyl groups in the structure of α,α'-trehalose and α and β methyl D-glucopyranoside, similar reactions had been previously described in the literature both for cellulose and for other saccharides.[103,143-146] In the last years, allyl derivatives of cellulose were obtained also in our laboratory.[97]

The present work focused on improving the conditions of the reactions on mono- and disaccharides, so as to obtain a better efficiency and final products with tunable hydrophilic/hydrophobic features. Accordingly, several molar ratios between α,α'-trehalose and the allyl bromide were tested, obtaining values of degree of substitution that increase as the molar ratio between the reagents increases (**Table 2**). At the end, a molar ratio of 6 was chosen as the optimal value for the functionalization of α,α'-trehalose because it corresponds to an average degree of substitution per molecule of disaccharide of about 1-2. The use of monomers with a low degree of substitution (i.e. mono- or disubstituted) reduces the possibility of a cross-linking during the polymerization. In this way, the formation of polymers with linear chains, that can easily penetrate into the structure of wood or paper is promoted. In a similar way, a molar ratio of 4 was chosen as the optimal value for the allyl methyl D-glucopyranoside synthesis.

Generally, the degree of substitution is an average value related to the presence of functional groups on the units of a polymer. However, in this research in order to compare the behavior of a mono- and a disaccharide, the degree of substitution was evaluated on the whole molecule of the saccharide using the integral values of the characteristic signals in the ^{1}H-NMR spectra. On the basis of these calculations, the molecular weights of the monomers were evaluated.

Table 2 Tested molar ratios between the α,α'-trehalose and the allyl bromide

Molar ratio (allyl bromide/α,α'-trehalose)	Degree of substitution per molecule of α,α'-trehalose
2	0.4
4	0.8
6	1.3
16	4.0

Concerning the allyl α,α'-trehalose, the degree of substitution is given by the following formula:

$$DS = \frac{A \cdot N}{(B'-2A)+(B''-2A)}$$

where:

- A = value of the integral of the signal at about 5.90 ppm (-CH_2-C**H**=CH_2 allyl group)
- B' = value of the integral of the signal at 5.20-5.40 ppm (H_1, H_1' α,α'-trehalose and -CH_2-CH=C**H_2** allyl group)
- B" = value of the integral of the signal at 3.40-4.40 ppm (H_2-H_6, H_2'-H_6' α,α'-trehalose and -C**H_2**-CH=CH_2 allyl group)
- N = total number of the protons of the disaccharide giving signals at 5.20-5.40 ppm and at 3.40-4.40 ppm (14 for α,α'-trehalose)

The calculation for allyl methyl D-glucopyranoside is easier. In the ^{1}H-NMR spectrum the signals of H_2-H_6 and –O-C**H_3** of both α and β form of the methyl D-glucopyranoside (9 protons) are all between 4.00 and 3.18 ppm. Therefore, by setting the integral of the signal at 4.00-3.18 ppm equal to 9, the value obtained for the signal at about 6.00 ppm (-CH_2-C**H**=CH_2 allyl group) corresponds to the degree of substitution.

The *work-up* procedures were also improved compared to the previous synthesis of allyl saccharides or allyl cellulose derivatives.[97,143-146] In particular, in the present work KOH was used instead of NaOH to promote the nucleophilic substitution in order to obtain more easily removable salts

as byproducts. Indeed, ethanol is the solvent used to purify the final products and potassium salts have lower solubility in this solvent compared to sodium salts.[147] In order to quantify the impurities present in the final product, ICP elemental analyses were performed at the end of the *work-up* (**Table 3**). The potassium salts formed during the reaction and the *work-up* include KBr (molecular weight 119.00 g/mol) and KCl (molecular weight 74.55 g/mol). Considering the hypothesis that all the potassium found in the elemental analysis corresponds to KBr (the heaviest among the possible byproducts), it can be estimated that 100 mg of the final product contain 10 mg of impurities (10%).

Table 3 Results of ICP elemental analysis

	Na%	K%	P%
Allyl α,α'-trehalose extracted with ethanol at 20°C	0.1949	2.5520	0.0273

4.1.2 Synthesis and characterization of the allyl α,α'-trehalose

In the literature, a fully substituted allyl α,α'-trehalose has already been synthesized using dimethyl sulfoxide as a solvent.[107] This product is insoluble in water and other polar solvents like alcohols. On the contrary, in the present work the water was used as a greener solvent and the final monomer is only monosubstituted or, at most, disubstituted in order to avoid cross-linking in the subsequent polymerization and to maintain the solubility in polar solvents (**Scheme 3**).

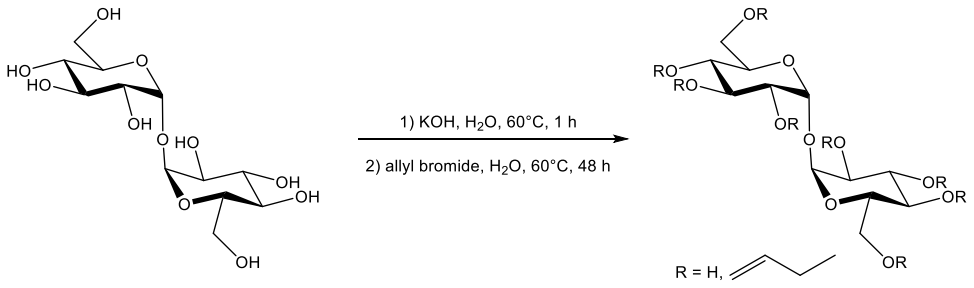

Scheme 3 Synthesis of the allyl α,α'-trehalose

The functionalization of α,α'-trehalose was performed in water as a solvent and under nitrogen atmosphere to avoid the oxidation of the allyl groups.

In the first step of the reaction strongly basic conditions were created using KOH as a base. The amount of the base was calculated in order to have a stoichiometric ratio between KOH and the hydroxyl groups of the disaccharide (8 -OH per molecule). In this way it was possible to promote the nucleophilic substitution on the allyl bromide in the second step, maintaining a basic pH during the reaction. Then, the allyl bromide was added and maintained in dispersion using vigorous stirring. As previously mentioned, several molar ratios between allyl bromide and α,α'-trehalose were tested and different values of degree of substitution in the final products were obtained. In the end, a ratio of 6 was chosen because it led to a monosubstituted or, at most, disubstituted allyl α,α'-trehalose.

At the end of the reaction, the pH of the mixture was adjusted to neutrality using HCl. Then, the solvent and the residual allyl bromide were distilled at reduced pressure. Finally, on the basis of some solubility tests, ethanol was chosen to extract and therefore purify the final product, because allyl α,α'-trehalose is soluble in this solvent unlike α,α'-trehalose and the byproducts.

After the extraction, a white solid was obtained and it was characterized by NMR and FT-IR spectroscopies. In ^{1}H-NMR spectrum (**Figure 25**), the presence of signals related to the allyl group from 4.09 to 4.37 ppm (-C**H$_2$**-CH=CH$_2$), from 5.28 to 5.41 ppm (-CH$_2$-CH=C**H$_2$**) and at 5.97 ppm (-CH$_2$-C**H**=CH$_2$) confirms the formation of the desired product. On the basis of the ^{1}H-NMR spectrum a degree of substitution of 1.3 and a molecular weight of 394.27 g/mol were evaluated.

In the ^{1}H-NMR spectrum, the signals of the structure of the disaccharide functionalized with allyl groups appear much broader than those of the starting α,α'-trehalose. This can be due to the functionalization on different hydroxyl groups in different positions, that may have caused a slight shift of the signals related to the closest protons compared to those of the starting molecule. This hypothesis is confirmed by the ^{13}C-NMR spectrum (**Figure 26**), in which the signals of the functionalized disaccharide structure are split and many new signals have appeared. In particular, the signals at 68.4, 77.4 and

78.0 ppm are very interesting because they are related to a carbon in a functionalized position (respectively to C_6 or C_6', C_4 or C_4' and C_2 or C_2'). This assignment can be performed on the basis of the data reported in the literature for a fully functionalized allyl α,α'-trehalose.[107] The signals related to the allyl group are present also in the ^{13}C-NMR spectrum at 73.9 ppm (-**C**H_2-CH=CH_2), 118.3, 118.5, 118.7, 118.8, 119.2 ppm (-CH_2-**C**H=CH_2) and 133.4, 133.5, 133.7 ppm (-CH_2-CH=**C**H_2).

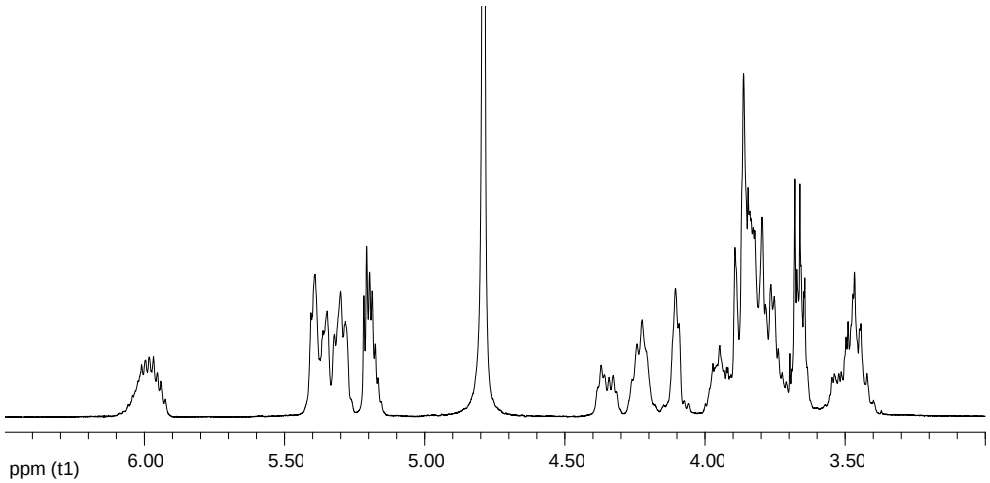

Figure 25 ^{1}H-NMR spectrum of the allyl α,α'-trehalose

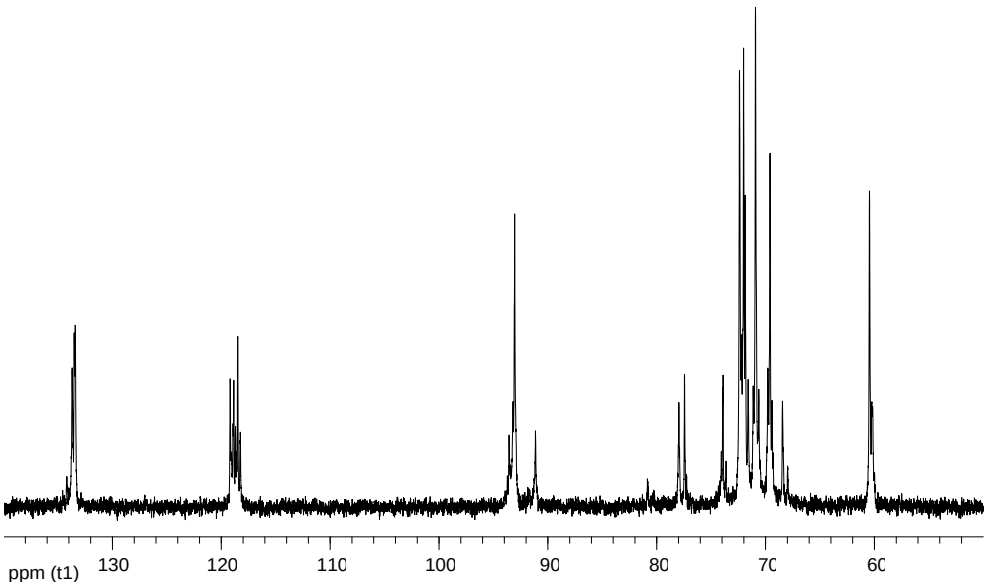

Figure 26 ^{13}C-NMR spectrum of the allyl α,α'-trehalose

Finally, the functionalization of the disaccharide is confirmed by the presence of several bands in the FT-IR spectrum (**Figure 27**) like the =C-H stretching at 3017 cm^{-1}, the C=C stretching at 1645 cm^{-1} and the =C-H out of plane bending at 941 cm^{-1}.

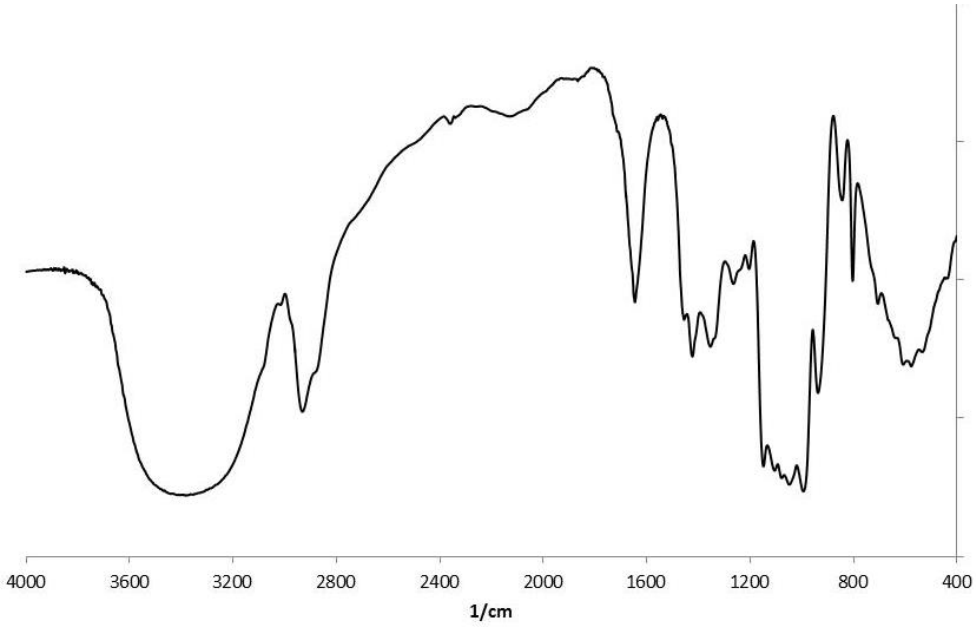

Figure 27 FT-IR spectrum of the allyl α,α'-trehalose

4.1.3 Synthesis and characterization of the allyl methyl D-glucopyranoside

As previously mentioned, several attempts had been made to directly synthesize allyl ethers from the D-cellobiose, but they led to unsatisfactory results. For this reason, a methylation reaction was performed to protect the anomeric position, but it led to the formation of a mixture of α and β methyl D-glucopyranoside.

This mixture was considered still interesting as starting material to obtain allyl monomers and, therefore, a reaction very similar to the synthesis of allyl α,α'-trehalose was performed (**Scheme 4**).

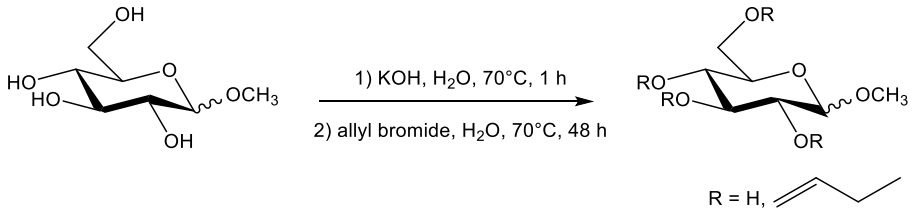

Scheme 4 Synthesis of the allyl methyl D-glucopyranoside

The functionalization of the methyl D-glucopyranoside was performed in water as a solvent and under nitrogen atmosphere to avoid the oxidation of the allyl groups.

In the first step of the reaction strongly basic conditions were created using KOH as a base. The amount of base was calculated in order to have a stoichiometric ratio between KOH and the hydroxyl groups of the saccharide (4 -OH per molecule). In this way it was possible to promote the nucleophilic substitution on the allyl bromide in the second step, maintaining a basic pH during the reaction. Then, the allyl bromide was added and maintained in dispersion using vigorous stirring. In this case, a molar ratio of 4 between allyl bromide and methyl D-glucopyranoside was chosen among all the tested molar ratios because it led to a monosubstituted or, at most, disubstituted allyl methyl D-glucopyranoside.

At the end of the reaction, the pH of the mixture was adjusted to neutrality using HCl. Then, the solvent and the residual allyl bromide were distilled at reduced pressure. Finally, on the basis of some solubility tests, ethanol was chosen to extract and then purify the final product because allyl methyl D-glucopyranoside is soluble in this solvent unlike methyl D-glucopyranoside and the byproducts.

After the extraction, a pale yellow solid was obtained and it was characterized by NMR and FT-IR spectroscopies. As in the case of allyl α,α'-trehalose, the signals of the functionalized saccharide in ^{1}H-NMR spectrum (**Figure 28**) are broader compared to those of the starting methyl D-glucopyranoside and those in ^{13}C-NMR spectrum (**Figure 29**) are split and many new signals have appeared. This behavior was attributed to the functionalization of the molecule on different hydroxyl groups in different

positions. In the ^{1}H-NMR spectrum the presence of signals of the allyl group from 4.13 to 4.38 ppm (-C**H$_2$**-CH=CH$_2$), from 5.30 to 5.42 ppm (-CH$_2$-CH=C**H$_2$**) and at 6.01 ppm (-CH$_2$-C**H**=CH$_2$) confirms the formation of the desired product. On the basis of the ^{1}H-NMR spectrum a degree of substitution of 1.1 and a molecular weight of 238.19 g/mol were evaluated.

Signals related to allyl group are present also in the ^{13}C-NMR spectrum at 71.7, 72.0, 73.7 ppm (-**C**H$_2$-CH=CH$_2$), 118.7 ppm (-CH$_2$-CH=**C**H$_2$) and 133.6 ppm (-CH$_2$-**C**H=CH$_2$). Moreover, it is possible to identify the signals related to the functionalized positions, i.e. 68.4, 68.6, 68.8 (C_6^{α} or C_6^{β}), 77.4 (C_4^{α} or C_4^{β}) and 78.3 (C_2^{α} or C_2^{β}).

Finally, the FT-IR spectrum (**Figure 30**) confirms the formation of the product because the bands related to the double bond can be observed at 3080, 3011 cm^{-1} (=C-H stretching), 1645 cm^{-1} (C=C stretching) and 930 cm^{-1} (=C-H out of plane bending).

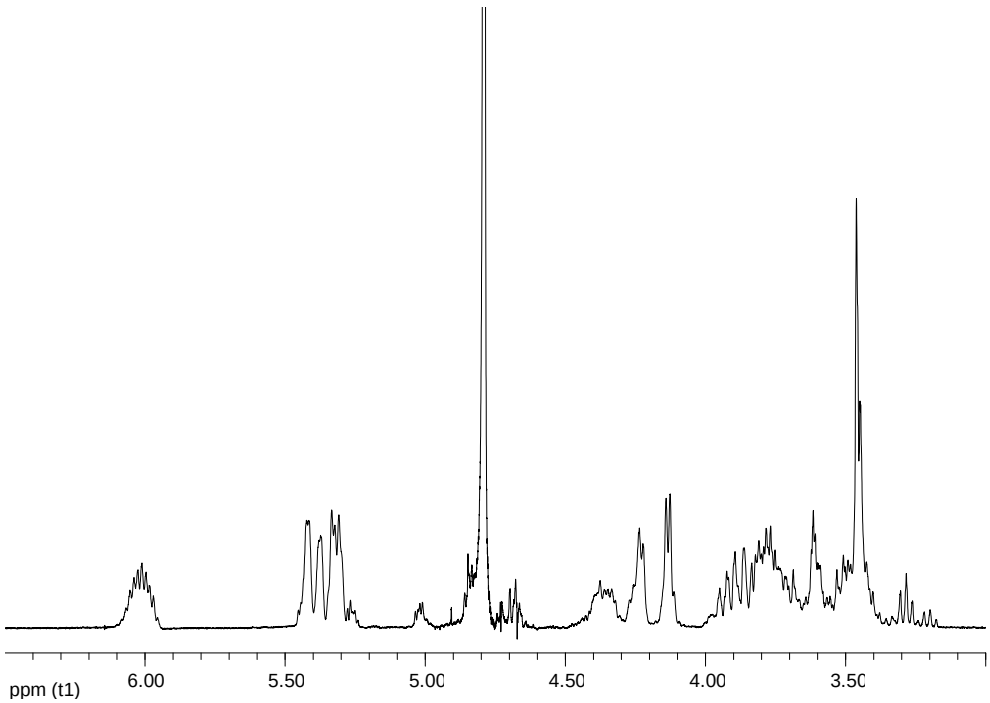

Figure 28 ^{1}H-NMR spectrum of the allyl methyl D-glucopyranoside

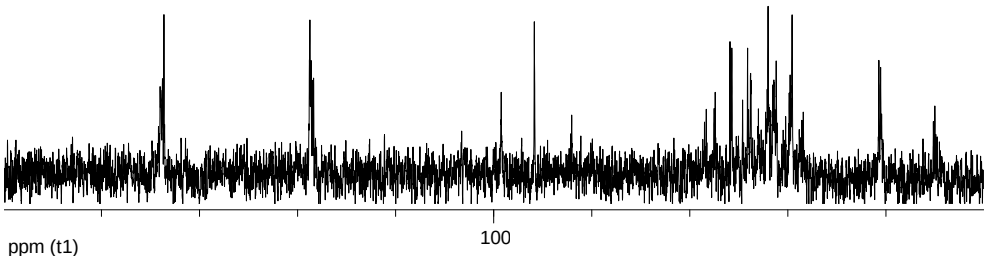

Figure 29 ^{13}C-NMR spectrum of the allyl methyl D-glucopyranoside

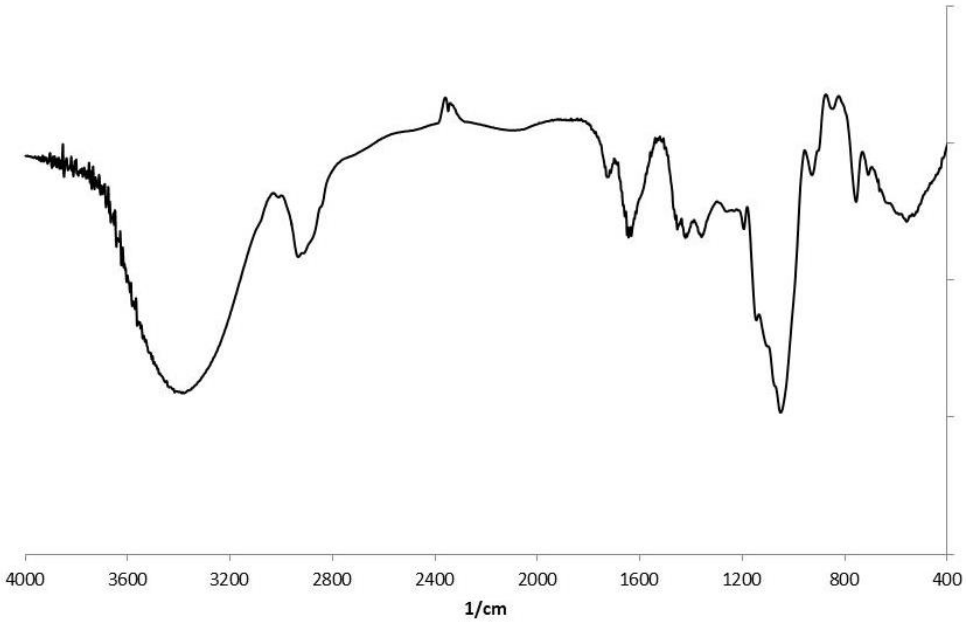

Figure 30 FT-IR spectrum of the allyl methyl D-glucopyranoside

4.2 Synthesis and characterization of vinyl acetate copolymers

4.2.1 General considerations

In this research, allyl α,α'-trehalose and allyl methyl D-glucopyranoside were initially used to obtain homopolymers through radical polymerizations (**Scheme 5**).

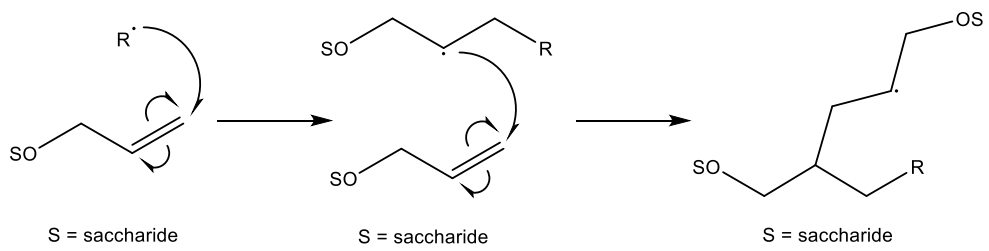

Scheme 5 Mechanism of the radical homopolymerization

Several reaction conditions (temperature and time) and several different radical initiators (tert-butyl hydroperoxide, 4,4' azo bis(4-cyanopentanoic acid) and azobisisobutyronitrile) were tested to optimize the synthesis of the desired products. Nevertheless, the results were not satisfactory in terms of yields and chain length of the final products. This behavior is consistent with the well-known poor reactivity of the allyl group, which is subject to autoinhibition phenomena.[148]

For this reason, the allyl saccharides were used with vinyl acetate to obtain copolymers via radical copolymerization (**Scheme 6**).

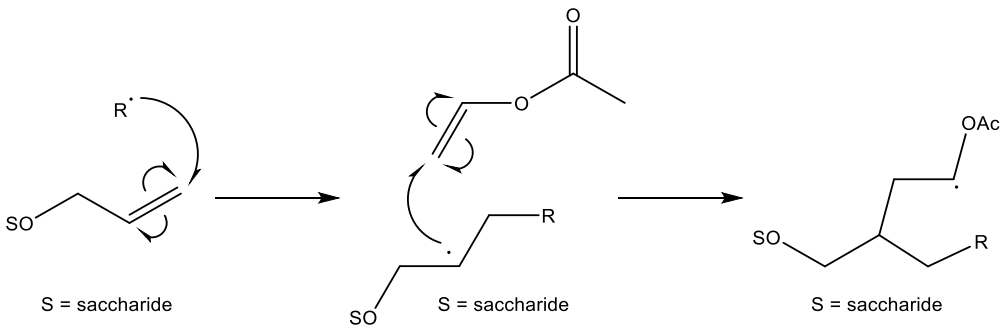

Scheme 6 Mechanism of the radical copolymerization

Even if water is commonly used as dispersion medium for the homo- and copolymerization of vinyl acetate, in this research an alcoholic solvent was used (i.e. methanol). In this way, it was possible to obtain pure copolymers and characterize them avoiding the presence of all the additives that are essential for their synthesis in water dispersion (i.e. protective colloid, surfactants, buffers). The characterization of the copolymers obtained in methanol was useful also for a parallel preliminary research performed in

our laboratory about the development of new formulations of modified polyvinyl acetate, produced as water-based dispersions to be used as adhesives for wood.[149] Furthermore, the absence of the additives makes the final vinyl copolymers more suitable to be used in the conservation field.

4.2.2 Synthesis and characterization of the allyl α,α'-trehalose/vinyl acetate copolymer

The reaction was performed in methanol using azobisisobutyronitrile (AIBN) as radical initiator and under nitrogen atmosphere in order to exclude the oxygen, which is an inhibitor of the free radical polymerizations and which could also oxidize the allyl and vinyl groups (**Scheme 7**).

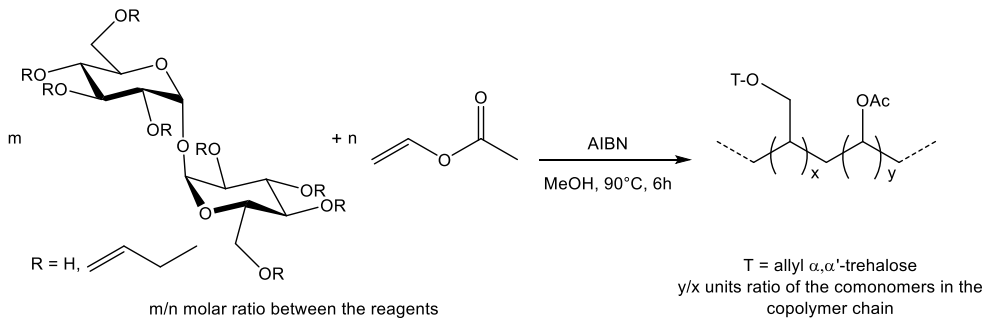

Scheme 7 Synthesis of the allyl α,α'-trehalose/vinyl acetate copolymer

At the end of the reaction, the solvent and the residual vinyl acetate were removed by distillation at reduced pressure. Then, an extraction in acetone was performed to separate the desired product from the unreacted allyl α,α'-trehalose and from the salts which could be present as impurities. Indeed, the synthesized copolymer is soluble in acetone as well as the homopolymer of vinyl acetate, which can be possibly present. On the contrary, solubility tests showed that the allyl disaccharide monomer and the salts are insoluble in acetone. Therefore, the separation of the copolymer by extraction was successfully achieved and this result was confirmed by the spectroscopic characterization of soluble and insoluble fractions. In particular, in the ^{1}H-NMR spectrum of the fraction insoluble in acetone only

the signals related to the allyl α,α'-trehalose monomer can be observed (**Figure 31**).

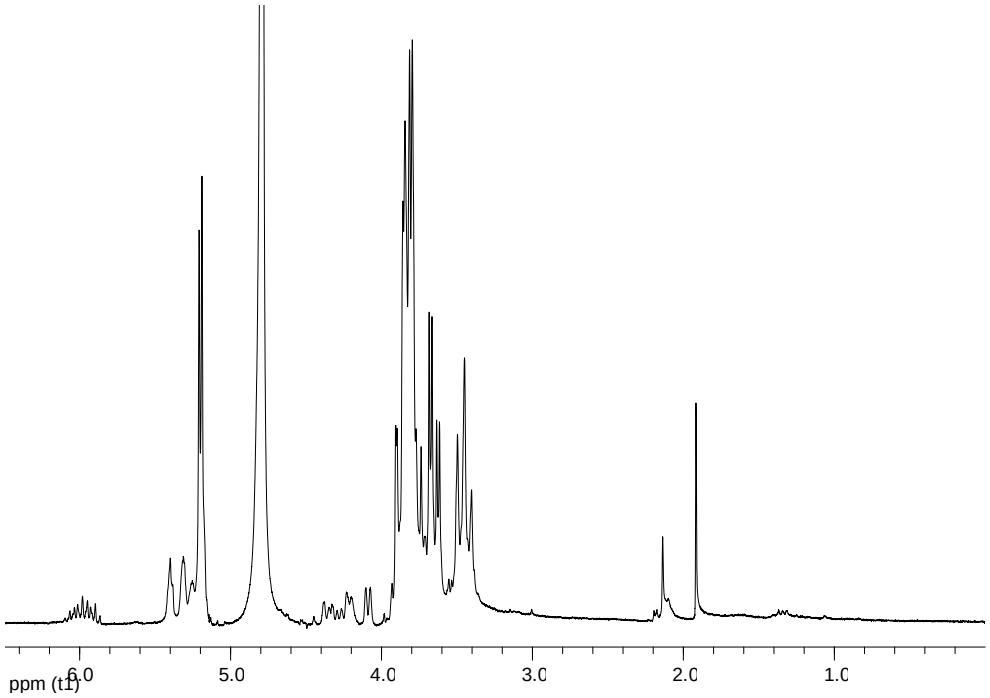

Figure 31 ^{1}H-NMR spectrum of the fraction insoluble in acetone

On the contrary, the presence of the copolymer in the fraction soluble in acetone (indicated as <u>fraction A+B</u>) is confirmed by the ^{1}H-NMR and the ^{13}C-NMR spectra (**Figure 32**). The signals of the α,α'-trehalose structure present as side group in the repeat unit are shifted compared to the starting monomer, while the signals related to vinyl acetate unit are visible respectively at 1.84 ppm (CH_3-CO-CH-C**H$_2$**-), 2.00, 2.03, 2.05 ppm (C**H$_3$**-CO-CH-CH_2-) and 4.87 ppm (CH_3-CO-C**H**-CH_2-) in the ^{1}H-NMR spectrum and at 21.3 ppm (**C**H_3-CO-CH-CH_2-), 40.0, 40.4, 40.7, 41.1 ppm (CH_3-CO-CH-**C**H_2-), 62.8 ppm (CH_3-CO-**C**H-CH_2-) and 172.4 ppm (CH_3-**C**O-CH-CH_2-) in the ^{13}C-NMR spectrum. The characteristic signals of the allyl group are still observable in the spectra, even if their intensity is lower compared to the spectra of the starting allyl α,α'-trehalose. This is due to the fact that in the starting monomer the average value of the degree of substitution was in agreement with the presence of some α,α'-trehalose molecules with more than one functionalizing group. Being the reactivity of the allyl group lower than that

of the vinyl group, during the copolymerization not all the allyl groups reacted and it is the reason why their signals are still visible in the spectra.

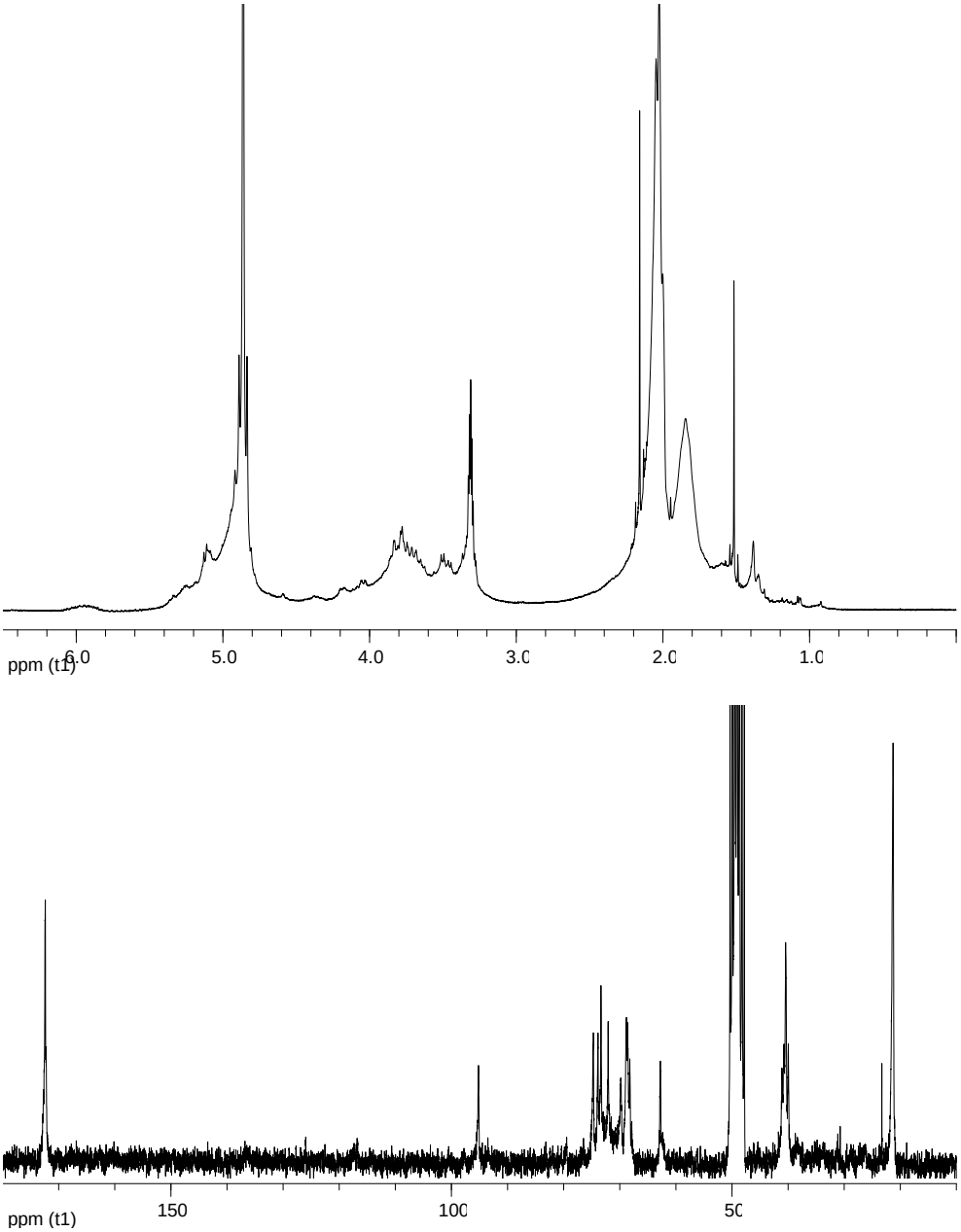

Figure 32 ^{1}H-NMR and ^{13}C-NMR spectra of the allyl α,α'-trehalose/vinyl acetate copolymer (fraction A+B)

Finally, the FT-IR spectrum of the fraction A+B (**Figure 33**) shows the characteristic bands of the acetate group such as the C=O stretching at 1736 cm^{-1}, the CH_3- bending at 1433 and 1375 cm^{-1}, the C-O stretching at 1244 cm^{-1} together with the bands of the disaccharide between 1146 and 995 cm^{-1} (C-OH stretching, C-O-C stretching). Also in this spectrum bands related to the allyl group are observable (1647, 945 cm^{-1}), even if their intensity is decreased with respect to the spectrum of allyl α,α'-trehalose.

The fraction A+B was obtained as a pale yellow solid with a yield of 65%.

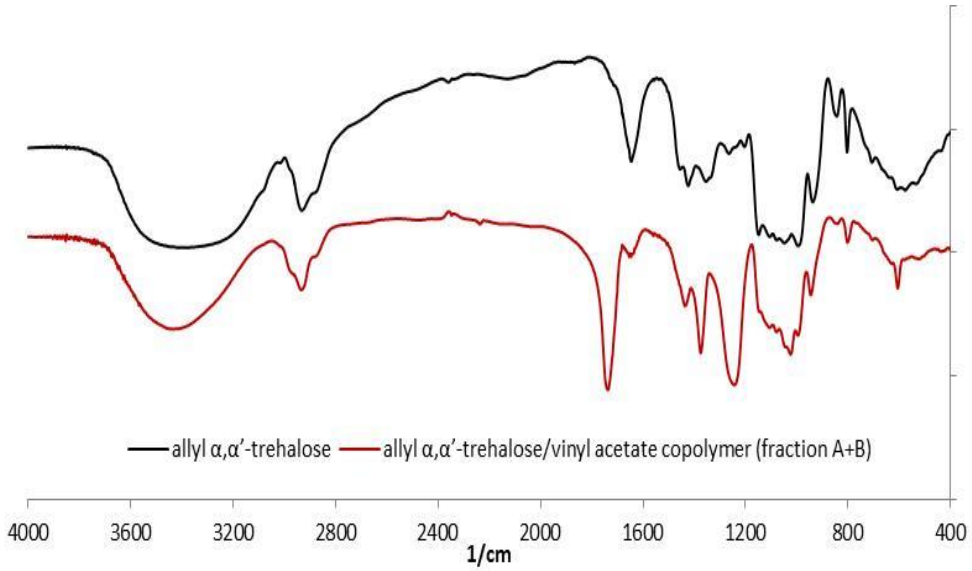

Figure 33 FT-IR spectra of the allyl α,α'-trehalose (black line) and of the allyl α,α'-trehalose/vinyl acetate copolymer (fraction A+B) (red line)

To fully characterize the product, the fraction A+B was extracted with water obtaining the separation of two fractions: <u>fraction A</u> (soluble in water) and <u>fraction B</u> (insoluble in water). The presence of two fractions with different solubility is in agreement with the different ratios between the comonomers in the copolymer chains (**Table 4**). Those ratios were calculated by integrating the signals related to the vinyl acetate and the disaccharide units in the ^{1}H-NMR spectra of the two fractions (**Figure 34**). The fraction B shows

higher vinyl acetate/allyl disaccharide units ratio compared to the fraction A, in agreement with the presence of copolymers with a high content of vinyl acetate units. However, in fraction B also vinyl acetate homopolymers can be present in the mixture, according to the known insolubility of this product in water.

The amount of the two different fractions and the yields of the reactions change according to the different molar ratios between the reagents (vinyl acetate/ally α,α'-trehalose) which were tested (**Table 4**). In particular, the more is the vinyl acetate used as a reagent, the higher are both the yield and the amount of fraction B. This result is in agreement with the higher reactivity of the vinyl group compared to the allyl one. The increase in yield and amount of fraction B can be explained with the increase in the percentage of vinyl acetate unit in the copolymer and/or with the increase in the amount of vinyl acetate homopolymer in fraction B.

Table 4

	Molar ratio*	Yield[y] (%)	Fraction A[a]		Fraction B[b]	
			Amount (%)	Comonomer units ratio**	Amount (%)	Comonomer units ratio**
Ally α,α'-trehalose/vinyl acetate copolymer	10	65	25	2	75	>5
	20	76	20	4	80	14
	50	94	0	-	100	47

* Moles of vinyl acetate/(moles of disaccharide comonomer·degree of substitution), [y] Calculated considering the fraction A+B, [a] Soluble in acetone, soluble in water, [b] Soluble in acetone, insoluble in water, ** Vinyl acetate units/allyl disaccharide units

After the separation, the fraction A and the fraction B were characterized by NMR and FT-IR spectroscopies. **Figure 34** and **Figure 35** show the ^{1}H-NMR and ^{13}C-NMR spectra and **Figure 36** shows the FT-IR spectra of the two

fractions. As previously said, the units of the two comonomers are present in the spectra of both fractions but, as expected, the signals/bands related to the different comonomers have different relative intensities. In particular, the intensity of the vinyl acetate signals is higher in the spectra of fraction B compared to those of fraction A, due to the presence in this fraction of copolymer chains with a higher vinyl acetate/allyl disaccharide units ratio together with vinyl acetate homopolymer chains.

Another interesting result is the presence of the signals related to the vinyl acetate in the spectrum of fraction A. This can be justified with the presence of vinyl acetate units in a copolymer rich in disaccharide units because, otherwise, the vinyl acetate homopolymer or a copolymer rich in vinyl acetate units could not be found in water due to their insolubility in this solvent. Moreover, the ^{1}H-NMR signals related to the disaccharide monomer units are sharp and the presence of short-chain copolymers in fraction A can be hypothesized based on the analysis of the shape of these signals. Indeed, in general in the ^{1}H-NMR spectrum of a polymer, the signals related to the monomer units in the polymer chain have a different shape compared to those of the monomers. In particular, the longer the polymeric chain, the broader the shape of the signals of the monomer units because these signals result from an average of the different steric arrangements of the pendant groups of the chain (tacticity) and from the consequently different chemical environments of the side groups (as for example the allyl α,α'-trehalose units, which are present in the structure of the copolymer as side groups). The signals of the disaccharide monomer units in fraction B, on the contrary, are broad and it indicates the presence of long-chain copolymers. The presence of short-chain copolymers in fraction A and long-chain copolymers in fraction B was confirmed also by the results of the SEC analysis (paragraph 4.2.4).

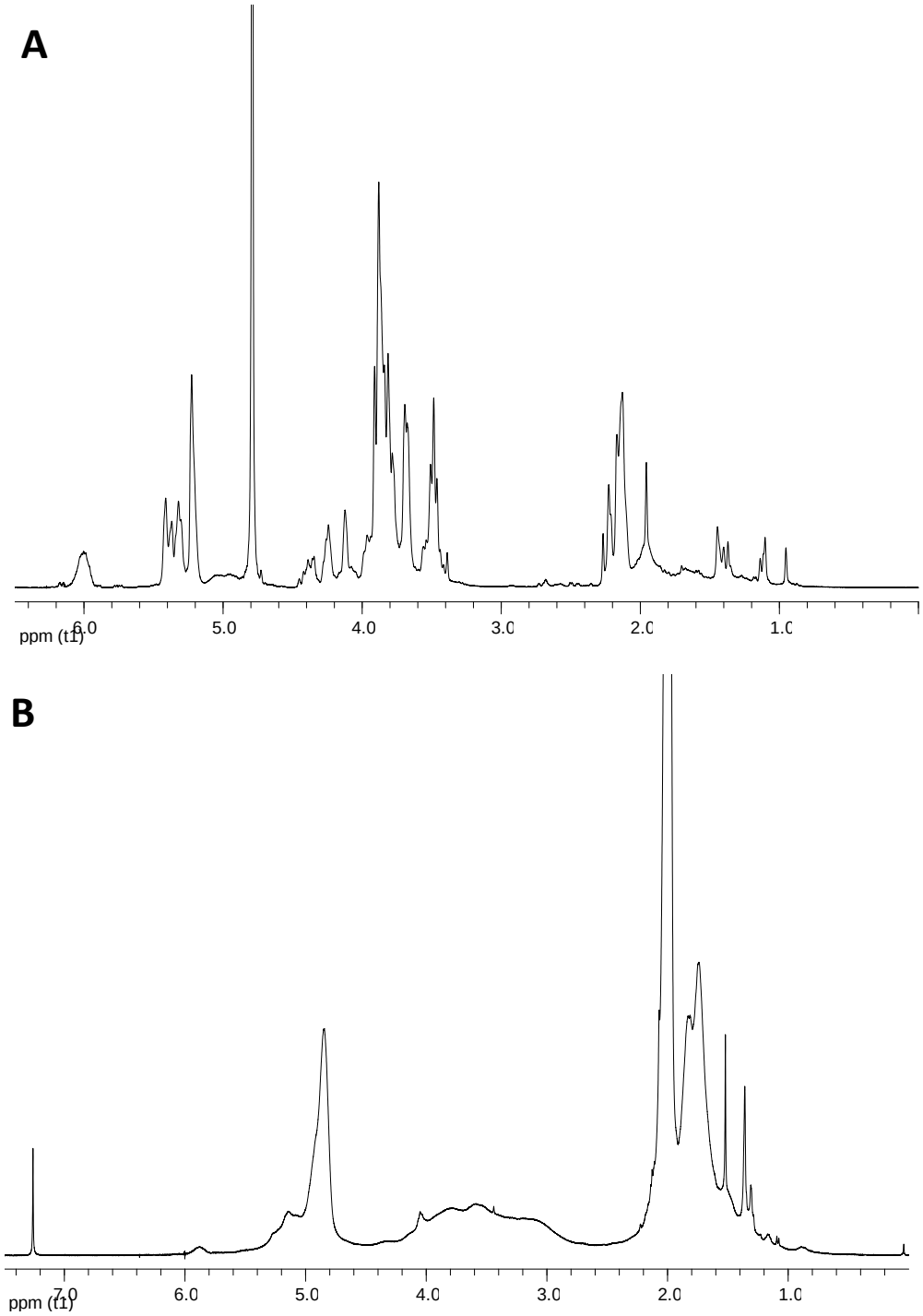

Figure 34 ^{1}H-NMR spectra of the fraction A (**A**) and of the fraction B (**B**) of the allyl α,α'-trehalose/vinyl acetate copolymer

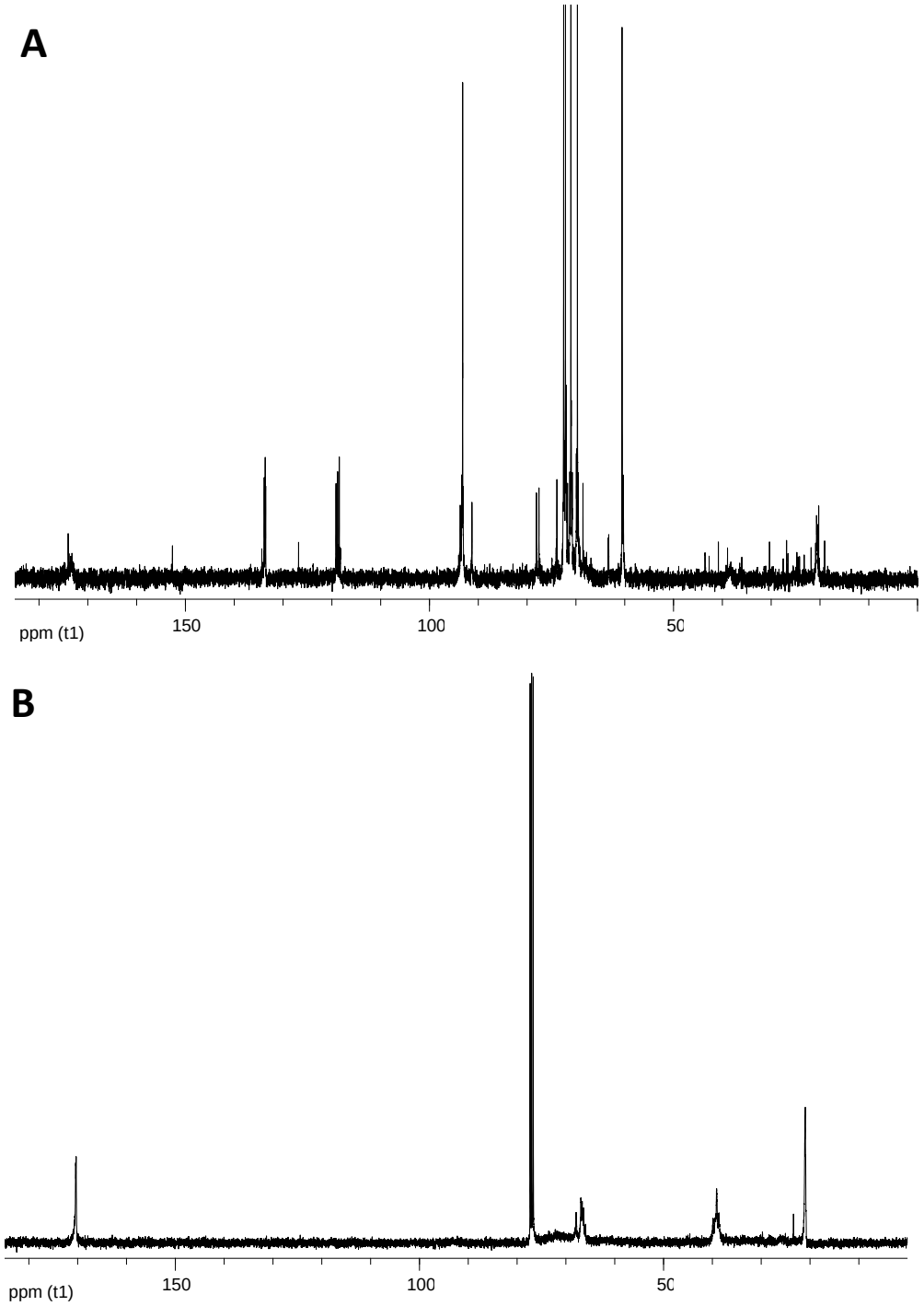

Figure 35 ^{13}C-NMR spectra of the fraction A (**A**) and of the fraction B (**B**) of the allyl α,α'-trehalose/vinyl acetate copolymer

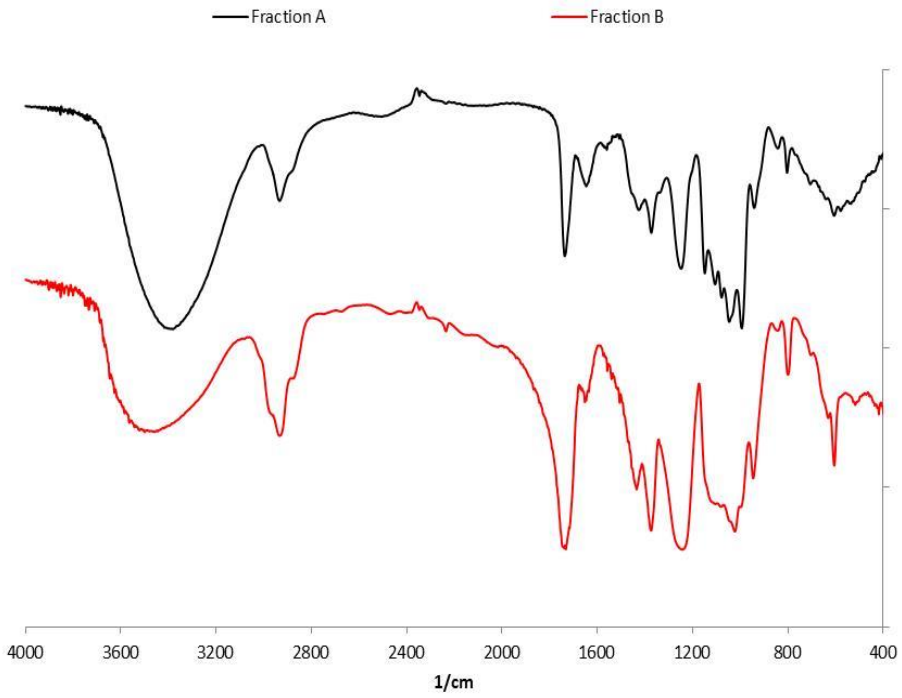

Figure 36 FT-IR spectra of the fraction A (black line) and the fraction B (red line) of the allyl α,α'-trehalose/vinyl acetate copolymer

4.2.3 Synthesis and characterization of the allyl methyl D-glucopyranoside/vinyl acetate copolymer

The reaction between the methyl D-glucopyranoside and the vinyl acetate was performed using the same reaction conditions used for the synthesis of the previous copolymer (**Scheme 8**).

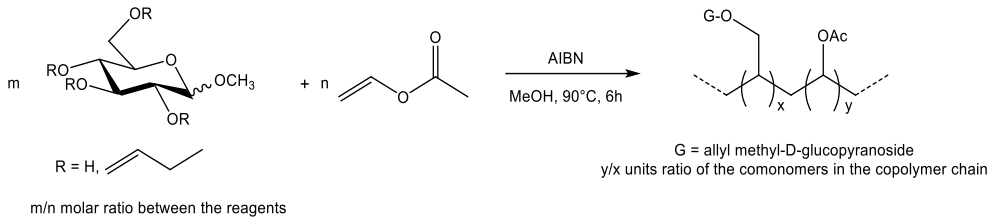

Scheme 8 Synthesis of the allyl methyl D-glucopyranoside/vinyl acetate copolymer

At the end of the reaction, the solvent and the residual vinyl acetate were removed by distillation at reduced pressure. Then, following the same *work-up* procedure described for the allyl α,α'-trehalose/vinyl acetate copolymer, the product was separated from the not reacted allyl methyl D-glucopyranoside and from the salts by an extraction in acetone. The separation was confirmed by the ^{1}H-NMR spectrum of the fraction insoluble in acetone in which only the signals related to the allyl methyl D-glucopyranoside can be observed (**Figure 37**).

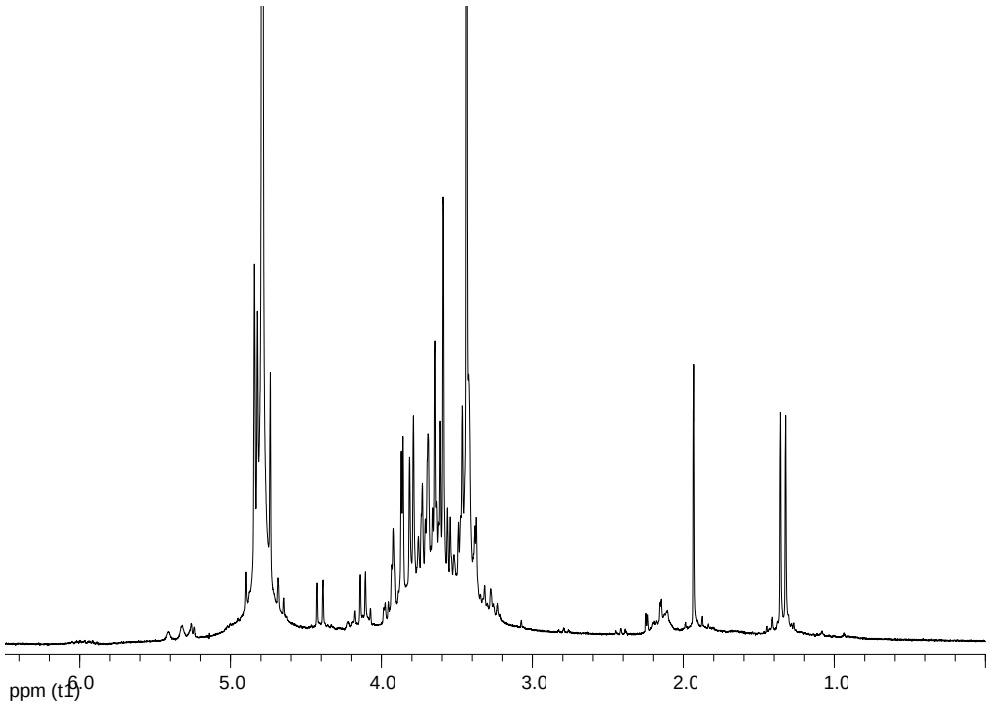

Figure 37 ^{1}H-NMR spectrum of the fraction insoluble in acetone

As regards the soluble fraction, after having distilled the acetone at reduced pressure, an orange solid (indicated as fraction A+B) was obtained with a yield of 57%. The product was characterized by NMR and FT-IR spectroscopies. In **Figure 38** the ^{1}H-NMR and the ^{13}C-NMR spectra of the fraction A+B are reported.

In the ^{1}H-NMR spectrum the signals related to the vinyl acetate comonomer are visible at 1.82 ppm (CH_3-CO-CH-C**H$_2$**-), 1.99, 2.02, 2.04 ppm (C**H$_3$**-CO-CH-CH_2-) and from 4.01 to 5.40 ppm (CH_3-CO-C**H**-CH_2-), together with the signals of the saccharide units. Not all the allyl groups on the allyl methyl D-glucopyranoside reacted during the polymerization and their characteristic signals are still visible in the spectrum of the copolymer. However, the intensity of these signals is lower than in the spectrum of the starting monomer, as it can be seen also comparing the ^{13}C-NMR spectra. This indicates that the allyl groups reacted, even if only partially. In the ^{13}C-NMR spectrum new signals related to the vinyl acetate units are present at 21.2 ppm (**C**H_3-CO-CH-CH_2-), 39.9, 40.3, 40.7, 41.0 ppm (CH_3-CO-CH-**C**H_2-), 62.8 ppm (CH_3-CO-**C**H-CH_2-) and 172.3 ppm (CH_3-**C**O-CH-CH_2-) together with the signals of the methyl D-glucopyranoside structure.

Finally, the FT-IR spectrum of the fraction A+B (**Figure 39**) shows the characteristic bands of a vinyl acetate moiety such as the C=O stretching at 1734 cm^{-1}, the CH_3- bending at 1437 and 1373 cm^{-1} and the C-O stretching at 1244 cm^{-1} together with the bands of the saccharide between 1147 and 1026 cm^{-1} (C-OH stretching, C-O-C stretching). Bands related to the allyl group are visible (1647, 946 cm^{-1}), even if their intensity is decreased compared to the spectrum of the allyl methyl D-glucopyranoside.

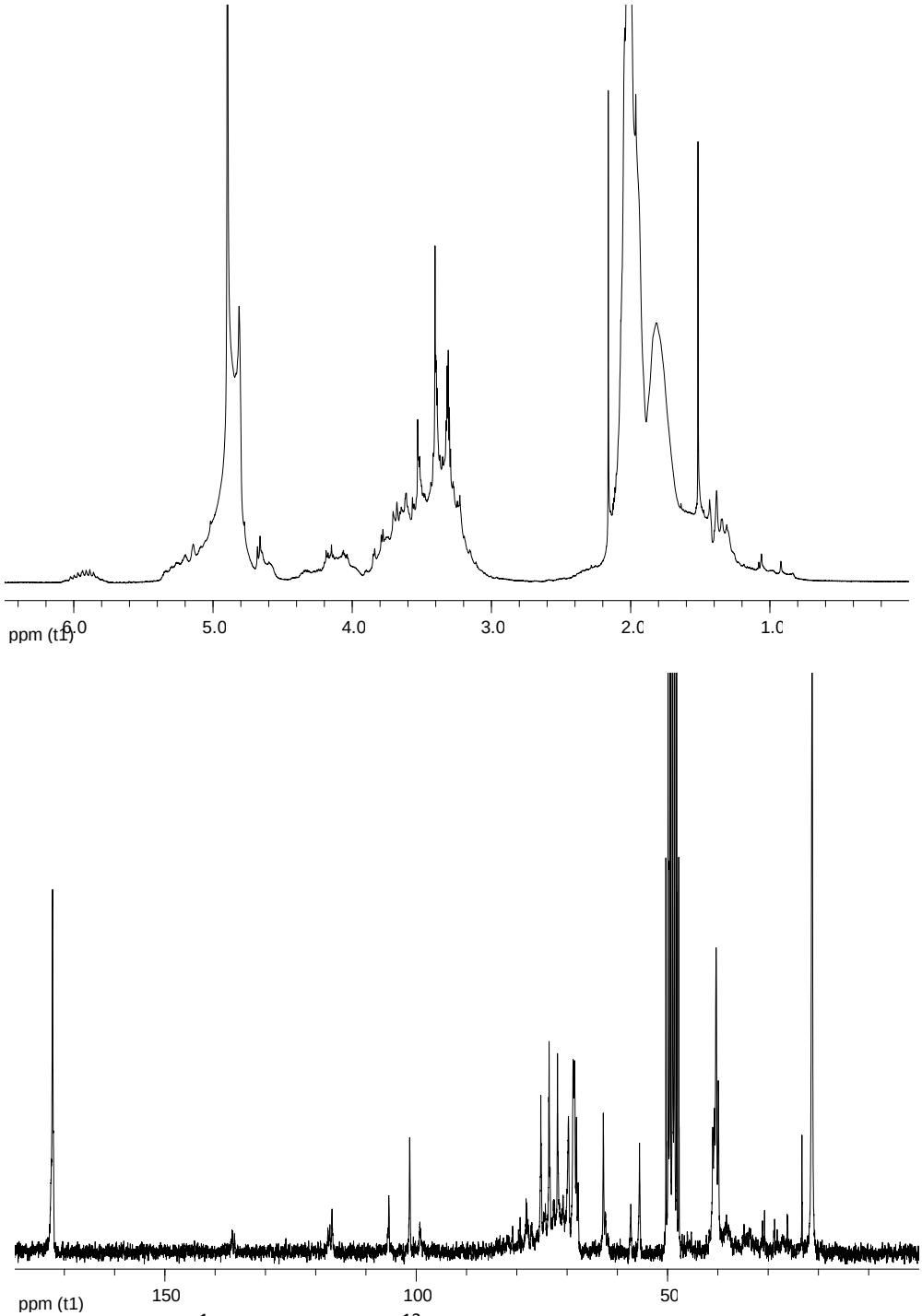

Figure 38 ^{1}H-NMR and the ^{13}C-NMR spectra of the allyl methyl D-glucopyranoside/vinyl acetate copolymer (fraction A+B)

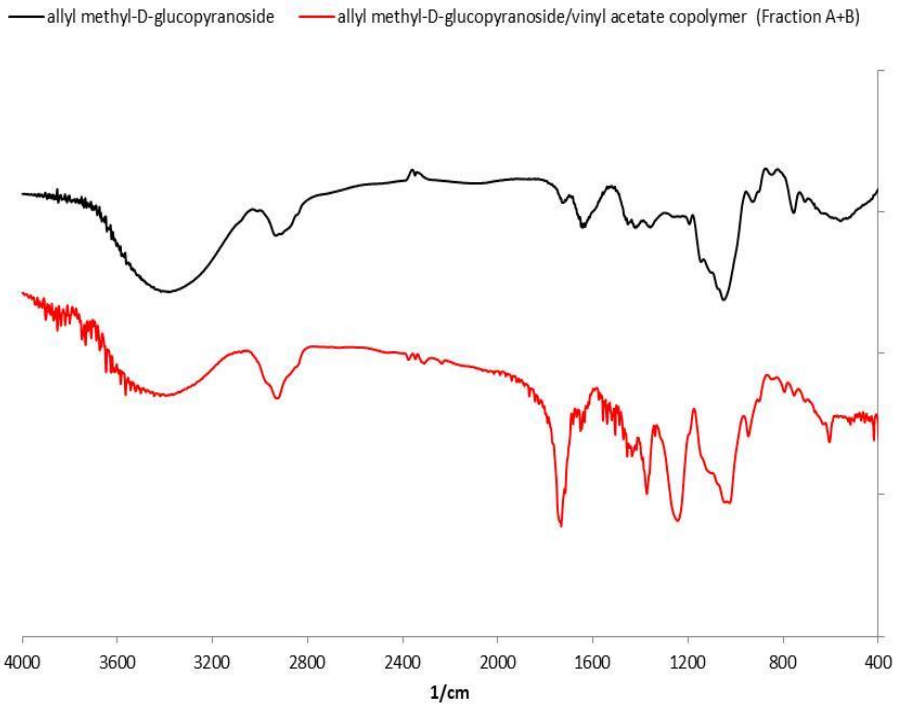

Figure 39 FT-IR spectra of the allyl methyl D-glucopyranoside (black line) and of the allyl methyl D-glucopyranoside/vinyl acetate copolymer (fraction A+B) (red line)

To fully characterize the product, the allyl methyl D-glucopyranoside/vinyl acetate copolymer was extracted with water and two fractions were separated: fraction A (soluble in water) and fraction B (insoluble in water). This behavior is in agreement with the formation of copolymer chains which have different ratios between the comonomers (**Table 5**). Those ratios were calculated by integrating the signals related to the vinyl acetate and the monosaccharide units in the ^{1}H-NMR spectra of the two fractions (**Figure 40**).

The fraction B shows higher vinyl acetate/saccharide units ratio compared to the fraction A and this is consistent with the presence of copolymers with a high content of vinyl acetate comonomer. However, in fraction B also vinyl acetate homopolymers can be present, according to the known insolubility of this product in water.

Table 5

	Molar ratio*	Yield[y] (%)	Fraction A[a]		Fraction B[b]	
			Amount (%)	Comonomer units ratio**	Amount (%)	Comonomer units ratio**
Allyl methyl D-glucopyranoside/ vinyl acetate copolymer	5	60	23	1	77	6
	9	57	20	1	80	10

* Moles of vinyl acetate/(moles of sugar comonomer·degree of substitution), [y] Calculated considering the fraction A+B, [a] Soluble in acetone, soluble in water, [b] Soluble in acetone, insoluble in water, ** Vinyl acetate units/allyl monosaccharide units

The fraction A and the fraction B were characterized after the separation by NMR and FT-IR spectroscopies. **Figure 40** and **Figure 41** show the ^{1}H-NMR and ^{13}C-NMR spectra and **Figure 42** shows the FT-IR spectra of the two fractions.

As previously said, the units of the two comonomers are present in the spectra of both fractions, but the signals/bands related to the different comonomers have different relative intensities, as expected from the ratios between the comonomers reported in **Table 5**. In particular, the intensity of the vinyl acetate signals is higher in the spectra of fraction B compared to those of fraction A, due to the presence in this fraction of copolymer chains with a higher vinyl acetate/allyl saccharide units ratio together with vinyl acetate homopolymer chains.

The presence of the signals related to the vinyl acetate in the spectra of fraction A can be justified, as in the case of the ally α,α'-trehalose/vinyl acetate copolymer, with the presence of vinyl acetate units in a copolymer rich in saccharide units. Furthermore, the ^{1}H-NMR signals related to the saccharide units are sharp and the presence of short-chain copolymers in fraction A can be supposed based on the analysis of the shape of these signals. On the contrary, the signals of the saccharide units in fraction B are broad and it indicates the presence of long-chain copolymers. Those two results were confirmed by the SEC analyses (paragraph 4.2.4).

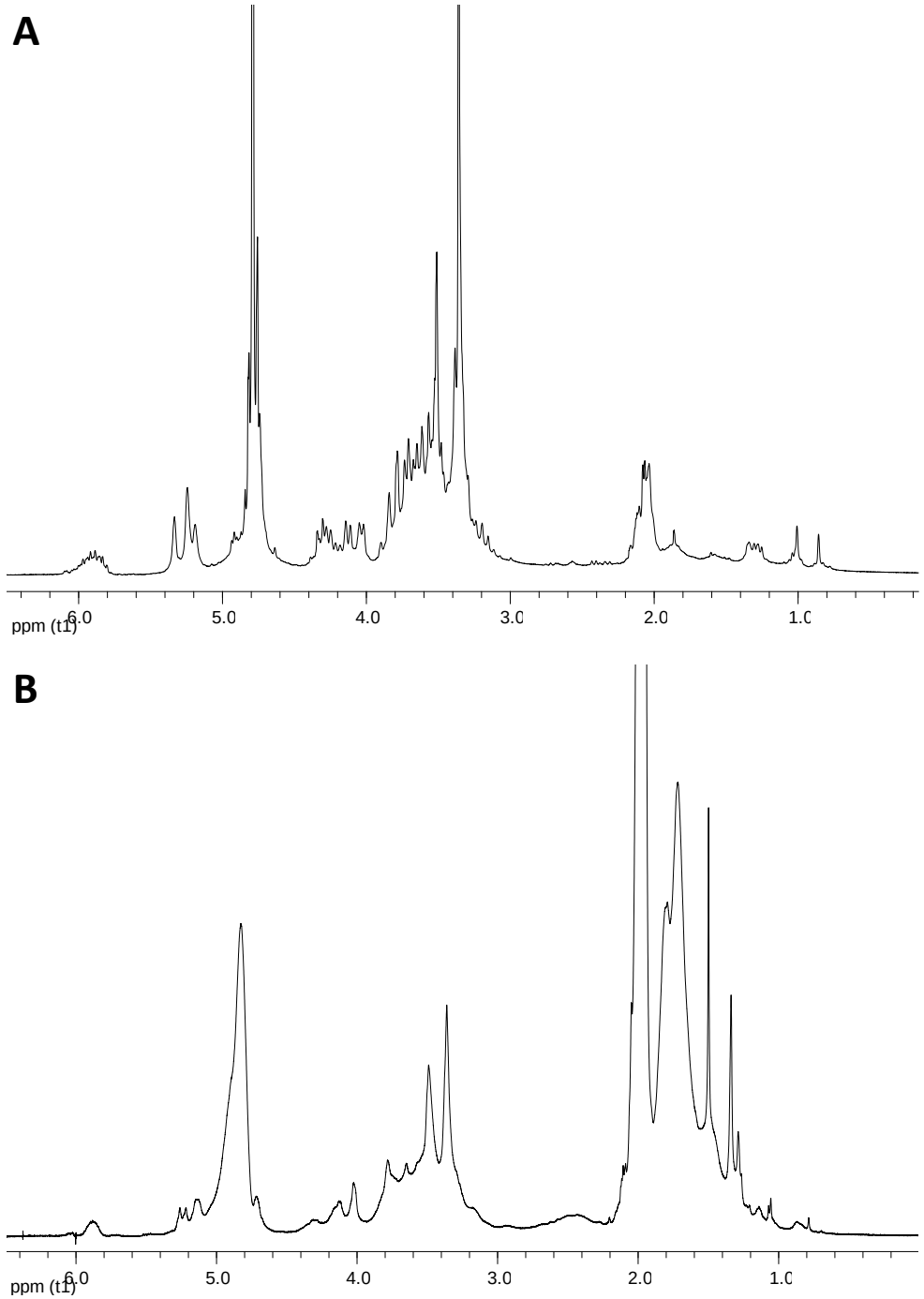

Figure 40 ^{1}H-NMR spectra of the fraction A (**A**) and of the fraction B (**B**) of the allyl methyl D-glucopyranoside/vinyl acetate copolymer

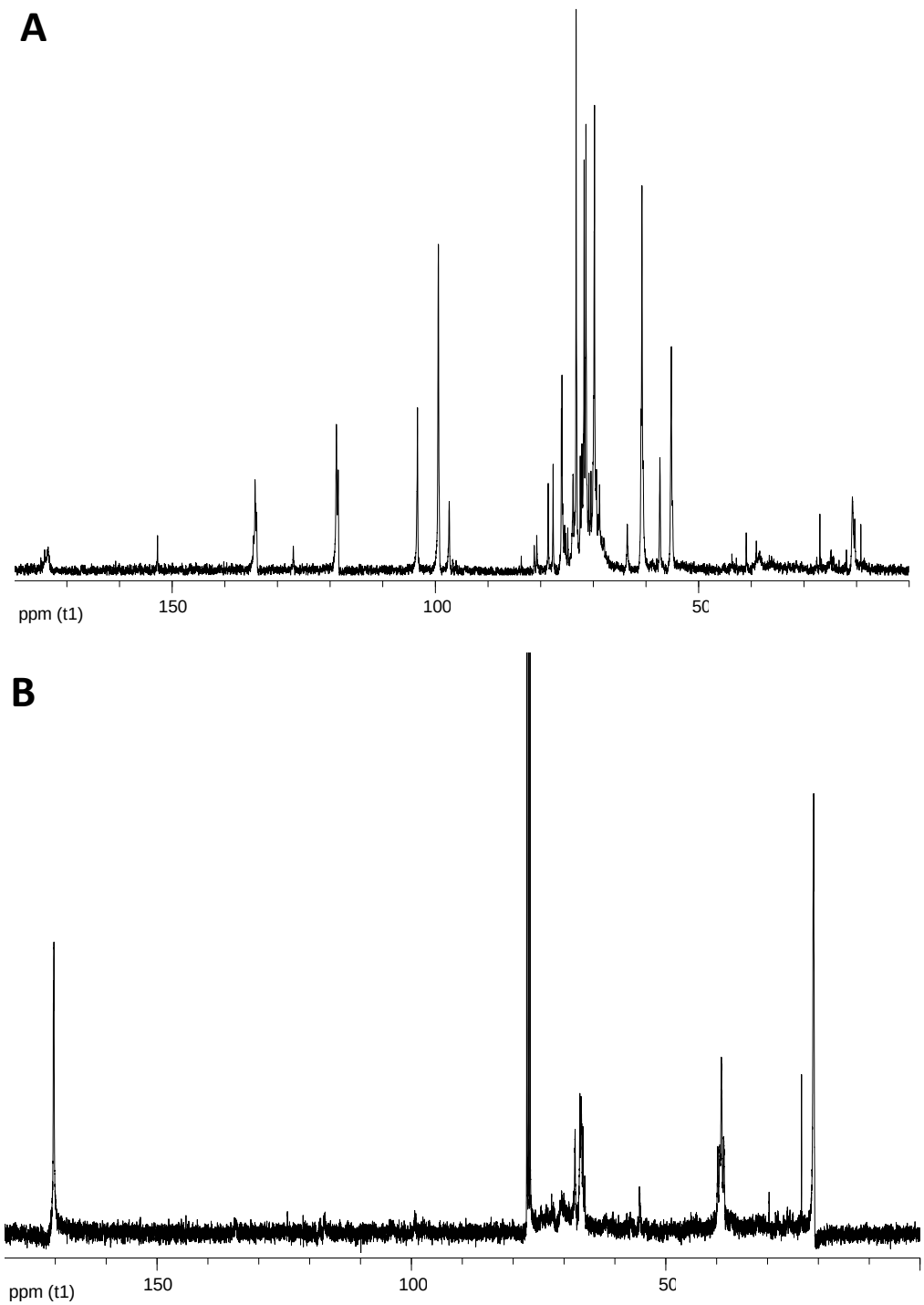

Figure 41 ^{13}C-NMR spectra of the fraction A (**A**) and of the fraction B (**B**) of the allyl methyl D-glucopyranoside/vinyl acetate copolymer

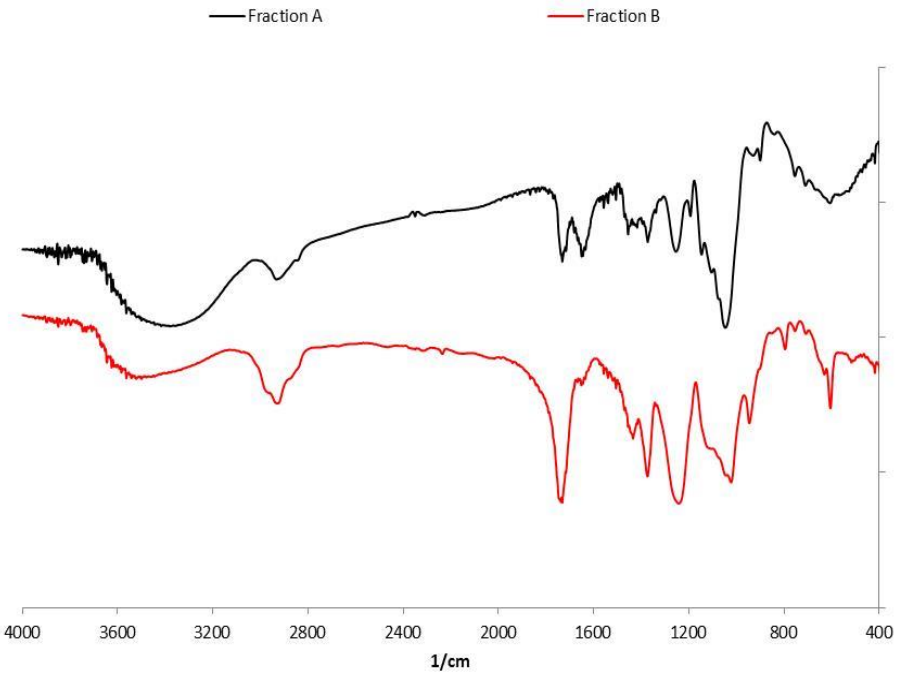

Figure 42 FT-IR spectra of the fraction A (black line) and the fraction B (red line) of the allyl methyl D-glucopyranoside/vinyl acetate copolymer

4.2.4 Characterization of the copolymers by differential scanning calorimetry (DSC) and size exclusion chromatography (SEC)

The allyl α,α'-trehalose/vinyl acetate and allyl methyl D-glucopyranoside/vinyl acetate copolymers (fraction A+B) and the two fractions obtained from each copolymer after the extraction in water (fraction A and fraction B) were analyzed by differential scanning calorimetry (DSC) and size exclusion chromatography (SEC).

Concerning the DSC analysis, two heating scans (from -10°C to 100°C, 10°C/min) were performed and the results for the two copolymers are reported in **Figure 43** (allyl α,α'-trehalose/vinyl acetate copolymer) and **Figure 44** (allyl methyl D-glucopyranoside/vinyl acetate copolymer).

Fraction A (**Figure 43**, black line) of allyl α,α'-trehalose/vinyl acetate copolymer has a glass transition (T_g) at about 0°C, which could have been seen better by starting the heating scan from a temperature lower than -10°C.

The behavior observed for fraction B (**Figure 43**, blue line) is different in the first scan compared to the second scan. In particular, the first scan shows an enthalpy recovery coupled with the glass transition, visible as endothermic signal. This feature is due to the fact that amorphous materials can age or relax over time. This behavior is a consequence of the rearrangement of the chains due to the interaction of the copolymer with the surrounding environment and is not an intrinsic feature, as it is instead the T_g. In effect, the second scan shows a normal T_g at a temperature of about 49°C. This value is coherent with the one reported in the literature for polyvinyl acetate (i.e. 30°C) and this is in agreement with the high content of vinyl acetate comonomer in the copolymer chains which are present in this fraction.

Finally, the fraction A+B (**Figure 43**, red line) has a T_g of about 40°C which is an intermediate value between the two T_g of the separated fractions. This result is in agreement with the contemporary presence inside this fraction of the two types of chains containing different ratios of the comonomers (fraction A and fraction B). The presence of a single T_g suggests that these chains strongly interact with each other.

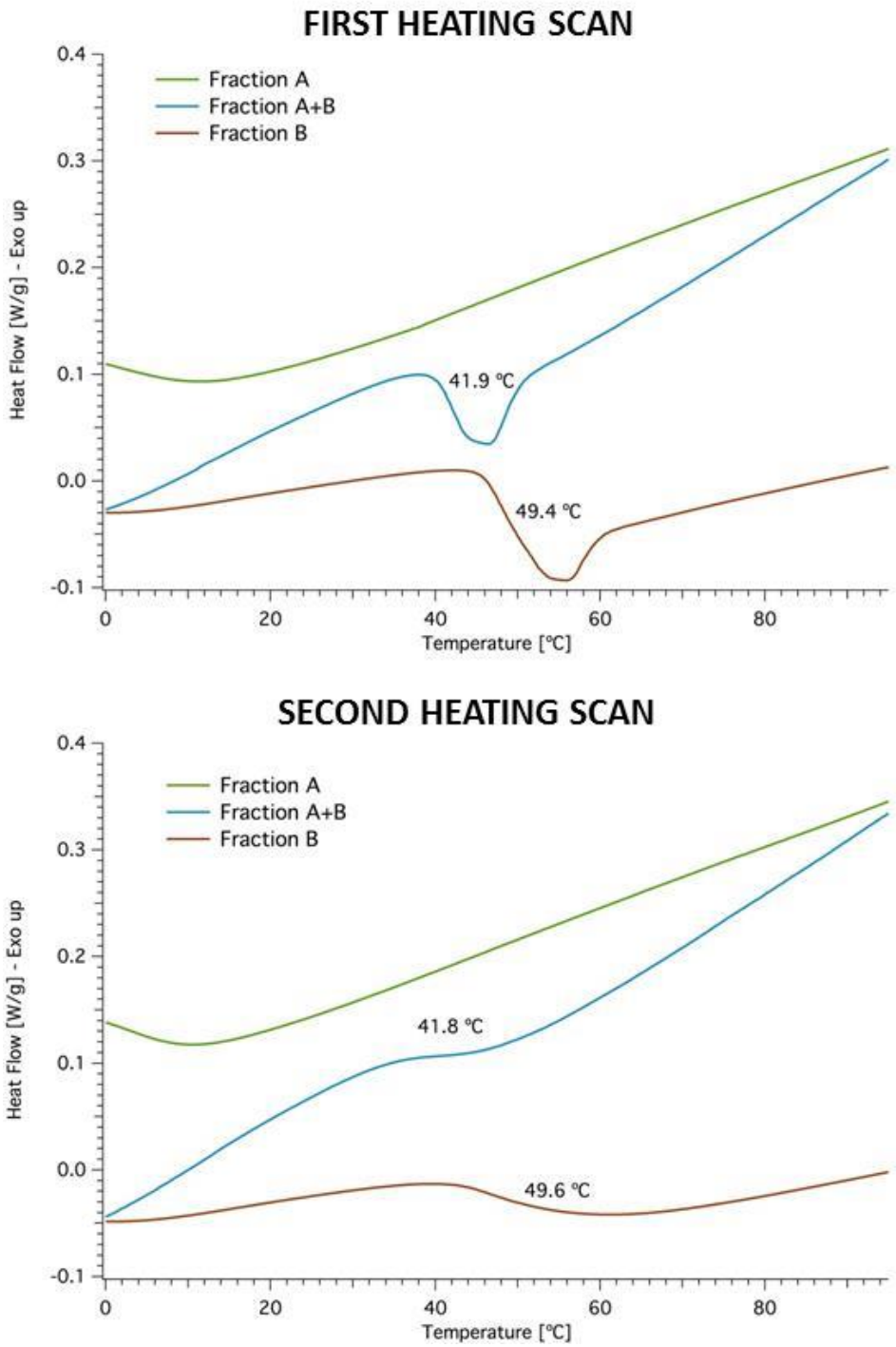

Figure 43 DSC analysis of the α,α'-trehalose/vinyl acetate copolymer: fraction A (green line), fraction B (red line) and fraction A+B (blue line)

The behavior of the three fractions of allyl methyl D-glucopyranoside/vinyl acetate copolymer is very similar (**Figure 44**).

For fraction A (**Figure 44**, green line) a T_g can be seen both in the first (9°C) and in the second (5°C) heating scan.

Concerning the fraction B (**Figure 44**, red line), the same enthalpy recovery which was observed for the fraction B of the allyl α,α'-trehalose/vinyl acetate copolymer is visible in the first scan. The second scan shows a well-defined T_g at a temperature of about 40°C, which is coherent with the one reported in the literature for polyvinyl acetate (i.e. 30°C). This behavior is in agreement with the high content of vinyl acetate comonomer in the copolymer chains which are present in this fraction.

Finally, the fraction A+B (**Figure 44**, blue line) has a T_g of about 28°C, which is an intermediate value between the two T_g values of the separated fractions. This result is in agreement with the contemporary presence inside this fraction of the two types of chains containing different ratios of the comonomers (fraction A and fraction B). The presence of a single T_g suggests that these chains strongly interact with each other.

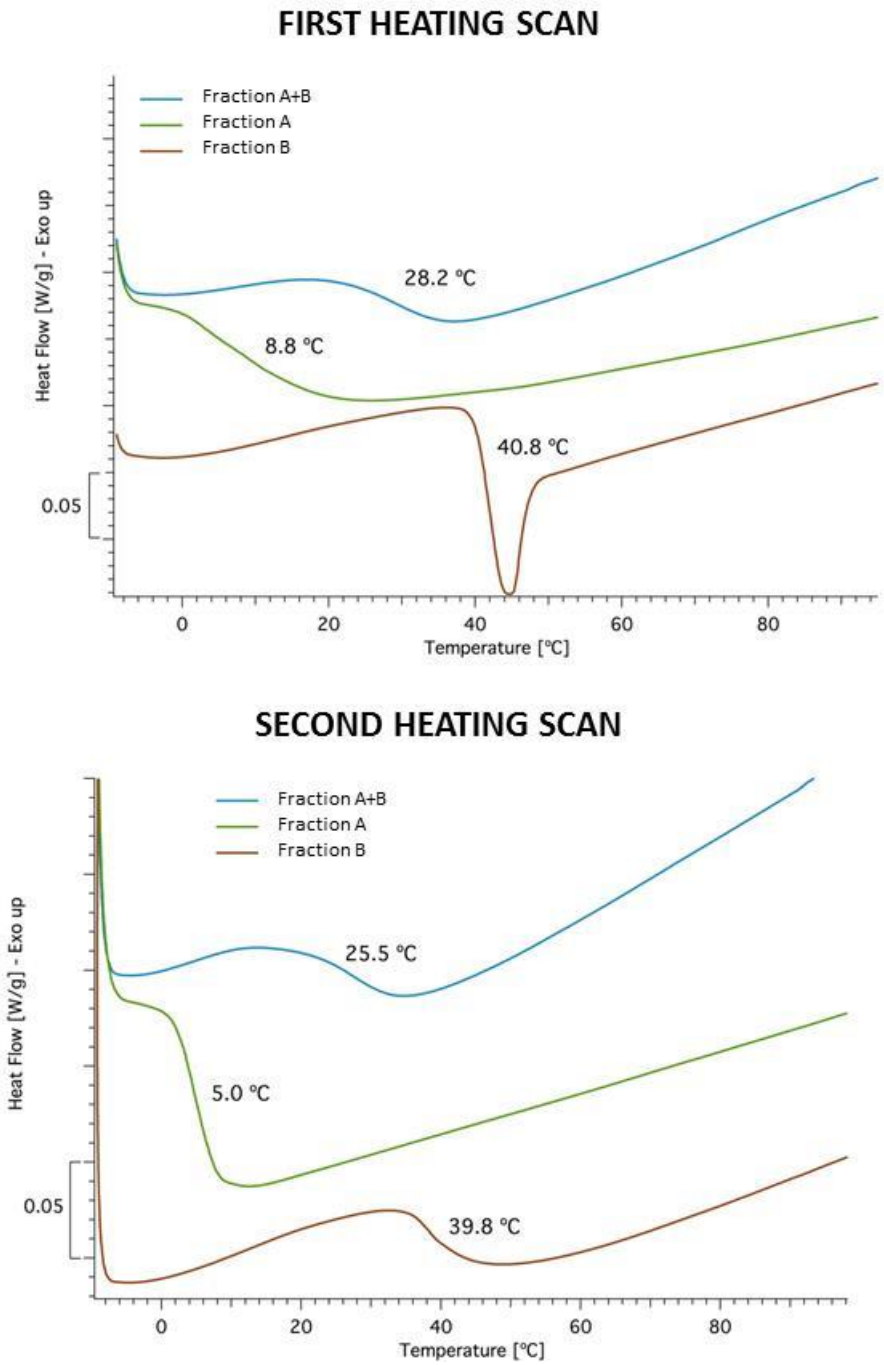

Figure 44 DSC analysis of the allyl methyl D-glucopyranoside/vinyl acetate copolymer: fraction A (green line), fraction B (red line) and fraction A+B (blue line)

The SEC results for the allyl α,α'-trehalose/vinyl acetate and allyl methyl D-glucopyranoside/vinyl acetate copolymers are reported respectively in **Figure 45** and **Figure 46**. Firstly, two remarks must be made:

1. the peak at about 37-38 minutes refers to the internal reference (1,2-dichlorobenzene);
2. peaks with a low retention time correspond to high hydrodynamic volume species and vice versa.

The results obtained for the two copolymers are very similar, despite the presence in their chains of two saccharides with different molecular size (i.e. a disaccharide and a monosaccharide). The curves related to the fraction A+B (in blue) of both copolymers show a very large peak centered at about 25 minutes and a narrow peak at about 31 minutes. The first peak is related to copolymers with a behavior similar to that reported in **Figure 47**, which shows the SEC analysis of a polyvinyl acetate homopolymer synthesized as a standard reference with the same procedure used for the synthesis of the copolymers. The second peak is sharper than the other and it can be attributed to copolymers with lower molecular weights, also because its retention time is too low to correspond to one of the starting monomers.

The SEC analyses were also performed on the fractions A and B, which were separated after the extraction of each copolymer with water. In the curves of fraction B (in red) of both copolymers only the broad peak at low time related to a copolymer similar to polyvinyl acetate is visible, while for fraction A (in green) of both copolymers only the peak related to a shorter copolymer can be observed. These results are consistent with the solubility of these fractions and with the comonomer unit ratios in the copolymer chains calculated by ^{1}H-NMR spectroscopy (paragraphs 4.2.2 and 4.2.3).

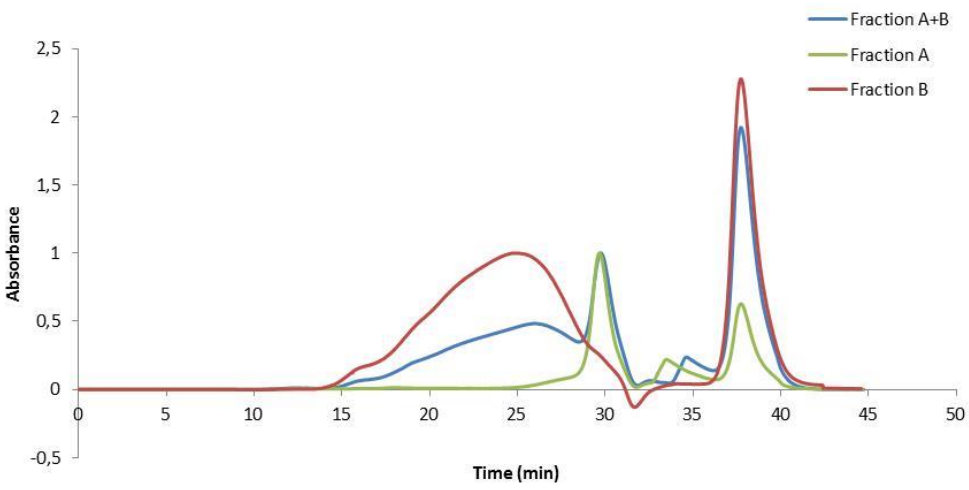

Figure 45 SEC analysis of the allyl α,α'-trehalose/vinyl acetate copolymer

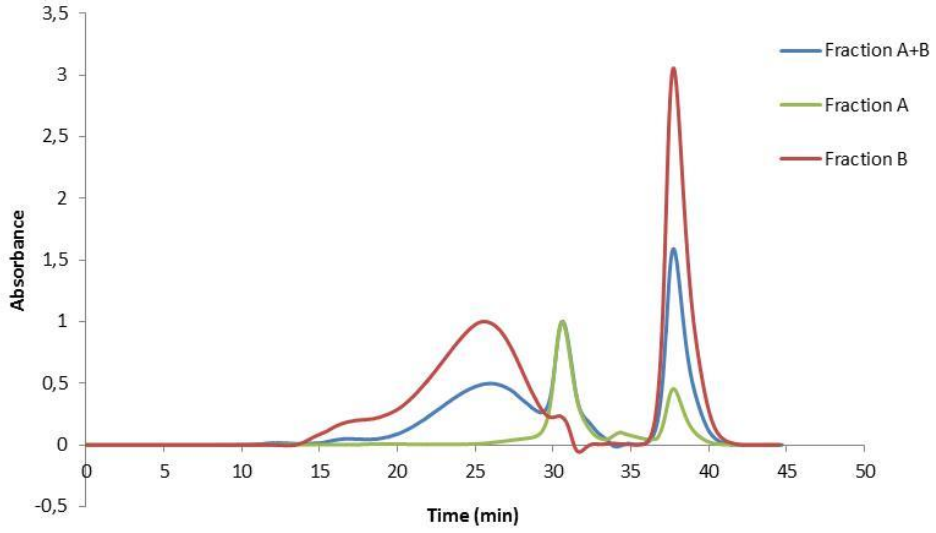

Figure 46 SEC analysis of the allyl methyl D-glucopyranoside/vinyl acetate copolymer

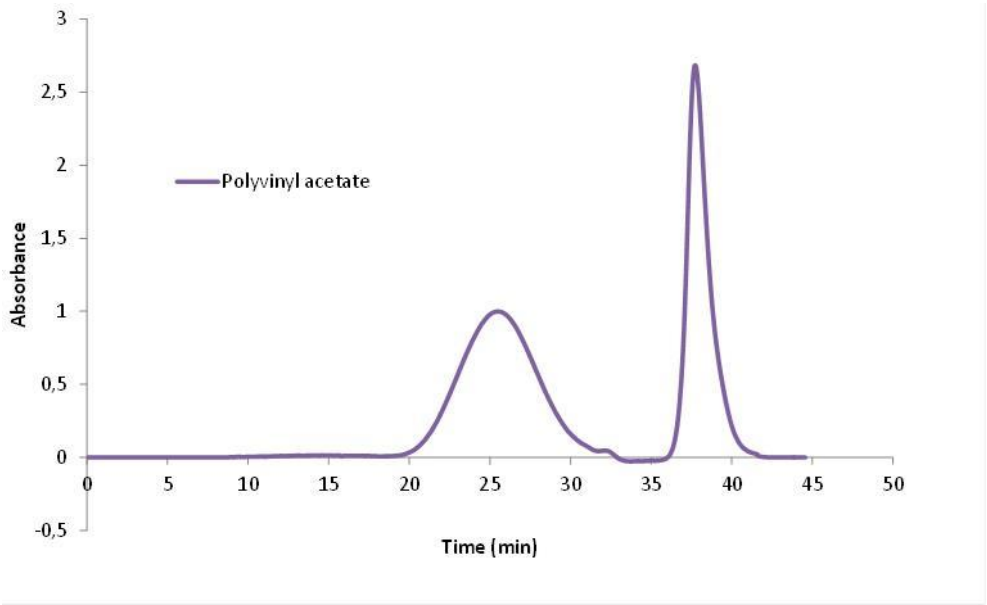

Figure 47 SEC analysis of the polyvinyl acetate

The molecular weights and the dispersity index of each fraction of the two copolymers (**Table 6**) were obtained from the SEC analyses as relative values using a monodispersed polystyrene standard and the following formulas:

$$M_n \text{ (number average molecular weight)} = \frac{\sum N_i M_i}{\sum N_i} \left[\frac{g}{mol}\right]$$

where M_i is the molecular weight of a chain and N_i is the number of chains with that molecular weight

$$M_w \text{ (weight average molecular weight)} = \frac{\sum N_i M_i^2}{\sum N_i M_i} \left[\frac{g}{mol}\right]$$

where M_i is the molecular weight of a chain and N_i is the number of chains with that molecular weight

$$Đ \text{ (dispersity index)} = \frac{M_w}{M_n}$$

As regards M_p, it represents the molecular weight of the highest peak in the curve and it is a useful parameter because is not an average value as M_n and M_w and so it is independent of the way in which the baseline and the integration extremes are chosen. In this case, being the peak at about 31 minutes the highest for fraction A+B and for fraction A of both the

copolymers, the M_p value is almost the same for these two fractions even if in fraction A+B also the peak at about 25 minutes is present. In fraction B of both the copolymers the highest peak is the one at about 25 minutes, which corresponds to a higher M_p value. Đ is the dispersity index and it is used as a measure of the molecular weight distribution of the polymer. The larger is the index, the broader is the molecular weight distribution. The Đ values obtained for all the fractions are high, considering that the typical polydispersity index for conventional free-radical polymerizations range from 1.50 to 2.00.[150]

Table 6

		M_n (g/mol)	M_w (g/mol)	M_p (g/mol)	Đ
Allyl α,α'-trehalose/vinyl acetate copolymer	**Fraction A+B**	4800	64200	5900	13.40
	Fraction A	6000	6800	6000	1.14
	Fraction B	19300	102200	26900	5.28
Allyl methyl D-glucopyranoside/ vinyl acetate copolymer	**Fraction A+B**	8200	97900	4300	11.97
	Fraction A	2400	4300	4400	1.79
	Fraction B	20600	103700	21900	5.03

M_n = number average molecular weight, M_w = weight average molecular weight, M_p = peak molecular weight, Đ = dispersity index

4.3 Synthesis and characterization of vinyl alcohol copolymers

4.3.1 General considerations

The hydrolysis of vinyl acetate copolymers was performed in order to obtain copolymers completely soluble in water and to prevent the hydrolysis of acetate groups from happening after the application of these products on the degraded material. Indeed, the hydrolysis of acetate groups produce acetic acid emission and can cause a hazardous decrease of the pH which, paradoxically, could accelerate the degradation, achieving an effect that is the opposite to the desired one.

The hydrolysis of vinyl acetate units was performed through a transesterification reaction with KOH in methanol (**Scheme 9**).[151] To perform the hydrolysis, the fraction A+B of each copolymer was chosen as starting product.

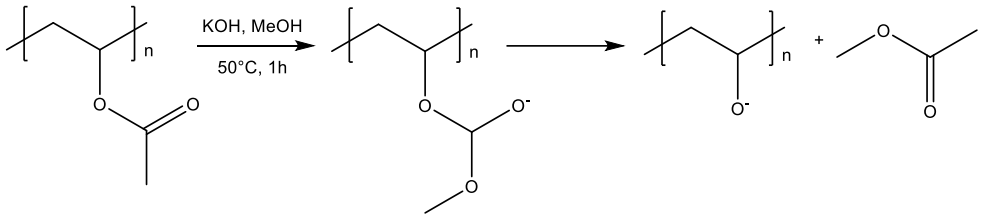

Scheme 9 Hydrolysis of a vinyl acetate polymer

4.3.2 Synthesis and characterization of the allyl α,α'-trehalose/vinyl alcohol copolymer

The hydrolysis of allyl α,α'-trehalose/vinyl acetate copolymer was performed under nitrogen atmosphere with KOH in anhydrous methanol (**Scheme 10**).

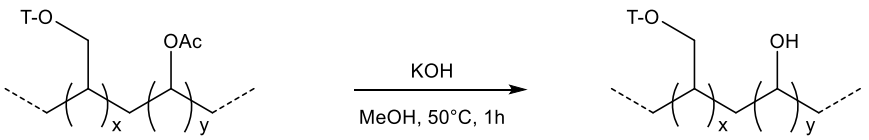

T = allyl α,α'-trehalose
y/x units ratio of the comonomers in the copolymer chain

T = allyl α,α'-trehalose
y/x units ratio of the comonomers in the copolymer chain

Scheme 10 Synthesis of the allyl α,α'-trehalose/vinyl alcohol copolymer

The standard procedure for the hydrolysis of polyvinyl acetate[151] provides for the precipitation of the polyvinyl alcohol because of its insolubility in methanol. In this case, the starting reagent (fraction A+B of allyl α,α'-trehalose/vinyl acetate copolymer) contains copolymer chains with different amount of vinyl acetate units in their structure. Therefore, at the end of the reaction, a part of the final product precipitated and it was separated from the methanol solution by centrifugation (fraction 1), while another part remained soluble in methanol and it was recovered by distilling the solvent

at reduced pressure (fraction 2). The product in fraction 1, which derives from the product in the fraction B of the vinyl acetate copolymer, has a high vinyl alcohol/disaccharide units ratio in the chains and therefore it precipitated as it was formed during the hydrolysis reaction. On the contrary, the product in fraction 2, which derives from the product in fraction A of the vinyl acetate copolymer, has a low vinyl alcohol/disaccharide units ratio in the chains and therefore it remained soluble in methanol.

The fraction 1 and the fraction 2 were characterized by NMR and FT-IR spectroscopy. All the spectra confirmed that the hydrolysis took place but was not complete, as generally occurs when polyvinyl acetate is hydrolyzed to polyvinyl alcohol. In **Figure 48** and **Figure 49** the characteristic signals of the vinyl acetate units at about 1.80, 2.00 and 4.90 ppm in the ^{1}H-NMR spectra and at about 21.0, 41.0, 63.0 and 172.0 ppm in the ^{13}C-NMR spectra are visible even if they have very low intensities compared to the spectra of the allyl α,α'-trehalose/vinyl acetate copolymer. On the contrary, new signals at about 1.60 and 4.00 ppm and at about 44.0 and 66.0 ppm have appeared respectively in ^{1}H and ^{13}C-NMR spectra and they are related to the $\underline{CH_2}$-$\underline{CH}$(OH)- units. In the FT-IR spectra of the two fractions (**Figure 50**) the C=O stretching of the acetate group is still present (1736 cm^{-1}) even if it has a very low intensity compared to the analogous band in the spectrum of the allyl α,α'-trehalose/vinyl acetate copolymer.

Concerning the degree of hydrolysis, when polyvinyl acetate is hydrolyzed to polyvinyl alcohol it is usually evaluated using the integrals of the characteristic signals of vinyl acetate (2.00 ppm, C**H$_3$**-CO) and vinyl alcohol (4.00 ppm, C**H$_2$**-CH(OH)-) units in the ^{1}H-NMR spectra. However, in the case of the allyl α,α'-trehalose/vinyl alcohol copolymer this evaluation was not possible due to the overlapping of the signal of vinyl alcohol units at 4.00 ppm (C**H$_2$**-CH(OH)-) with those of the saccharide structure.

Finally, the comparison of the intensity of the signals related to vinyl alcohol units in the different spectra of fraction 1 and fraction 2 confirms the presence of a higher amount of vinyl alcohol units in the chains of fraction 1 with respect to fraction 2.

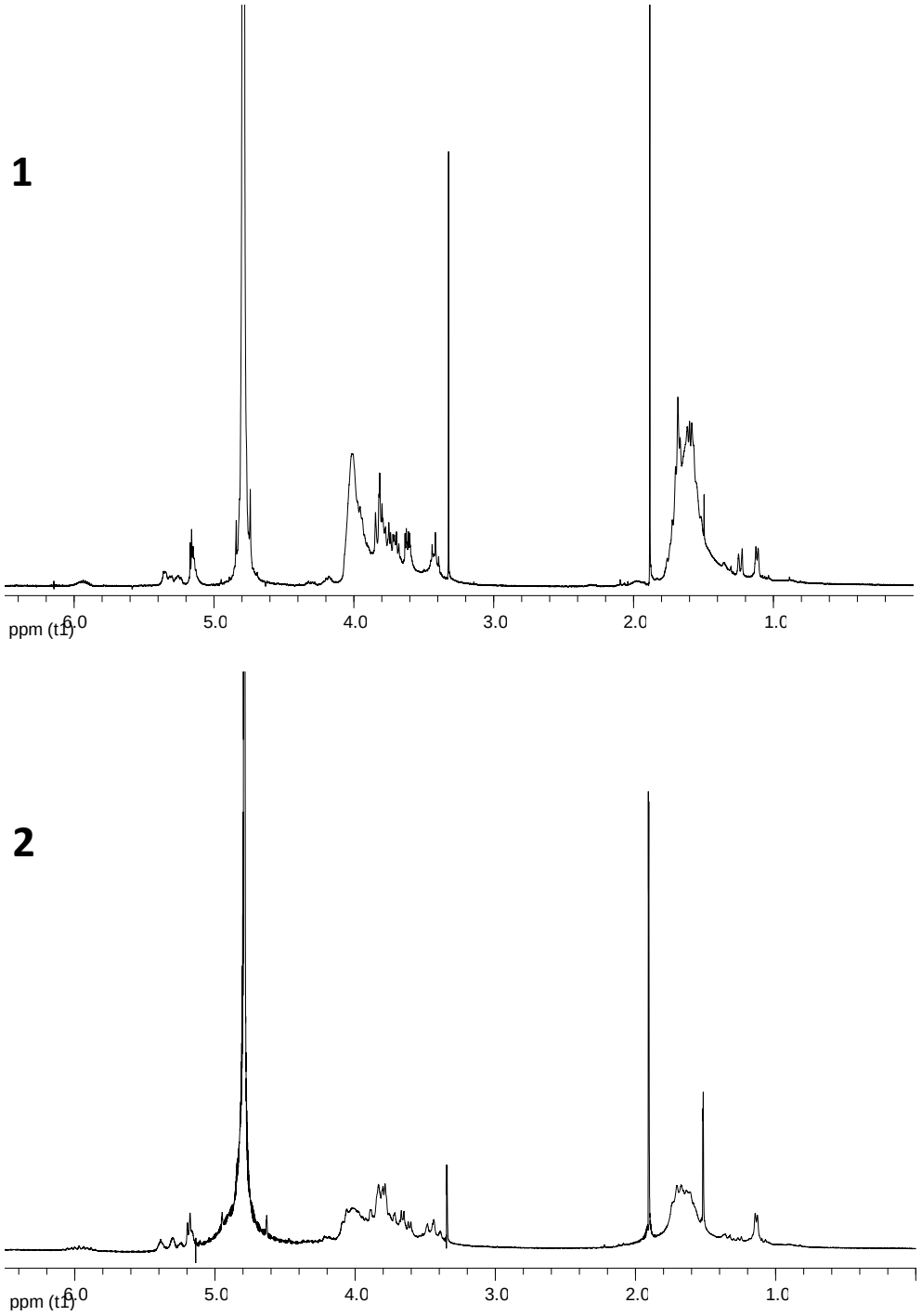

Figure 48 ^{1}H-NMR spectra of the allyl α,α'-trehalose/vinyl alcohol copolymer (**1** fraction 1, **2** fraction 2)

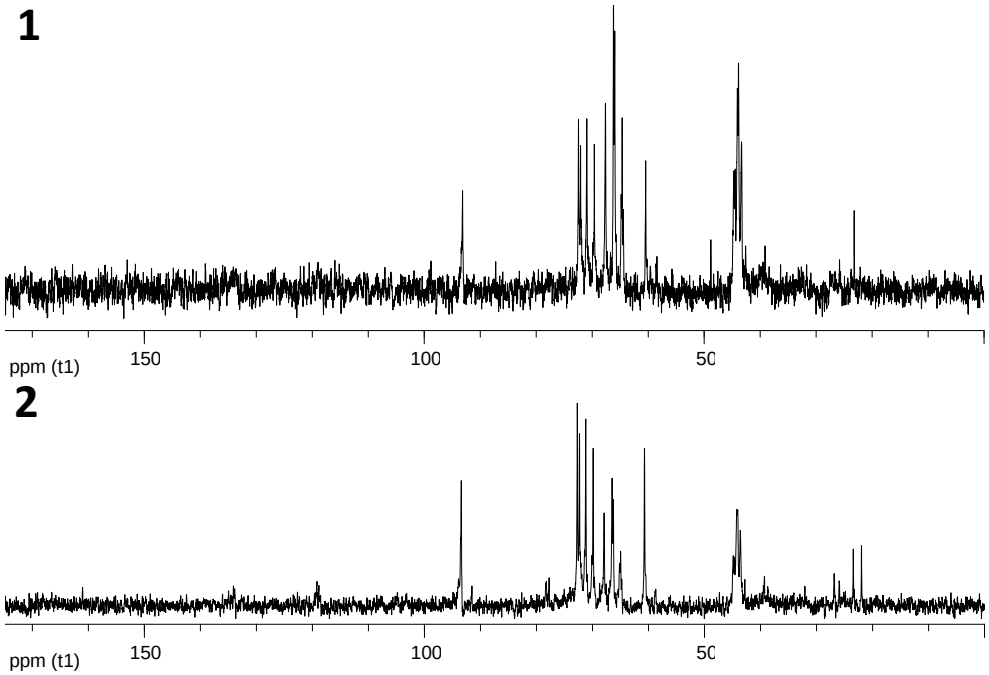

Figure 49 ^{13}C-NMR spectra of the allyl α,α'-trehalose/vinyl alcohol copolymer (**1** fraction 1, **2** fraction 2)

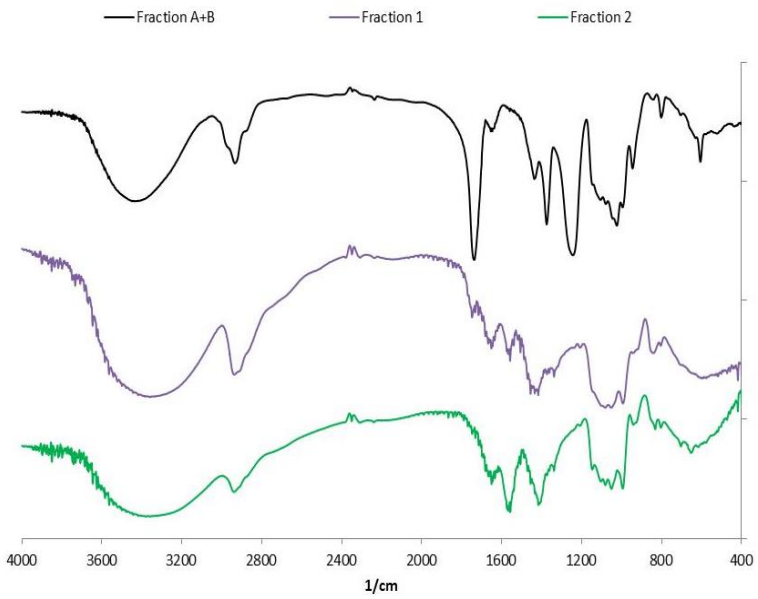

Figure 50 Comparison between the FT-IR spectra of the allyl α,α'-trehalose/vinyl alcohol copolymer (fraction 1 purple line, fraction 2 green line) and the spectrum of the allyl α,α'-trehalose/vinyl acetate copolymer (fraction A+B black line)

4.3.3 Synthesis and characterization of the allyl methyl D-glucopyranoside/vinyl alcohol copolymer

The hydrolysis of allyl methyl D-glucopyranoside/vinyl acetate copolymer was performed under nitrogen atmosphere with KOH in anhydrous methanol (**Scheme 11**).

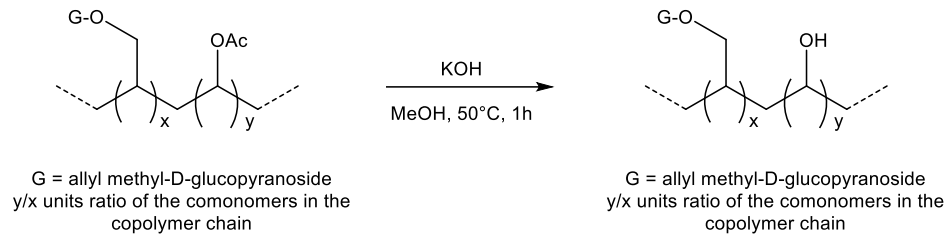

Scheme 11 Synthesis of the allyl methyl D-glucopyranoside/vinyl alcohol copolymer

At the end of the hydrolysis two fractions were obtained and characterized by NMR and FT-IR spectroscopy. Fraction 1 was recovered as a solid which had precipitated during the reaction, while fraction 2 was obtained after having distilled the solvent at reduced pressure.

All the spectra confirmed that the hydrolysis occurred but not completely. In the NMR spectra (**Figure 51** and **Figure 52**) the characteristic signals of vinyl acetate units at about 1.80, 2.00 and 4.90 ppm in the ^{1}H-NMR spectra and at about 21.0, 41.0, 63.0 and 172.0 ppm in the ^{13}C-NMR spectra have very low intensities compared to the spectra of the allyl methyl D-glucopyranoside/vinyl acetate copolymer. On the contrary, new signals at about 1.60 and 4.00 ppm and at about 44.0 and 66.0 ppm have appeared respectively in ^{1}H and ^{13}C-NMR spectra and they are related to the $\underline{CH_2}$-$\underline{CH}$(OH)- units. In the FT-IR spectra of the two fractions (**Figure 53**) the C=O stretching of the acetate group is still present (1736 cm^{-1}) even if it has a very low intensity compared to the analogous band in the spectrum of the allyl methyl D-glucopyranoside/vinyl acetate copolymer. As in the case of allyl α,α'-trehalose/vinyl alcohol copolymer, the evaluation of the degree of hydrolysis was not possible due to the overlapping of the signal of vinyl

alcohol units at 4.00 ppm (C**H$_2$**-CH(OH)-) with those of the saccharide structure.

Finally, the comparison of the intensity of the signals related to vinyl alcohol units in the different spectra of fraction 1 and fraction 2 confirms the presence of a higher amount of vinyl alcohol units in the chains of fraction 1 with respect to fraction 2.

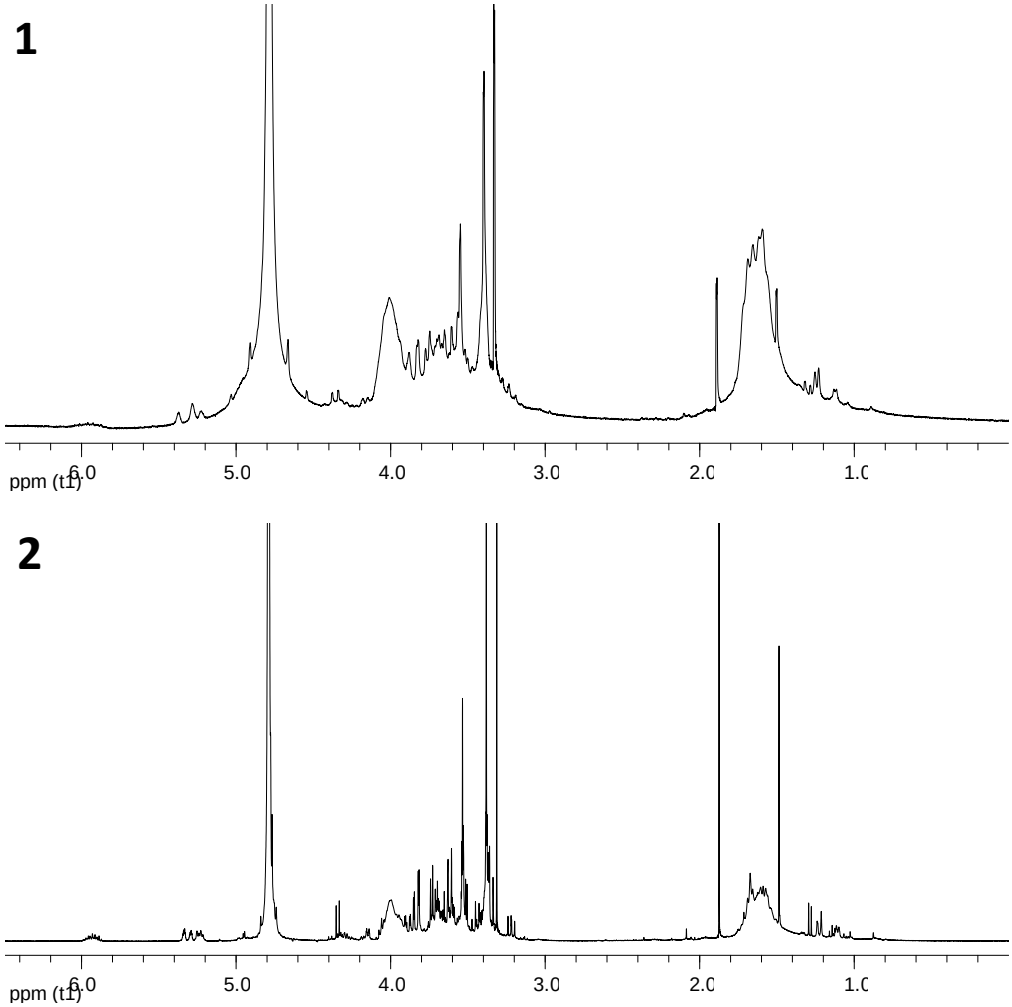

Figure 51 ^{1}H-NMR spectra of the allyl methyl D-glucopyranoside/vinyl alcohol copolymer (**1** fraction 1, **2** fraction 2)

1

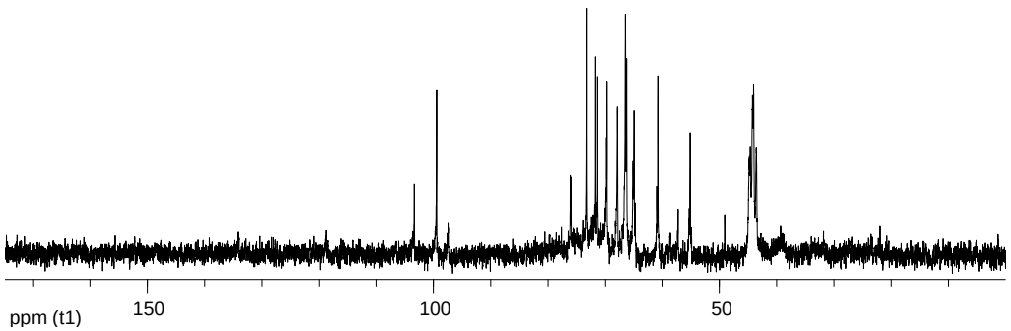

2

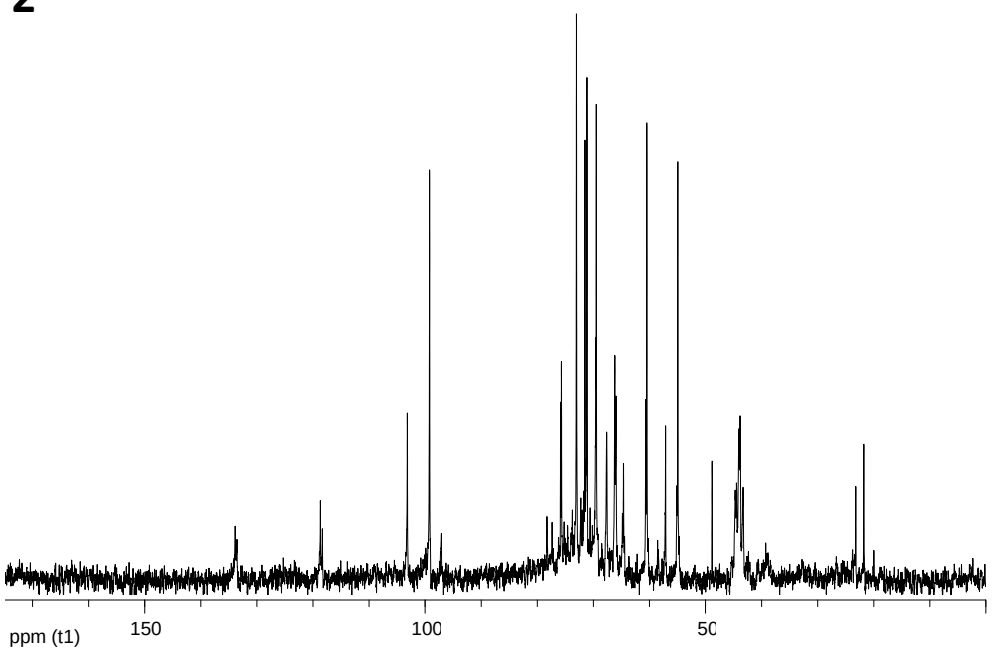

Figure 52 ^{13}C-NMR spectra of the allyl methyl D-glucopyranoside/vinyl alcohol copolymer (**1** fraction 1, **2** fraction 2)

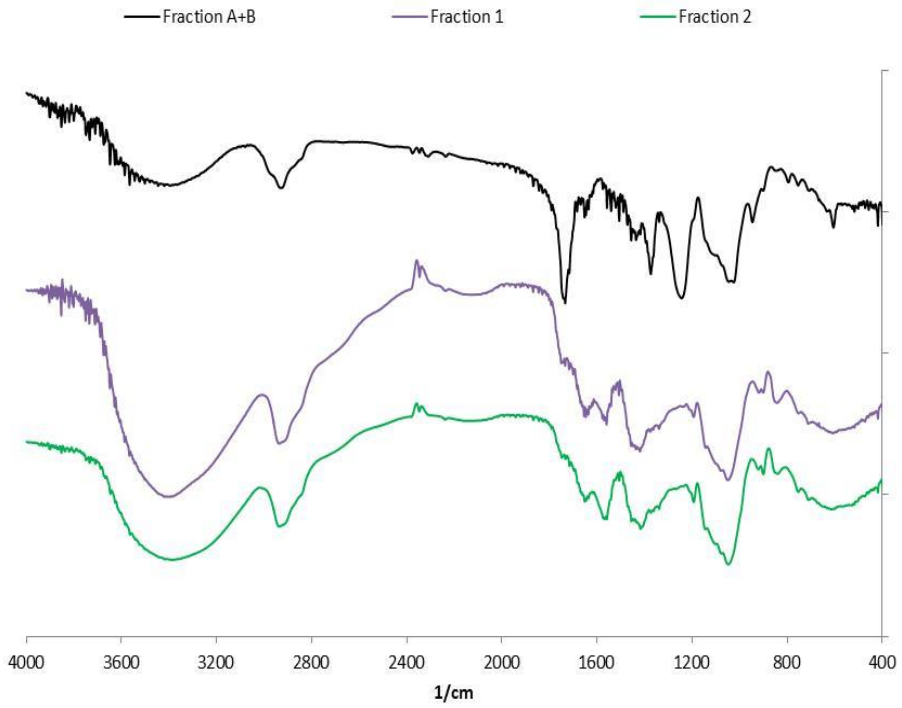

Figure 53 Comparison between the FT-IR spectra of the allyl methyl D-glucopyranoside/vinyl alcohol copolymer (fraction 1 purple line, fraction 2 green line) and the spectrum of the allyl methyl D-glucopyranoside/vinyl acetate copolymer (fraction A+B black line)

4.4 Nanocomposites

4.4.1 General considerations

The preparation of the nanocomposites allows to obtain materials with better properties compared to that of the single components (i.e. nanoparticles or organic matrices). As regard the conservation of cellulosic materials, a further advantage of using a nanocomposite is that it is possible to combine the positive effects of both the components, i.e. deacidification or antimicrobial activity of nanoparticles and consolidation properties of polymers, by performing a single application.

In this research the preparation of two nanocomposites was studied: allyl saccharide/vinyl alcohol copolymer/$Ca(OH)_2$ nanoparticles and allyl saccharide/vinyl acetate copolymer/TiO_2 nanoparticles.

4.4.2 Nanocomposites with $Ca(OH)_2$ nanoparticles and allyl saccharide/vinyl alcohol copolymers

In recent years, $Ca(OH)_2$ nanoparticles have been widely studied and used in the deacidification of paper or other cellulosic materials.[51-53]

In this research, an attempt to obtain a nanocomposite by mixing $Ca(OH)_2$ nanoparticles and allyl saccharide/vinyl alcohol copolymers was performed.

Vinyl alcohol copolymers were chosen instead of vinyl acetate copolymers in order to prevent the hydrolysis of the acetate group in the presence of a strong base, as the $Ca(OH)_2$ nanoparticles.

However, a stable dispersion was not obtained when nanoparticles and vinyl alcohol copolymers were mixed. The system (2% of the copolymer and 4g/L of nanoparticles in 2-propanol/water 75/25) flocculated in a very short time. **Figure 54** shows photos of the two systems containing $Ca(OH)_2$ nanoparticles and allyl α,α'-trehalose/vinyl alcohol copolymer (T) or allyl methyl D-glucopyranoside/vinyl alcohol copolymer (G) compared to a dispersion of 4g/L of nanoparticles in the same solvent system (NPs). The three photos were taken immediately after the mixing (photo 1), after one hour (photo 2) and after 24 hours (photo 3). This behavior can be attributed to the strong interaction between the nanoparticles and the large amount of hydroxyl groups on the structure of the copolymers, which cause aggregation and consequently flocculation. The result underlines the need for a better formulation of these nanocomposites to prevent or minimize the flocculation by adopting different formulation/mixing conditions.

However, before proceeding to the improvement of this formulation, the interest for a treatment that provides for the simultaneous presence of the consolidant and the nanoparticles on the cellulosic material was evaluated.

To do this, the vinyl alcohol copolymers were studied as nanocomposites with $Ca(OH)_2$ nanoparticles by performing subsequent applications of the two separate dispersions (consolidant and nanoparticles) on Whatman paper samples (paragraph 4.5.3).

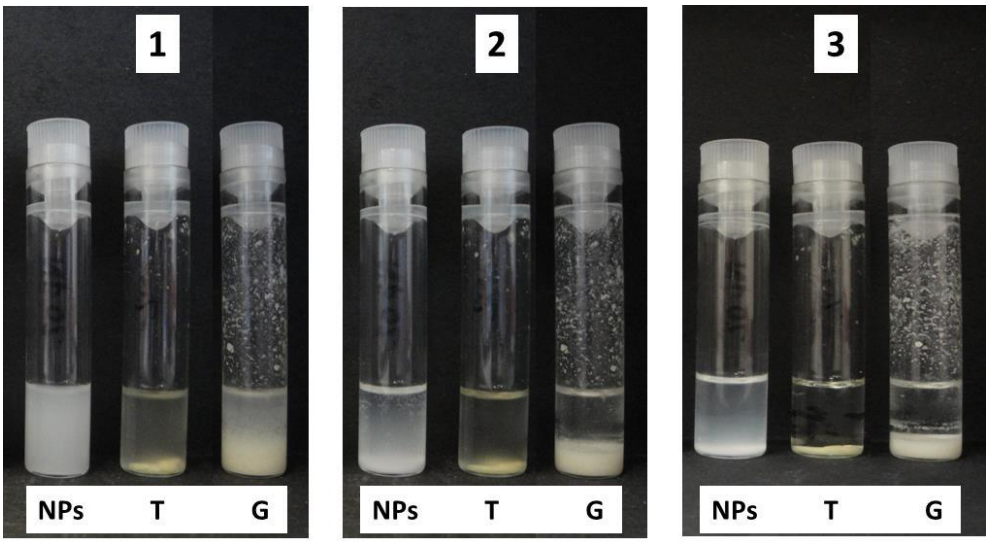

Figure 54 Photos of the three systems (**NPs** $Ca(OH)_2$ nanoparticles, **T** allyl α,α'-trehalose/vinyl alcohol copolymer+$Ca(OH)_2$ nanoparticles, **G** allyl methyl D-glucopyranoside/vinyl alcohol copolymer+$Ca(OH)_2$ nanoparticles) taken immediately after the mixing (**1**), after one hour (**2**) and after 24 hours (**3**)

4.4.3 Nanocomposites with TiO_2 anatase nanoparticles and allyl saccharide/vinyl acetate copolymers

In recent years, nanocomposites between TiO_2 anatase nanoparticles and oligoamides were synthesized from renewable resources and their antimicrobial activity against the attack of the fungus *Trametes Versicolor* was tested on wood specimens.[152]

On the basis of these results, in this research new nanocomposites were designed with the aim of obtaining new products with antimicrobial activity for cellulosic artifacts. In particular, nanocomposites between TiO_2 anatase nanoparticles and allyl saccharide/vinyl acetate copolymers were obtained

by grafting the copolymers on properly functionalized nanoparticles. Several steps were performed before arriving at the final products:

- activation of the TiO_2 nanoparticles,
- functionalization of the TiO_2 nanoparticles with vinyltriethoxysilane,
- in situ copolymerization of the allyl saccharide with vinyl acetate in the presence of functionalized TiO_2 nanoparticles.

4.4.3.1 Activation of the TiO_2 anatase nanoparticles

In a previous research carried out in our laboratory[153], several methods for the activation of powder TiO_2 anatase nanoparticles were tested and the best results were obtained using a modified version of a procedure found in the literature.[154]

The activation was performed at 95°C for 8 hours using commercial powder TiO_2 anatase nanoparticles and HNO_3 2M (**Scheme 12**). Then the dispersion was centrifuged and the solid was dispersed in water (4.5% w/w, pH 1-2) obtaining a highly stable system, unlike that obtained using not activated powder TiO_2 anatase nanoparticles.

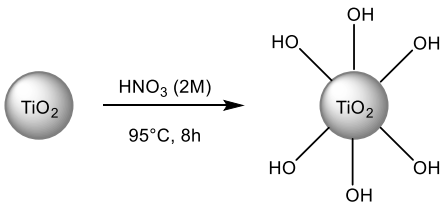

Scheme 12 Activation of the TiO_2 anatase nanoparticles

Nanoparticles were characterized by FT-IR spectroscopy and TEM. The analyses were performed on the solid obtained from the water dispersion after having distilled the solvent at reduced pressure. In the FT-IR spectrum (**Figure 55**) two bands at 3396 and 1635 cm^{-1} and a very broad and intense band from 450 to 800 cm^{-1} are visible. According to the literature[131], the first two bands are related to the stretching and bending of the hydroxyl groups on the surface of the nanoparticles, while the third band is related to the Ti-

O stretching. The band at 1386 cm^{-1} is related to the stretching of the NO_3^-, which is present as impurity.

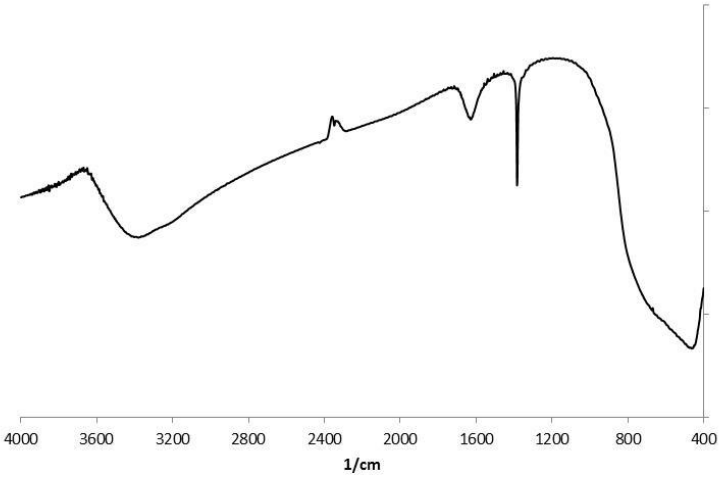

Figure 55 FT-IR spectrum of the activated TiO_2 anatase nanoparticles

TEM image (**Figure 56**) confirm the presence of dispersed nanoparticles with a diameter of about 10-20 nm.

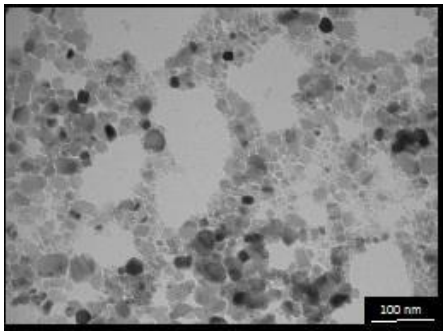

Figure 56 TEM image of the activated TiO_2 anatase nanoparticles

4.4.3.2 Functionalization of the TiO_2 anatase nanoparticles with vinyltriethoxysilane

In this step, the activated TiO_2 nanoparticles were functionalized in methanol under nitrogen atmosphere with a coupling agent, i.e. vinyltriethoxysilane

(**Scheme 13**), in order to have vinyl groups on their surface. A molar ratio between TiO_2 nanoparticles and vinyltriethoxysilane of 2:1 was used.

In a previous research[155] an attempt to perform the reaction without changing the pH of the starting dispersion was made, but the strongly acidic conditions promoted the complete hydrolysis of the ethoxy groups on the silane with a consequent condensation of the –SiOH groups to Si-O-Si. Therefore, before starting the reaction, the pH of the water dispersion of the nanoparticles was adjusted to 4 (evaluated with litmus paper) using a saturated solution of $NaHCO_3$.

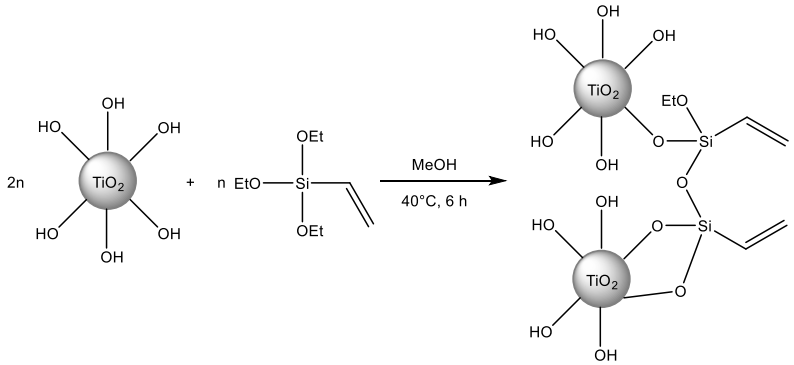

Scheme 13 Functionalization of the TiO_2 anatase nanoparticles with vinyltriethoxysilane

Although, this step and the subsequent are generally performed directly one after the other, a test to evaluate the result of the functionalization was performed. The reaction was stopped and, after an extraction in acetone, the obtained products were analyzed by FT-IR spectroscopy. In **Figure 57** the FT-IR spectra of the fractions soluble and insoluble in acetone together with the spectrum of the vinyltriethoxysilane are reported. The soluble fraction (black line) is characterized by the absence of the broad band between 450 and 800 cm^{-1} typical of the Ti-O stretching. Moreover, the Si-O stretching bands at 1110 and 1080 cm^{-1} are shifted and also wider compared to that of the vinyltriethoxysilane (**Figure 57**, green line). Finally, saturated C-H stretching bands are visible at 2973, 2928 cm^{-1} and they demonstrate an incomplete hydrolysis of the ethoxy groups on the silane. All this experimental evidences are in agreement with the formation of not grafted

$[CH_2=CH\text{-}SiO_x(OR)_{2-x}]_n$ oligomers, where x varies from 1 to 2 according to the formation of linear chains or reticular structures. On the contrary, in the spectrum of the insoluble fraction (red line) the broad band at 450-800 cm^{-1} related to the Ti-O stretching is visible and this confirms the presence of TiO_2 nanoparticles. The Si-O stretching bands shift at 1127 and 1047 cm^{-1} and become wider, probably because of the formation of Si-O-Ti bridges. Moreover, saturated C-H stretching bands are lower in intensity compared to those in the spectrum of soluble fraction because in this case ethoxy groups have almost completely hydrolyzed to form of Si-O-Ti bridges. Finally, as in the spectrum of activated nanoparticles, the very intense band at 1384 cm^{-1} corresponds to the presence of NO_3^- as impurity. The spectrum of the fraction insoluble in acetone is in agreement with the formation of functionalized nanoparticles.

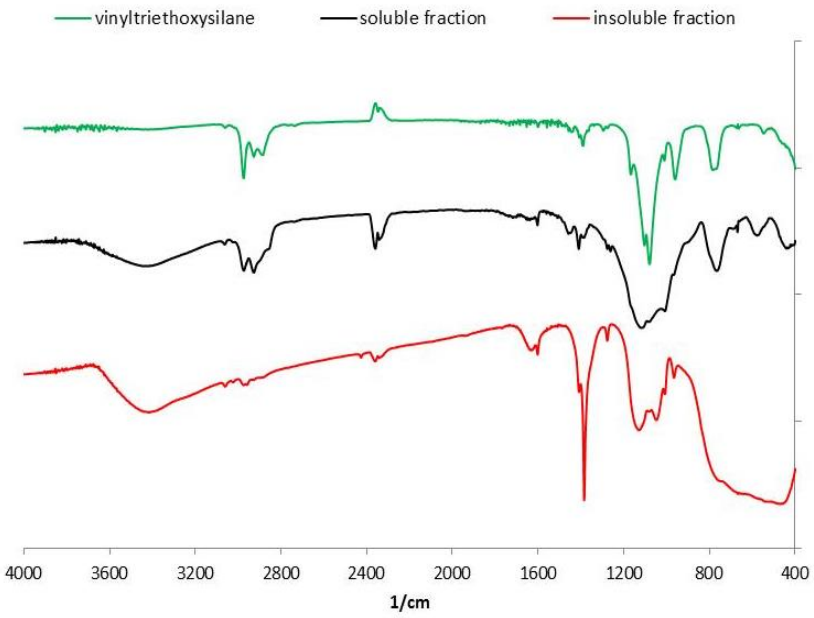

Figure 57 FT-IR of the vinyltriethoxysilane (green line), the acetone soluble fraction (black line) and the acetone insoluble fraction (red line) of the TiO_2 nanoparticles functionalized with vinyltriethoxysilane

4.4.3.3 In situ copolymerization of the allyl α,α'-trehalose with vinyl acetate in the presence of functionalized TiO_2 nanoparticles

In general, the functionalization of the nanoparticles with vinyltriethoxysilane (paragraph 4.4.3.2) was directly followed by the in situ polymerization. This reaction was performed by adding the allyl α,α'-trehalose, the vinyl acetate and the radical initiator azobisisobutyronitrile (AIBN) to the dispersion of functionalized TiO_2 nanoparticles in methanol (**Scheme 14**).

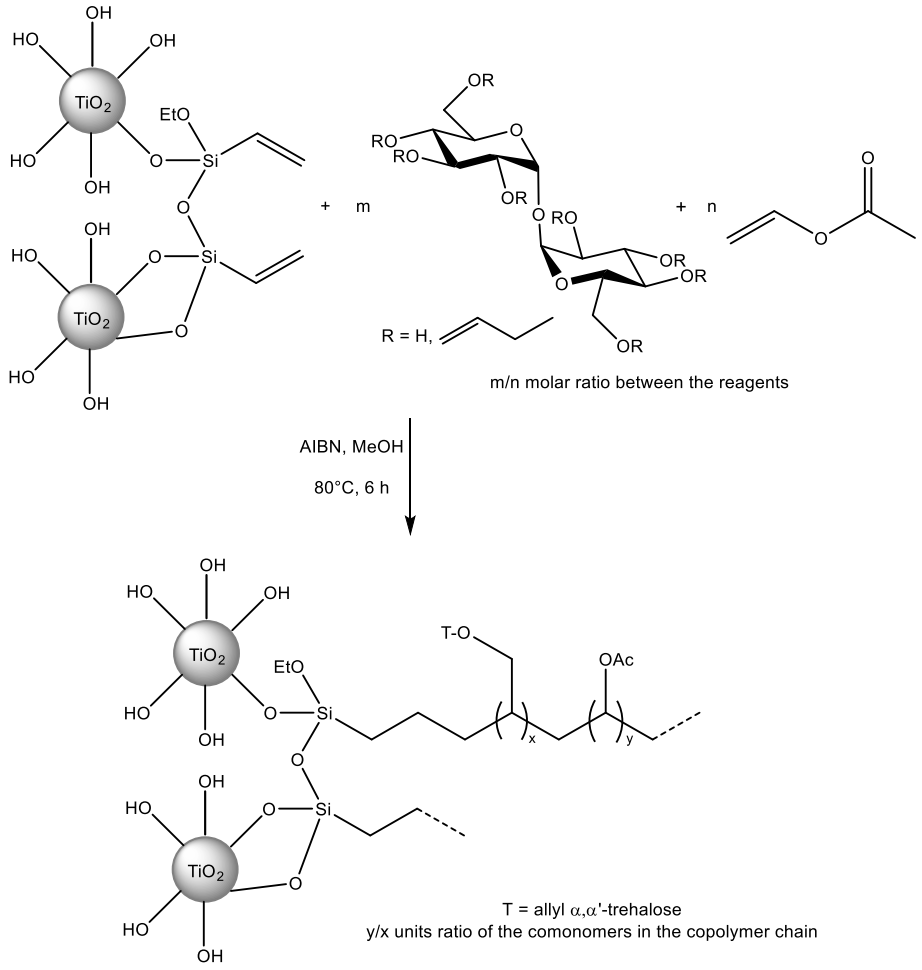

Scheme 14 Synthesis of the allyl α,α'-trehalose/vinyl acetate copolymer on functionalized TiO_2 nanoparticles

The amounts of reagents used to perform the reaction were evaluated considering the following molar ratios:

$$\frac{\text{mol (VA)}}{\text{mol (ATR)} \cdot \text{DS}} = 10 \qquad \frac{\text{mol (VA)} + (\text{mol (ATR)} \cdot \text{DS})}{\text{mol (VTEOS)}} = 28$$

where mol (VA) are the moles of vinyl acetate, mol (ATR) are the moles of allyl α,α'-trehalose, mol (VTEOS) are the moles of vinyltriethoxysilane and DS is the degree of substitution of the allyl α,α'-trehalose molecule.

The molar ratio of 28 is the same used in a previous research carried out in our laboratory with the aim of synthesizing polyvinyl acetate homopolymers on TiO_2 nanoparticles.[156]

At the end of the reaction the solvent and the residual vinyl acetate were distilled at reduced pressure and the solid was extracted with acetone to separate the not grafted allyl α,α'-trehalose/vinyl acetate copolymer and the not grafted vinyltriethoxysilane that may be possibly present. The SEM images of the soluble and insoluble fractions (**Figure 58** and **Figure 59**) confirm that it was possible to separate the nanocomposite (insoluble fraction) from a polymeric matrix not grafted on the nanoparticles (soluble fraction). In particular, the SEM image of the fraction insoluble in acetone confirms that it contains TiO_2 nanoparticles immersed in a polymeric matrix.

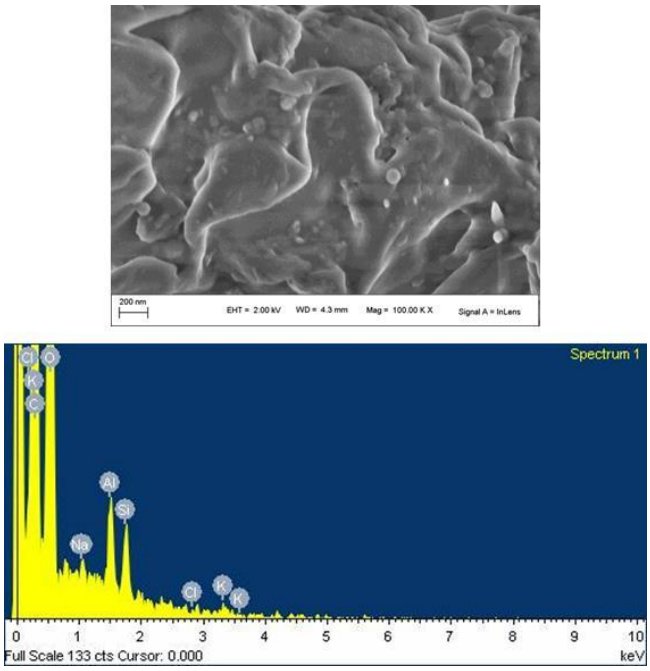

Figure 58 SEM-EDS analysis of the acetone soluble fraction of the allyl α,α'-trehalose/vinyl acetate copolymer/TiO_2 nanocomposite

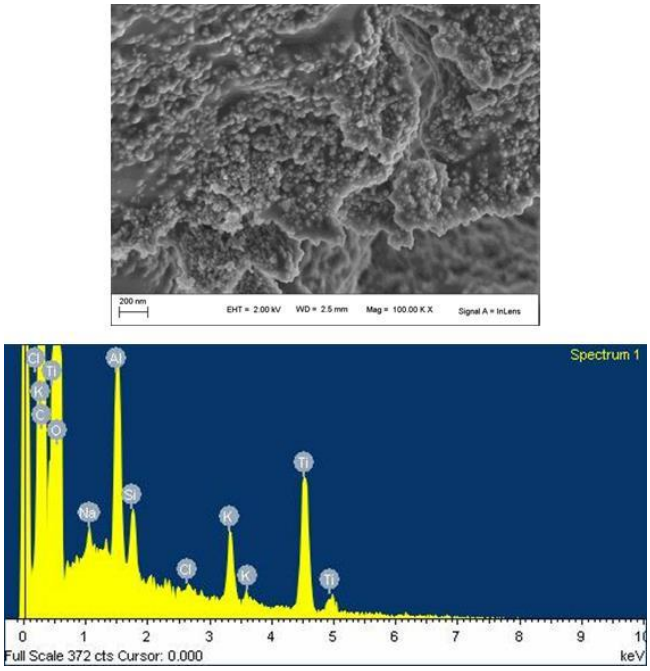

Figure 59 SEM-EDS analysis of the acetone insoluble fraction of the allyl α,α'-trehalose/vinyl acetate copolymer/TiO_2 nanocomposite

The white solid insoluble in acetone was characterized also by FT-IR spectroscopy. In **Figure 60** the FT-IR spectrum of this product is reported together with the spectrum of the nanoparticles functionalized with vinyltriethoxysilane and with that of the allyl α,α'-trehalose/vinyl acetate copolymer. The presence of the nanoparticles in the insoluble fraction is confirmed by the broad band at 450-800 cm^{-1}, which is visible also in the spectrum of functionalized nanoparticles. The bands related to the acetate group of the allyl α,α'-trehalose/vinyl acetate copolymer grafted on the nanoparticles are visible in the spectrum of the insoluble fraction at 1736 and 1248 cm^{-1} and they are comparable with those in the spectrum of the copolymer. Moreover, the shape of the group of bands between 1150 and 990 cm^{-1} is different in the various spectra. In particular, for the insoluble fraction it results from the overlapping of the Si-O stretching, which is characteristics of the functionalized nanoparticles, and the C-OH and C-O-C stretching of the allyl α,α'-trehalose/vinyl acetate copolymer.

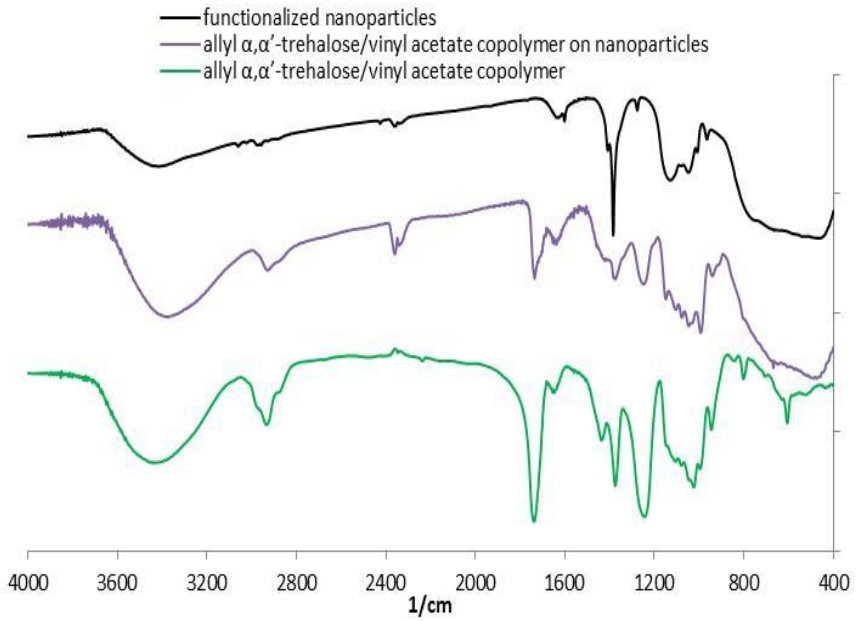

Figure 60 FT-IR spectra of the TiO_2 nanoparticles functionalized with vinyltriethoxysilane (black line), the fraction insoluble in acetone of the allyl α,α'-trehalose/vinyl acetate copolymer/TiO_2 nanocomposite (purple line) and the fraction A+B of the allyl α,α'-trehalose/vinyl acetate copolymer (green line)

4.4.3.4 In situ copolymerization of the allyl methyl D-glucopyranoside with vinyl acetate in the presence of functionalized TiO_2 nanoparticles

The TiO_2 nanoparticles functionalized with vinyltriethoxysilane were directly used as methanol dispersion together with the allyl methyl D-glucopyranoside, the vinyl acetate and the radical initiator azobisisobutyronitrile (AIBN) to perform the in situ polymerization (**Scheme 15**).

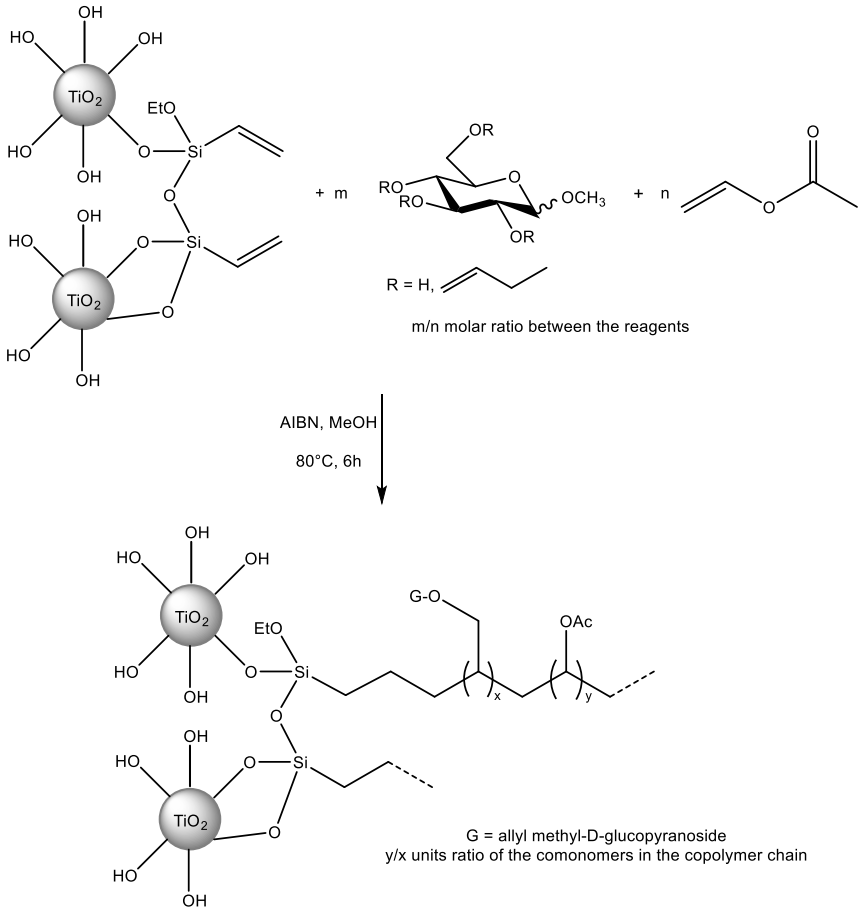

Scheme 15 Synthesis of the allyl methyl D-glucopyranoside/vinyl acetate copolymer on functionalized TiO_2 nanoparticles

The amounts of reagents used to perform the reaction were evaluated considering the following molar ratios:

$$\frac{\text{mol (VA)}}{\text{mol (AMG)} \cdot \text{DS}} = 9 \qquad \frac{\text{mol (VA)} + (\text{mol (AMG)} \cdot \text{DS})}{\text{mol (VTEOS)}} = 28$$

where mol (VA) are the moles of vinyl acetate, mol (AMG) are the moles of allyl methyl D-glucopyranoside, mol (VTEOS) are the moles of vinyltriethoxysilane and DS is the degree of substitution of the allyl methyl D-glucopyranoside molecule.

The molar ratio of 28 is the same used in a previous research carried out in our laboratory with the aim of synthesizing polyvinyl acetate on TiO_2 nanoparticles.[156]

At the end of the reaction the solvent and the residual vinyl acetate were distilled at reduced pressure and the solid was extracted with acetone to separate the not grafted allyl methyl D-glucopyranoside/vinyl acetate copolymer and the not grafted vinyltriethoxysilane that may be possibly present. The insoluble white solid was characterized by FT-IR spectroscopy and SEM-EDS. The SEM images of the soluble and insoluble fractions (**Figure 61** and **Figure 62**) confirmed that after the extraction in acetone it was possible to separate the nanocomposite (insoluble fraction) from a polymeric matrix not grafted on the nanoparticles (soluble fraction). In particular, the SEM image of the fraction insoluble in acetone confirmed that it contains TiO_2 nanoparticles immersed in a polymeric matrix.

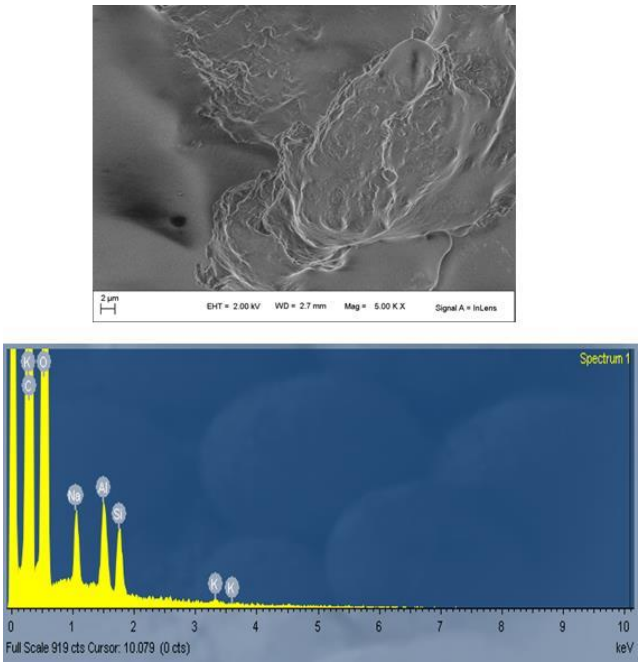

Figure 61 SEM-EDS analysis of the acetone soluble fraction of the allyl methyl D-glucopyranoside/vinyl acetate copolymer/TiO_2 nanocomposite

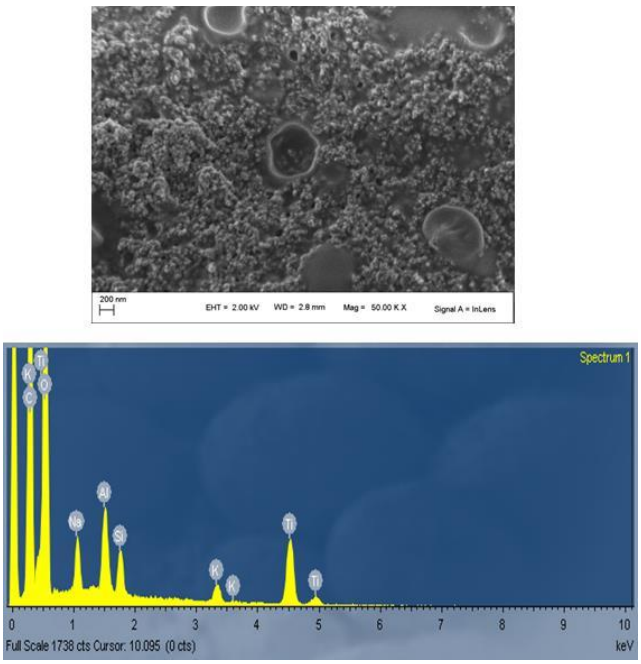

Figure 62 SEM-EDS analysis of the acetone insoluble fraction of the allyl methyl D-glucopyranoside/vinyl acetate copolymer/TiO_2 nanocomposite

In **Figure 63** the FT-IR spectrum of the insoluble fraction is reported together with the spectrum of the TiO_2 nanoparticles functionalized with vinyltriethoxysilane and with that of the allyl methyl D-glucopyranoside/vinyl acetate copolymer. The presence of the nanoparticles in the insoluble fraction is confirmed by the broad band at 450-800 cm^{-1}, which is visible also in the spectrum of functionalized nanoparticles. The bands related to the acetate group of the allyl methyl D-glucopyranoside/vinyl acetate copolymer grafted on the nanoparticles are visible in the spectrum of insoluble fraction at 1732 and 1250 cm^{-1} and they are comparable with those in the spectrum of the allyl methyl D-glucopyranoside/vinyl acetate copolymer. Moreover, the shape of the group of bands between 1150 and 990 cm^{-1} is different in the various spectra. In particular, for the insoluble fraction it results from the overlapping of the Si-O stretching, which is characteristics of the functionalized nanoparticles, and the C-OH and C-O-C stretching of the allyl methyl D-glucopyranoside/vinyl acetate copolymer.

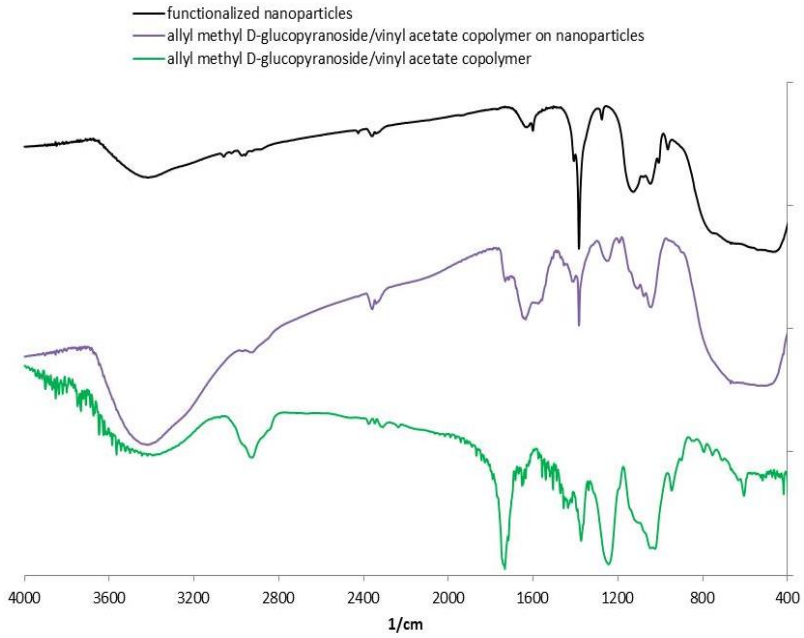

Figure 63 FT-IR spectra of the TiO_2 nanoparticles functionalized with vinyltriethoxysilane (black line), the fraction insoluble in acetone of the allyl methyl D-glucopyranoside/vinyl acetate copolymer/TiO_2 nanocomposite (purple line) and the fraction A+B of the allyl methyl D-glucopyranoside/vinyl acetate copolymer (green line)

4.5 Applicative studies

4.5.1 Consolidation of archaeological waterlogged wood

In the past years, the consolidating properties of some cellulose derivatives were tested on waterlogged archaeological wood.[97] They were chosen because of their structural affinity for the wood and its principal components. In particular, their structure is similar to that of the cellulosic component which has been lost in heavily degraded wood. Unfortunately, their penetration ability resulted insufficient because of their too high molecular weights (MW > 50000 g/mol). Consequently, other polymers or oligomers have been designed and synthesized in order to have different structures and lower molecular weights, thus enhancing the penetration ability of the final products in the wood structure.

More recently, several oligoamides were synthesized and tested as consolidants for waterlogged wood.[98,99] They showed good consolidating properties and good penetration ability thanks to their low molecular weights (MW 1000-10000 g/mol).

In this research, new products (i.e. allyl saccharide/vinyl alcohol copolymers) with higher molecular weight compared to the oligoamides, but at the same time different structure compared to that of the cellulose derivatives were studied as consolidants for waterlogged archaeological wood in order to verify the influence of the different structure and molecular weight on the penetration ability and the consolidating action. The use of an allyl derivative as comonomer was chosen as a possible method to reduce the molecular weight of the final copolymers according to the lower reactivity of the allyl group compared to the vinyl group. Moreover, the presence of a small amount of unreacted allyl groups could lead to cross-linking inside the consolidated materials, thus decreasing the mobility of the consolidant and, accordingly, improving the efficacy of the treatment. On the other hand, the choice of a saccharide derivative as comonomer and its presence in the chain improves the chemical and physical affinity of the copolymers for cellulosic substrates.

Among the new products synthesized in this research, allyl α,α'-trehalose/vinyl alcohol copolymer was studied as consolidant for waterlogged archaeological wood because it is soluble in water and has more affinity for wood compared to the analogous vinyl acetate copolymer. Moreover, the use of a hydrolyzed vinyl acetate copolymer allows to avoid the emission of acetic acid during an eventual future degradation of the consolidant inside the treated object.

The consolidating properties of the allyl α,α'-trehalose/vinyl alcohol copolymer were evaluated by performing treatment tests on degraded wood samples, using in parallel some other products which have been previously synthesized and in some cases tested (**Figure 64**):

- oligo ethylene-L-tartaramide,[99]
- copolymer between ethylenediamine, adipic acid and tartaric acid,[153]
- oligo esamethylene-L-tartaramide synthesized by Ditta Radici Chimica s.p.a..

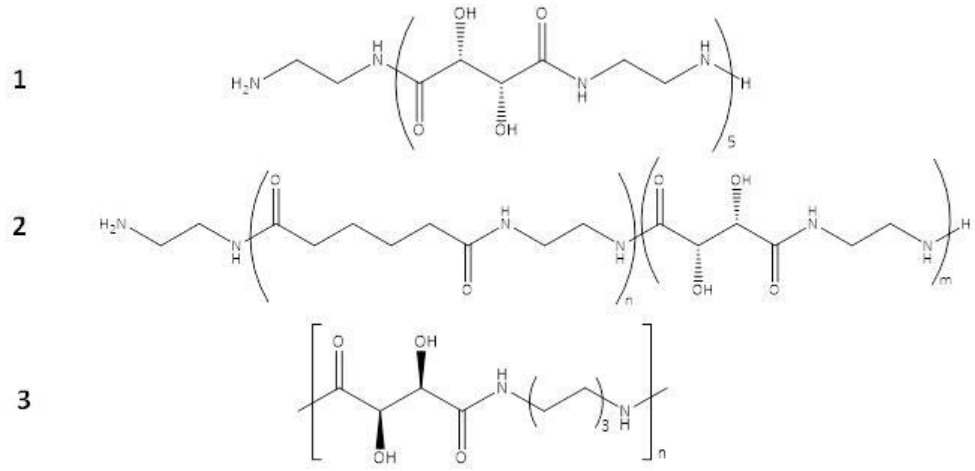

Figure 64 Structure of the oligoamides used in the test (**1** oligo ethylene-L-tartaramide; **2** copolymer between ethylenediamine, adipic acid and tartaric acid; **3** oligo esamethylene-L-tartaramide)

Firstly, solutions of these consolidants were prepared by dissolving the solid products in Milli-Q water, maintaining the concentrations under the limit of saturation (**Table 7**). It should be noticed that the oligo esamethylene-L-tartaramide is less soluble in water than the other products because of a

longer apolar chain between the amidic groups. Therefore, to prepare its solution it was necessary to perform several extractions in water. Then, after having decanted the solution, a further centrifugation was performed in order to separate the insoluble fraction. The final solution obtained from this centrifugation was used to perform the treatment.

Table 7

Product	Concentration	Color of the solution
allyl α,α'-trehalose/vinyl alcohol copolymer	4.5%	pale orange
oligo ethylene-L-tartaramide	4.3%	pale orange
copolymer between ethylenediamine, adipic acid and tartaric acid	2.5%	pale orange
oligo esamethylene-L-tartaramide	1.8%	orange

In this study, a diagnostic protocol which has been specifically designed in the past years in our laboratory was slightly modified and used to quickly assess the performances of new consolidants for waterlogged wood and to compare products with different structures.[100,101] These changes were designed to assess how and how much the inhomogeneity of the degraded wood may affect the analytical results.

The first step of this protocol was the evaluation of the affinity of the products for the wooden substrate. Lignin samples were chosen to perform affinity tests because in the degraded wood the cellulosic component is partially lost and the residual material is mainly composed of lignin. Oak lignin was obtained with the Klason procedure. Then, it was dispersed in the solutions of the various consolidants and kept under continuous stirring for 24 hours at room temperature. Finally, after filtration and drying, the lignin was characterized by FT-IR spectroscopy. These spectra were compared to the spectrum of the starting lignin (**Figure 65**, **Figure 66**, **Figure 67**, **Figure 68**).

Then, the treated lignin samples were used to perform reversibility tests. They were kept under continuous stirring in demineralized water for 24

hours at room temperature and then they were filtrated and dried. Finally, FT-IR spectra were recorded after the reversibility tests and they were compared with those recorded on treated lignin before the reversibility tests and with the spectrum of untreated lignin (**Figure 65**, **Figure 66**, **Figure 67**, **Figure 68**).

As regard the allyl α,α'-trehalose/vinyl alcohol copolymer (**Figure 65**), the characteristic bands of the consolidant are similar to those of the untreated lignin and so the evaluation of the affinity and reversibility was possible only analyzing and comparing the differences in the intensities of some bands between one spectrum to the others. A variation in the intensity and the width of the bands at 2938, 1604, 1507, 1460, 1324, 1118 and 1033 cm^{-1} can be observed by comparing the spectra before and after the treatment. The variation can be due to the overlapping of the lignin bands with those of the consolidant. This behavior is consistent with the absorption of the product on the lignin sample. Moreover, there are no significant variations in the spectrum recorded after the reversibility test and it can be due to a modification in the solubility of the consolidant related to the possibility of the allyl groups to perform cross-linking reactions.

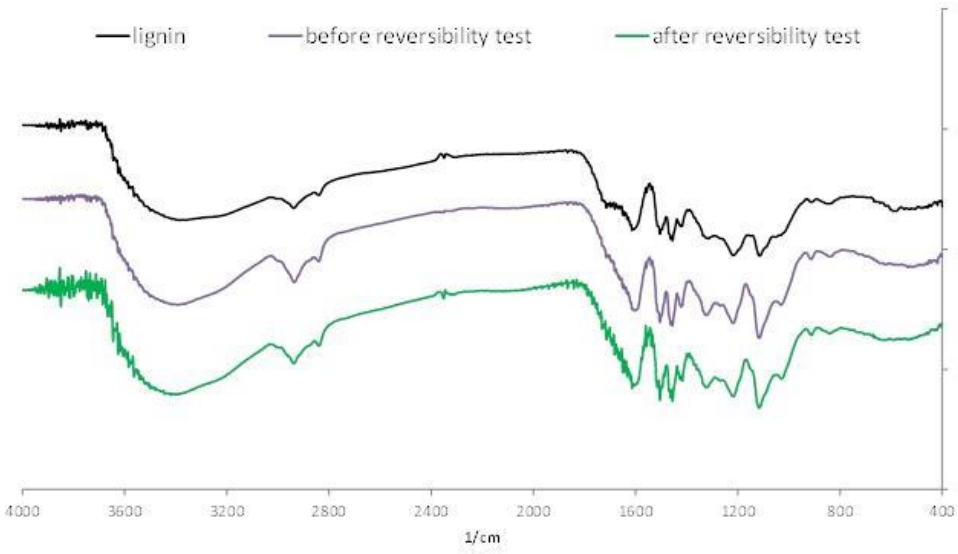

Figure 65 FT-IR spectra related to the affinity and reversibility tests performed on lignin samples using the allyl α,α'-trehalose/vinyl alcohol copolymer

On the contrary, the comparison between the spectra of the lignin treated with the oligoamides and that of untreated lignin was easier because in all the spectra recorded after the treatment the typical bands of the amidic group (C=O stretching at about 1650 cm^{-1} and N-H bending at 1550 cm^{-1}) are visible. Therefore, the good affinity of oligoamides was easily demonstrated. The reversibility tests show that the reversibility of the oligoamides was in general higher with respect to that of the allyl α,α'-trehalose/vinyl alcohol copolymer, even if for a consolidant which has penetrated into the wood is not complete anyway. Moreover, the extent of the reversibility is different for the different oligoamides on the basis of their solubility in water and of their tendency to form crystals. In particular, among the oligoamides, the oligo ethylene-L-tartaramide shows the highest reversibility, while the oligo esamethylene-L-tartaramide has the lowest (**Figure 66**, **Figure 67**, **Figure 68**).

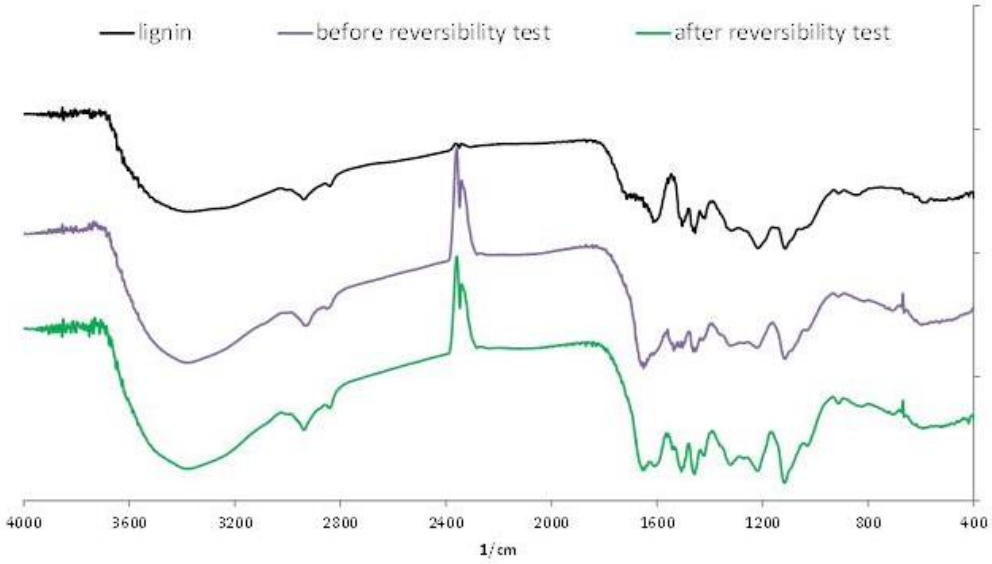

Figure 66 FT-IR spectra related to the affinity and reversibility tests performed on lignin samples using the oligo ethylene-L-tartaramide

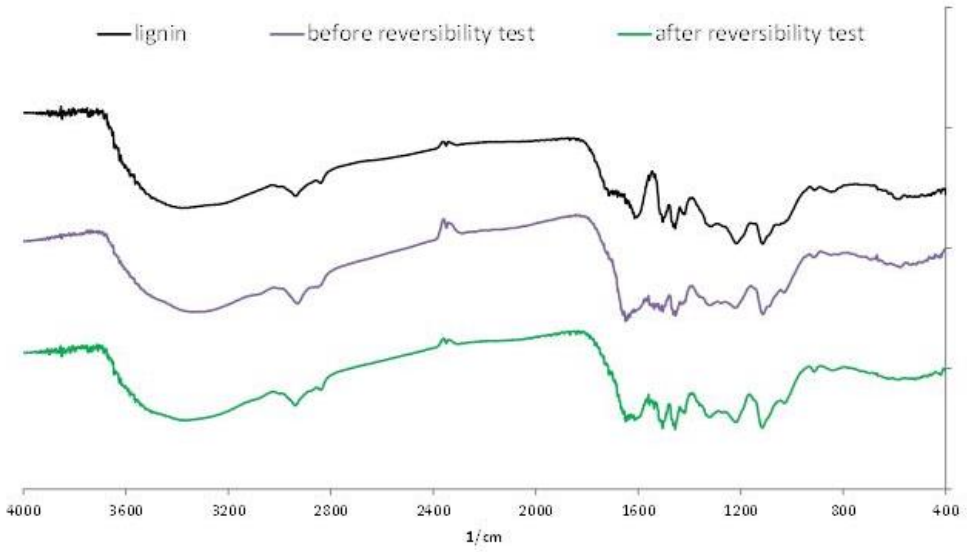

Figure 67 FT-IR spectra related to the affinity and reversibility tests performed on lignin samples using the copolymer between ethylenediamine, adipic acid and tartaric acid

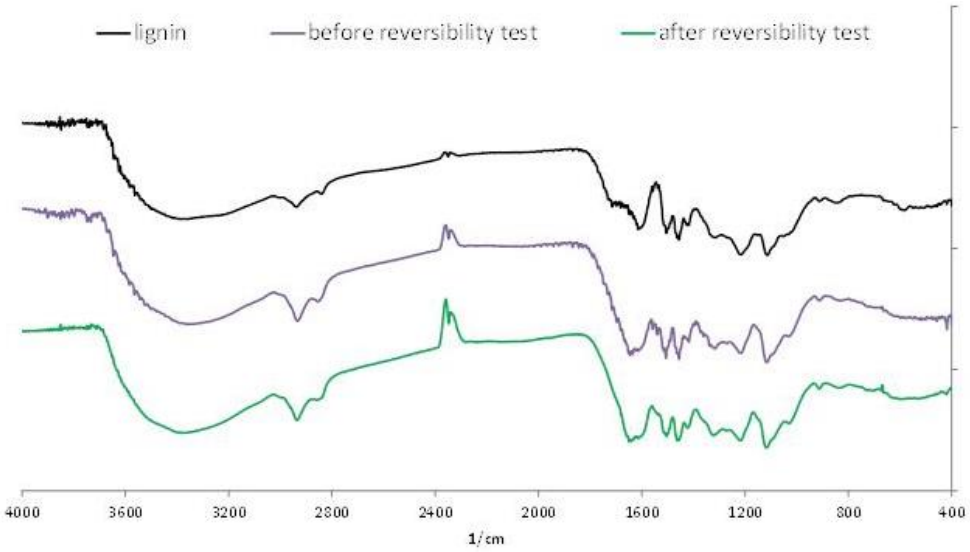

Figure 68 FT-IR spectra related to the affinity and reversibility tests performed on lignin samples using the oligo esamethylene-L-tartaramide

After having demonstrated that all the products have good affinity for a degraded wood which contains a high amount of lignin, the treatment on

real archaeological waterlogged wood samples was performed. For each consolidant, 5 initial cubic samples (volume 1 cm^3) were used to perform the test. Four of them were *Quercus* samples (less degraded wood) and one was a *Fraxinus* sample (more degraded wood). As a modification to the previously used diagnostic protocol[100,101], in this research the initial samples were divided in half so as to have for each treated half a corresponding other untreated half (used as control sample). This was done to evaluate the role of the intrinsic inhomogeneity of the degraded wood. Therefore, the 5 initial cubic samples were divided and one half was immersed in 3.5 mL of the solution of the chosen consolidant while the other half was immersed in 3.5 mL of deionized water (**Figure 69**).

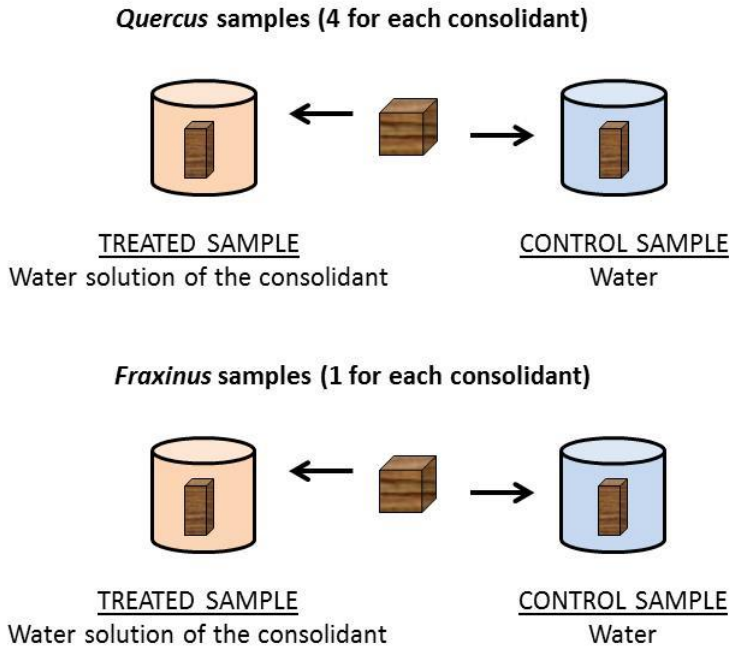

Figure 69 Preparation of the samples used in the test

The treatment was performed by keeping all the treated and control samples in a climate-controlled room at 20°C for 48 days (**Figure 70**). In **Table 8** the set-up of the treatment is reported. The weights and the volumes of all the treated samples were evaluated at the end of the treatment using respectively an analytical balance and the water displacement method, a procedure based on the Archimedes' principle (see paragraph 6.4.1.5).

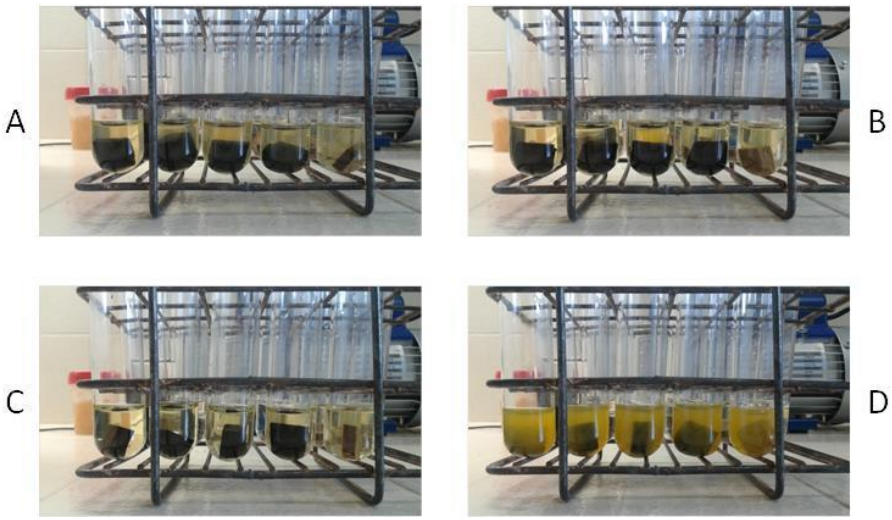

Figure 70 Treatment of the wooden samples (**A** samples treated with allyl α,α'-trehalose/vinyl alcohol copolymer, **B** samples treated with oligo ethylene-L-tartaramide, **C** samples treated with copolymer between ethylenediamine, adipic acid and tartaric acid, **D** samples treated with oligo esamethylene-L-tartaramide)

Table 8

Consolidant	***Quercus* samples**		***Fraxinus* samples**	
	Treated half	**Untreated half (control sample)**	**Treated half**	**Untreated half (control sample)**
allyl α,α'-trehalose/vinyl alcohol copolymer	1, 2, 3, 4	1c, 2c, 3c, 4c	21F	21Fc
oligo ethylene-L-tartaramide	5, 6, 7, 8	5c, 6c, 7c, 8c	22F	22Fc
copolymer between ethylenediamine, adipic acid and tartaric acid	9, 10, 11, 12	9c, 10c, 11c, 12c	23F	23Fc
oligo esamethylene-L-tartaramide	13, 14, 15, 16	13c, 14c, 15c, 16c	24F	24Fc

After the treatment, according to the international technical standard UNI ISO 483[157] the samples were dried by keeping them in a closed system which was balanced to decreasing values of relative humidity (**Figure 71**). This progressive decrease of relative humidity allowed a gradual reaching of the hygroscopic equilibrium and reduced the physical-mechanical risks for the samples. For all the duration of the procedure, a beaker containing xylene was present inside the system to prevent microbiological attacks. The weights of the specimens treated with the different consolidants were evaluated at each relative humidity value used during the drying procedure (100%, 86%, 65%). Finally, according to the standard UNI ISO 3130[158] the last step consisted in drying the samples in an oven. Actually, the standard provides for a drying temperature of 104°C, which corresponds to a value of relative humidity of 0% (anhydrous state). However, in this test a temperature of 50°C was used in order to be not too above the T_g of the consolidants. The weights and the volumes of the samples which were evaluated after this step were used together with those which had been evaluated soon after the treatment to obtain some physical properties as the maximum water content (MWC), the basic density (ρ_b) and the volumetric shrinkage (β_v), which will be discussed in detail later.

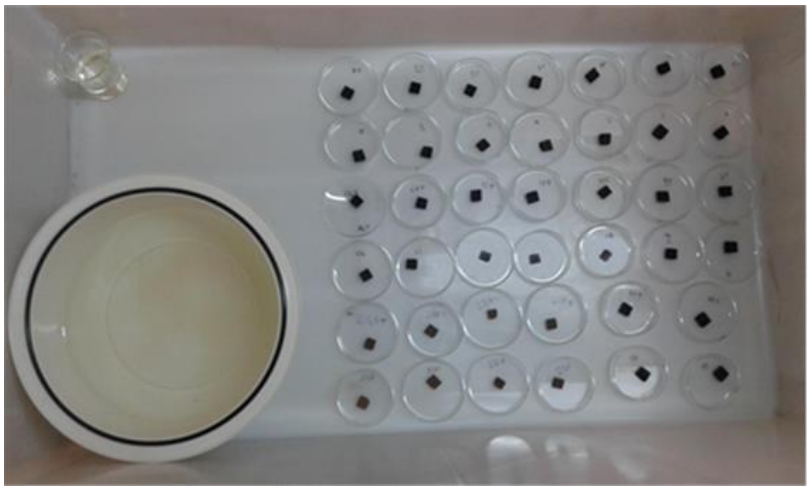

Figure 71 Closed system used to dry the samples

Then, to assess the penetration ability of the various consolidants inside the wooden samples, FT-IR spectra of the treated and control samples were recorded.

The FT-IR spectrum of a *Quercus* control sample (1c) was compared with that of one treated *Quercus* sample for each consolidant (samples 1, 7, 12, 14). The *Quercus* treated samples were cut into two halves in order to record an FT-IR spectrum from the external section and one from the internal section. Therefore, the presence of the consolidant in the treated samples was verified by comparing the spectra of the internal and external sections with the spectrum of the control sample.

As regard the *Fraxinus* wood, the treated samples were too thin to be cut so the identification of the internal and the external sections was not possible. Therefore, the presence of the consolidant in these samples was verified by comparing the spectrum of the control sample (21Fc) with that of one treated *Fraxinus* sample for each consolidant (samples 21F, 22F, 23F, 24F) without the separation in internal and external section.

Concerning the allyl α,α'-trehalose/vinyl alcohol copolymer, in **Figure 72** the FT-IR spectra related to the *Quercus* wood are reported. In the spectrum of the treated sample the presence of the consolidant in the external section is confirmed by the significant variation of the intensity of the bands at 3380, 2900 and 1650 cm^{-1} and also by the increasing in the complexity of the group of overlapping bands between 1200 and 1000 cm^{-1} with respect to the spectrum of the control sample. The penetration of the consolidant is confirmed by the presence of its characteristic bands in the spectra of both the external and the internal sections. A similar behavior was observed for the *Fraxinus* wood, even if the product appears to be penetrated less (**Figure 73**). For both types of wood, the presence of the consolidant is confirmed also by the observation of the treated samples with the digital microscope because it can be seen on the surface but also inside the vessels, where it forms filamentous aggregates (**Figure 74**).

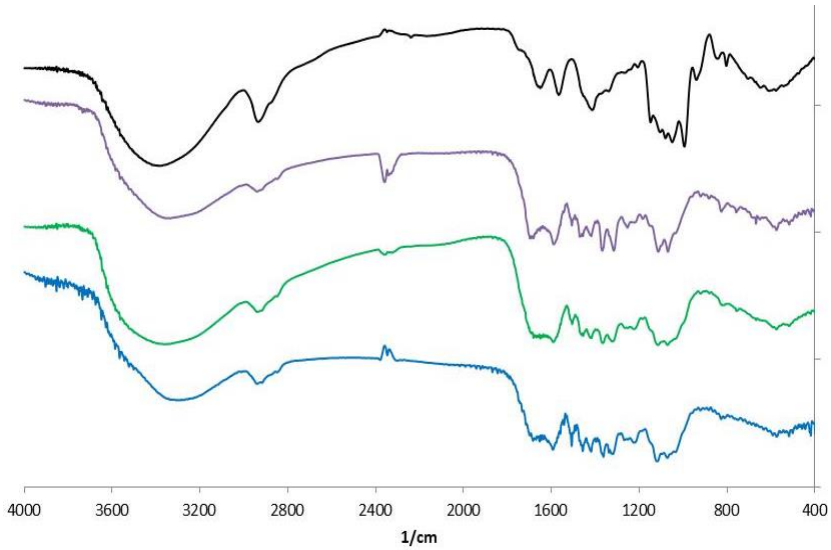

Figure 72 FT-IR spectra of the *Quercus* wood treated with allyl α,α'-trehalose/vinyl alcohol copolymer (black line consolidant, purple line control sample 1c, green line external section of treated sample 1, blue line internal section of treated sample 1)

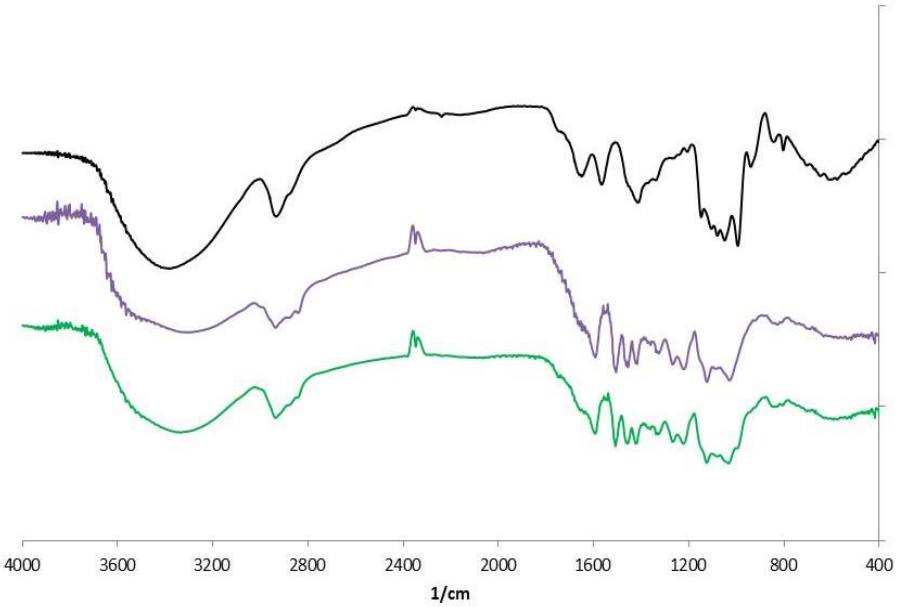

Figure 73 FT-IR spectra of the *Fraxinus* wood treated with allyl α,α'-trehalose/vinyl alcohol copolymer (black line consolidant, purple line control sample 21Fc, green line treated sample 21F)

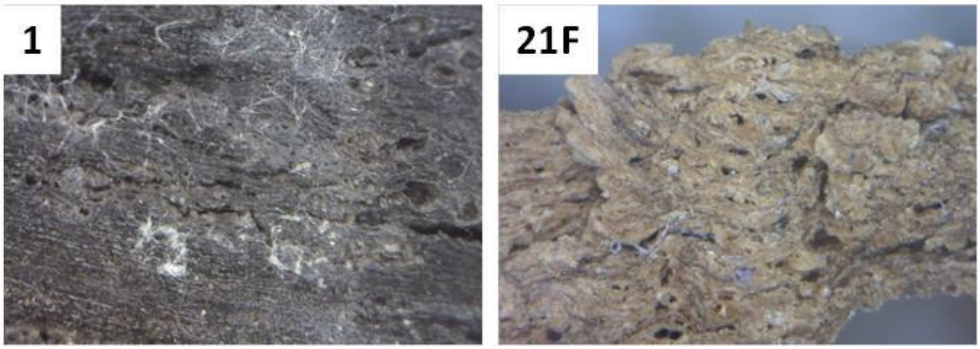

Figure 74 Digital microscope photos of the surfaces of the samples treated with allyl α,α'-trehalose/vinyl alcohol copolymer (**1** *Quercus*, **21F** *Fraxinus*)

As regards the three oligoamides, their presence in the *Quercus* treated samples and their penetration ability are confirmed by the bands at 1650 and 1540 cm^{-1} and by the increasing of the intensity of the bands at about 3300, 2900, 1130 and 1070 cm^{-1} (**Figure 75**, **Figure 78**, **Figure 81**). The same results were obtained also for the *Fraxinus* treated samples, in which the presence of the consolidant is confirmed by the bands at 1650, 1540 and 1050 cm^{-1} (**Figure 76**, **Figure 79, Figure 82**). Finally, another confirmation was obtained from the observation of the treated samples with the digital microscope (**Figure 77**, **Figure 80**, **Figure 83**). In particular, as regards the copolymer between ethylenediamine, adipic acid and tartaric acid some little crystals are visible inside the porosity of the samples of both wood types, while filaments are present especially on *Fraxinus*. Finally, the oligo esamethylene-L-tartaramide forms dark orange crystals visible to the naked eye on the surface of the *Quercus* samples, altering the aspect of the material. On *Fraxinus* samples, on the contrary, the presence of the consolidant gives the surface a translucent appearance, characterized in some points by the presence of some filaments.

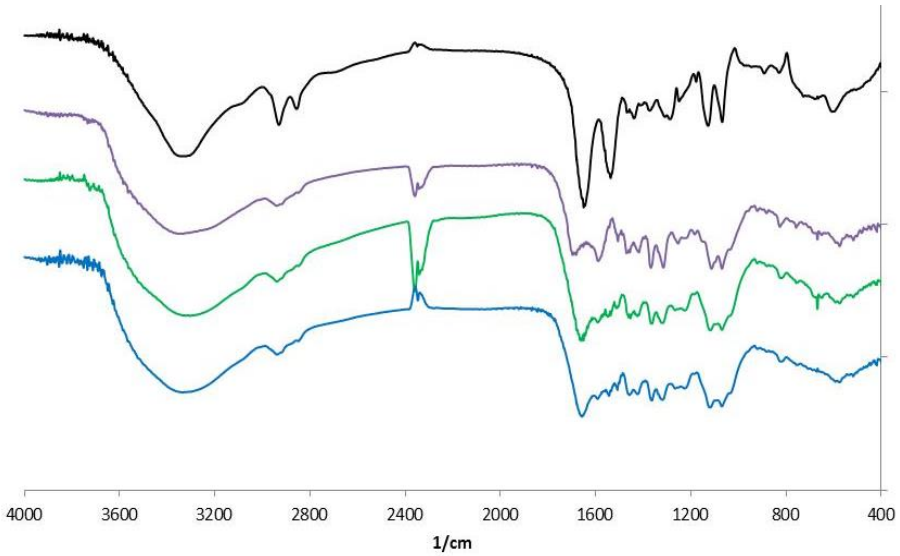

Figure 75 FT-IR spectra of the *Quercus* wood treated with oligo ethylene-L-tartaramide (black line consolidant, purple line control sample 1c, green line external section of treated sample 7, blue line internal section of treated sample 7)

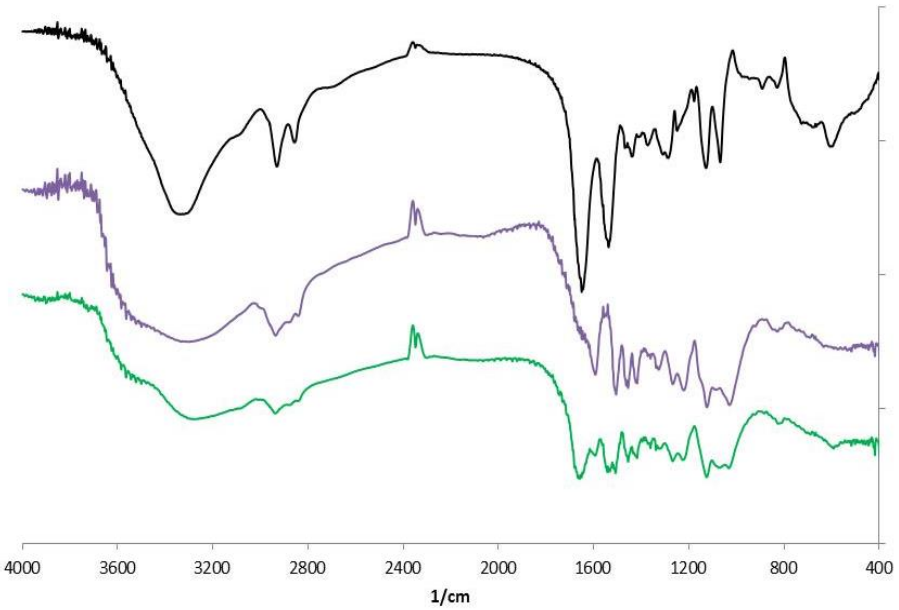

Figure 76 FT-IR spectra of the *Fraxinus* wood treated with oligo ethylene-L-tartaramide (black line consolidant, purple line control sample 21Fc, green line treated sample 22F)

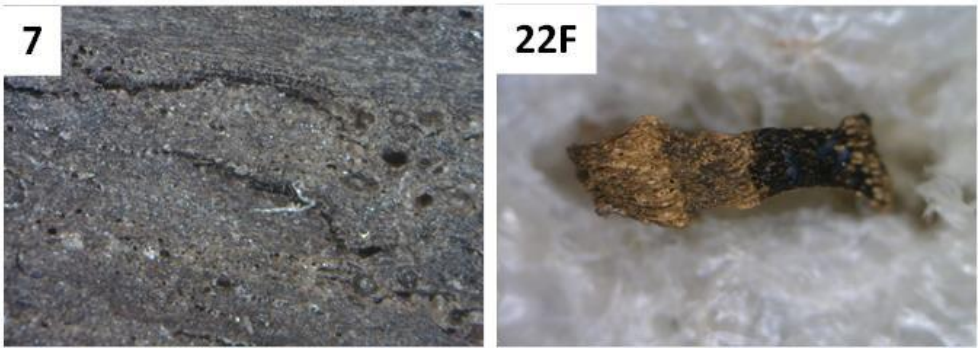

Figure 77 Digital microscope photos of the surfaces of the samples treated with oligo ethylene-L-tartaramide (**7** *Quercus*, **22F** *Fraxinus*)

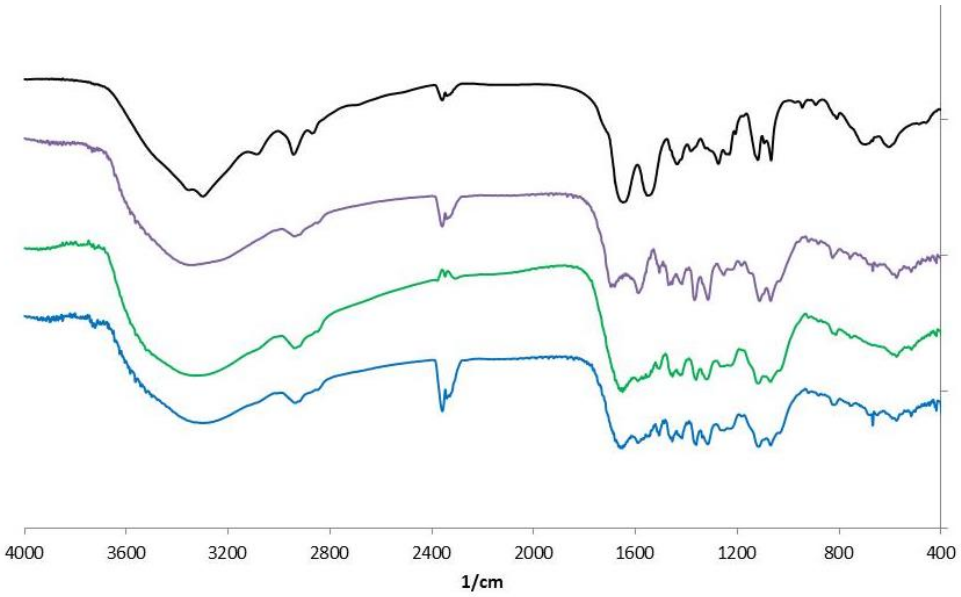

Figure 78 FT-IR spectra of the *Quercus* wood treated with copolymer between ethylenediamine adipic acid and tartaric acid (black line consolidant, purple line control sample 1c, green line external section of treated sample 12, blue line internal section of treated sample 12)

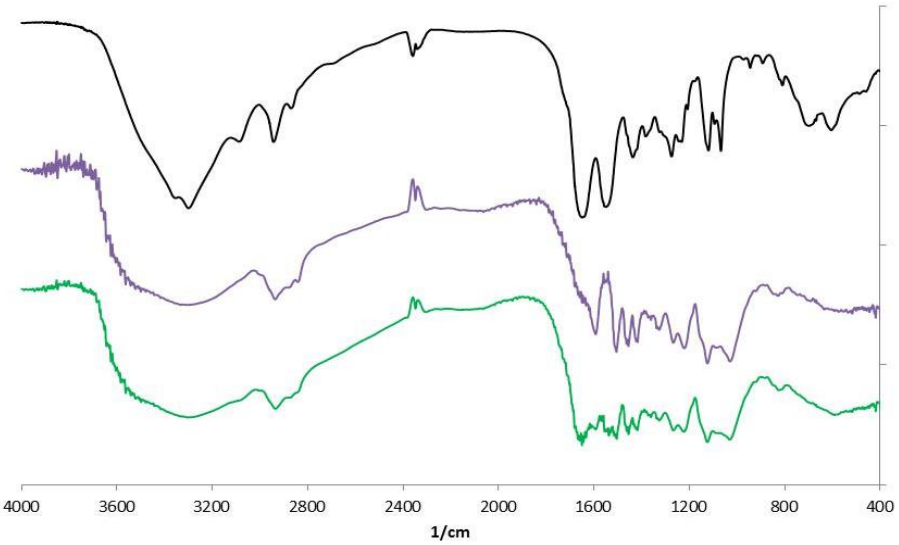

Figure 79 FT-IR spectra of the *Fraxinus* wood treated with copolymer between ethylenediamine adipic acid and tartaric acid (black line consolidant, purple line control sample 21Fc, green line treated sample 23F)

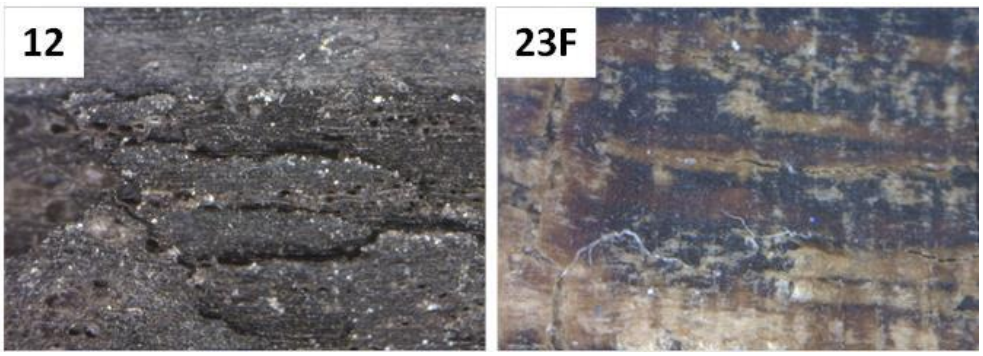

Figure 80 Digital microscope photos of the surfaces of the samples treated with copolymer between ethylenediamine adipic acid and tartaric acid (**12** *Quercus*, **23F** *Fraxinus*)

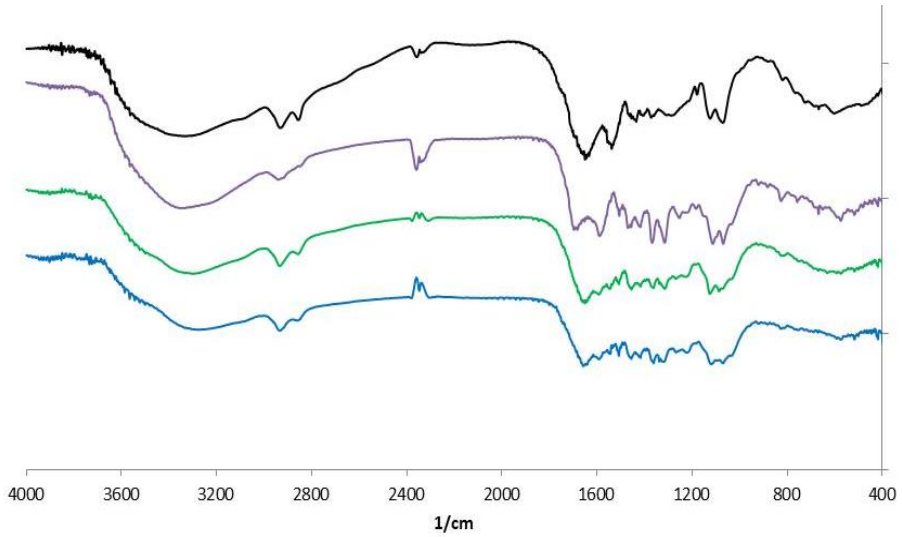

Figure 81 FT-IR spectra of the *Quercus* wood treated with oligo esamethylene-L-tartaramide (black line consolidant, purple line control sample 1c, green line external section of treated sample 14, blue line internal section of treated sample 14)

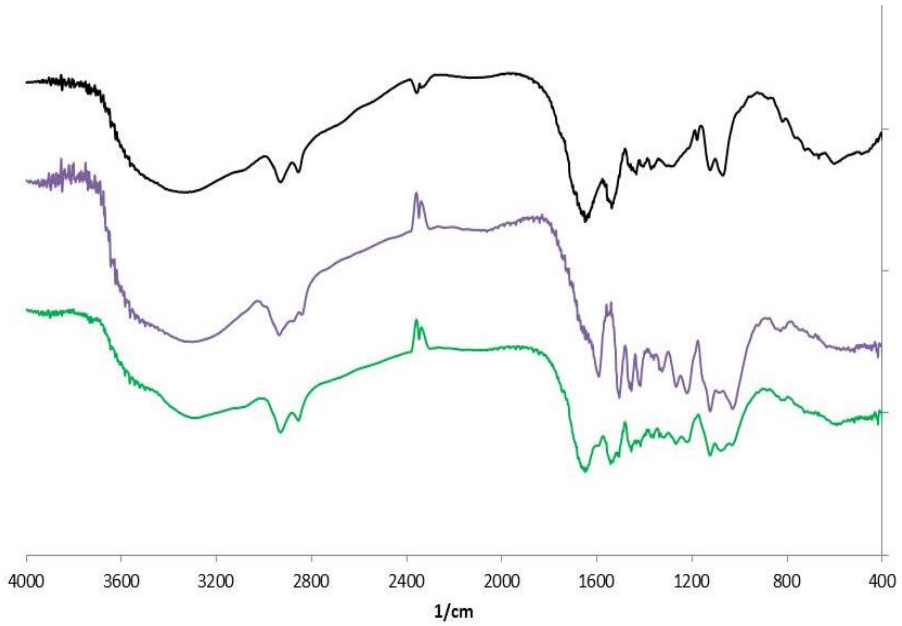

Figure 82 FT-IR spectra of the *Fraxinus* wood treated with oligo esamethylene-L-tartaramide (black line consolidant, purple line control sample 21Fc, green line treated sample 24F)

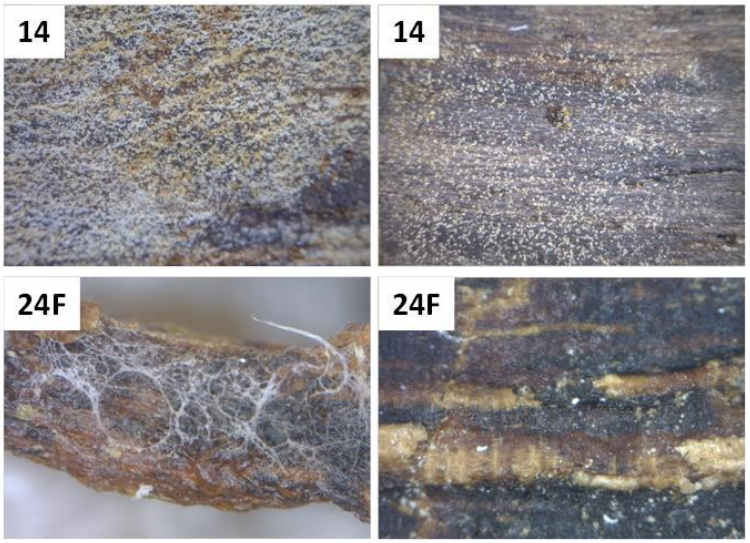

Figure 83 Digital microscope photos of the surfaces of the samples treated with oligo esamethylene-L-tartaramide (**14** *Quercus*, **24F** *Fraxinus*)

To perform the physical characterization of each sample, the weights and the volumes recorded after the treatment (indicated as "green") and after the drying procedure (indicated as "anhydrous") were used. Some physical properties as the maximum water content (MWC), the basic density (ρ_b) and the volumetric shrinkage (β_v) were evaluated following the diagnostic protocol.[100,101]

- **Maximum water content (MWC)**

  The maximum water content is a physical parameter used to characterize the decay of waterlogged archaeological wood and it measures the water content in relation to the mass of the dried wood. Each sample was weighed after the treatment ("green" weight) and at the end of the drying procedure ("anhydrous" weight) and the MWC was evaluated as reported in the experimental section (paragraph 6.4.1.7). In **Table 9** and **Figure 84** the MWC values relative to all the treated samples and their corresponding control samples are reported.

  As regards *Quercus* untreated samples (1c-16c), their MWC values show a considerable variability due to the high intrinsic inhomogeneity of the material. Their average MWC value is 334% ± 39%. Nevertheless, in general the treated samples have a lower MWC value with respect to the

corresponding control samples, except for samples 2 and 2c for which the result can have been altered by the presence of a knot (**Figure 85**).

Table 9 MWC values of the treated and the control samples

CONSOLIDANT	TREATED SAMPLES				CONTROL SAMPLES			
		MWC (%)	AVERAGE MWC (%)	σ		MWC (%)	AVERAGE MWC (%)	σ
allyl α,α'-trehalose/vinyl alcohol copolymer	1	268	300*	34	1c	364	361*	16
	2	310			2c	285		
	3	335			3c	344		
	4	298			4c	376		
oligo ethylene-L-tartaramide	5	281	275	34	5c	321	340	26
	6	315			6c	369		
	7	233			7c	315		
	8	271			8c	356		
copolymer between ethylenediamine adipic acid and tartaric acid	9	353	278	50	9c	439	337	69
	10	252			10c	291		
	11	249			11c	308		
	12	258			12c	310		
oligo esamethylene-L-tartaramide	13	242	222	30	13c	312	316	9
	14	239			14c	329		
	15	228			15c	314		
	16	178			16c	308		
allyl α,α'-trehalose/vinyl alcohol copolymer	21F	691			21Fc	983		
oligo ethylene-L-tartaramide	22F	653			22Fc	972		
copolymer between ethylenediamine adipic acid and tartaric acid	23F	776			23Fc	946		
oligo esamethylene-L-tartaramide	24F	642			24Fc	1016		
* Values calculated excluding samples 2 and 2c								

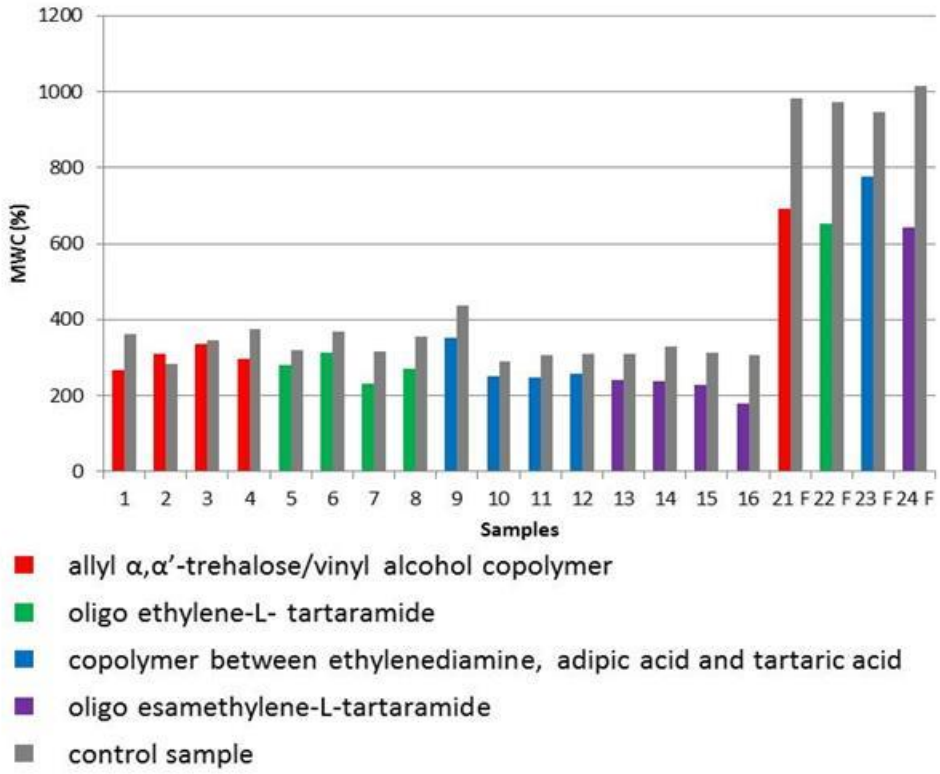

Figure 84 Maximum water content of the treated and the control samples

Figure 85 Knot in the sample 2c

The lower MWC values of the treated samples compared to those of the control samples are consistent with the presence of the consolidant. After the penetration, the consolidant substitutes the water molecules that, due to the degradation of the cellulosic component, have created

secondary interactions with the residual components of the wood (paragraph 1.2.3). This substitution results in a reduction of the MWC of the treated wood.

The values obtained for *Fraxinus* control samples are considerably higher (average MWC 979% ± 29%) because these sample are more degraded compared to *Quercus* ones. In general, the more the wood is degraded the less cellulose and hemicelluloses are present inside its structure, consequently increasing the porosity of the material. This allows a greater amount of water to penetrate and create secondary interactions with the residual components of the wood (paragraph 1.2.3) Nevertheless, as in the case of *Quercus* wood, the values obtained for *Fraxinus* treated samples are lower than that of the corresponding control samples and this confirms the presence of the consolidant. In particular, the percentage decrease of the MWC values for the treated *Fraxinus* samples are 37% for oligo esamethylene-L-tartaramide, 33% for oligo ethylene-L-tartaramide, 30% for the allyl α,α'-trehalose/vinyl alcohol copolymer and 18% for the copolymer between ethylenediamine adipic acid and tartaric acid.

To evaluate the action of the consolidants on *Quercus* wood samples reducing the error due to the inhomogeneity of the material, the arithmetic averages of the MWC values of the treated samples were evaluated and compared with the arithmetic averages of the MWC values of their corresponding control samples (**Table 9**, **Figure 86**). Samples 2 and 2c were excluded from the calculation because, due to the presence of the knot, their MWC values are outliers that would distort the average. Also other samples, like 9 and 9c, could increase the error because they show very different MWC values with respect to the other *Quercus* samples. However, they were not excluded from the calculation of the average because the decrease of MWC due to the presence of the consolidant results comparable with those observed for the other *Quercus* treated samples. Nevertheless, results like those of samples 2, 2c, 9 and 9c confirm the variability of the wood characteristics and the need for a critical analysis of the collected data.

After the evaluation of the arithmetic averages, it was possible to quantify the percentage decrease of the MWC values for the treated *Quercus* samples with respect to the MWC of the control samples. These percentage decreases are 30% for oligo esamethylene-L-tartaramide, 19% for oligo ethylene-L-tartaramide, 18% for the copolymer between ethylenediamine, adipic acid and tartaric acid and 17% for the allyl α,α'-trehalose/vinyl alcohol copolymer.

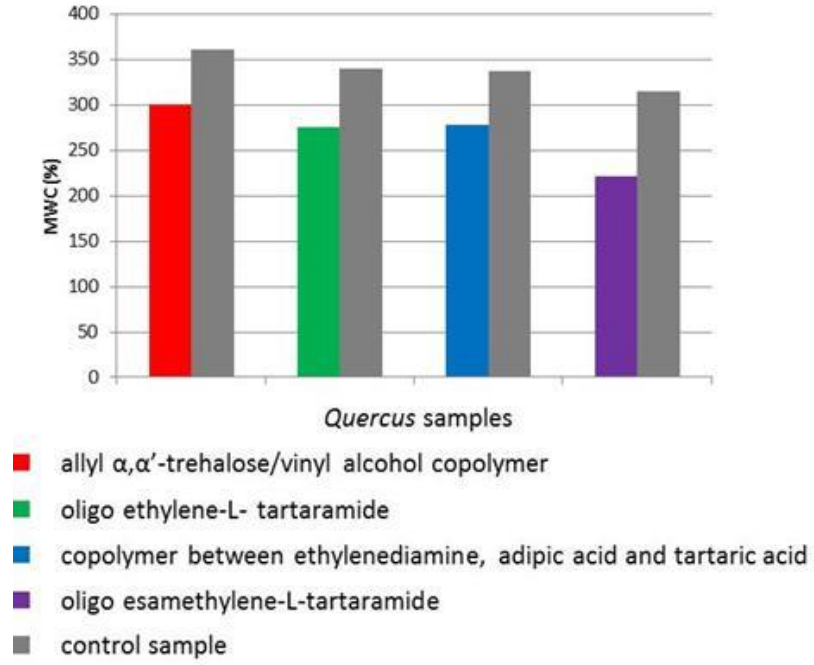

Figure 86 Average maximum water content values of the treated and the control samples (*Quercus* wood)

Considering the maximum water content, the oligo esamethylene-L-tartaramide gave the best results for *Quercus* wood, while oligo esamethylene-L-tartaramide, oligo ethylene-L-tartaramide and allyl α,α'-trehalose/vinyl alcohol copolymer gave good results for *Fraxinus* wood.

Concerning the allyl α,α'-trehalose/vinyl alcohol copolymer, the better results obtained for the *Fraxinus* samples compared to those obtained when the same consolidant was used for the treatment of the *Quercus* samples can be explained considering that the more severe degradation

of *Fraxinus* wood has made it more porous. In general, the high porosity promotes the penetration of consolidants with higher molecular weight inside the sample and the allyl α,α'-trehalose/vinyl alcohol copolymer has the highest molecular weight between the tested consolidants. Therefore, it has penetrated better in *Fraxinus* wood compared to *Quercus*, giving better results in terms of MWC decrease.

- **Basic density (ρ_b)**

The basic density is the ratio between the "anhydrous" weight of the wood, obtained after the drying procedure, and the "green" volume, obtained soon after the treatment (paragraph 6.4.1.7). It can be used as an indicator of the residual wood or of the presence of a consolidant. The values obtained for the basic density of all the treated and control samples are reported in **Table 10** and **Figure 87**. As regards the control samples, the values obtained both for *Quercus* and *Fraxinus* are typical of a degraded wood, even if those for *Quercus* are higher because it is less degraded compared to *Fraxinus*. Moreover, as previously said for MWC, the values of basic density for the control samples reflect the inhomogeneity of the *Quercus* wood since they fluctuate from 0.211 to 0.302 g/cm^3 (average value 0.268 ± 0.024 g/cm^3). The average value for *Fraxinus* control samples is 0.107 ± 0.003 g/cm^3. The typical basic density values for recent wood are generally above 0.500 g/cm^3, even if they strongly depends on the species, the storage conditions and the provenance of the wood. For example, the basic density of a recent *Quercus* wood measured at the GESAAF (Gestione dei Sistemi Agrari, Alimentari e Forestali) department is 0.700 g/cm^3, while as regards recent *Fraxinus* in the literature there can be found values between 0.570 and 0.940 g/cm^3.

Considering the treated samples, all the values are higher compared to those of their corresponding control samples, except values obtained for the sample 2, because its control sample contains a knot. This general increase of the basic density is consistent with the penetration of the consolidant inside the wood structure.

With respect to the basic density of the control sample, the percentage increase of the values for the treated *Fraxinus* samples are 31% for oligo ethylene-L-tartaramide, 29% for oligo esamethylene-L-tartaramide, 21% for allyl α,α'-trehalose/vinyl alcohol copolymer and 15% for the copolymer between ethylenediamine, adipic acid and tartaric acid.

Table 10 Basic density values of the treated and the control samples

CONSOLIDANT	TREATED SAMPLES				CONTROL SAMPLES			
		ρ_b (g/cm^3)	AVERAGE ρ_b (g/cm^3)	σ		ρ_b (g/cm^3)	AVERAGE ρ_b (g/cm^3)	σ
allyl α,α'-trehalose/vinyl alcohol copolymer	1	0.324	0.298*	0.03	1c	0.247	0.250*	0.01
	2	0.284			2c	0.302		
	3	0.268			3c	0.262		
	4	0.302			4c	0.240		
oligo ethylene-L-tartaramide	5	0.316	0.320	0.03	5c	0.265	0.262	0.02
	6	0.289			6c	0.249		
	7	0.362			7c	0.283		
	8	0.315			8c	0.251		
copolymer between ethylenediamine adipic acid and tartaric acid	9	0.261	0.318	0.04	9c	0.211	0.268	0.04
	10	0.337			10c	0.300		
	11	0.345			11c	0.283		
	12	0.330			12c	0.277		
oligo esamethylene-L-tartaramide	13	0.343	0.370	0.04	13c	0.275	0.279	0.01
	14	0.351			14c	0.268		
	15	0.363			15c	0.283		
	16	0.422			16c	0.289		
allyl α,α'-trehalose/vinyl alcohol copolymer	21F	0.142			21Fc			
oligo ethylene-L-tartaramide	22F	0.161			22Fc			
copolymer between ethylenediamine adipic acid and tartaric acid	23F	0.132			23Fc			
oligo esamethylene-L-tartaramide	24F	0.145			24Fc			

* Values calculated excluding samples 2 and 2c

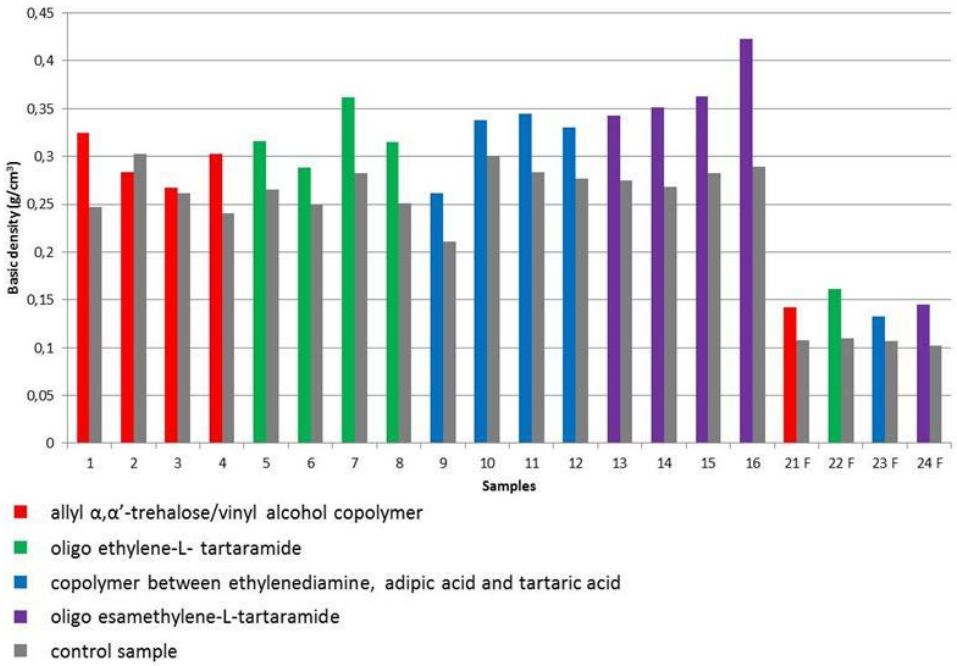

Figure 87 Basic density of the treated and the control samples

To evaluate the action of the consolidants on *Quercus* wood samples reducing the error due to the inhomogeneity of the material, the arithmetic averages of the basic density values of the treated samples were evaluated and compared to the arithmetic averages of the basic density values of the control samples (**Table 10**, **Figure 88**). As it was done for MWC, even in this case the values for the samples 2 and 2c were not considered because they were distorted by the presence of the knot.

With respect to the basic density of the control samples, the percentage increase of the values for the treated *Quercus* samples are 24% for oligo esamethylene-L-tartaramide, 19% for oligo ethylene-L-tartaramide, 17% for allyl α,α'-trehalose/vinyl alcohol copolymer and 16% for the copolymer between ethylenediamine, adipic acid and tartaric acid.

Therefore, for both species the most efficient consolidants are oligo esamethylene-L-tartaramide and oligo ethylene-L-tartaramide, while the

allyl α,α'-trehalose/vinyl alcohol copolymer gave better results for *Fraxinus* than for *Quercus* wood. This behavior can be justified by the different penetration ability of the various consolidants. Nevertheless, for a more comprehensive analysis of the consolidating effectiveness, the different basic density values should be also related to the formation of filamentous aggregates or crystals on the surface of the samples, which were observed in the case of the oligo esamethylene-L-tartaramide.

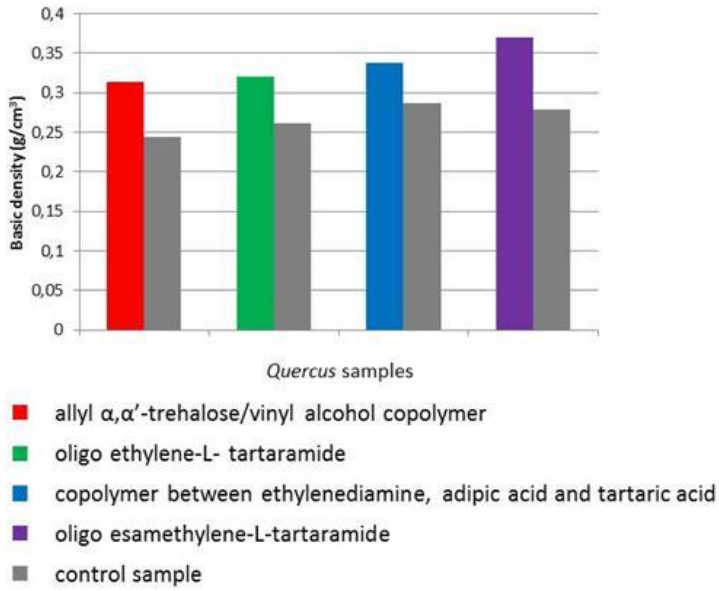

Figure 88 Average basic density values of the treated and the control samples (*Quercus* wood)

- **Volumetric shrinkage (β_v)**

  The last physical property taken in consideration was the volumetric shrinkage. Volumes were not geometrically determined because of the small dimensions and irregular form of the samples, which could produce significant errors. Therefore, the volumes were obtained through the water displacement method, a procedure based on the Archimedes' principle (paragraph 6.4.1.7). In order to have a precise measurement, it is necessary a rapid acquisition of the value before the complete absorption of water. However, in this study very small samples were used and so the evaluation of the volumes was difficult because of the

high water absorption speed and the great influence of other factors, like the formation of surface bubbles. Therefore, the absolute values obtained for the samples using this method cannot be considered quantitatively reliable, but they can be used for a preliminary assessment. To confirm this observation, the volumetric shrinkage of the control samples was evaluated but, as expected, the results show big fluctuations and so cannot be considered significant (**Figure 89**).

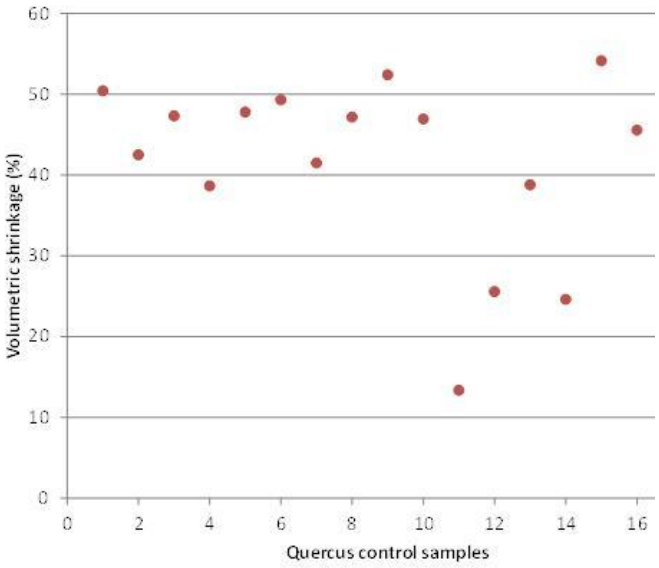

Figure 89 Volumetric shrinkage values of the *Quercus* control samples

Consequently, the volumetric shrinkage was assessed only qualitatively comparing the photos taken with a digital microscope of the treated samples with the photos of the corresponding control samples (**Figure 90**).

The volumetric shrinkage generally increases with the degradation of the wood. Considering the approximate values of shrinkage calculated using the volumes obtained with the water displacement method, the *Fraxinus* control samples have higher shrinkage values (89/90%) compared to the *Quercus* ones (40-50%) because they are more degraded. All those shrinkage values are in turn extremely large if compared to the values

obtained for recent *Quercus* (13.2% *Robur* section or 19.2% *Cerris* section) and recent *Fraxinus* (14.2%).

Considering the qualitative evaluation, all the treated samples have a lower volumetric shrinkage compared to the control samples, some of which were fractured during the drying procedure (e.g. sample 9c in **Figure 90**). This behavior allows to confirm the positive effect of the consolidants on the dimensional stabilization of the wood.

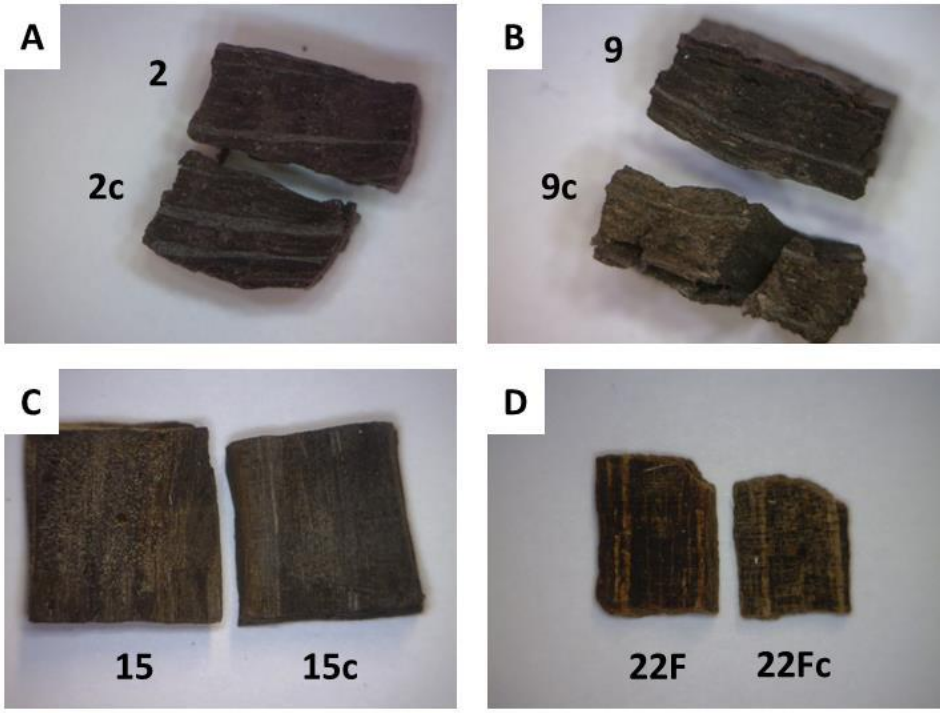

Figure 90 Qualitative evaluation of the volumetric shrinkage (**A** allyl α,α'-trehalose/vinyl alcohol copolymer, **B** copolymer between ethylenediamine adipic acid and tartaric acid; **C** oligo esamethylene-L-tartaramide; **D** oligo ethylene-L-tartaramide)

4.5.2 Antifungal treatment

The antifungal properties of the nanocomposite obtained by grafting allyl α,α'-trehalose/vinyl acetate copolymer on functionalized TiO_2 anatase

nanoparticles were evaluated by performing two tests on wooden samples exposed to the fungus *Trametes Versicolor*.

The samples were taken from recent European beech (*Fagus Selvatica L.*), a wood species that is well known for its low natural durability and high susceptibility to fungi and bacteria, which make it one of the most suitable species to test the performances of antimicrobial or antifungal products. Samples were prepared using a material free of any previous biological alteration. All specimens were obtained by cutting the wood along the longitudinal faces parallel to the grain up to a final size of 10x20x2 mm. Before the treatment, the wood samples were equilibrated at 20°C and 65% relative humidity inside a desiccator, which contained also xylene as inhibitor of fungal activity.

Treatment with the nanocomposite containing the not grafted polymer

In the first test both the acetone soluble and insoluble fractions of the nanocomposite were used, even if the soluble fraction contains only polymer not grafted on the nanoparticles. Indeed, in a previous study performed in our laboratory regarding the application of some oligoamides/TiO_2 nanocomposites, the presence of a fraction of free polymer did not affect the antifungal activity of the TiO_2 nanoparticles.[152]

Therefore, a dispersion in water/acetone 1:1 of the nanocomposite containing also free allyl α,α'-trehalose/vinyl acetate copolymer was applied by brushing on all the faces of 16 wooden samples. After the treatment, the samples were dried in an oven for 2 days at 35°C and observed with a digital microscope to check the uniformity of the applied film. The treated samples appeared covered by a white layer consisting for the most part of free polymer. Indeed, the average w/w ratio between the fraction soluble in acetone (free polymer) and the fraction insoluble in acetone (grafted polymer and nanoparticles) is 3. Other 16 samples were left untreated.

Then, all the treated and untreated samples were placed on the *Trametes Versicolor* cultures, using a small sterile net to hold them up in order to avoid the direct contact with the mycelium. 4 samples (2 treated and 2 untreated) were placed on each of the 8 plates. Then 4 plates were placed under a lamp

end exposed to the UV radiation (365 nm), while the other 4 plates were kept in the dark (**Figure 91**). The experiment lasted 3 weeks and the exposition was carried out so as to simulate the behavior of the sunlight. In particular, for the whole duration of the test the lamp was kept lit for 12 hours and turned off for 12 more using a timer. The samples exposed to the UV light have been turned upside down every day in the middle of the illumination period, in order to expose both sides to the radiation during the experiment.

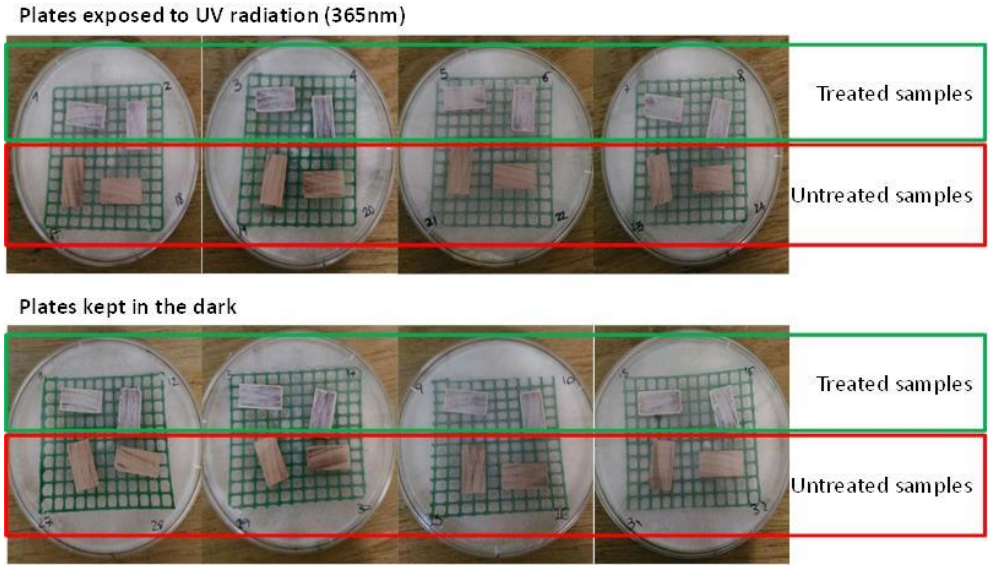

Figure 91 Set-up at the beginning of the first test

After 12 days all the samples were analyzed with the digital microscope (**Figure 92**). It is worth noting that the mycelium of the *Trametes Versicolor* is present on all the treated and untreated samples. In particular, it is visible also on the treated samples exposed to the UV light, even if the nanocomposite was supposed to inhibit the fungal growth thanks to the presence of the TiO_2 anatase nanoparticles. This unsatisfactory result was attributed to the presence of an excessive quantity of allyl α,α'-trehalose/vinyl acetate copolymer, in particular in the "free form", which can have neutralized the antifungal effect of the nanoparticles by incorporating them in a layer of polymer so thick as to reduce the absorption of light required to activate them. Furthermore, the presence of the free copolymer

can promote the fungal growth because of the susceptibility of the α,α'-trehalose and the vinyl acetate to the fungal attack.[159-160]

The excessive quantity of free allyl α,α'-trehalose/vinyl acetate copolymer may also be the cause of the formation of a sticky dark orange exudate under all the treated samples kept in the dark and also under some of those exposed to the UV light. This exudate was already visible after 6 days since the beginning of the test.

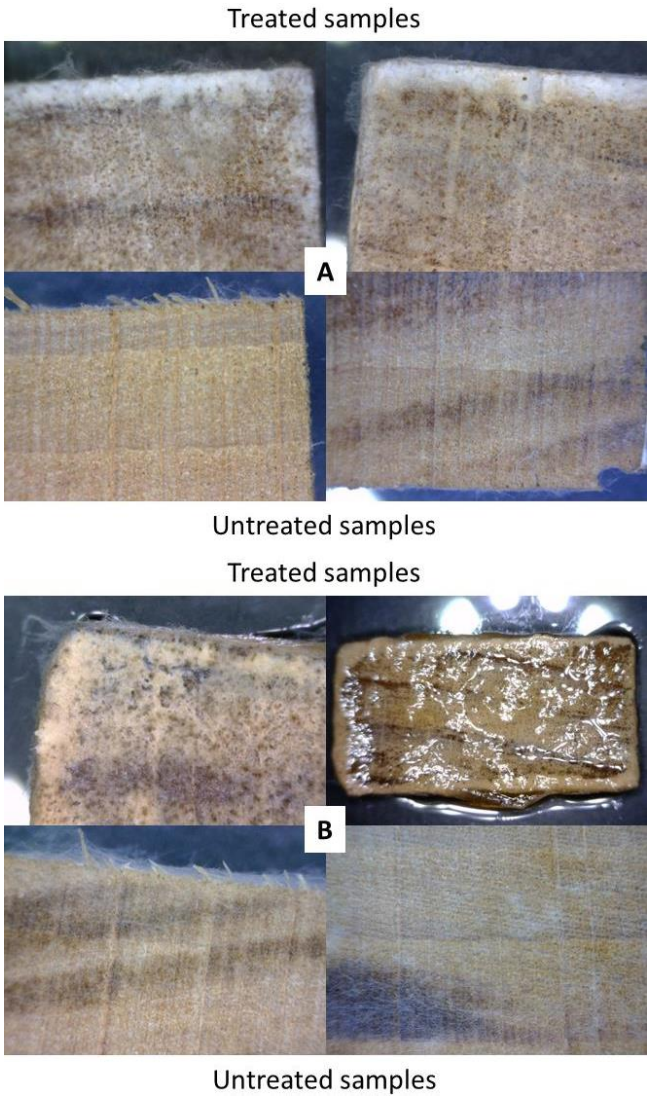

Figure 92 Photos of some samples after 12 days (**A** samples exposed to the UV light, **B** samples kept in the dark)

At the end of the experiment (after 3 weeks), photos of all samples were taken with the digital microscope (**Figure 93**) and they confirm the fungal growth on the all samples regardless the presence of the nanocomposite and the exposition to the UV radiation.

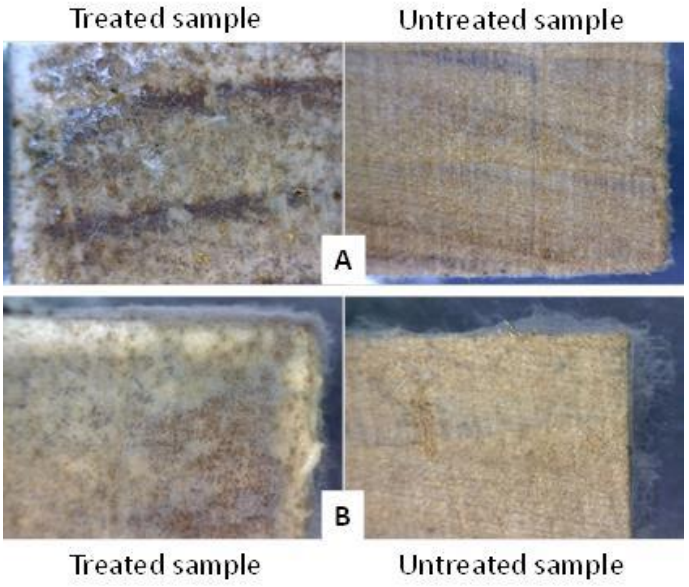

Figure 93 Photos of some samples at the end of the treatment (**A** samples exposed to the UV light, **B** samples kept in the dark)

Treatment with the nanocomposite without the not grafted polymer

To overcome the problem of the excessive amount of free polymer on the samples, in the second test only the fraction insoluble in acetone of the nanocomposite containing allyl α,α'-trehalose/vinyl acetate copolymer grafted on TiO_2 nanoparticles was used. Moreover, 2-propanol was used to disperse the product instead of the mixture water/acetone because, being more volatile than water, it allows the samples to dry faster without the need to place them in an oven. Furthermore, 2-propanol is also a well-known bacteriostatic, whereas water and humidity generally promote a microbiological attack.

Before the test, a preliminary assessment of the photocatalytic activity of the nanocomposite was performed using the test of the methylene blue. The

methylene blue is commonly used to test the photocatalytic activity of TiO_2 nanoparticles through the study of its photocatalytic decomposition.[161-163] In particular, in this test an aqueous solution of methylene blue was exposed to the UV light (365 nm) both alone and in the presence of the nanocomposite until a discoloration of the solution in the presence of the nanocomposite was observed. **Figure 94** shows that the degradation of the methylene blue started after 30 minutes of exposure and it can be considered almost completed after 60 minutes, while the solution without nanocomposite did not undergo any color variation. In the previous study with oligoamides/TiO_2 nanocomposites[153], the methylene blue was completely decomposed in 20 minutes. This difference can be explained with a lower photoactivity of the nanoparticles in the allyl α,α'-trehalose/vinyl acetate copolymer/TiO_2 nanocomposite.

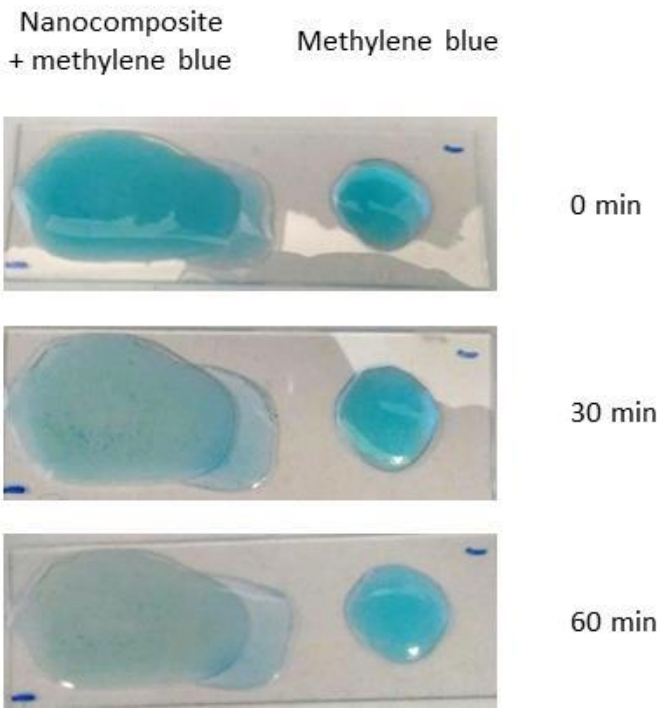

Figure 94 Test of the methylene blue

To test also the resistance of the nanocomposite to photodegradation, a water dispersion of the fraction insoluble in acetone of the nanocomposite was deposited on a Petri dish and dried in an oven. Then, the Petri dish was

exposed to the UV radiation (365 nm). The weight was monitored regularly and, after 58 hours of exposure, an FT-IR spectrum was recorded and compared with that of the product before the irradiation (**Figure 95**). After 58 hours, the weight has increased of about 3 mg probably because of water absorption, while the FT-IR spectrum shows a decrease in the intensity of the characteristics band of the acetate group (C=O stretching at 1736 cm^{-1} and C-O stretching at 1248 cm^{-1}) with respect to the bands of the saccharide structure (1148-994 cm^{-1}). Probably, the UV radiation caused the break of the bond with the acetate group and the increase in the amount of hydroxyl groups on the polymer with a consequent increase in the water absorption capacity. Indeed, the intensity of the bands at 3390 cm^{-1} and 1645 cm^{-1} (related to the presence of humidity) increases in the spectrum after 58 hours compared to that before the exposure.

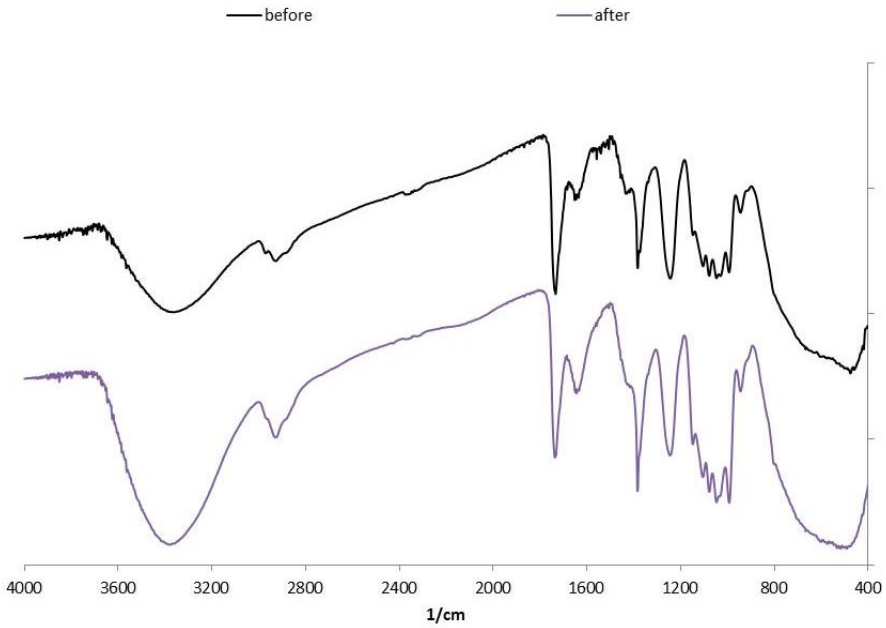

Figure 95 FT-IR spectra of the fraction insoluble in acetone of the allyl α,α'-trehalose/vinyl acetate copolymer/TiO_2 nanocomposite before (black line) and after (purple line) 58 hours of UV exposure

Nevertheless, the dispersion of the nanocomposite was applied by brushing on all the faces of 16 wooden samples. The application was performed after sonication, but the dispersion was unstable and consequently a relatively

large amount of product remained on the bottom of the container (about 42% of the initial quantity of the product). After the treatment, the samples were observed with a digital microscope to check the uniformity of the applied film. The final appearance of the samples was good, with a layer of product homogeneously distributed and a whitening effect not as evident as in the case of the samples used in the first test.

Moreover, a 2-propanol dispersion of TiO_2 anatase nanoparticles with no grafted polymer was used to treat other 8 samples. This was done in order to verify the influence of the presence of the grafted allyl α,α'-trehalose/vinyl acetate copolymer on the antifungal activity of TiO_2 nanoparticles. The application of the dispersion of TiO_2 anatase nanoparticles had the same difficulties described for the application of the nanocomposite, because also this dispersion was not stable and, therefore, less nanoparticles than that provided for the treatment were applied (about 20% less). As regards the final appearance, this treatment had a very evident whitening effect.

Finally, 2 samples were treated only with 2-propanol to check the influence of the solvent on the fungal activity, while 10 other samples were left untreated.

After the treatment all samples were placed on the *Trametes Versicolor* cultures (**Figure 96**) using a small sterile net to hold them up in order to avoid the direct contact with the mycelium. In particular, the following plates were prepared:

- 8 plates containing 2 samples treated with the nanocomposite, 1 sample treated with TiO_2 nanoparticles and 1 untreated sample (4 plates were exposed to the UV light and 4 plates were kept in the dark);
- 1 plate containing 2 samples treated with 2-propanol and 2 untreated samples (kept in the dark).

The experiment lasted 3 weeks and the UV exposition was carried out so as to simulate the behavior of the sunlight. In particular, the lamp was kept lit for 12 hours and turned off for 12 more using a timer for the whole duration of the test. The samples exposed to the UV light have been turned upside

down every day in the middle of the illumination period so as to expose both sides to the radiation during the treatment.

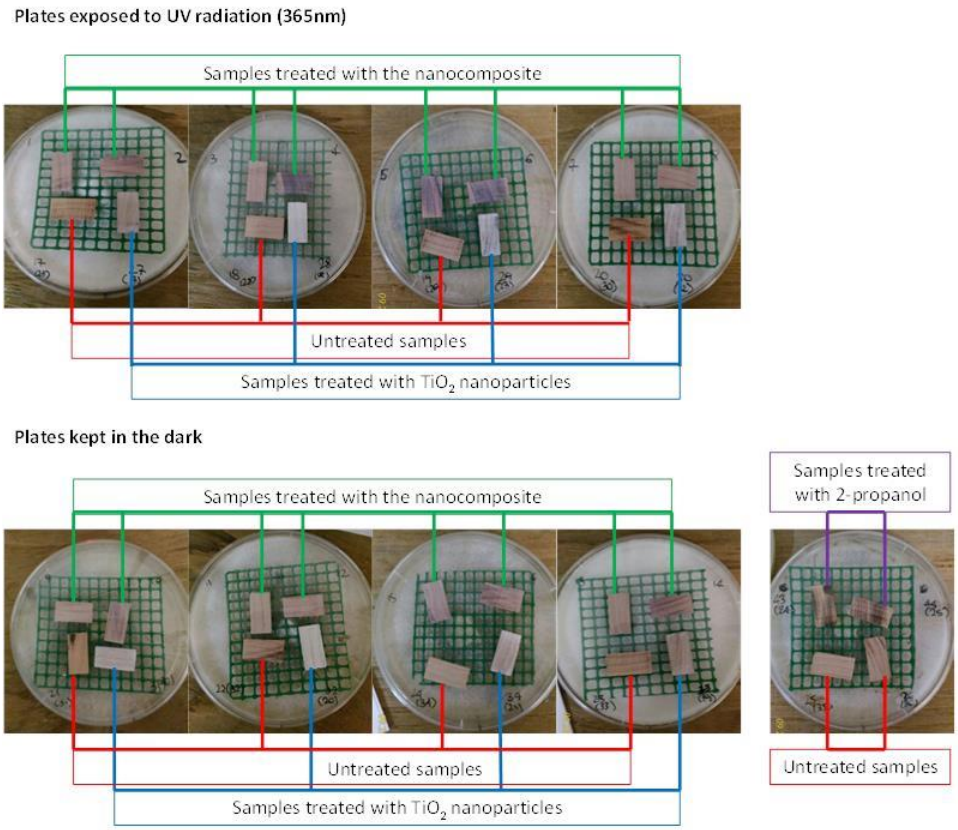

Figure 96 Set-up at the beginning of the second test

After 12 days photos of all samples were taken with the digital microscope (200x). Unlike the previous test, the dark orange sticky exudate did not form. This behavior confirms that the presence of that product was related to the large amount of free polymer on the samples used in the first test. As regards the *Trametes Versicolor*, in the plates kept in the dark the fungus has grown in the same extent on all samples. On the contrary, in the plates exposed to the UV light the presence of the fungus seems to depend on the treatment. In particular, it is visible on some samples treated with the nanocomposite and on some untreated samples, while it is not visible on the samples treated with the TiO_2 nanoparticles. However, this observation was

difficult and in some cases not so reliable because the photos after 12 days were taken keeping the plates closed and so it was not possible to zoom in.

At the end of the experiment (after 3 weeks) photos of all samples were taken with a digital microscope (400x) (**Figure 97**, **Figure 98**) and the following observation can be made:

- The growth of the fungus is visible on all samples except those treated with the TiO_2 nanoparticles and exposed to the UV light.
- Comparing the samples exposed to the UV radiation, the growth on the samples treated with the nanocomposite is lower than that on the untreated samples, while is higher than that on the samples treated with TiO_2 nanoparticles. Therefore, it can be said that to a certain extent the presence of the nanocomposite limits the fungal growth, though the attack is not completely stopped.
- As regard the samples kept in the dark, the fungal growth took place in the same extent on all the samples regardless of the type of treatment (nanocomposite, nanoparticles, 2-propanol or untreated).

Comparing the behavior observed in this test with that observed in the previous study performed with oligoamides/TiO_2 nanocomposites[152], it is worth noting that the ratio between the amounts of organic and inorganic part (polymer and nanoparticles) which are present in the two different nanocomposites is the same. However, the amount of nanoparticles applied per sample in the previous study was higher than that applied in this test (14 mg/sample versus 8 mg/sample) due to the fact that during the treatment about 42% of the initial quantity of the product was lost as precipitate. Therefore, the growth of the fungus observed in this test cannot be caused by a higher amount of polymer grafted on the nanoparticles (because the ratio organic/inorganic part is equal to that of the previous study), but by the lower amount of nanoparticles applied on each sample and by the lower photoactivity of the nanocomposite, as demonstrated by the test of the methylene blue. Furthermore, also the intrinsic susceptibility of the vinyl acetate and of the disaccharide to microbial attack can have influenced the result of this test.

Finally, the plates which had been exposed to the radiation were kept in the dark for 1 week and then photos were taken with the digital microscope (200x). The growth was increased and clearly visible on all the samples, thus confirming that the antifungal activity of the TiO_2 nanoparticles is possible only when exposed to the UV light.

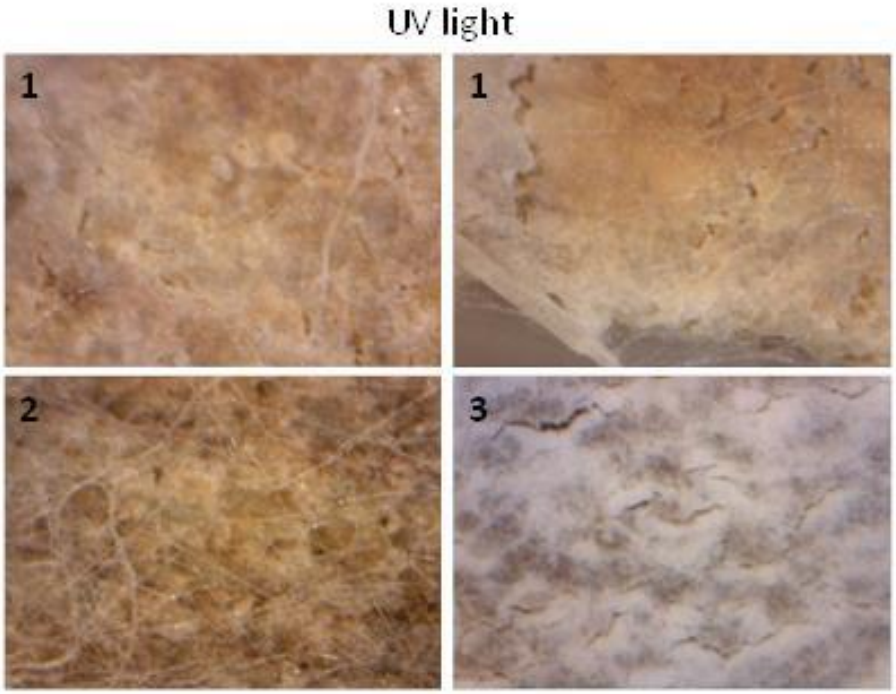

Figure 97 Photos of some samples exposed to the UV light at the end of the treatment (**1** samples treated with the nanocomposite, **2** untreated sample, **3** sample treated with TiO_2 nanoparticles)

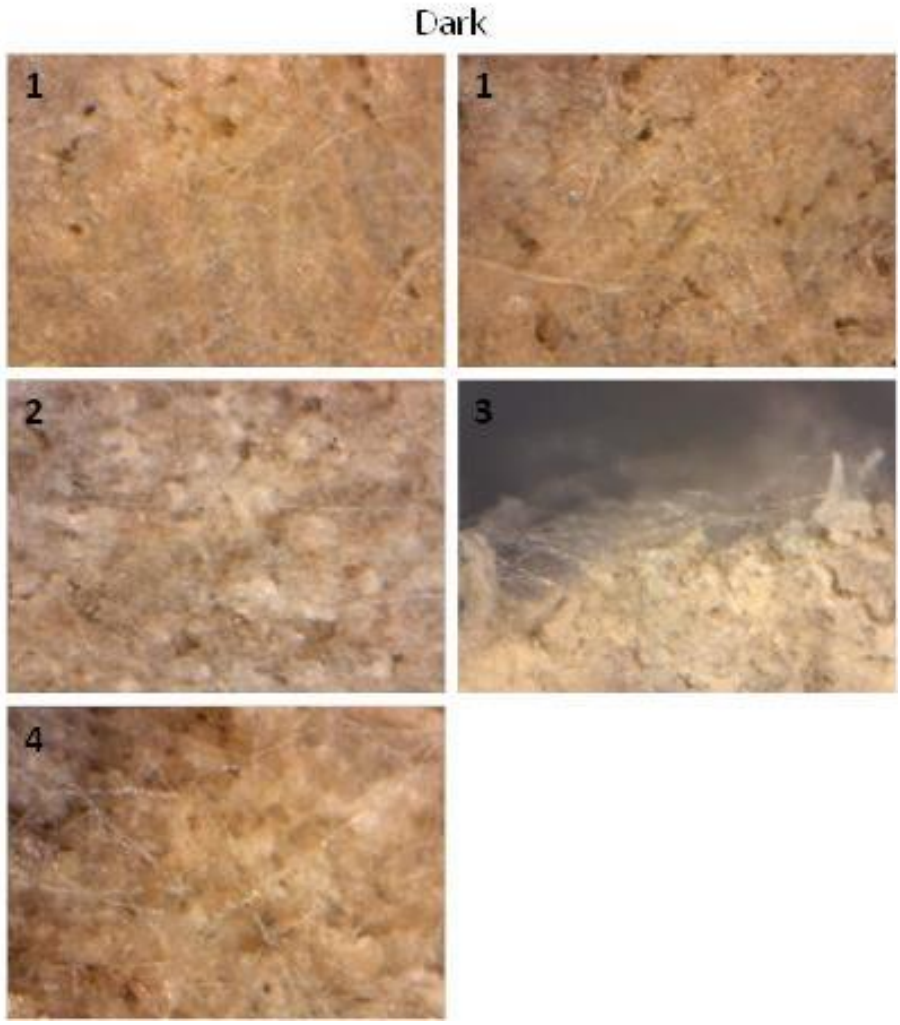

Figure 98 Photos of some samples kept in the dark at the end of the treatment (**1** samples treated with the nanocomposite, **2** untreated sample, **3** sample treated with TiO_2 nanoparticles, **4** sample treated with 2-propanol)

4.5.3 Study of new formulations for paper treatment

During this research, a study on new consolidants for degraded paper was started. In particular, preliminary tests on the newly synthesized allyl saccharide/vinyl alcohol copolymers were performed in order to evaluate the interest in their use for the conservation of aged paper-made works of art. In those preliminary tests, the behavior of the allyl saccharide/vinyl alcohol copolymers was compared to that of other biopolymers previously synthesized in our laboratory[97,98,153,165], also when TiO_2 anatase or $Ca(OH)_2$ nanoparticles were present on the samples.

The preliminary screening performed in this research had the aim of assessing the resistance of the chosen products when exposed to natural radiation by evaluating the color changes induced on the paper by the presence of the consolidant alone or together with the nanoparticles. A simple protocol was developed to quickly compare different formulations using an exposure of 24 hours at room temperature under an UV lamp at 365 nm. The aim of those preliminary tests was the identification of the product which gives the best results in term of color changes both alone or in the presence of the nanoparticles. The UV exposure of the paper treated with the best product is going to be extended for a more meaningful duration. In this way it will be possible to study the degradation reactions which could take place in consequence of the UV exposure of the cellulose and of multifunctional polymers, such as those used in this research. Furthermore, the selected product will be used for the treatment of artificially aged samples.

As previously mentioned, the allyl α,α'-trehalose/vinyl alcohol and allyl methyl D-glucopyranoside/vinyl alcohol copolymers were used to perform preliminary tests on Whatman paper samples and their behavior was compared to that of three products previously synthesized in our laboratory, i.e. an oligoamide dimethyl-L-tartrate/L-lysine[165], an allyl n-hydroxypropyl cellulose[97] and an oligo ethylene adipoamide[153] (**Figure 99**).

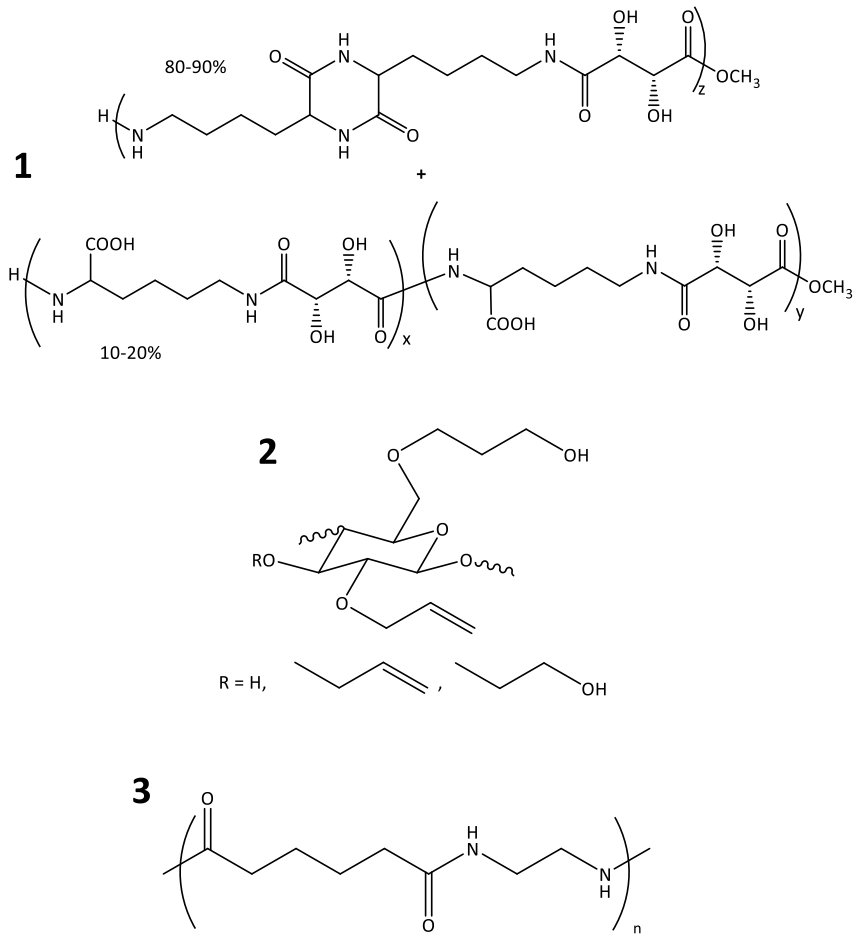

Figure 99 Structure of the oligoamide dimethyl-L-tartrate/L-lysine (**1**), the allyl n-hydroxypropyl cellulose (**2**) and the oligo ethylene adipoamide (**3**)

Firstly, some tests were performed to identify the best solvent between 2-propanol and dimethyl carbonate to prepare the dispersions of the selected biopolymers. Dimethyl carbonate was chosen because it is a well-known non-toxic reagent, which shows several main green-chemistry features[166,167], while 2-propanol was chosen because it is commonly used as a solvent for the dispersions used to perform paper treatments.[51,168] The tests were performed by dispersing 10 mg of each consolidant in 2 mL of each solvent. The best results in terms of homogeneity of the dispersions were obtained using 2-propanol and, therefore, it was chosen as a solvent to prepare the

dispersions of the consolidants. In particular, for the treatment of each single disk of paper a dispersion containing 25 mg of the consolidant in 5 mL of 2-propanol was prepared.

The second step was the treatment of the Whatman samples. The first attempt of treatment was performed by dripping the dispersions of the consolidants on the paper discs and evaporating the solvent at room temperature. However, the amount of the deposited product and the homogeneity of the treatment were not satisfactory. Therefore, the second attempt was performed by spraying the dispersions on the samples and evaporating the solvent at room temperature. The results obtained with this method were satisfactory both in terms of amount of product deposited and in terms of homogeneity (**Table 11**, **Figure 100**).

Table 11

Treatment	Product	Product deposited
Spray 25 mg/5 mL	allyl α,α'-trehalose/vinyl alcohol copolymer	10.9 mg
	allyl methyl D-glucopyranoside/vinyl alcohol copolymer	16.6 mg
	oligoamide dimethyl-L-tartrate/L-lysine	12.8 mg
	allyl n-hydroxypropyl cellulose	22.1 mg
	oligo ethylene adipoamide	13.6 mg

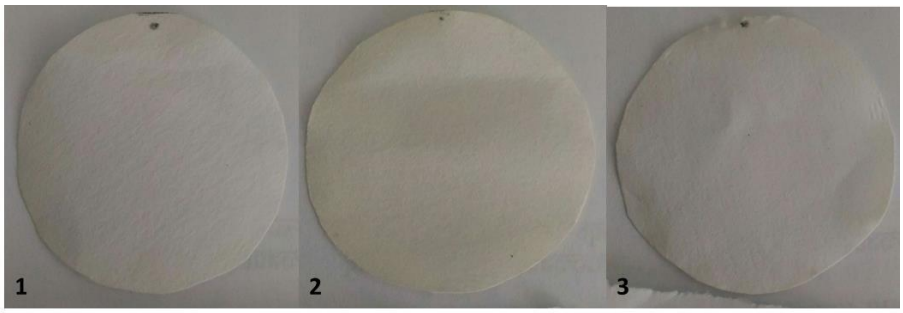

Figure 100 Samples treated by spray (**1** allyl α,α'-trehalose/vinyl alcohol copolymer, **2** oligo ethylene adipoamide, **3** allyl n-hydroxypropyl cellulose)

The comparison between the FT-IR spectra of each treated sample, of an untreated disc and of the corresponding consolidant are reported in **Figure 101**, **Figure 102**, **Figure 103**, **Figure 104**, **Figure 105**. The evaluation through FT-IR spectroscopy of the presence of the consolidant on the samples treated with allyl α,α'-trehalose/vinyl alcohol copolymer, allyl methyl D-glucopyranoside/vinyl alcohol copolymer and allyl n-hydroxypropyl cellulose was difficult because their structures are very similar to that of the paper. For these products, only a slightly difference in the spectra of treated paper samples can be observed due to the overlapping of the bands of paper with the bands of the consolidant (**Figure 101**, **Figure 102**, **Figure 104**). On the contrary, the presence of the oligoamides was more easily detectable thanks to the presence of the C=O stretching of the amide at about 1650 cm^{-1} (**Figure 103**, **Figure 105**).

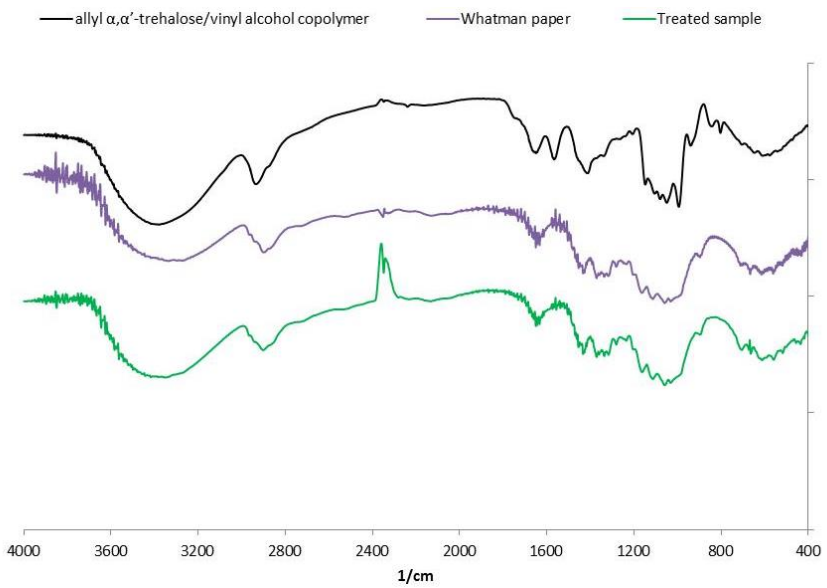

Figure 101 FT-IR spectra of the allyl α,α'-trehalose/vinyl alcohol copolymer (dark line), the Whatman paper (purple line) and the paper treated with allyl α,α'-trehalose/vinyl alcohol copolymer (green line)

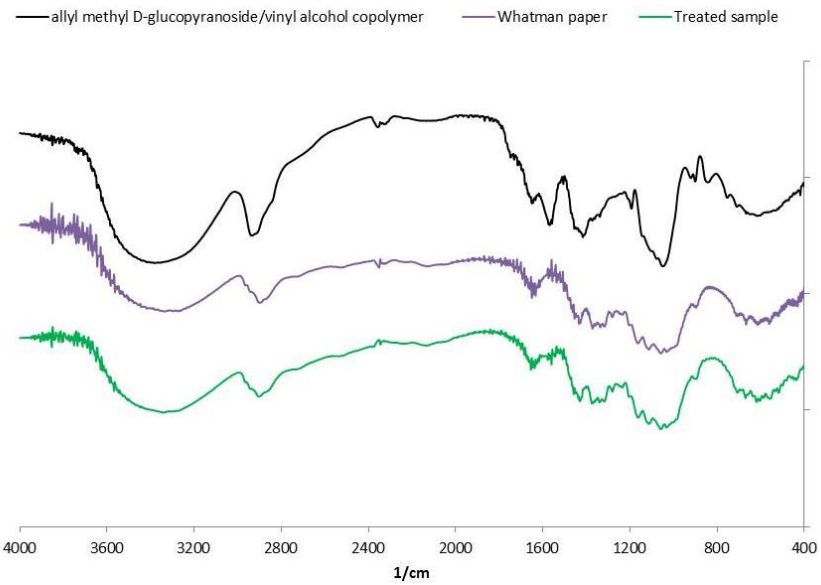

Figure 102 FT-IR spectra of the allyl methyl D-glucopyranoside/vinyl alcohol copolymer (dark line), the Whatman paper (purple line) and the paper treated with allyl methyl D-glucopyranoside/vinyl alcohol copolymer (green line)

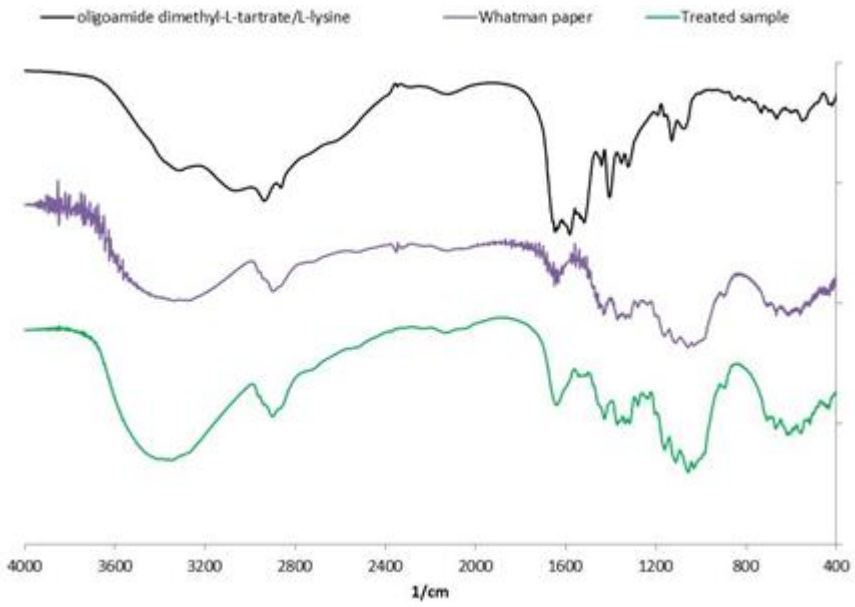

Figure 103 FT-IR spectra of the oligoamide dimethyl-L-tartrate/L-lysine (dark line), the Whatman paper (purple line) and the paper treated with oligoamide dimethyl-L-tartrate/L-lysine (green line)

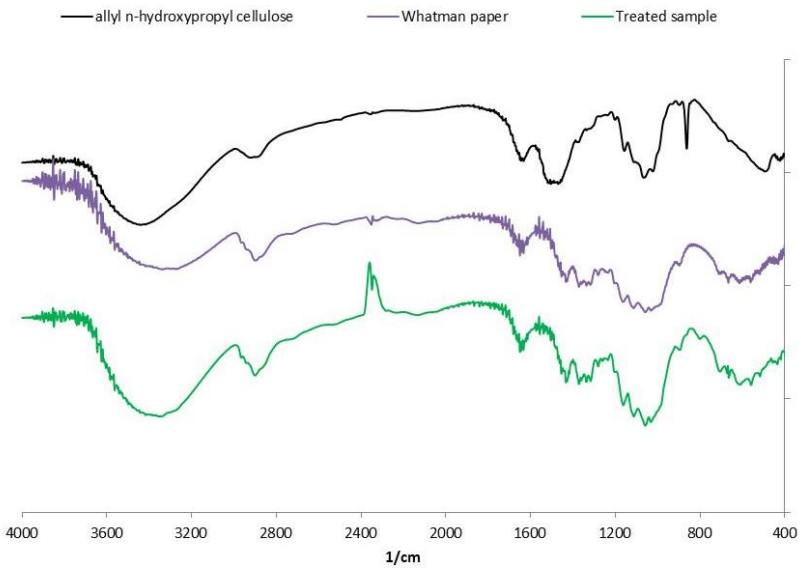

Figure 104 FT-IR spectra of the allyl n-hydroxypropyl cellulose (dark line), the Whatman paper (purple line) and the paper treated with allyl n-hydroxypropyl cellulose (green line)

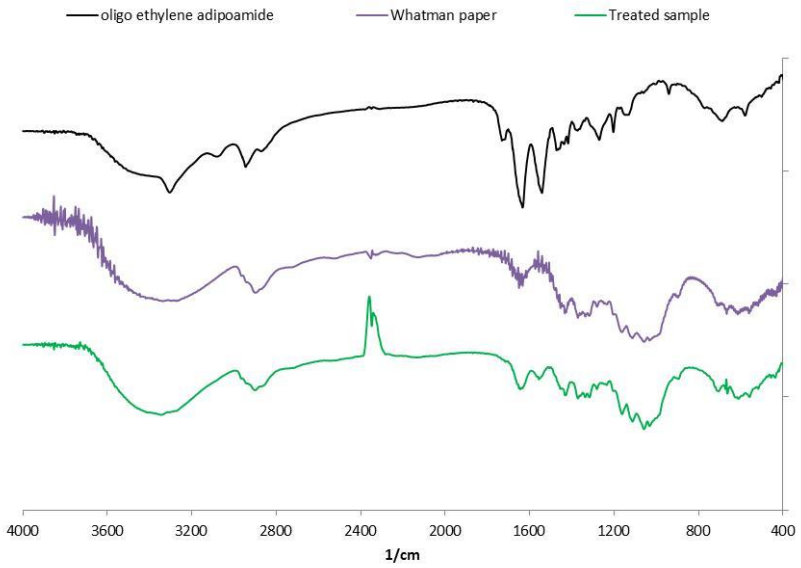

Figure 105 FT-IR spectra of the oligo ethylene adipoamide (dark line), the Whatman paper (purple line) and the paper treated with oligo ethylene adipoamide (green line)

Then, the treated samples were exposed to the UV light for 24 hours at 365 nm. Colorimetric measurements were performed according to the CIEL*a*b* system on the Whatman paper before the treatment, after the treatment and after the exposition to the UV radiation. In order to achieve meaningful results, the various samples were analyzed always in the same spot using a mask that allowed the correct positioning of the colorimeter. The *color difference* (ΔE*) was evaluated using the following equation (**Table 12**):

$$\Delta E^* = \sqrt{\Delta L^{*2} + \Delta a^{*2} + \Delta b^{*2}}$$

where, in the case of the evaluation after the treatment ΔL* = L* (after the treatment) – L* (before the treatment), Δa* = a* (after the treatment) – a* (before the treatment) and Δb* = b* (after the treatment) – b* (before the treatment), while in the case of the evaluation after the UV exposition: ΔL* = L* (after UV exposure) – L* (before the treatment), Δa* = a* (after UV exposure) – a* (before the treatment) and Δb* = b* (after UV exposure) – b* (before the treatment).

Table 12

Product	ΔE* after treatment	ΔE* after 24h UV
allyl α,α'-trehalose/vinyl alcohol copolymer	3.5	3.5
allyl methyl D-glucopyranoside/vinyl alcohol copolymer	6.3	5.3
oligoamide dimethyl-L-tartrate/L-lysine	4.5	4.8
allyl n-hydroxypropyl cellulose	2.6	1.8
oligo ethylene adipoamide	4.0	7.2

Considering that ΔE* values less than or equal to 3.0 correspond to color variations which are imperceptible to the human eye, the best results after the treatment and after the exposure were obtained with the allyl n-

hydroxypropyl cellulose and the allyl α,α'-trehalose/vinyl alcohol copolymer, which gave the lowest color variations.

Furthermore, it is worth noting that the variations recorded for allyl methyl D-glucopyranoside/vinyl alcohol copolymer and allyl n-hydroxypropyl cellulose had a decrease after 24 hours of UV exposure. This behavior can be attributed to the effect of the UV light on chromophores or auxochromes groups. Indeed, after the exposure a discoloration is observed for paper treated with these allyl derivatives because the conjugate system, which is responsible of the coloring, can be simplified upon exposure to radiation, for example by the reduction of the double bonds of allyl groups to single bonds.

On the contrary, the ΔE* values observed for paper treated with oligo ethylene adipoamide show a very strong variation from ΔE* 4.0 (after the treatment) to ΔE* 7.2 (after 24 hours of UV exposure). In this case, probably the UV radiation caused the formation of chromophores, thus increasing the color variation after the exposure.

In order to better evaluate how the ΔE* values in **Table 12** are influenced by the various components of ΔE* (i.e. ΔL*, Δa*, Δb*), in **Figure 106** and **Figure 107** all the values of ΔL*, Δa*, Δb*, ΔE* recorded for the various samples after the treatment and after the UV exposure are reported. It is evident from the graphs that for all the samples Δb* is the colorimetric coordinate which contributes more to ΔE* variations. In the CIEL*a*b* system b* has values ranging from -60 (blue) to +60 (yellow). Therefore, a positive variation of this coordinate means that the color of the paper after the treatments and the UV exposure changed to yellow.

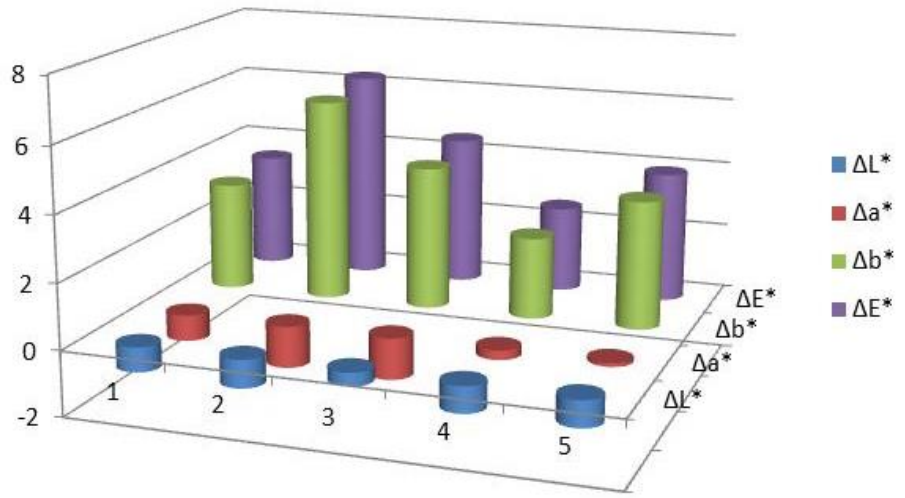

Figure 106 Colorimetric changes after the treatment (**1** allyl α,α'-trehalose/vinyl alcohol copolymer, **2** allyl methyl D-glucopyranoside/vinyl alcohol copolymer, **3** oligoamide dimethyl-L-tartrate/L-lysine, **4** allyl n-hydroxypropyl cellulose, **5** oligo ethylene adipoamide)

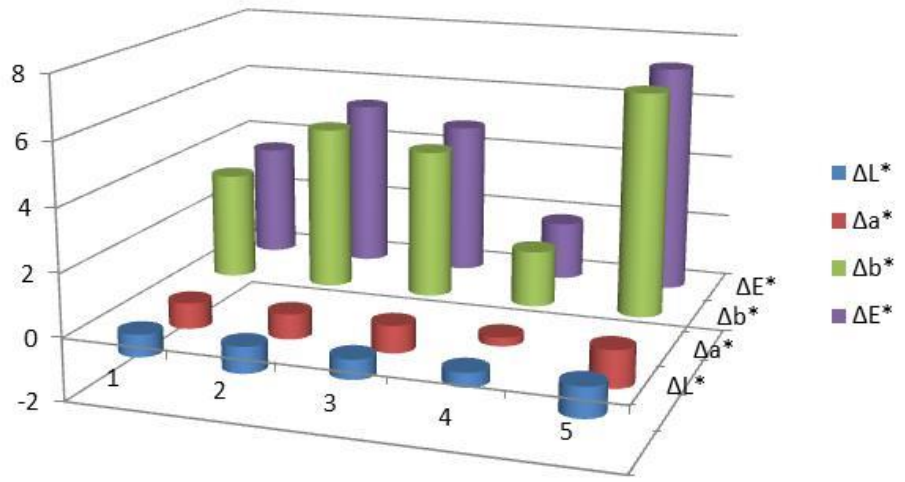

Figure 107 Colorimetric changes after the UV exposure (**1** allyl α,α'-trehalose/vinyl alcohol copolymer, **2** allyl methyl D-glucopyranoside/vinyl alcohol copolymer, **3** oligoamide dimethyl-L-tartrate/L-lysine, **4** allyl n-hydroxypropyl cellulose, **5** oligo ethylene adipoamide)

On the basis of these tests, the two products which gave the best results in terms of ΔE* after the UV exposure, i.e. allyl n-hydroxypropyl cellulose and allyl α,α'-trehalose/vinyl alcohol copolymer, were selected to perform the next step. This step consisted in the evaluation of the influence on the colorimetric changes of the simultaneous presence of TiO_2 or $Ca(OH)_2$ nanoparticles on Whatman paper treated with the two chosen products. Indeed, the presence of TiO_2 anatase nanoparticles could modify the structure of the organic compounds present on the paper surface by reducing chromophores which are formed in the degradative oxidation processes. Instead, the $Ca(OH)_2$ nanoparticles reduce the acidity of the paper and the consequent hydrolysis and oxidation reactions.

As previously mentioned, an attempt to obtain the nanocomposite with $Ca(OH)_2$ nanoparticles and allyl α,α'-trehalose/vinyl alcohol copolymer or allyl methyl D-glucopyranoside/vinyl alcohol copolymer was performed by mixing them (mixing conditions 2% of the copolymer and 4g/L of nanoparticles in 2-propanol/water 75/25), but the dispersions were not stable (paragraph 4.4.2). Therefore, in this preliminary study nanocomposite coatings were obtained by subsequent applications of the dispersions of the consolidant and the nanoparticles.

The nanoparticles were applied on Whatman paper as alcoholic dispersions. In particular, the TiO_2 nanoparticles were dispersed in 2-propanol, while the $Ca(OH)_2$ nanoparticles were used as supplied by the C.S.G.I. laboratory (i.e. dispersion in ethanol). The application was performed by brushing the dispersions on the paper samples and the amount of nanoparticles applied on each samples was 5 mg.

Another aim of this step was the choice of the best treatment procedure in terms of color differences. With this purpose, two different types of treatment procedures were used:

I. spray treatment with the dispersion of the consolidant and then brushing treatment with the dispersion of the nanoparticles;
II. brushing treatment with the dispersion of the nanoparticles and then spray treatment with the dispersion of the consolidant.

The allyl n-hydroxypropyl cellulose was used to perform this choice. The samples were treated and dried at room temperature and colorimetric measurements were performed. Then, the treated samples were exposed to the UV light for 24 hours at 365 nm and colorimetric measurements were performed after the exposition. In **Table 13** the amount of consolidant and nanoparticles applied are reported for each sample, together with the ΔE* values obtained after the treatment and after the UV exposure. As previously mentioned, in order to achieve meaningful results, all colorimetric measurements were performed always in the same spot of the samples using a mask that allowed the correct positioning of the colorimeter. Moreover, in order to better evaluate how the ΔE* values reported in **Table 13** are influenced by the various components of ΔE* (i.e. ΔL*, Δa*, Δb*), in **Figure 108** and **Figure 109** all the values of ΔL*, Δa*, Δb* and ΔE* recorded for the various samples after the treatment and after the UV exposure are reported.

Table 13

Product/Nanoparticles		Treatment	Product deposited	ΔE* after treatment	ΔE* after 24h UV
allyl n-hydroxypropyl cellulose	TiO_2	Nanoparticles – consolidant	14.4 mg	2.6	1.6
		Consolidant – nanoparticles	12.4 mg	2.1	1.1
	$Ca(OH)_2$	Nanoparticles – consolidant	21.8 mg	2.2	0.9
		Consolidant – nanoparticles	18.8 mg	2.3	0.8

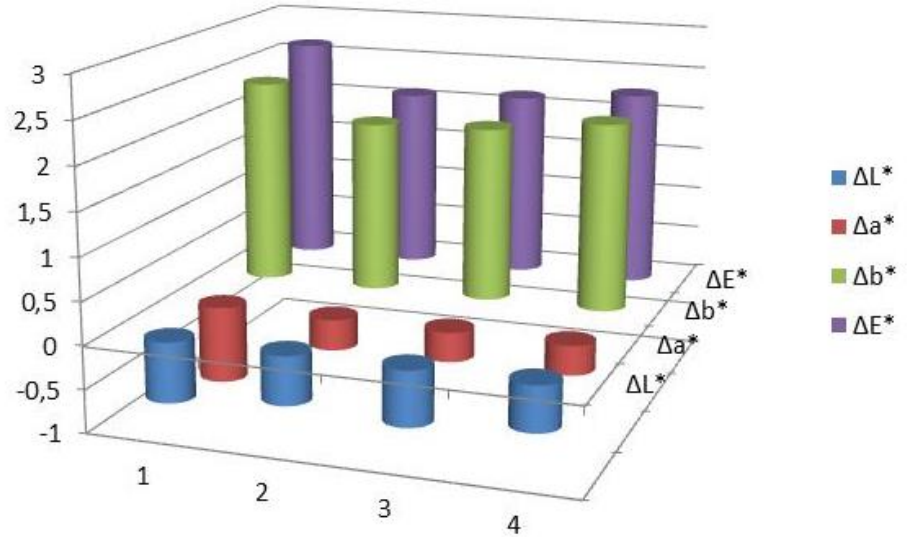

Figure 108 Colorimetric changes after the treatment (**1** TiO_2 nanoparticles/allyl n-hydroxypropyl cellulose, **2** allyl n-hydroxypropyl cellulose/TiO_2 nanoparticles, **3** $Ca(OH)_2$ nanoparticles/allyl n-hydroxypropyl cellulose, **4** allyl n-hydroxypropyl cellulose/$Ca(OH)_2$ nanoparticles)

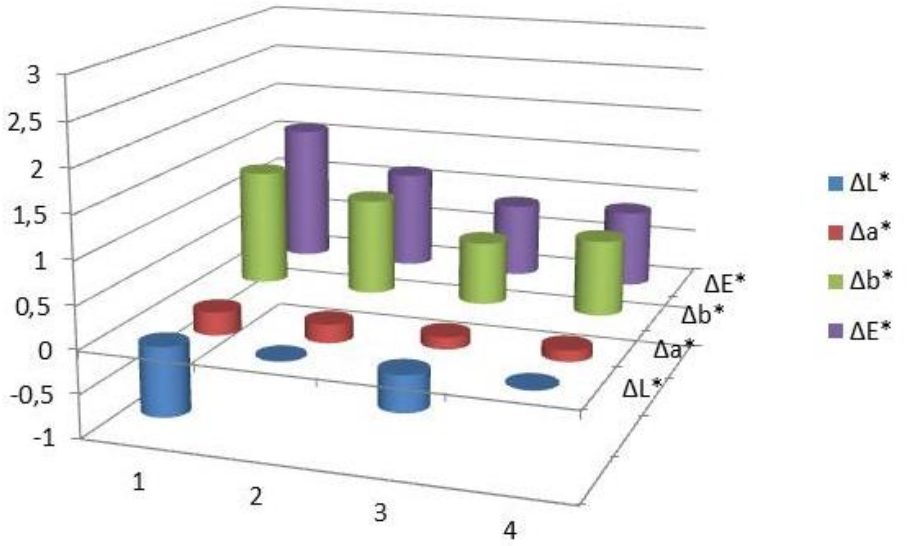

Figure 109 Colorimetric changes after the UV exposure (**1** TiO_2 nanoparticles/allyl n-hydroxypropyl cellulose, **2** allyl n-hydroxypropyl cellulose/TiO_2 nanoparticles, **3** $Ca(OH)_2$ nanoparticles/allyl n-hydroxypropyl cellulose, **4** allyl n-hydroxypropyl cellulose/$Ca(OH)_2$ nanoparticles)

The ΔE* values are smaller than 3 for all the samples both after the treatment and after the UV exposure. As regards the influence of the simultaneous presence of the nanoparticles, different results in terms of color changes were obtained with TiO_2 or $Ca(OH)_2$ nanoparticles after 24 hours of UV exposure (ΔE* 1.6-0.8, **Table 13**) with respect to that obtained by treating with only the consolidant (ΔE* 1.8, **Table 12**). In particular, the type of treatment procedure seems to influence the results. Moreover, as observed for the treatment with only the consolidant, even in this case the ΔE* values recorded after the UV exposition are decreased with respect to those recorded after the treatment.

Figure 109 show that, as for the treatment with only the consolidant, also in this case the b* coordinate contributes more than the others to the ΔE* variations. However, when TiO_2 or $Ca(OH)_2$ nanoparticles are applied before the consolidant there is also a variation of L*, which expresses the brightness in the CIEL*a*b* system. This negative variation means that the color tended to be less bright and it had a darkening (the so-called *wet look*).

As regard the treatment with TiO_2 nanoparticles, the best result in terms of ΔE* values was obtained with the nanoparticles applied after the consolidant maybe because they can have a sort of "whitening" effect, which quenches the colorimetric changes due to the consolidant. Furthermore, a higher photoactivity of the nanoparticles not covered by the polymer with respect to those covered by the polymer cannot be excluded. Concerning the $Ca(OH)_2$ nanoparticles, the ΔE* values obtained with the two different treatment procedures after 24 hours of UV exposition are very similar. Therefore, in this case the best procedure was chosen considering that the presence of the consolidant over the layer of nanoparticles can reduce their mobility.

Finally, the best treatment procedures selected for allyl n-hydroxypropyl cellulose were used for the treatment of paper samples with the allyl α,α'-trehalose/vinyl alcohol copolymer in the presence of TiO_2 and $Ca(OH)_2$ nanoparticles. The samples were treated, dried at room temperature and then exposed to the UV light (24 hours, 365 nm). In **Table 14** the ΔE* values obtained from the colorimetric measurements performed after the

treatment and after the UV exposure are reported, together with the amount of product and nanoparticles deposited on each sample after the treatment. As previously mentioned, in order to achieve meaningful results, all colorimetric measurements were performed always in the same spot of the samples using a mask that allowed the correct positioning of the colorimeter. In order to better evaluate how the ΔE* values reported in **Table 14** are influenced by the various components of ΔE* (i.e. ΔL*, Δa*, Δb*), in **Figure 110** and **Figure 111** all the values of ΔL*, Δa*, Δb* and ΔE* recorded for the various samples after the treatment and after the UV exposure are reported.

Even in this case, a decrease in the ΔE* values after the UV exposition compared to those recorded after the treatment can be observed. **Figure 111** shows that the b* coordinate contributes more than the others to the ΔE* variations as in all the other previous cases. Moreover, also a negative variation of L* is visible, which means that the color tended to be less bright and it had a darkening (the so-called *wet look*). Considering the influence of the simultaneous presence of the nanoparticles, it has a small positive effect on the ΔE* values after the UV exposure (ΔE* 3.2-2.6, **Table 14**) compared to the correspondent result obtained for paper treated with only the allyl α,α'-trehalose/vinyl alcohol copolymer (ΔE* 3.5, **Table 12**).

In conclusion, the two treatment procedures gave good results, as in the case of allyl n-hydroxypropyl cellulose, because the ΔE* values obtained resulted lower than 3.

Table 14

Product/Nanoparticles		Treatment	Product deposited	ΔE* after treatment	ΔE* after 24h UV
allyl α,α'-trehalose/vinyl alcohol copolymer	TiO_2	Consolidant – nanoparticles	12.1	4.4	3.0
	$Ca(OH)_2$	Nanoparticles – consolidant	16.5	4.1	2.6

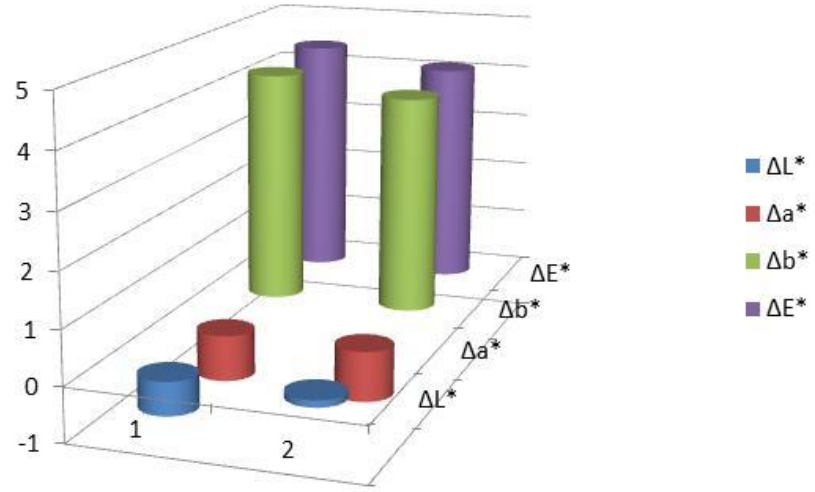

Figure 110 Colorimetric changes after the treatment (**1** allyl α,α'-trehalose/vinyl alcohol copolymer/TiO_2 nanoparticles, **2** $Ca(OH)_2$ nanoparticles/allyl α,α'-trehalose/vinyl alcohol copolymer)

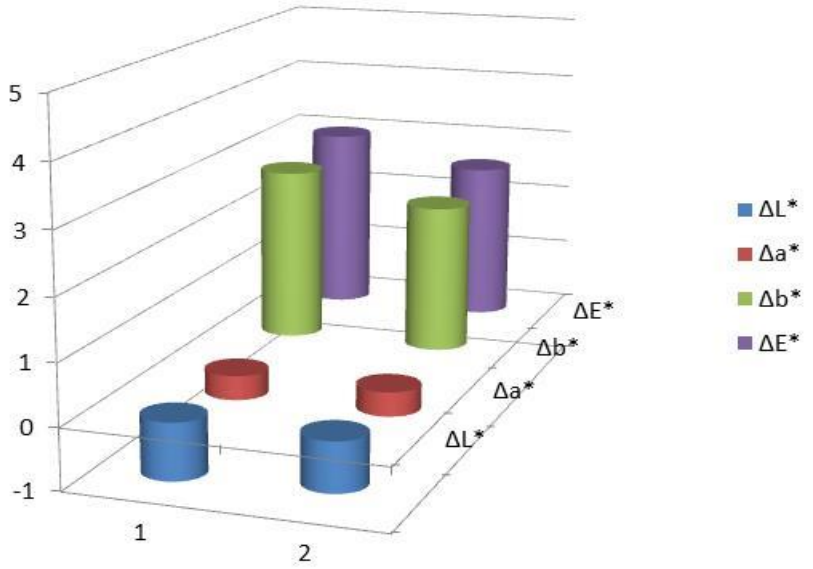

Figure 111 Colorimetric changes after the UV exposure (**1** allyl α,α'-trehalose/vinyl alcohol copolymer/TiO_2 nanoparticles, **2** $Ca(OH)_2$ nanoparticles/allyl α,α'-trehalose/vinyl alcohol copolymer)

5 Conclusions

In this research work, new formulations were obtained and studied for applications in the field of cultural heritage, in particular for the conservation of cellulosic artifacts. New biopolymers and new nanocomposites were synthesized using α,α'-trehalose and D-cellobiose as feedstocks. The choice of renewable starting materials was made taking in consideration the growing interest of academia and industry for the exploitation of lignocellulosic biomasses from which α,α'-trehalose and D-cellobiose are obtained. Moreover, focusing on cultural heritage conservation, the use of bio-based materials has further advantages like the compatibility and the affinity for the works of art, especially those made of the same chemical species that constitute the biomass (i.e. wood and paper).

The synthetic methodologies for the preparation of the new copolymers and the new nanocomposites were selected taking into account their future use in the conservation of the cultural heritage and the application properties of these new synthesized products were studied on cellulosic substrates such as wood and paper.

Synthesis of the monomers

Saccharides like α,α'-trehalose and D-cellobiose were selected as starting materials for the synthesis of bio-based monomers, in order to introduce units with a structure similar to that of the cellulosic materials which constitute some works of art in the new products.

Before the synthesis of the monomers, the anomeric position of the D-cellobiose was subjected to a protection using methanol and a ion exchange resin, Amberlite IR-120H. However, this reaction led not only to the methylation but also to the simultaneous cleavage of the 1,4-β-glycosidic bond of the disaccharide. Therefore, instead of a methyl D-cellobioside, a mixture of methyl α-D-glucopyranoside and methyl β-D-glucopyranoside was obtained. Anyhow, the reaction was considered interesting for a biorefinery process as a possible procedure for the depolymerization of the cellulose from biomass with solid acid catalysts. Indeed, in order to overcome the disadvantages of the two main hydrolysis methods currently used in cellulose saccharification (i.e. enzymatic and homogeneous acid catalyzed),

in recent years several researches were carried out on the use of solid acid catalysts, which are more easily removable. Moreover, the methyl D-glucopyranoside was considered interesting in view of the production of bio-based products for cultural heritage since it has a carbohydrate structure, as the starting D-cellobiose, and therefore it maintains the positive characteristics of affinity and compatibility that make it suitable for application on cellulosic artifacts.

Allyl saccharide monomers were synthesized using allyl bromide as functionalizing agent for α,α'-trehalose or methyl D-glucopyranoside. The reaction was performed in water with advantages in terms of costs and sustainability with respect to a previously published procedure in which dimethyl sulfoxide was used as a solvent.[107]

Moreover, KOH was used instead of NaOH to promote the nucleophilic substitution on the allyl bromide and to favor the formation of more easily removable byproducts. Indeed, the potassium salts formed during the reaction have lower solubility in ethanol (the solvent used to purify the final products) compared to the analogous sodium salts.[147] In this way, it was possible to obtain allyl derivatives which contains only 10% of impurities, with yield ranging between 90% and 97%.

Several molar ratio between the reagents were tested and they led to the synthesis of monomers with different degrees of substitution. Finally a molar ratio allyl bromide/α,α'-trehalose of 6 and a molar ratio allyl bromide/methyl D-glucopyranoside of 4 were chosen because they allowed to obtain a degree of substitution of 1-2 on the final monomer, thus decreasing the possibility of a cross-linking in the subsequent copolymerization reactions.

Synthesis of the vinyl acetate copolymers

Starting from the allyl saccharide monomers, preliminary tests on the synthesis of homopolymers were performed but they gave unsatisfactory results in terms of yields and chain length. This behavior is consistent with the well-known poor reactivity of the allyl bond.[148] Therefore, the allyl monomers were used with vinyl acetate to obtain copolymers through radical polymerization reactions.

The synthesis of the copolymers was performed using methanol as a solvent instead of water, which is commonly used as dispersion medium for the homo- and copolymerization of vinyl acetate. Methanol allowed to obtain pure copolymers avoiding the presence of all the additives that are essential for their synthesis in water dispersion (i.e. protective colloid, surfactants, buffers). In this way the pure copolymers can be more easily characterized and they are also more suitable to be used in the cultural heritage conservation.

Allyl α,α'-trehalose/vinyl acetate and allyl methyl-D-glucopyranoside/vinyl acetate copolymers were obtained with yields of about 60% (for a molar ratio between the reagents vinyl acetate/allyl saccharide = 10). These copolymers are soluble in chloroform and acetone, while after an extraction in water the presence of two fractions with different solubility in this solvent was observed: fraction A, soluble in water, and fraction B, insoluble in water. This different solubility was explained by the different ratios between the comonomer units in the copolymers chains. In particular, the fraction A of each copolymer contains water soluble chains rich in saccharide monomer units, with low molecular weights (M_w of about 27000 g/mol for allyl α,α'-trehalose/vinyl acetate copolymer and of about 4000 g/mol for allyl methyl-D-glucopyranoside/vinyl acetate copolymer) and T_g values lower than room temperature. On the contrary, the fraction B of each copolymer contains chains insoluble in water and rich in vinyl acetate monomer units, with higher molecular weights with respect to those contained in fraction A (M_w of about 100000 g/mol for both allyl α,α'-trehalose/vinyl acetate and allyl methyl-D-glucopyranoside/vinyl acetate copolymer) and T_g values of about 40-49°C. It cannot be excluded that chains of polyvinyl acetate homopolymer can be present in this fraction together with the copolymers.

Synthesis of the vinyl alcohol copolymers

Allyl α,α'-trehalose/vinyl alcohol and allyl methyl-D-glucopyranoside/vinyl alcohol copolymers were obtained by hydrolyzing the correspondent vinyl acetate copolymers in anhydrous methanol at 50°C for 1 hour.

These products were synthesized in order to have water soluble copolymers suitable for the treatment of wood and paper and to prevent the hydrolysis of the vinyl acetate groups which could take place after the application if the

vinyl acetate copolymers are used to treat the degraded material. Indeed, during the hydrolysis, acetic acid can be formed causing a hazardous decrease of the pH which, paradoxically, could accelerate the degradation of the artifact, achieving an effect that is the opposite to the desired one.

The vinyl alcohol copolymers are composed of two fractions (fraction 1 and fraction 2) which show different ratios of the comonomer units in the chains, different molecular weights and different solubility in methanol. In particular, the fraction 1 is a solid insoluble in methanol which precipitates as it is formed during the reaction, composed of chains with high molecular weight and rich in vinyl alcohol units. On the contrary, the fraction 2 is soluble in methanol and therefore is recovered after the reaction from the methanol solution. It is composed of chains with low molecular weights and rich in allyl saccharide units.

Synthesis of the TiO_2 anatase nanocomposites

New nanocomposites were designed with the aim of obtaining new products with antimicrobial activity for cellulosic artifacts. In particular, nanocomposites between TiO_2 anatase nanoparticles and allyl saccharide/vinyl acetate copolymers were obtained by grafting the copolymers on properly functionalized nanoparticles.

The nanoparticles were firstly activated and then functionalized with a coupling agent (vinyltriethoxysilane). Finally, the allyl saccharide/vinyl acetate copolymers were grafted on functionalized TiO_2 nanoparticles through an in situ radical copolymerization. The nanocomposites were recovered as insoluble fraction after an extraction in acetone and characterized by FT-IR spectroscopy and SEM images.

Applicative studies

Consolidation of archaeological waterlogged wood

The performances of the allyl α,α'-trehalose/vinyl alcohol copolymer as consolidant for archaeological waterlogged wood were compared to those of some oligoamides previously synthesized in our laboratory. A diagnostic protocol designed to quickly compare the consolidating properties of different products was used.[100-101]

Firstly, a good affinity for a degraded wood rich in lignin was demonstrated for all the tested consolidants by performing impregnation tests on archaeological lignin samples and monitoring the results with the FT-IR spectroscopy. The reversibility of the treatments was tested on the treated lignin samples and the oligoamides showed higher reversibility than allyl α,α'-trehalose/vinyl alcohol copolymer. This was probably due to a modification in the solubility of this last consolidant as a result of cross-linking reactions which could have involved the allyl groups still present in its structure.

Then, samples of two different wood species (*Quercus*, less degraded, and *Fraxinus*, more degraded) were treated with water solutions of the various consolidants and dried according to international technical standards UNI ISO 483[157] and UNI ISO 3130.[158]

The penetration ability of the consolidants was evaluated by FT-IR spectroscopy and it was generally good for all the tested products.

Finally, some physical properties of the treated samples like the maximum water content, the basic density and the volumetric shrinkage were evaluated. As regards the maximum water content and the basic density, the results obtained with allyl α,α'-trehalose/vinyl alcohol copolymer for *Fraxinus* wood are comparable with those obtained with oligo esamethylene-L-tartaramide and oligo ethylene-L-tartaramide, while a lower effectiveness of this product was observed for *Quercus* wood. This behavior is probably due to the high porosity of the more degraded *Fraxinus* wood, which allowed a better penetration of this copolymer, that has the highest molecular weight among the tested consolidants. The volumetric shrinkage was evaluated only qualitatively and it was generally lower for all the treated samples compared with the untreated ones.

Antifungal treatment

The antifungal properties of the nanocomposite obtained by grafting allyl α,α'-trehalose/vinyl acetate copolymer on functionalized TiO_2 anatase nanoparticles were evaluated by performing tests on recent wood exposed to the fungus *Trametes Versicolor*. In particular, two tests were performed using wooden samples treated in different ways (treated with

nanocomposite, untreated or treated with a dispersion of TiO_2 nanoparticles). In each test the samples were placed on plates containing the culture of the fungus. Then, some of the plates were exposed to the UV light (365 nm) and some other were kept in the dark for 3 weeks.
The first test was performed using the nanocomposite containing not grafted copolymer and underlined the need of a proper purification of the nanocomposite. The presence of the not grafted allyl α,α'-trehalose/vinyl acetate copolymer caused a significant alteration of the aspect of treated samples and promoted the growth of the fungus also on samples exposed to the UV light.

On the contrary, in the second test a nanocomposite purified from the not grafted copolymer was used and the aspect of the treated samples was not altered significantly. Moreover, the fungal growth on samples treated with the nanocomposite and exposed to the UV light was lower than that on the untreated samples, while it was higher than that on the samples treated with TiO_2 nanoparticles.

Therefore, the presence of the nanocomposite limits the fungal growth, though the attack is not completely stopped. This behavior highlights the need for a future improvement of the formulation in terms of photoactivity.

Finally, a photodegradation test performed on the nanocomposite purified from the not grafted copolymer showed that the UV radiation cause the break of bond with the acetate group of the nanocomposite and the consequent emission of acetic acid. To prevent this emission from occurring within the treated wooden artifacts, in the future it will be necessary to design the synthesis of a nanocomposite containing the vinyl alcohol copolymer.

Study of new formulations for paper treatment

A study on new formulations for degraded paper was performed through a preliminary screening of the resistance of several consolidants to the exposition to natural radiation.
The color changes induced on the paper by the presence of the consolidants or of their nanocomposites were evaluated after the treatment and after an exposure of 24 hours at room temperature under an UV lamp (365 nm). The

allyl α,α'-trehalose/vinyl alcohol and allyl methyl D-glucopyranoside/vinyl alcohol copolymers were used to perform these treatments and their behavior was compared with that of three products previously synthesized in our laboratory, i.e. an oligoamide dimethyl-L-tartrate/L-lysine, an allyl n-hydroxypropyl cellulose and an oligo ethylene adipoamide. The analysis of the components of ΔE* (i.e. ΔL*, Δa*, Δb*) showed a significant variation of b* to positive values, which means that the material has undergone a yellowing. Nevertheless, good results in terms of ΔE* after the treatment and after 24 hours of exposure were obtained with allyl α,α'-trehalose/vinyl alcohol copolymer and allyl n-hydroxypropyl cellulose.

Those two products were also tested as nanocomposites obtained by performing subsequent applications of the dispersions of the consolidants and of the TiO_2 or $Ca(OH)_2$ nanoparticles on Whatman paper. The color changes were evaluated after the treatment and after 24 hours of UV exposure and a positive effect was observed with both the nanoparticles because there was a small reduction of the ΔE* values with respect to those obtained with only the consolidant.

The products which have given the best results (i.e. allyl α,α'-trehalose/vinyl alcohol copolymer and allyl n-hydroxypropyl cellulose also in the form of nanocomposite with TiO_2 or $Ca(OH)_2$ nanoparticles) are promising for the treatment of paper and the study of their effect on artificially aged samples in terms of consolidating properties and colorimetric changes after a period of exposition of the samples to the UV light in a solarbox is currently underway.

6 Experimental

6.1 Materials

D-cellobiose, α,α'-trehalose, allyl bromide, Amberlite IR-120H resin, hydrochloric acid, ethanol, methanol, vinyl acetate, 2-propanol, sodium bicarbonate, methylene blue, TiO_2 anatase nanoparticles, vinyltriethoxysilane, ethylenediamine, N,N-dimethylacetamide, potassium chloride, lithium chloride, ammonium nitrate, 3-bromo-1-propanol, L-lysine, deuterium oxide, methanol-d_4 and chloroform-d were purchased from Sigma Aldrich. Potassium hydroxide, diethyl ether, triethylamine and L-tartaric acid were purchased from Carlo Erba. Sulfuric acid and azobisisobutyronitrile were purchased from Fluka Co. Acetone was purchased from VWR International. Nitric acid and sodium hydroxide were purchased from Honeywell Riedel-de Haën.

Amberlite IR-120H resin (250 mg) was activated by washing it with methanol (3 x 1.25 mL, 10' + 1 x 1.25 mL overnight).

Dimethyl-L-tartrate was synthesized using a literature procedure.[97]

Dimethyl adipate was synthesized by Ditta Radici Chimica s.p.a.

Oligo esamethylene-L-tartaramide was synthesized by Ditta Radici Chimica s.p.a. ^{1}H-NMR (D_2O, 200 MHz, ppm): 1.2-1.7 (m, 8H, $NHCH_2\mathbf{(CH_2)_4}CH_2NH$); 2.98 (m, 2H, $CH_2NH_3^+$ salt); 3.22 (m, 2H, $C\mathbf{H_2}NHCO$); 4.28 (s, 1H, C**H**OH salt); 4.42-4.50 (m, 1H, C**H**OH). FT-IR (KBr pellets): peaks at 3221 (w, OH stretching); 2927, 2854 (w, C-H stretching); 1635 (s, C=O stretching); 1541 (s, C=O stretching); 1120, 1066 (s, C-O stretching) cm^{-1}.

$Ca(OH)_2$ nanoparticles were supplied by the C.S.G.I. laboratory (ethanol dispersion, 3g/L).

Whatman paper Cat No 1001-055 (55 mm diameter) was purchased from Sigma Aldrich.

6.2 Instruments

^{1}H-NMR, ^{13}C-NMR spectra were recorded with a Varian Mercury Plus 400 spectrometer and a Varian VXR 200 spectrometer, working at 399.921 MHz and 199.985 MHz, respectively. The chemical shifts are reported in ppm and referred to TMS as internal standard. Spectra elaboration was performed with the software MestRe-C 4.3.2.0.

FT-IR spectra were recorded with a Shimadzu FT-IR-8400S model and elaborated with the software Shimadzu IRsolution 1.04.

Elemental analysis were performed with a Perkin-Elmer Analyzer 2400 Series II CHNS/O.

Electrospray mass spectrometry (ESI-MS) and tandem mass spectrometry (MS/MS) analyses were performed with a ESI/LTQ Orbitrap, a hybrid linear ion trap orbitrap high resolution mass spectrometer (Thermo Fisher Scientific, Bremen, Germany). ESI-MS analyses were performed as follows: the solution of the product in D_2O was diluted 1:20 in LC-MS grade water. Then it was analyzed by infusion (at 5 uL/min flow rate) in the ESI interface of a LTQ Orbitrap. Spectra were recorded in negative ion mode, in scan mode in the 150-450 m/z range. MS/MS spectra were recorded isolating the $[M-H]^-$ of the two molecules and colliding them in the ion trap, at 22% and 25% for m/z 193 and m/z 355, respectively. The ESI parameters were as follows: spray voltage -4 kV, capillary voltage -39 V, capillary temperature 270°C, tube lens voltage -103 V; nitrogen were used as nebulizer and auxiliary gas, at 15 and 2 values (arbitrary units), respectively. Data were acquired and analyzed using the Xcalibur software (ver. 3.0).

Differential Scanning Calorimetry (DSC) experiments were performed with a DSC Q2000 (TA Instruments) calorimeter. Samples were pre-dried using a vacuum pump. Then, they were closed in aluminum hermetic pans and analyzed from -10°C to 100°C at 10°C/min.

SEC system was composed of a Waters 1515 Isocratic HPLC pump and a three Phenogel columns set (443-K0, 445-K0, 446) equipped with a Waters 2487 Dual λ Absorbance Detector set at 230 nm using 1 mL/min flow rate

and 20 µL as injection volume. Samples were prepared dissolving 10-20 mg of polymer in 1 mL of anhydrous DMF. Before the analysis, the solution was filtered with 0.45 µm filters, therefore the reported results refer only to the polymer present in solution. The molecular weights were determined using a calibration made with monodisperse polystyrene standards.

Scanning electron microscope (SEM) images were collected on uncoated samples with a field-emission ΣIGMA (Carl Zeiss) microscope, with an accelerating potential of 2 kV.

Transmission electron microscopy (TEM) analyses were performed with a TEM Philips CM 12 equipped with an Olympus Megaview G2 camera and using an accelerating voltage of 100 kV. Samples were prepared by depositing a drop of the dispersion on a carbon film of 200 mesh Cu grid and on holey carbon.

Photos of the samples were taken with a Dino-Lite Pro Portable Digital Microscope AD413T (1.3 megapixel image sensor, magnification of 200x) and a Dino-Lite Pro Portable Digital Microscope AM4113ZT4 (1.3 megapixel image sensor, polarized light, magnification of 400x).

Exposure to UV radiation was carried out using a Spectroline Lamp, Model ENF-260C/FE, with an emission in the UV-A range at wavelength 365 nm (tube of 6W).

Colorimetric analyses were performed using a SP60 X·Rite portable spectrophotometer. The color coordinates were based on CIEL*a*b* system, a D65 illuminant and an observer angle of 10 were used. The measurements were performed in SPEX mode.

6.3 Syntheses

6.3.1 Synthesis of the allyl α,α'-trehalose

In a Sovirel® tube an aqueous solution of KOH (6.00 mL, 2.11 M) was added under nitrogen atmosphere to α,α'-trehalose (1.59 mmol) and the mixture

was heated at 60°C for 1 hour. After cooling to room temperature, allyl bromide (0.82 mL, 9.47 mmol) was added under nitrogen atmosphere and the reaction mixture was allowed to react at 60°C for 48 hours under vigorous stirring. After cooling to room temperature, the pH was adjusted to neutrality using HCl (2 N) and finally the solvent and the residual allyl bromide were distilled at reduced pressure. The resulting solid was extracted in ethanol to separate the product from salts. The alcoholic phase was distilled at reduced pressure and a white solid was obtained (673.02 mg, DS = 1.3, 97% yield). ^{1}H-NMR (D_2O, 400 MHz, ppm): from 3.40 to 3.97 (m, 12H, H_2-H_6, H_2'-H_6'); from 4.09 to 4.37 (m, 2H, -C**H$_2$**-CH=CH_2 allyl group); 5.21 (m, 2H, H_1, H_1'); from 5.28 to 5.41 (m, 2H, -CH_2-CH=C**H$_2$** allyl group); 5.97 (m, 1H, -CH_2-C**H**=CH_2 allyl group). ^{13}C-NMR (D_2O, 100 MHz, ppm): 60.0, 60.2, 60.5 (C_6, C_6'); 68.4 (C_6 functionalized, C_6' functionalized); 69.4, 69.6, 69.8 (C_4, C_4'); 70.6, 70.9, 71.1 (C_2, C_2'); from 71.6 to 72.4 (C_5, C_5', C_3, C_3'); 73.9 (-**C**H_2-CH=CH_2 allyl group); 77.4 (C_4 functionalized, C_4' functionalized); 78.0 (C_2 functionalized, C_2' functionalized); 91.1, 93.1, 93.2, 93.6 (C_1, C_1'); 118.3, 118.5, 118.7, 118.8, 119.2 (-CH_2-**C**H=CH_2 allyl group); 133.4, 133.5, 133.7 (-CH_2-CH=**C**H_2 allyl group). FT-IR (KBr pellets): peaks at 3390 (s, O-H stretching); 3081, 3017 (w, =C-H stretching); 2933 (m, -C-H stretching); 1645 (m, C=C stretching); 1149, 1105, 1076, 1047, 993 (s, C-OH stretching, C-O-C stretching); 941 (m, =C-H out of plane bending) cm^{-1}.

6.3.2 Synthesis of the allyl α,α'-trehalose/vinyl acetate copolymer

In a Sovirel® tube vinyl acetate (6.46 mmol, 0.60 mL) and a solution of allyl α,α'-trehalose in methanol (0.51 mmol in 2.50 mL) were added under nitrogen atmosphere to azobisisobutyronitrile (AIBN) (22.70 mg). Then, the reaction mixture was allowed to react at 90°C for 6 hours under continuous stirring. After cooling to room temperature, the solvent and the residual vinyl acetate were distilled at reduced pressure and the solid was extracted in acetone. The soluble fraction was distilled at reduced pressure and a pale orange solid was obtained (fraction A+B). Finally, the solid was extracted in

Milli-Q water and two fractions were obtained: fraction A (soluble in water) and fraction B (insoluble in water).

Fraction A+B (491.40 mg, 65% yield). ^{1}H-NMR (CD_3OD, 200 MHz, ppm): 1.51 (s, 6H, C**H$_3$** AIBN); 1.84 (m, 2H, CH_3-CO-CH-C**H$_2$**- vinyl acetate unit); 2.00, 2.03, 2.05 (m, 3H, C**H$_3$**-CO-CH-CH_2- vinyl acetate unit); from 3.40 to 4.50 (m, 12H, H_2-H_6, H_2'-H_6' and 2H, -C**H$_2$**-CH=CH_2 allyl group); 4.87 (m, 1H, CH_3-CO-C**H**-CH_2- vinyl acetate unit); from 5.05 to 5.38 (m, 2H, H_1, H_1' and 2H, -CH_2-CH=C**H$_2$** allyl group); 5.95 (m, 1H, -CH_2-C**H**=CH_2 allyl group). ^{13}C-NMR (CD_3OD, 50 MHz, ppm): 21.3 (**C**H_3-CO-CH-CH_2- vinyl acetate unit); 23.3 (**C**H_3 AIBN); 40.0, 40.4, 40.7, 41.1 (CH_3-CO-CH-**C**H_2- vinyl acetate unit); 62.8 (C_6, C_6'); from 68.2 to 74.9 (CH_3-CO-**C**H-CH_2- vinyl acetate unit, C_2-C_5, C_2'-C_5'); 95.2 (C_1, C_1'); 116.7, 116.8, 117.3 (-CH_2-**C**H=CH_2 allyl group); 136.5, 136.8 (-CH_2-CH=**C**H_2 allyl group); 172.4 (CH_3-**C**O-CH-CH_2- vinyl acetate unit). FT-IR (KBr pellets): peaks at 3435 (s, O-H stretching); 2935 (m, -C-H stretching); 1736 (s, C=O stretching acetate group); 1647 (m, C=C stretching); 1433, 1375 (m, CH_3- bending acetate group); 1244 (s, C-O stretching acetate group); 1146, 1105, 1080, 1043, 1024, 995 (s, C-OH stretching, C-O-C stretching); 945 (m, =C-H out of plane bending) cm^{-1}.

Fraction A (122.28 mg, 16% yield). ^{1}H-NMR (D_2O, 400 MHz, ppm): 1.96 (m, 2H, CH_3-CO-CH-C**H$_2$**- vinyl acetate unit); 2.13, 2.17, 2.23, 2.27 (m, 3H, C**H$_3$**-CO-CH-CH_2- vinyl acetate unit); from 3.39 to 3.97 (m, 12H, H_2-H_6, H_2'-H_6'), from 4.12 to 4.45 (2H, -C**H$_2$**-CH=CH_2 allyl group); 4.97, 5.06 (m, 1H, CH_3-CO-C**H**-CH_2- vinyl acetate unit); 5.23 (m, 2H, H_1, H_1'); from 5.30 to 5.41 (2H, -CH_2-CH=C**H$_2$** allyl group); 6.00 (m, 1H, -CH_2-C**H**=CH_2 allyl group). ^{13}C-NMR (D_2O, 100 MHz, ppm): 20.7 (**C**H_3-CO-CH-CH_2- vinyl acetate unit); 38.3 (CH_3-CO-CH-**C**H_2- vinyl acetate unit); 60.2, 60.3, 60.5 (C_6, C_6'); 63.3, 63.4 (CH_3-CO-**C**H-CH_2- vinyl acetate unit); 68.5 (C_6, C_6' functionalized); 69.5, 69.7, 69.9 (C_4, C_4'); 70.7, 71.0, 71.2 (C_2, C_2'); from 71.7 to 72.5 (C_5, C_5', C_3, C_3'); 73.9 (-**C**H_2-CH=CH_2 allyl group); 77.6 (C_4, C_4' functionalized); 78.1 (C_2, C_2' functionalized); 91.3, 93.1, 93.2, 93.3 (C_1, C_1'); 118.2, 118.5, 118.8, 119.1 (-CH_2-**C**H=CH_2 allyl group); 133.5, 133.6, 133.9 (-CH_2-CH=**C**H_2 allyl group); 173.3 (CH_3-**C**O-CH-CH_2- vinyl acetate unit). FT-IR (KBr pellets): peaks at 3381 (s, O-H stretching); 2933 (m, -C-H stretching); 1738 (m, C=O stretching acetate group); 1647 (m, C=C stretching); 1425, 1373 (m, CH_3- bending acetate group); 1247 (m, C-O

stretching acetate group); 1149, 1105, 1078, 1047, 993 (s, C-OH stretching, C-O-C stretching); 941 (m, =C-H out of plane bending) cm^{-1}.

Fraction B (368.55 mg, 49% yield). ^{1}H-NMR ($CDCl_3$, 400 MHz, ppm): 1.52 (s, 6H, C**H$_3$** AIBN); 1.74, 1.83 (m, 2H, CH_3-CO-CH-C**H$_2$**- vinyl acetate unit); 1.97, 2.00, 2.01 (m, 3H, C**H$_3$**-CO-CH-CH_2- vinyl acetate unit); from 2.70 to 4.40 (m, 12H, H_2-H_6, H_2'-H_6' and 2H, -C**H$_2$**-CH=CH_2 allyl group); 4.84 (m, 1H, CH_3-CO-C**H**-CH_2- vinyl acetate unit); from 4.90 to 5.30 (m, 2H, H_1, H_1' and 2H, -CH_2-CH=C**H$_2$** allyl group); 5.88 (m, 1H, -CH_2-C**H**=CH_2 allyl group). ^{13}C-NMR ($CDCl_3$, 100 MHz, ppm): 21.0 (**C**H_3-CO-CH-CH_2- vinyl acetate unit); 23.4 (**C**H_3 AIBN); 38.6, 39.1, 39.8 (CH_3-CO-CH-**C**H_2- vinyl acetate unit); 66.0, 66.3, 66.7, 66.9, 67.9 (CH_3-CO-**C**H-CH_2- vinyl acetate unit); 170.3 (CH_3-**C**O-CH-CH_2- vinyl acetate unit). FT-IR (KBr pellets): peaks at 3460 (m, O-H stretching); 2933 (m, -C-H stretching); 1738 (s, C=O stretching acetate group); 1652 (w, C=C stretching); 1435, 1373 (s, CH_3- bending acetate group); 1244 (s, C-O stretching acetate group); 1105, 1022, 997 (s, C-OH stretching, C-O-C stretching); 945 (m, =C-H out of plane bending) cm^{-1}.

6.3.3 Synthesis of the allyl α,α'-trehalose/vinyl alcohol copolymer

In a dry two-necked flask equipped with a bubble condenser and an isobaric dropping funnel, 3.20 mL of anhydrous methanol were added to KOH (32.09 mg) under nitrogen atmosphere and the mixture was maintained at room temperature (25°C) until the solid was dissolved. Then, a solution of the copolymer between allyl α,α'-trehalose and vinyl acetate in anhydrous methanol (8.13 mmol in 4.70 mL) was added and the mixture was allowed to react at 50°C for 1 hour under continuous stirring. During the reaction a solid precipitated while it was formed and at the end it was separated from the solution through a centrifugation. The solid (fraction 1) was dried under vacuum while the solution (fraction 2) was distilled at reduced pressure. The two obtained solids were characterized separately.

Fraction 1 (332.60 mg). ^{1}H-NMR (D_2O, 400 MHz, ppm): 1.61, 1.64, 1.68, 1.70 (m, 2H, C**H$_2$**-CH(OH)- vinyl alcohol unit); from 3.39 to 4.20 (m, H_2-H_6, H_2'-H_6',

CH_2-C**H**(OH)- vinyl alcohol unit and 2H, -C**H_2**-CH=CH_2 allyl group); 5.18 (m, 2H, H_1, H_1'); from 5.24 to 5.39 (m, 2H, -CH_2-CH=C**H_2** allyl group); 5.96 (m, 1H, -CH_2-C**H**=CH_2 allyl group). ^{13}C-NMR (D_2O, 100 MHz, ppm): 43.6, 44.1, 44.2, 44.6, 44.9 (**C**H_2-CH(OH)- vinyl alcohol unit); 60.7 (C_6, C_6'); 64.8, 65.0, 65.2 (CH_2-**C**H(OH)- vinyl alcohol unit); from 66.3 to 72.7 (C_2-C_5, C_2'-C_5'); 93.4 (C_1, C_1'), 119.2 (-CH_2-**C**H=CH_2 allyl group); 134.1 (-CH_2-CH=**C**H_2 allyl group). FT-IR (KBr pellets): peaks at 3355 (s, O-H stretching); 2937 (m, -C-H stretching); 1747 (w, C=O stretching acetate group); 1645 (m, C=C stretching); 1436 (m, CH_3- bending acetate group); 1144, 1104, 1082, 1051, 993 (s, C-OH stretching, C-O-C stretching); 942 (w, =C-H out of plane bending) cm^{-1}.

Fraction 2 (171.20 mg). ^{1}H-NMR (D_2O, 200 MHz, ppm): 1.58, 1.60, 1.61, 1.67 1.68 (m, 2H, C**H_2**-CH(OH)- vinyl alcohol unit); from 3.39 to 4.32 (m, H_2-H_6, H_2'-H_6', CH_2-C**H**(OH)- vinyl alcohol unit and 2H, -C**H_2**-CH=CH_2 allyl group); 5.16 (m, 2H, H_1, H_1'); from 5.24 to 5.36 (m, 2H, -CH_2-CH=C**H_2** allyl group); 5.94 (m, 1H, -CH_2-C**H**=CH_2 allyl group). ^{13}C-NMR (D_2O, 50 MHz, ppm): 43.3, 43.9, 44.1, 44.5, 44.7 (**C**H_2-CH(OH)- vinyl alcohol unit); 60.4 (C_6, C_6'); 64.8, 65.0, 65.2 (CH_2-**C**H(OH)- vinyl alcohol unit); from 66.3 to 72.7 (C_2-C_5, C_2'-C_5'); 93.4 (C_1, C_1'), 119.2 (-CH_2-**C**H=CH_2 allyl group); 134.0 (-CH_2-CH=**C**H_2 allyl group). FT-IR (KBr pellets): peaks at 3360 (s, O-H stretching); 2943 (m, -C-H stretching); 1650 (m, C=C stretching acetate group); 1411 (m, CH_3- bending acetate group); 1148, 1102, 1082, 1050, 995 (m, C-OH stretching, C-O-C stretching); 943 (w, =C-H out of plane bending) cm^{-1}.

6.3.4 Synthesis of the methyl D-glucopyranoside (mixture of methyl α-D-glucopyranoside and methyl β-D-glucopyranoside)

In a Sovirel® tube D-cellobiose (0.73 mmol) and methanol (5.00 mL) were added under nitrogen atmosphere to 250.00 mg of activated Amberlite IR-120H resin and the reaction mixture was allowed to react at 95°C for four days under gentle stirring. After cooling to room temperature, the product was recovered after filtration on a Büchner funnel and distillation at reduced pressure of the solution (237.00 mg, 83% yield). ^{1}H-NMR (D_2O, 400 MHz, ppm): 3.28 (t, 1H, H_2^{α}); from 3.37 to 3.42 (m, 2H, H_5^{α}, H_5^{β}); 3.44 (s, 3H,

–O-C**H**$_3^{\alpha}$); from 3.46 to 3.53 (m, 2H, H_2^{β}, H_3^{β}); 3.57 (m, 1H, H_4^{α}); 3.59 (s, 3H, –O-C**H**$_3^{\beta}$); from 3.64 to 3.67 (m, 2H, H_3^{α}, H_4^{β}); from 3.71 to 3.96 (m, 4H, H_6^{α}, H_6^{β}); 4.40 (d, 1H, H_1^{β}); 4.83 (d, 1H, H_1^{α}). ^{13}C-NMR (D_2O, 100 MHz, ppm): 55.0 (–O-**C**H_3^{α}); 57.1 (–O-**C**H_3^{β}); 60.5 (C_6^{α}); 60.7 (C_6^{β}); 69.5 (C_5^{α}); 69.6 (C_5^{β}); 71.2 (C_4^{α}); 71.5 (C_3^{α}); 73.0 (C_2^{α}, C_4^{β}); 75.7 (C_3^{β}); 75.8 (C_2^{β}); 99.2 (C_1^{α}); 103.2 (C_1^{β}). FT-IR (KBr pellets): peaks at 3383 (s, O-H stretching); 2912 (m, -C-H stretching); 1144, 1102, 1074, 1047, 1029 (s, C-OH stretching, C-O-C stretching) cm^{-1}.

6.3.5 Synthesis of the allyl methyl D-glucopyranoside

In a Sovirel® tube an aqueous solution of KOH (1.00 mL, 3.90 M) was added under nitrogen atmosphere to methyl D-glucopyranoside (0.98 mmol) and the mixture was heated at 70°C for 1 hour. After cooling to room temperature, allyl bromide (0.28 mL, 3.23 mmol) was added under nitrogen atmosphere and the reaction mixture was allowed to react at 70°C for 48 hours under vigorous stirring. After cooling to room temperature, the pH was adjusted to neutrality using HCl (2N) and the solvent and the residual allyl bromide were distilled at reduced pressure. The resulting solid was extracted in ethanol to separate the product from salts. The alcoholic phase was distilled at reduced pressure and a pale yellow solid was obtained (239.39 mg, DS = 1.1, 90% yield). ^{1}H-NMR (D_2O, 400 MHz, ppm): from 3.18 to 3.36 (m, 1H, H_2^{α}); 3.46 (s, 3H, –O-C**H**$_3^{\alpha}$); 3.62 (s, 3H, –O-C**H**$_3^{\beta}$); from 3.37 to 3.94 (m, H_3^{α}-H_6^{α}, H_2^{β}-H_6^{β}); from 4.13 to 4.38 (m, 2H, -C**H**$_2$-CH=CH_2 allyl group); from 4.64 to 4.74 (m, 1H, H_1^{β}); from 4.83 to 4.86, from 5.00 to 5.03, from 5.24 to 5.28 (m, 1H, H_1^{α}); from 5.30 to 5.42 (m, 2H, -CH_2-CH=C**H**$_2$ allyl group); 6.01 (m, 1H, -CH_2-C**H**=CH_2 allyl group). ^{13}C-NMR (D_2O, 100 MHz, ppm): 54.7 (–O-**C**H_3^{α}); 57.1 (–O-**C**H_3^{β}); 60.3, 60.5, 60.7 (C_6^{α}, C_6^{β}); 68.4, 68.6, 68.8 (C_6^{α} functionalized, C_6^{β} functionalized); 69.6, 69.8 (C_5^{α}, C_5^{β}); 71.2, 71.4 (C_4^{α}); 71.5 (C_3^{α}); 71.7, 72.0, 73.7 (-**C**H_2-CH=CH_2 allyl group); 74.0, 74.6 (C_2^{α}, C_4^{β}); 75.7, 75.9 (C_2^{β}, C_3^{β}); 77.4 (C_4^{α} functionalized, C_4^{β} functionalized); 78.3 (C_2^{α} functionalized, C_2^{β} functionalized); 95.8 (C_1^{α}); 99.2 (C_1^{β}); 118.7 (-CH_2-CH=**C**H_2 allyl group); 133.6 (-CH_2-**C**H=CH_2 allyl group). FT-IR (KBr pellets): peaks at 3381(s, O-H stretching); 3080, 3011 (w, =C-H stretching); 2935 (m, -

C-H stretching); 1645 (m, C=C stretching); 1146, 1103, 1076, 1051 (s, C-OH stretching, C-O-C stretching); 930 (w, =C-H out of plane bending) cm^{-1}.

6.3.6 Synthesis of the allyl methyl D-glucopyranoside/vinyl acetate copolymer

In a Sovirel® tube a solution of allyl methyl D-glucopyranoside in methanol (0.90 mmol in 2.5 mL) and vinyl acetate (5.80 mmol, 0.54 mL) were added under nitrogen atmosphere to azobisisobutyronitrile (AIBN) (20.25 mg). Then, the reaction mixture was allowed to react at 90°C for 6 hours under continuous stirring. After cooling to room temperature, the solvent and the residual vinyl acetate were distilled at reduced pressure and the solid was extracted in acetone. The soluble fraction was distilled at reduced pressure and a yellow-orange solid was obtained (fraction A+B). Finally, the solid was extracted in with Milli-Q water and two fractions were obtained: fraction A (soluble in water) and fraction B (insoluble in water).

Fraction A+B (402.10 mg, 57% yield). ^{1}H-NMR (CD_3OD, 200 MHz, ppm): 1.52 (s, 6H, C**H$_3$** AIBN); 1.82 (m, 2H, CH_3-CO-CH-C**H$_2$**- vinyl acetate unit); 1.99, 2.02, 2.04 (m, 3H, C**H$_3$**-CO-CH-CH_2- vinyl acetate unit); 3.40 (m, 3H, -OC**H$_3^{\alpha}$**); 3.53 (m, 3H, -OC**H$_3^{\beta}$**); from 3.00 to 4.00 (m, 12H, H_2^{α}-H_6^{α}, H_2^{β}-H_6^{β}); from 4.01 to 5.40 (m, 1H, H_1^{α}, 1H, H_1^{β}, 2H, -C**H$_2$**-CH=CH_2 allyl group, 1H, CH_3-CO-CH_2-C**H**- vinyl acetate unit, 2H, -CH_2-CH=C**H$_2$** allyl group); 5.91 (m, 1H, -CH_2-C**H**=CH_2 allyl group). ^{13}C-NMR (CD_3OD, 100 MHz, ppm): 21.2 (**C**H_3-CO-CH-CH_2- vinyl acetate unit); 23.3 (**C**H_3 AIBN); 39.9, 40.3, 40.7, 41.0 (CH_3-CO-CH-**C**H_2- vinyl acetate unit); 55.6 (–O-**C**H_3^{α}); 57.3 (–O-**C**H_3^{β}); 62.8 (C_6^{α}, C_6^{β}); from 62.3 to 78.1 (CH_3-CO-**C**H-CH_2- vinyl acetate unit, C_2^{α}-C_5^{α}, C_2^{β}-C_5^{β}, C_2^{α} functionalized, C_2^{β} functionalized, C_4^{α} functionalized, C_4^{β} functionalized, C_6^{α} functionalized, C_6^{β} functionalized, -**C**H_2-CH=CH_2 allyl group); 99.3, 101.3, 105.5 (C_1^{α}, C_1^{β}); 116.7, 117.2, 117.6 (-CH_2-CH=**C**H_2 allyl group); 136.1, 136.5 (-CH_2-**C**H=CH_2 allyl group); 172.3 (CH_3-**C**O-CH-CH_2- vinyl acetate unit). FT-IR (KBr pellets): peaks at 3420 (m, O-H stretching); 2926 (m, -C-H stretching); 1734 (s, C=O stretching acetate group); 1647 (w, C=C stretching); 1437, 1373 (s, CH_3-bending acetate group); 1244 (s, C-O stretching acetate group); 1147, 1103,

1079, 1047, 1026 (s, C-OH stretching, C-O-C stretching); 946 (m, =C-H out of plane bending) cm^{-1}.

Fraction A (80.42 mg, 12% yield). ^{1}H-NMR (D_2O, 200 MHz, ppm): 1.86 (m, 2H, CH_3-CO-CH-C**H$_2$**- vinyl acetate unit); 2.04, 2.07, 2.08, 2.10 (m, 3H, C**H$_3$**-CO-CH-CH_2- vinyl acetate unit); 3.36 (m, 3H, -OC**H$_3^{\alpha}$**); 3.51 (m, 3H, -OC**H$_3^{\beta}$**); from 3.07 to 3.90 (m, 12H, H_2^{α}-H_6^{α}, H_2^{β}-H_6^{β}); from 4.02 to 5.33 (m, 1H, H_1^{α}, 1H, H_1^{β}, 2H, -C**H$_2$**-CH=CH_2 allyl group, 1H, CH_3-CO-CH_2-C**H**- vinyl acetate unit, 2H, -CH_2-CH=C**H$_2$** allyl group); 5.88 (m, 1H, -CH_2-C**H**=CH_2 allyl group). ^{13}C-NMR (D_2O, 50 MHz, ppm): 20.3, 20.8 (**C**H_3-CO-CH-CH_2- vinyl acetate unit); 38.4, 39.0, 41.0 (CH_3-CO-CH-**C**H_2- vinyl acetate unit); 55.2 (–O-**C**H_3^{α}); 57.3 (–O-**C**H_3^{β}); 62.8 (C_6^{α}, C_6^{β}); 60.8 (CH_3-CO-**C**H-CH_2- vinyl acetate unit); from 62.3 to 81.2 (C_2^{α}-C_5^{α}, C_2^{β}-C_5^{β}, C_2^{α} functionalized, C_2^{β} functionalized, C_4^{α} functionalized, C_4^{β} functionalized, C_6^{α} functionalized, C_6^{β} functionalized, -**C**H_2-CH=CH_2 allyl group); 97.4, 99.4, 103.4 (C_1^{α}, C_1^{β}); 118.5, 118.8 (-CH_2-CH=**C**H_2 allyl group); 164.0, 134.3 (-CH_2-**C**H=CH_2 allyl group); 173.5 (CH_3-**C**O-CH-CH_2- vinyl acetate unit). FT-IR (KBr pellets): peaks at 3383 (s, O-H stretching); 2932 (m, -C-H stretching); 1732 (m, C=O stretching acetate group); 1645 (m, C=C stretching); 1456, 1373 (m, CH_3- bending acetate group); 1253 (m, C-O stretching acetate group); 1148, 1105, 1074, 1047 (s, C-OH stretching, C-O-C stretching); 930 (w, =C-H out of plane bending) cm^{-1}.

Fraction B (321.68 mg, 46% yield). ^{1}H-NMR ($CDCl_3$, 400 MHz, ppm): 1.50 (s, 6H, C**H$_3$** AIBN); 1.71, 1.79 (m, 2H, CH_3-CO-CH-C**H$_2$**- vinyl acetate unit); 1.95, 1.98, 2.00 (m, 3H, C**H$_3$**-CO-CH-CH_2- vinyl acetate unit); 3.36 (m, 3H, -OC**H$_3^{\alpha}$**); 3.49 (m, 3H, -OC**H$_3^{\beta}$**); from 2.90 to 3.90 (m, 12H, H_2^{α}-H_6^{α}, H_2^{β}-H_6^{β} e); from 4.02 to 5.26 (m, 1H, H_1^{α}, 1H, H_1^{β}, 2H, -C**H$_2$**-CH=CH_2 allyl group, 1H, CH_3-CO-CH_2-C**H**- vinyl acetate unit, 2H, -CH_2-CH=C**H$_2$** allyl group); 5.88 (m, 1H, -CH_2-C**H**=CH_2 allyl group). ^{13}C-NMR ($CDCl_3$, 100 MHz, ppm): 20.9, 21.0 (**C**H_3-CO-CH-CH_2- vinyl acetate unit); 23.3 (**C**H_3 AIBN); 38.6, 39.0, 39.4, 39.8 (CH_3-CO-CH-**C**H_2- vinyl acetate unit); 55.2 (–O-**C**H_3^{α}); 57.0 (–O-**C**H_3^{β}); 62.8 (C_6^{α}, C_6^{β}); 60.8 (CH_3-CO-**C**H-CH_2- vinyl acetate unit); from 62.0 to 74.5 (CH_3-CO-**C**H-CH_2- vinyl acetate unit, C_2^{α}-C_6^{α}, C_2^{β}-C_6^{β}, C_2^{α} functionalized, C_2^{β} functionalized, C_4^{α} functionalized, C_4^{β} functionalized, C_6^{α} functionalized, C_6^{β} functionalized, -**C**H_2-CH=CH_2 allyl group); 170.3, 170.4 (CH_3-**C**O-CH-CH_2- vinyl acetate unit). FT-IR (KBr pellets): peaks at 3495 (m, O-H stretching); 2930 (m, -C-H stretching);

1732 (s, C=O stretching acetate group); 1647 (w, C=C stretching); 1435, 1373 (m, CH_3- bending acetate group); 1242 (s, C-O stretching acetate group); 1105, 1045, 1022 (s, C-OH stretching, C-O-C stretching); 947 (m, =C-H out of plane bending) cm^{-1}.

6.3.7 Synthesis of the allyl methyl D-glucopyranoside/vinyl alcohol copolymer

In a dry two-necked flask equipped with a bubble condenser and an isobaric dropping funnel, 2.30 mL of anhydrous methanol were added to KOH (22.84 mg) under nitrogen atmosphere and the mixture was maintained at room temperature (25°C) until the solid was dissolved. Then, a solution of copolymer between allyl methyl D-glucopyranoside and vinyl acetate in anhydrous methanol (6.12 mmol in 3.30 mL) was added and the mixture was allowed to react at 50°C for 1 hour under continuous stirring. During the reaction a solid precipitated while it was formed and at the end it was separated from the solution through a centrifugation. The solid (fraction 1) was dried under vacuum while the solution (fraction 2) was distilled at reduced pressure. The two obtained solids were characterized separately.

Fraction 1 (232.30 mg). ^{1}H-NMR (D_2O, 200 MHz, ppm): 1.60, 1.62, 1.66, 1.69 (m, 2H, C**H$_2$**-CH(OH)- vinyl alcohol unit); from 3.20 to 3.88 (m, 18H, H_2^{α}-H_6^{β}, H_2^{α}-H_6^{β}, -OC**H$_3$**$^{\alpha}$, -OC**H$_3$**$^{\beta}$); 4.01 (m, 1H, CH_2-C**H**(OH)- vinyl alcohol unit); from 4.15 to 5.37 (m, 1H, H_1^{α}, H_1^{β}, 2H, -C**H$_2$**-CH=CH_2 allyl group, 2H, -CH_2-CH=C**H$_2$** allyl group); 5.96 (m, 1H, -CH_2-C**H**=CH_2 allyl group). ^{13}C-NMR (D_2O, 50 MHz, ppm): 43.6, 44.1, 44.3, 44.7, 44.9 (**C**H_2-CH(OH)- vinyl alcohol unit); 55.2 (–O-**C**H_3^{α}); 57.3 (–O-**C**H_3^{β}); 60.7 (C_6^{α}, C_6^{β}); 64.8, 65.0, 66.1 (CH_2-**C**H(OH)- vinyl alcohol unit); from 66.3 to 76.0 (C_2^{α}-C_5^{α}, C_2^{β}-C_5^{β} C_2^{α} functionalized, C_2^{β} functionalized, C_4^{α} functionalized, C_4^{β} functionalized, C_5^{α} functionalized, C_5^{β} functionalized, -**C**H_2-CH=CH_2 allyl group); 97.4, 99.4, 103.4 (C_1^{α}, C_1^{β}). FT-IR (KBr pellets): peaks at 3399 (s, O-H stretching); 2938 (m, -C-H stretching); 1750 (w, C=O stretching acetate group); 1652 (m, C=C stretching); 1435 (m, CH_3- bending acetate group); 1141, 1080, 1050 (s, C-OH stretching, C-O-C stretching); 920 (w, =C-H out of plane bending) cm^{-1}.

Fraction 2 (426.50 mg). ^{1}H-NMR (D_2O, 400 MHz, ppm): 1.57, 1.59, 1.60, 1.65, 1.67, 1.69 (m, 2H, C**H$_2$**-CH(OH)- vinyl alcohol unit); from 3.20 to 3.91 (m, 18H, H_2^{α}-H_6^{β}, H_2^{α}-H_6^{β}, -OC**H$_3$**$^{\alpha}$, -OC**H$_3$**$^{\beta}$); 4.00 (m, 1H, CH_2-C**H**(OH)- vinyl alcohol unit); from 4.14 to 5.33 (m, 1H, H_1^{α}, H_1^{β}, 2H, -C**H$_2$**-CH=CH_2 allyl group, 2H, -CH_2-CH=C**H$_2$** allyl group); 5.93 (m, 1H, -CH_2-C**H**=CH_2 allyl group). ^{13}C-NMR (D_2O, 100 MHz, ppm): 43.3, 43.8, 44.1, 44.6, 44.7 (**C**H_2-CH(OH)- vinyl alcohol unit); 55.0 (–O-**C**H_3^{α}); 57.1 (–O-**C**H_3^{β}); 60.5, 60.6 (C_6^{α}, C_6^{β}); 64.5, 64.6, 64.8 (CH_2-**C**H(OH)- vinyl alcohol unit); from 65.9 to 75.8 (C_2^{α}-C_5^{α}, C_2^{β}-C_5^{β} C_2^{α} functionalized, C_2^{β} functionalized, C_4^{α} functionalized, C_4^{β} functionalized, C_5^{α} functionalized, C_5^{β} functionalized, -**C**H_2-CH=CH_2 allyl group); 97.1, 99.2, 103.1 (C_1^{α}, C_1^{β}); 118.7 (-CH_2-CH=**C**H_2 allyl group); 133.7 (-CH_2-**C**H=CH_2 allyl group). FT-IR (KBr pellets): peaks at 3394 (s, O-H stretching); 2943 (m, -C-H stretching); 1747 (w, C=O stretching acetate group); 1647 (m, C=C stretching); 1420 (m, CH_3- bending acetate group); 1146, 1104, 1079, 1050 (s, C-OH stretching, C-O-C stretching); 920 (w, =C-H out of plane bending) cm^{-1}.

6.3.8 Activation of the TiO_2 anatase nanoparticles

In a dry flask equipped with a bubble condenser, TiO_2 anatase nanoparticles (20 mmol) and HNO_3 (2M) were allowed to react at 95°C for 8 hours under continuous stirring. After cooling to room temperature, the activated nanoparticles were centrifuged and dispersed in Milli-Q water (4.5% dispersion). FT-IR (KBr pellets): peaks at 3396 (w, O-H stretching); 1635 (w, O-H bending); 1386 (m, N-O stretching); 800-450 (s, Ti-O stretching) cm^{-1}. TEM: the diameter of nanoparticles is about 10-20 nm.

6.3.9 Functionalization of the TiO_2 anatase nanoparticles with vinyltriethoxysilane

In a Sovirel® tube the pH of the TiO_2 anatase nanoparticles dispersion (1.85 mL) was adjusted to 4 using a saturated solution of $NaHCO_3$. Then, vinyltriethoxysilane (0.505 mmol, 0.106 mL) and methanol (4 mL) were

added under nitrogen atmosphere to the nanoparticles dispersion. The mixture was heated at 40°C for 6 hours under continuous stirring. After cooling to room temperature, the solvent was distilled at reduced pressure and the solid was extracted with acetone three times. Finally, the insoluble fraction was dried under vacuum and a white solid was obtained (107.80 mg, 97% yield). FT-IR (KBr pellets): peaks at 3426 (m, O-H stretching); 3063 (w, -C=H stretching); 2973 (w, -C-H stretching); 1637, 1601 (w, C=C stretching); 1384 (s, N-O stretching); 1276 (w, C-O stretching); 1127, 1047 (m, Si-O stretching); 1008, 965 (w, =C-H out of plane bending); 800-450 (s, Ti-O stretching) cm^{-1}.

6.3.10 Synthesis of the allyl α,α'-trehalose/vinyl acetate copolymer on functionalized TiO_2 anatase nanoparticles

In a Sovirel® tube azobisisobutyronitrile (AIBN) (16.22 mmol), vinyl acetate (6.21 mmol, 0.57 mL) and a solution of allyl α,α'-trehalose in methanol (0.49 mmol in 2.45 mL) were added to the water dispersion of functionalized nanoparticles (0.50 mmol, 0.90 mL). The mixture was allowed to react at 80°C for 6 hours under continuous stirring. After cooling to room temperature, the solvent and the residual vinyl acetate were distilled at reduced pressure and the solid was extracted in acetone to obtain a white insoluble product (101.90 mg, 13% yield). ^{1}H-NMR (D_2O, 200 MHz, ppm): 2.08 (m, 3H, C**H$_3$**-CO-CH-CH_2- vinyl acetate unit); from 3.30 to 4.00 (m, 12H, H_2-H_6, H_2'-H_6' and 2H, Si-O-C**H$_2$**-CH_3); from 4.01 to 4.40 (m, 2H, -C**H$_2$**-CH=CH_2 allyl group); 5.18, 5.19 (m, 2H, H_1, H_1'); from 5.24 to 5.40 (m, 2H, -CH_2-CH=C**H$_2$** allyl group); 5.97 (m, 1H, -CH_2-C**H**=CH_2 allyl group). FT-IR (KBr pellets): peaks at 3381 (m, O-H stretching); 2926 (m, -C-H stretching); 1736 (m, C=O stretching acetate group); 1637 (w, C=C stretching); 1420, 1375 (m, CH_3- bending acetate group); 1248 (s, C-O stretching acetate group); 1150, 1105, 1078, 1047, 1032, 993 (s, C-OH stretching, C-O-C stretching, Si-O stretching); 941 (m, =C-H out of plane bending, Ti-O-Si stretching); 800-450 (s, Ti-O stretching) cm^{-1}.

6.3.11 Synthesis of the allyl methyl D-glucopyranoside/vinyl acetate copolymer on functionalized TiO_2 anatase nanoparticles

In a Sovirel® tube azobisisobutyronitrile (AIBN) (0.06 mmol), vinyl acetate (2.90 mmol, 0.27 mL) and a solution of allyl methyl D-glucopyranoside in methanol (0.45 mmol in 1.24 mL) were added to the water dispersion of functionalized nanoparticles (0.23 mmol, 0.4 mL). The mixture was allowed to react at 80°C for 6 hours under continuous stirring. After cooling to room temperature, the solvent and the residual vinyl acetate were distilled at reduced pressure and the solid was extracted in acetone to obtain a white insoluble product (37.20 mg, 10% yield). ^{1}H-NMR (D_2O, 200 MHz, ppm): 2.06 (m, 3H, C**H$_3$**-CO-CH-CH_2- vinyl acetate unit); 3.39 (-OC**H$_3^{\alpha}$**); 3.54 (-OC**H$_3^{\beta}$**); from 3.10 to 3.90 (m, 12H, H_2^{α}-H_6^{α}, H_2^{β}-H_6^{β} and 2H, Si-O-C**H$_2$**-CH_3); from 4.01 to 5.37 (m, 2H, -C**H$_2$**-CH=CH_2 allyl group, 2H, H_1^{α}, H_1^{β}, 2H, -CH_2-CH=C**H$_2$** allyl group); 5.94 (m, 1H, -CH_2-C**H**=CH_2 allyl group). FT-IR (KBr pellets): peaks at 3422 (s, O-H stretching); 2936 (m, -C-H stretching); 1732 (w, C=O stretching acetate group); 1645 (m, C=C stretching); 1412, 1384 (m, CH_3- bending acetate group); 1250 (m, C-O stretching acetate group); 1107, 1078, 1045, (m, C-OH stretching, C-O-C stretching, Si-O stretching); 574 (s, Ti-O stretching) cm^{-1}.

6.3.12 Synthesis of the oligo ethylene-L-tartaramide

In a Sovirel® tube, triethylamine (0.55 mmol, 0.08 mL) was added under nitrogen atmosphere and continuous stirring to a methanol solution of dimethyl L-tartrate (2.02 mmol, 9.00 mL). Then, ethylenediamine (2.02 mmol, 0.13 mL) was added and the mixture was heated at 80°C for 3 days. After cooling to room temperature, the mixture was filtered on a Büchner funnel and washed with methanol. The obtained solid was dried under vacuum (305.40 mg, 64% yield, T_g 104°C). ^{1}H-NMR (D_2O, 400 MHz, ppm): 3.09 (m, 4H, C**H$_2$**-NH_2); 3.48 (m, 4H, C**H$_2$**-NH-CO); 4.58 (m, 2H, C**H**-OH). ^{13}C-NMR (D_2O, 100 MHz, ppm): 38.5 (**C**H_2-NH-CO); 39.4 (**C**H_2-NH_2); 72.3 (**C**H-OH); 174.0 (**C**O-NH). FT-IR (KBr pellets): peaks at 3358, 3298 (s, N-H and O-H

stretching); 2941 (w, C-H stretching); 1659 (s, C-O amide stretching); 1539 (s, N-H amide bending); 1120, 1068 (w, C-O stretching) cm^{-1}.

6.3.13 Synthesis of the copolymer between ethylenediamine, adipic and tartaric acid

In a Sovirel® tube, dimethyl adipate (3.00 mmol) and dimethyl L-tartrate (3.00 mmol) were added under nitrogen atmosphere and continuous stirring to a methanol solution of ethylenediamine (6.00 mmol, 1.00 mL). The mixture was heated at 80 °C for 5 days. After cooling to room temperature, the mixture was filtered on a Büchner funnel and washed with diethyl ether. The obtained yellow solid was dried under vacuum (949.00 mg, 67% yield, T_g 109 °C).

6.3.14 Synthesis of the allyl n-hydroxypropyl cellulose

Into a dry two-necked flask equipped with a reflux condenser, powdered NaOH (16.00 mmol) was added under nitrogen atmosphere and continuous stirring to a LiCl/ N,N-dimethylacetamide (6% w/w) cellulose solution (500.00 mg, 20.00 mL) and the mixture was heated at 80°C for 40 minutes. After cooling to room temperature, a solution of 3-bromo-1-propanol in N,N-dimethylacetamide (8.00 mmol, 15.00 mL) was added and the mixture was allowed to react at 70°C for 18 hours. After cooling to room temperature, powdered NaOH (9.00 mmol) was added and the mixture was heated at 80°C for 40 minutes. After cooling to room temperature, a solution of allyl bromide in N,N-dimethylacetamide (4.50 mmol, 15 mL) was added and the mixture was allowed to react at 70°C for 5 hours. After cooling to room temperature, the reaction mixture was added to 250.00 mL of ethanol and the obtained precipitate was filtered on a Gooch funnel, washed with ethanol and dried under vacuum. The white solid was added to 100.00 mL of ethanol and kept under continuous stirring at room temperature for 3 hours. After filtration, the solid was dried in vacuum (620.00 mg, DS_{allyl} = 0.1, $DS_{n\text{-}hydroxypropyl}$ = 0.3, 98% yield). ^{1}H-NMR (D_2O, 400 MHz, ppm): 1.87 (m, 2H, -O-

CH_2-C**H_2**-CH_2-OH hydroxypropyl group); 3.23 (m, 1H, H_2); 3.68 (m, 4H, -O-C**H_2**-CH_2-**CH_2**-OH hydroxypropyl group); 3.83, 3.96, 3.98, 4.01 (m, 4H, H_3-H_6); 4.12 (m, 2H, -C**H_2**-CH=CH_2 allyl group); 4.54 (m, 1H, H_1); 5.33 (m, 2H, -CH_2-CH=C**H_2** allyl group); 5.99 (m, 1H, -CH_2-**CH**=CH_2 allyl group). FT-IR (KBr pellets): peaks at 3450 (s, O-H stretching); 2921, 2892 (w, C-H stretching); 1642 (s, C=C stretching); 1158, 1112, 1066, 1023 (s, C-OH stretching, C-O-C stretching) cm^{-1}.

6.3.15 Synthesis of the oligo di-ethylene triamino adipoamide

In a Sovirel® tube, dimethyl adipate (10.00 mmol) was added under nitrogen atmosphere to ethylene diamine (10.00 mmol). The reaction mixture was allowed to react at 80°C for 8 hours. After cooling to room temperature, a white solid was recovered after filtration, washed with diethyl ether and dried under vacuum at room temperature (1.04 g, 45% yield). 50.00 mg of the solid were extracted in water obtaining a soluble fraction (33.00 mg, 66% yield) and an insoluble one (17.00 mg, 34% yield).

Soluble fraction ^{1}H-NMR (D_2O, 400 MHz, ppm): 1.60 (m, 4H, C**H_2**-CH_2-CO-NH); 2.25 (m, 4H, CH_2-C**H_2**-CO-NH); 2.42 (m, 2H, C**H_2**-CO-OCH_3); 2.94 (m, 2H, C**H_2**-NH_2); from 3.20 to 3.45 (m, 4H, C**H_2**-NH-CO); 3.70 (s, 3H -OC**H_3**). ^{13}C-NMR (D_2O, 100 MHz, ppm): 23.6 (**C**H_2-CH_2-CO-OCH_3); 2.47 (**C**H_2-CH_2-CO-NH); 33.2 (**C**H_2-CO-OCH_3), 35.4 (**C**H_2-CO-NH); 38.5 (**C**H_2-NH-CO); 39.4 (**C**H_2-NH_2); 52.1 (-O**C**H_3); 176.7 (**C**O-NH); 177.1 (**C**O-OCH_3). FT-IR (KBr pellets): peaks at 3298 (s, N-H stretching); 3084, 2941, 2860 (m, C-H stretching); 1720 (m, C=O ester stretching); 1640 (s, C=O amide stretching); 1556 (s, N-H amide bending) cm^{-1}.

6.3.16 Synthesis of the oligoamide dimethyl-L-tartrate/L-lysine

In a Sovirel® tube, triethylamine (0.58 mmol) was added under nitrogen atmosphere to a methanol solution of L-lysine (2.15 mmol, 4.00 mL). Then, a methanol solution of dimethyl-L-tartrate (2.15 mmol, 4.00 mL) were added

and the mixture was allowed to react at 80°C for 7 days. After cooling to room temperature, the mixture was filtered on a Büchner funnel. The solid was washed with methanol and dried under vacuum at room temperature (375.00 mg, 54% yield). ^{1}H-NMR (D_2O, 400 MHz, ppm): 1.41 (m, 4H, H_γ); 1.59 (m, 4H, H_δ); 1.72 (m, 4H, $H_{\delta\ terminal}$); 1.88 (m, 4H, H_β); 3.02 (m, 4H, $H_{\varepsilon\ terminal}$, C**H$_2$**-$NH_2$); from 3.20 to 3.40 (m, 4H, H_ε, C**H$_2$**-NH-CO); 3.73, 4.22 (2H, H_α, C**H$_2$**-NH-CO, 1H, C**H**(COOH)NH-CO); 4.52 (m, 2H, C**H**-OH). ^{13}C-NMR (D_2O, 50 MHz, ppm): 20.8 (C_γ);25.6 ($C_{\delta\ terminal}$); 27.3 (C_δ); 29.3 (C_β); 37.9 (C_ε); 53.8 (C_α); 71.4 (**C**H-OH); 172.7, 173.9 (**C**O-NH). FT-IR (KBr pellets): peaks at 3323 (s, N-H and O-H stretching); 2939, 2864 (w, C-H stretching); 2630, 2131 (w, NH_3^+ stretching); 1645 (s, C=O amide stretching); 1582, 1516 (s, N-H amide bending); 1131, 1075 (m, C-O stretching) cm^{-1}.

6.4 Applicative studies

6.4.1 Consolidation of archaeological waterlogged wood

6.4.1.1 Preparation of the solutions of the consolidants

For all the tested consolidants, Milli-Q water was used as a solvent and concentrations under the limit of saturation were chosen to prepare the solutions:

- Allyl α,α'-trehalose/vinyl alcohol copolymer
  901.4 mg were dissolved in 19 mL of Milli-Q water (4.5%)
- Oligo ethylene-L-tartaramide
  904.2 mg were dissolved in 20 mL of Milli-Q water (4.3%)
- Copolymer between ethylenediamine, adipic acid and tartaric acid
  577.8 mg were dissolved in 22.5 mL of Milli-Q water (2.5%)
- Oligo esamethylene-L-tartaramide
  The brown hard solid (4.7 g) was grinded, put in a flask with 60 mL of Milli-Q water and the dispersion was kept under continuous stirring for 24 hours. Then, the mixture was centrifuged and the solution was separated from the solid. Several repetition of this procedure were performed and all the various saturated solutions were put together. The

opaque orange solution was decanted for 24 hours and finally it was centrifuged to separate the solution which was used for the treatment of the wooden samples (30 mL, 1.8%).

6.4.1.2 Preparation of the lignin samples

Oak wood flour was obtained by grinding the wood in an agate mortar and then passing it through a 300-µm sieve. The wood flour (116 mg) was introduced into a cellulose thimble and then placed into a Soxhlet extractor. The flask was filled with 200 mL of ethanol (95%) and after 6 hours of extraction the thimble was dried in an oven at 70°C for 24 hours.

The pre-extracted wood flour was added to 15 mL of sulfuric acid (72%) in a beaker and kept under continuous stirring at 0°C for 10 minutes. The beaker was then allowed to come back to room temperature and the stirring was continued for 2 hours. The solution was diluted to 3%, brought to the boiling point and kept at that temperature for 4 hours, adding water during the process to keep the volume constant. After cooling to room temperature, the solution was decanted and the lignin residue was filtered, washed and dried in an oven at 103°C.

6.4.1.3 Affinity tests on lignin samples

The lignin was kept under continuous stirring in the solution of the consolidant for 24 hours at room temperature (**Table 15**). Then the treated lignin was filtered, dried in an oven at 40°C and characterized by FT-IR spectroscopy.

Table 15 Affinity tests on lignin samples

Consolidant	Lignin (mg)	Solution of the consolidant (mL)
allyl α,α'-trehalose/vinyl alcohol copolymer	15	4.0
oligo ethylene-L-tartaramide	15	4.0
copolymer between ethylenediamine, adipic acid and tartaric acid	13	3.4
oligo esamethylene-L-tartaramide	15	4.0

6.4.1.4 Reversibility tests on treated lignin samples

The treated lignin was kept under continuous stirring in demineralized water for 24 hours at room temperature (**Table 16**). Then, the lignin was filtered, dried in an oven at 50°C and characterized by FT-IR spectroscopy.

Table 16 Reversibility test on treated lignin samples

Consolidant	Lignin (mg)	Water (mL)
allyl α,α'-trehalose/vinyl alcohol copolymer	6.5	1.5
oligo ethylene-L-tartaramide	13.4	2.5
copolymer between ethylenediamine, adipic acid and tartaric acid	10	2.0
oligo esamethylene-L-tartaramide	7.5	1.5

6.4.1.5 Preparation and treatment of the archaeological wooden samples

Two types of archaeological wood were used to obtain the samples which were used in this test:

1) wood of the genus *Quercus* from the archaeological site of Longola di Poggiomarino (NA), where a prehistoric stilt-house settlement (16^{th}-6^{th} century B.C.) was found in 2000 (**Figure 112**);

Figure 112 Archaeological site of Longola di Poggiomarino (NA)

2) wood of the genus *Fraxinus* from the archaeological site of the ancient roman harbor of Olbia (SA) (5^{th} century A.D.) (**Figure 113**).

Figure 113 Shipwreck in the ancient roman harbor of Olbia (SA)

Wooden finds were stored up to the time of use in test tubes filled with distilled water at 4°C in a climate-controlled room at the GESAAF

(Gestione dei Sistemi Agrari, Alimentari e Forestali) department of the University of Florence. These are the optimal conditions to preserve the archaeological waterlogged wood and to prevent microbial attacks.

16 cubical samples (volume 1 cm^3) were obtained from a suitable *Quercus* wood fragment (samples 1-16), while 4 slightly smaller cubical samples were obtained from a fragment of *Fraxinus* wood (samples 21F, 22F, 23F, 24F). Each sample was subsequently divided into two equal halves. One half of each specimen was treated with one of the chosen consolidants, while the corresponding other half (called control sample) was left untreated. For each of this 40 samples mass and volume were evaluated using, respectively, an analytical balance and the water displacement method, a procedure based on the Archimedes' principle. This procedure consists in immersing the wooden sample in a beaker filled with distilled water and placed on a digital balance. The sample is secured to the balance pan by an external support. The Archimedes' principle states that "*any object, wholly or partially immersed in a fluid, is buoyed up by a force equal to the weight of the fluid displaced by the object*". However, being the sample secured to the balance pan it cannot move, so the weight of the displaced water, which correspond to the volume of the sample, is discharged directly on the balance.

The samples were treated following the scheme in **Table 17**. Each consolidant was tested on four *Quercus* samples and one *Fraxinus* sample (5 samples in total) and the treatment was performed by immersing each wooden sample in a test tube containing 3.5 mL of the solution of the chosen consolidant. The control samples were immersed in test tubes containing 3.5 mL of deionized water. The treatment lasted 48 days and during this period all the test tubes were kept in a climate-controlled room at 20°C. At the end of the treatment, all the wooden specimens were extracted from the test tubes, dabbed to eliminate the residual solution from their surface and the "green" mass and "green" volume were measured respectively, with an analytical balance and with the water displacement method.

Table 17 Treated and untreated wooden samples

Consolidant	Treated *Quercus* samples	Treated *Fraxinus* samples	Control samples
allyl α,α'-trehalose/vinyl alcohol copolymer	1, 2, 3, 4	21F	1c, 2c, 3c, 4c, 21Fc
oligo ethylene-L-tartaramide	5, 6, 7, 8	22F	5c, 6c, 7c, 8c, 22Fc
copolymer between ethylenediamine, adipic acid and tartaric acid	9, 10, 11, 12	23F	9c, 10c, 11c, 12c, 23Fc
oligo esamethylene-L-tartaramide	13, 14, 15, 16	24F	13c, 14c, 15c, 16c, 24Fc

6.4.1.6 Controlled drying of the archaeological wooden samples

To dry the samples after the treatment, the method of exposing them to progressively decreasing humidity values was used. The treated and the control samples placed on glass Petri dishes were kept in a closed system which was maintained to a defined humidity value thanks to the presence of a saturated solution of salt. Moreover, a beaker containing xylene was put inside the system to prevent bacterial attacks. The basin was maintained in a climate-controlled room at 20°C until the end of the drying procedure.

According to the standard UNI ISO 483[157] three steps were performed by changing the salt solution and, consequently, the relative humidity (RH) inside the system (**Table 18**). At each step the samples were regularly weighted and only when the difference between two subsequent measurements was less than the 0.5% it was possible to move on the following step. As last step of the drying procedure, the standard UNI ISO 3130[158] provide for a heating at 104°C in an oven. However, in this case the temperature was maintained at 50°C in order to be not too above the T_g of the consolidants. At the end of this final step, the "anhydrous" weight and

the “anhydrous” volume of all the samples were measured respectively, with an analytical balance and with the water displacement method.

Table 18 Steps of the drying procedure

Steps	Conditions
1	RH 100% (distilled water) in a climate-controlled room (20°C)
2	RH 86% (saturated solution of KCl) in a climate-controlled room (20°C)
3	RH 65% (saturated solution of NH_4NO_3) in a climate-controlled room (20°C)
4	Oven (50°C)

6.4.1.7 Measure of the physical properties of the archaeological wooden samples

As regard the physical properties of the wooden samples, the maximum water content (MWC), the basic density (ρ_b) and the volumetric shrinkage (β_v) were evaluated using the weights and the volumes collected immediately after the treatment (“green” weight and “green” volume) and at the end of the drying procedure (“anhydrous” weight and “anhydrous” volume).

The maximum water content (MWC) was obtained using the following formula:

$$MWC = \frac{m_1 - m_0}{m_1} \cdot 100 \quad [\%]$$

where m_1 is the “green” weight of the sample and m_0 is the “anhydrous” weight of the sample.

The basic density (ρ_b) was obtained using the following formula:

$$\rho_b = \frac{m_o}{V_1} \quad \left[\frac{g}{cm^3}\right]$$

where m_0 is the “anhydrous” weight of the sample and $V_1$is the “green” volume of the sample.

The volumetric shrinkage (β_v) was obtained using the following formula:

$$\beta_v = \frac{V_1 - V_0}{V_1} \cdot 100 \quad [\%]$$

where V_1 is the "green" volume of the sample and V_0 is the "anhydrous" volume of the sample. The volumetric shrinkage was also evaluated qualitatively by comparing photos of treated and control samples taken with a digital microscope (200x).

6.4.1.8 Assessment of the penetration ability

The penetration ability of the tested consolidants was evaluated by recording FT-IR spectra of an internal and an external section of a treated sample and comparing them with the spectrum of the control sample (**Table 19**). For treated *Quercus* wood samples it was possible to identify an internal and an external section, while *Fraxinus* samples were too thin and did not allow to distinguish between the two sections. In this case, only one spectrum for each selected treated specimen was recorded and compared to that of the control sample.

Table 19 Sample selected to perform the assessment of the penetration ability

	Treated sample		Control sample
***Quercus* wood**	1	allyl α,α'-trehalose/vinyl alcohol copolymer	1c
	7	oligo ethylene-L-tartaramide	
	12	copolymer between ethylenediamine, adipic acid and tartaric acid	
	14	oligo esamethylene-L-tartaramide	
***Fraxinus* wood**	21F	allyl α,α'-trehalose/vinyl alcohol copolymer	21Fc
	22F	oligo ethylene-L-tartaramide	
	23F	copolymer between ethylenediamine, adipic acid and tartaric acid	
	24F	oligo esamethylene-L-tartaramide	

6.4.2 Antifungal treatment

6.4.2.1 Test of the methylene blue

A water dispersion containing 10 mg of the nanocomposite allyl α,α'-trehalose/vinyl acetate copolymer on functionalized TiO_2 anatase nanoparticles (only acetone insoluble fraction) was deposited on a glass microscope slide and dried overnight at room temperature. Then, a water solution of methylene blue ($2 \cdot 10^{-3}$ %) was dropped on the glass microscope slide both on the glass and above the nanocomposite (**Figure 114**). The glass microscope slide was then exposed to the UV light (365 nm) for 60 minutes and the discoloration of the methylene blue solution deposited on the nanocomposite was observed.

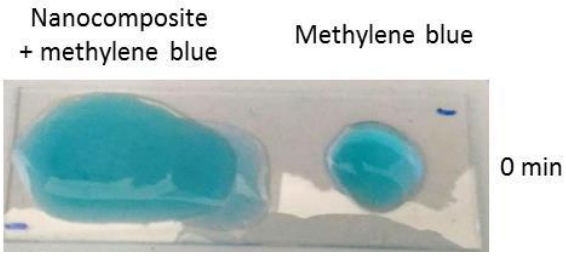

Figure 114 Set-up of the test of the methylene blue

6.4.2.2 Resistance of the nanocomposite to photodegradation

A water dispersion of the nanocomposite allyl α,α'-trehalose/vinyl acetate copolymer on functionalized TiO_2 anatase nanoparticles (only acetone insoluble fraction) (30 mg in 1 mL) was deposited on a Petri dish and dried in an oven at 40°C for 4 hours. Then, it was placed under the UV lamp (365 nm) and irradiated for 58 hours. The weight was monitored at regular intervals and, after 58 hours, an FT-IR spectrum of the product was recorded.

6.4.2.3 Microorganism and growth conditions

To assess the antifungal properties of the new nanocomposite, the fungus *Trametes versicolor* strain DSM 3086 was used. In particular, *Trametes versicolor* was grown on Malt Extract Agar (MEA, OXOID) plates and incubated to obtain a thick mycelium. The plates were incubates for 2-4 weeks and then used to perform the tests.

6.4.2.4 Preparation of the wooden samples

Recent wooden samples were obtained from *Fagus Selvatica L.* (European beech). Samples of 10x20x2 mm size were cut keeping the longitudinal faces parallel to the grain. Before the treatment, the wood samples were equilibrated at 20°C and 65% relative humidity by keeping them inside a basin together with a beaker filled of xylene which acted as fungal activity inhibitor.

6.4.2.5 Treatment of the samples and set-up of the tests

Two tests were performed to assess the antifungal properties of the nanocomposite allyl α,α'-trehalose/vinyl acetate copolymer on functionalized TiO_2 anatase nanoparticles. The first was performed with the nanocomposite which contained also not grafted polymer, while the second was performed with the nanocomposite purified from not grafted polymer.

32 wooden samples were used to perform the first test (**Figure 115**):

- 16 samples were treated with a dispersion of the allyl α,α'-trehalose/vinyl acetate copolymer/TiO_2 nanocomposite (both acetone soluble and insoluble fractions) in the mixture water/acetone 1:1 (2.08 g in 30 mL). This quantity was chosen in order to apply a theoretical amount of 14 mg of TiO_2 nanoparticles on each sample. The application was performed using a brush on all the faces of the samples and at the end the samples were dried in an oven at 35°C for 2 days.

- 16 samples were left untreated.

Before starting the exposition to the fungus, photos of the treated samples were taken using a digital microscope (200x) to verify the uniformity of the treatment. Then, the samples were placed on the *Trametes Versicolor* cultures, using a small sterile net to hold them up in order to avoid the direct contact with the mycelium. 4 samples (2 treated and 2 untreated) were placed on each plate. Finally, half of the plates were irradiated with the UV light, while the other half was kept in the dark (**Figure 115**). The exposition was carried out so as to simulate the behavior of the sunlight. In particular, the lamp was kept lit for 12 hours and turned off for 12 more using a timer for the whole duration of the test. The samples exposed to the UV light have been turned upside down every day in the middle of the illumination period so as to expose both sides to the radiation during the test. The experiment was performed in a climate-controlled room at 20°C and lasted 3 weeks. Photos were taken with the digital microscope (200x) after 12 days and at the end of the experiment.

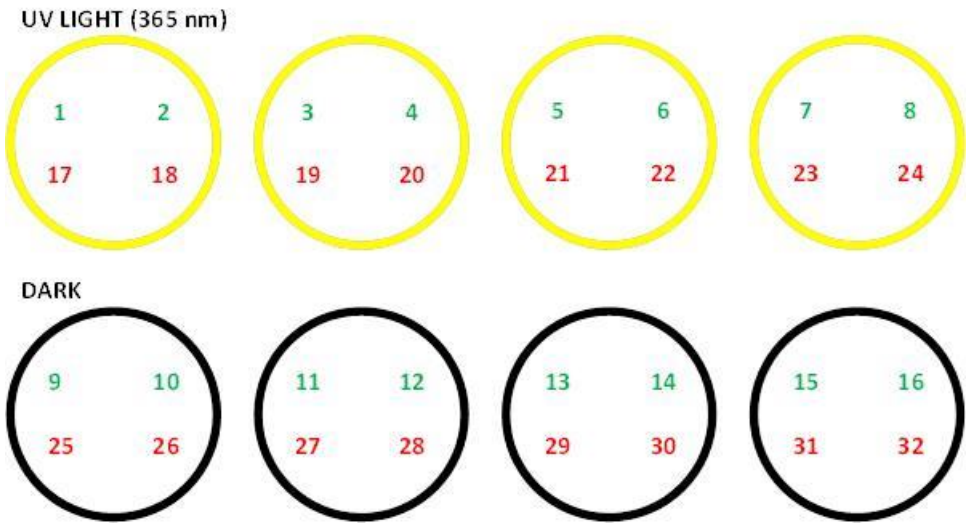

Figure 115 Set-up of the first test (1-16 treated samples, 17-32 untreated samples)

36 wooden samples were used to perform the second test (**Figure 116**):

- 16 samples were treated with a dispersion of the allyl α,α'-trehalose/vinyl acetate copolymer/TiO_2 nanocomposite (only acetone insoluble fraction) in 2-propanol (739.7 mg in 24 mL). This quantity was chosen in order to apply a theoretical amount of 20 mg of TiO_2 nanoparticles on each sample. The application was performed using a brush on all the faces of the samples and at the end the samples were dried at room temperature.
- 8 samples were treated with a dispersion of TiO_2 anatase nanoparticles in 2-propanol (165.52 mg in 4 mL). This quantity was chosen in order to apply a theoretical amount of 20 mg of TiO_2 nanoparticles on each sample. The application was performed using a brush on all the faces of the samples and at the end the samples were dried at room temperature.
- 2 samples were treated with 2-propanol (4 mL) using a brush on all the faces of the samples and at the end the samples were dried at room temperature.
- 10 samples were left untreated.

Before starting the exposition to the fungus, photos of the treated samples were taken using a digital microscope (200x) to verify the uniformity of the treatment. Then, the samples were placed on the *Trametes Versicolor* cultures, using a small sterile net to hold them up in order to avoid the direct contact with the mycelium. Some of the plates were irradiated with the UV light (365 nm), while the others was kept in the dark (**Figure 116**):

- 4 samples (2 treated with the nanocomposite, 1 treated with TiO_2 nanoparticles and 1 untreated) were placed on 8 plates (4 plates under the UV light, 4 plates in the dark).
- 4 samples (2 treated with 2-propanol and 2 untreated) were placed on another plate (in the dark).

The exposition was carried out so as to simulate the behavior of the sunlight. In particular, the lamp was kept lit for 12 hours and turned off for 12 more using a timer for the whole duration of the test. The samples exposed to the

UV light have been turned upside down every day in the middle of the illumination period so as to expose both sides to the radiation during the test. The experiment was performed in a climate-controlled room at 20°C and lasted 3 weeks. Photos were taken with the digital microscope (200x) after 7, 12, 17 days. At the end of the experiment photos of each sample were taken with the digital microscope (400x).

After 3 weeks of exposure, the plates which had been exposed to the UV radiation were moved outside the lamp keeping them in the dark for 1 week and then photos with the digital microscope (400x) were taken.

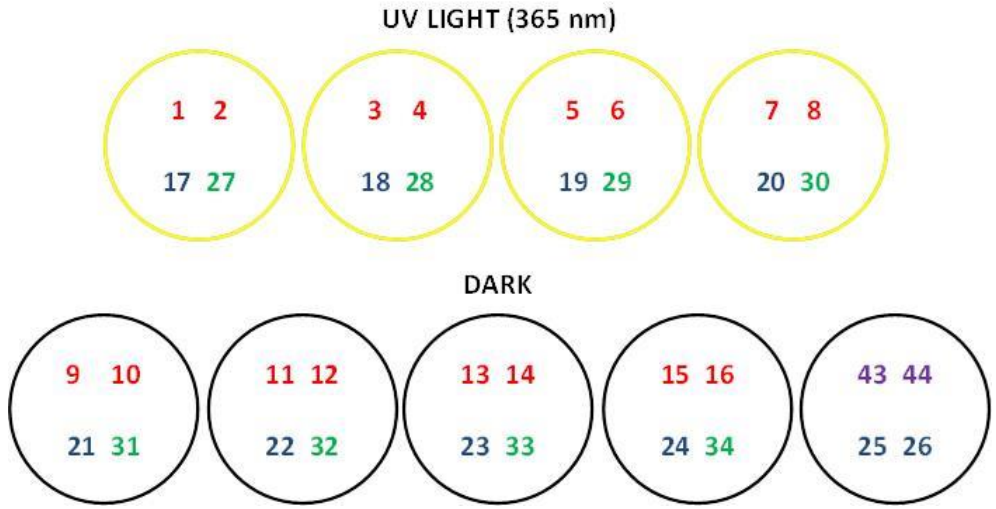

Figure 116 Set-up of the second test (1-16 samples treated with the nanocomposite, 17-16 untreated samples, 27-34 samples treated with the TiO_2 nanoparticles, 43-44 samples treated with 2-propanol)

6.4.3 Study of new formulations for paper treatment

6.4.3.1 Treatment of the samples

Whatman discs were treated with the dispersions of the consolidants in 2-propanol (5 mL of a dispersion with concentration of 5 mg/mL). The treatments were performed by spraying the dispersions on one face of each disk.

The TiO_2 nanoparticles were dispersed in 2-propanol (5 mg in 1 mL) while the $Ca(OH)_2$ nanoparticles were used as supplied (1.7 mL of an ethanol dispersion with concentration 3 g/L). The treatments with nanoparticles dispersions were performed with a plastic brush.

After the treatment, the samples were dried at room temperature and then exposed to the UV light (365 nm) for 24 hours. The FT-IR spectra of each sample were recorded after the treatment and after the exposition to the UV light.

6.4.3.2 Evaluation of the colorimetric changes

Colorimetric measures were performed on the untreated samples, after the treatment and after 24 hours of UV exposure using a portable spectrophotometer based on CIEL*a*b* system (**Figure 117**).

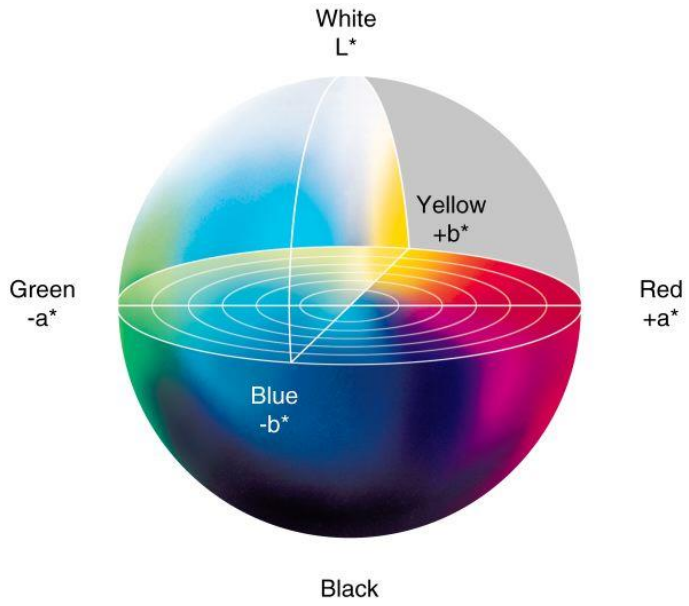

Figure 117 The CIEL*a*b* color space

This method is based on reflectance measurements that express the colors in numerical terms through a set of three space coordinates:

- L* that expresses the brightness and has values ranging from 0 (black) to 100 (white);
- a* that expresses the tint and has values ranging from -60 (green) to +60 (red);
- b* that expresses the tint and has values ranging from -60 (blue) to +60 (yellow).

Starting from the space coordinates of two samples or, as in this case, of the same sample in two subsequent stages, it is possible to evaluate the *color difference* (ΔE*) using the following equation:

$$\Delta E^* = \sqrt{\Delta L^{*2} + \Delta a^{*2} + \Delta b^{*2}}$$

However, to have a meaningful comparison the colorimetric measurements should always be carried out on the same spot of the sample. In order to do this, a mask was used because it allowed the correct positioning of the colorimeter. The ΔE*=3 value represents the detection limit of the human eye, so color differences less than or equal to this value correspond to imperceptible color variations.

Colorimetric measurements can be performed in SPIN or SPEX mode. In SPIN (specular component included) mode both the specular and the diffuse reflectance are recorded. In this way the total color appearance is measured regardless of surface conditions. In SPEX (specular component excluded) mode the specular reflectance is excluded and only the diffuse reflectance is recorded producing a color evaluation affine to the way in which an observer sees the color of an object. In this research, the colorimetric measurements on Whatman samples were performed in SPEX mode.

7 References

1. E. Sjöström, *Wood Chemistry Fundamentals and Applications*, Academic Press, Inc., Orlando, Florida, 1981

2. R. Whetten and R. Sederoff, *The Plant* Cell, 1995, **7**, 1001-1013

3. R. Vanholme, B. Demedts, K. Morreel, J. Ralph and W. Boerjan, *Plant Physiol.*, 2010, **153**, 895-905

4. G. Caneva, M. P. Nugari and O. Salvadori, *La biologia nel restauro*, Nardini Editore, Firenze, 2002

5. C. Gjelstrup Björdal, *Int. Biodeterior. Biodegrad.*, 2012, **70**, 126-140

6. G. Daniel, in *Secondary Xylem Biology*, ed. Y. S. Kim, R. Funada and A. P. Singh, Elsevier Inc., London, 2016, 8, 131-167

7. T. K. Kirk and D. Cullen, in *Environmentally Friendly Technologies for the Pulp and Paper Industry*, ed. R. A. Young and M. Akhtar, John Wiley & Sons, Inc., 605 Third Avenue, New York, NY, 1998, 9, 273-307

8. M.-L. E. Florian, *Adv. Chem. Ser.*, 1990, **225**, 3-32

9. R. A. Blanchette, *Int. Biodeterior. Biodegrad.*, 2000, **46**, 189-204

10. C. Gjelstrup Björdal, *Journal of Cultural Heritage*, 2012, **13S**, S118-S122

11. A. Gambetta, *Funghi e insetti nel legno. Diagnosi, prevenzione, controllo*, Nardini Editore, Firenze, 2010

12. Y. Kohdzuma, *Characteristics of Archeological Waterlogged Wood*, http://www.nara.accu.or.jp/elearning/2005/characterristics.pdf (accessed November 2016)

13. UNI 11205 (2007) *Cultural Heritage - Archaeological And Archaeo-Botanic Wood - Guidelines To The Characterization*

14. P. Jensen and D. J. Gregory, *J. Archaeol. Sci.*, 2006, **33**, 551-559

15. D. W. Grattan, *Stud. Conserv.*, 1982, **27**, 124-136

16. B. Kaye, D. J. Cole-Hamilton and K. Morphet, *Stud. Conserv.*, 2000, **45**, 233-252

17. S. Bugani, F. Modugno, J. J. Łucejko, G. Giachi, S. Cagno, P. Cloetens, K. Janssens and L. Morselli, *Anal. Bioanal. Chem.*, 2009, **395**, 1977-1985

18. G. M. Crisci, M. F. La Russa, M. Malagodi and S. A. Ruffolo, *Journal of Cultural Heritage*, 2010, **11**, 304-308

19. Code of Ethics and guidelines for practice, http://ethics.iit.edu/ecodes/node/3014, (accessed November 2016)

20. B. Appelbaum, *J. Am. Inst. Conserv.*, 1987, **26**(2), 65-73

21. R. M. Seborg and R. B. Inverarity, *Science*, 1962, **136**(3516), 649-650

22. B. L. Stark, *Stud. Conserv.*, 1976, **21**(3), 154-158

23. D. J. Graves, *SSCR Journal*, 2004, **15**(3), 13-17

24. E. Hocker, G. Almkvist and M. Sahlstedt, *Journal of Cultural Heritage*, 2012, **13S**, S175-S182

25. F. Kawai, *Appl. Microbiol. Biotechnol.*, 2002, **58**, 30-38

26. M. Bardet, G. Gerbaud, Q.-K. Trân and S. Hediger, *J. Archaeol. Sci.*, 2007, **34**, 1670-1676

27. J. M. Parrent, *Stud. Conserv.*, 1985, **30**(2), 63-72

28. D. Gregory, P. Jensen and K. Strætkvern, *Journal of Cultural Heritage*, 2012, **13S**, S139-S148

29. A. Morgós, S. Imazu and K. Ito, in *Condition.2015 conservation and digitalization Conference Proceedings*, K. Piotrowska and P. Konieczny, National Maritime Museum, Gdańsk ul. Olowianka, PL, 2015

30. A. Kennedy and E. R. Pennington, *Stud. Conserv.*, 2014, **59**(3), 194-201

31. A. Tahira, W. Howard, E. R. Pennington and A. Kennedy, *Stud. Conserv.*, 2016, DOI: 10.1080/00393630.2016.1169364

32. F. Fiesoli, F. Gennai, *Gradus*, 2010, **5.1**, 9-16

33. J. W. Baty, C. L. Maitland, W. Minter, M. A. Hubbe and S. K. Jordan-Mowery, *BioResources*, 2010, **5**(3), 1955-2023

34. M. C. Area and H. Cheradame, *BioResources*, 2011, **6**(4), 5307-5337

35. X. Zou, N. Gurnagul, T. Uesaka and J. Bouchard, *Polym. Degrad. Stab.*, 1994, **43**, 393-402

36. J. Kolar, *Restaurator*, 1997, **18**, 163-176

37. C. J. Knill and J. F. Kennedy, *Carbohydr. Polym.*, 2003, **51**, 281-300

38. V. Rouchon, M. Duranton, C. Burgaud, E. Pellizzi and B. Lavédrine, *Anal. Chem.*, 2011, **83**, 2589-2597

39. S. Margutti, G. Conio, P. Calvini and E. Pedemonte, *Restaurator*, 2001, **22**, 67-83

40. P. Baldrian and V. Valášková, *FEMS Microbiol. Rev.*, 2008, **32**, 501-521

41. M. Nittérus, *Restaurator*, 2000, **21**, 25-40

42. K. Sterflinger, *Fungal Biology Reviews*, 2010, **24**, 47-55

43. K. Sterflinger and F. Pinzari, *Environ. Microbiol.*, 2012, **14**(3), 559-566

44. F. Pinzari, G. Pasquariello and A. De Mico, *Macromol. Symp.*, 2006, **238**, 57-66

45. S. Zervos and I. Alexopoulou, *Cellulose*, 2015, **22**(5), 2859-2897

46. S. Sequeira, E. J. Cabrita and M. F. Macedo, *Int. Biodeterior. Biodegrad.*, 2012, **74**, 67-86

47. H. Wang, G. Lu, J. Zhang and D. Zheng, *Stud. Conserv.*, 2013, **58**(1), 23-29

48. A.W. Smith, *Restaurator*, 2012, **33**, 223-248

49. *PCT Int. Appl.*, WO 2013090684, 2013

50. R. Giorgi, C. Bozzi, L. Dei, C. Gabbiani, B. W. Ninham and P. Baglioni, *Langmuir*, 2005, **21**, 8495-8501

51. S. Sequeira, C. Casanova and E. J. Cabrita, *Journal of Cultural Heritage*, 2006, **7**, 264-272

52. E. Stefanis and C. Panayiotou, *Restaurator*, 2007, **28**, 185-200

53. G. Poggi, N. Toccafondi, L. N. Melita, J. C. Knowles, L. Bozec, R. Giorgi and P. Baglioni, *Appl. Phys. A*, 2014, **114**, 685-693

54. H. Bansa and R. Ishii, *Restaurator*, 1999, **20**, 198-224

55. S. M. Santos, J. M. Carbajo, N. Gómez, E. Quintana, M. Ladero, A. Sánchez, G. Chinga-Carrasco and J. C. Villar, *J. Mater. Sci.*, 2016, **51**, 1541-1552

56. A. M. A. Nada, A. A. Abd El-Hakim and A. S. Badran, *Restaurator*, 1999, **20**, 30-38

57. E. Princi and S. Vicini, *Eur. Polym. J.*, 2008, **44**, 2392-2403

58. E. Princi, S. Vicini, E. Pedemonte, V. Arrighi and I. McEwen, *J. Appl. Polym. Sci.*, 2005, **98**, 1157-1164

59. G. Abdel-Maksoud and Z. al-Saad, *Mediterranean Archaeology and Archeometry*, 2009, **9**, 69-87

60. E. Ardelean, R. Nicu (Parpalea), D. Asandei and E. Bobu, *European Journal of Science and Technology*, 2009, **5**(4), 67-75

61. C. V. Horie, *Materials for conservation: organic consolidants, adhesives and coatings*, Butterworth-Heinemann, Amsterdam, 2010

62. M. Seki, N. Sonoda, S. Hidaka, T. Morita and T. Okayama, *Restaurator*, 2010, **31**, 126-141

63. R. Mülhaupt, *Macromol. Chem. Phys.*, 2013, **214**, 159-174

64. P. T. Anastas and J. C. Warner, *J. C. Green Chemistry: Theory and Practice*, Oxford University Press, New York, 1998

65. A. K. Mohanty, M. Misra and G. Hinrichsen, *Macromol. Mater. Eng.*, 2000, **276/277**, 1-24

66. H. Ohara, *Appl. Microbiol. Biotechnol.*, 2003, **62**, 474-477

67. F. Cherubini, *Energy Convers. Manage.*, 2010, **51**, 1412-1421

68. A. Demirbas, in *Biofuels Securing the Planet's Future Energy Needs*, Springer-Verlag, London, 2009, 2, 45-85

69. Y. Hadar, in *Lignocellulose Conversion Enzymatic and Microbial Tools for Bioethanol Production*, V. Faraco, Springer-Verlag, Berlin Heidelberg, 2013, 2, 21-38

70. Y. Sun and J. Cheng, *Bioresour. Technol.*, 2002, **83**, 1-11

71. N. Mosier, C. Wyman, B. Dale, R. Elander, Y. Y. Lee, M. Holtzapple and M. Ladisch, *Bioresour. Technol.*, 2005, **96**, 673-686

72. C. E. Wyman, B. E. Dale, R. T. Elander, M. Holtzapple, M. R. Ladisch and Y. Y. Lee, *Bioresour. Technol.*, 2005, **96**, 1959-1966

73. F. Carvalheiro, L. C. Duarte and F. M. Gírio, *J. Sci. Ind. Res.*, 2008, **67**, 849-864

74. P. Alvira, E. Tomás-Pejó, M. Ballesteros and M. J. Negro, *Bioresour. Technol.*, 2010, **101**, 4851-4861

75. J. J. Bozell and G. R. Petersen, *Green Chem.*, 2010, **12**, 539-554

76. A. Gandini, T. M. Lacerda, A. J. F. Carvalho and E. Trovatti, *Chem. Rev.*, 2016, **116**(3), 1637-1669

77. I. Delidovich, P. J. C. Hausoul, L. Deng, R. Pfützenreuter, M. Rose and R. Palkovits, *Chem. Rev.*, 2016, **116**, 1540-1599

78. H. Danner and R. Braun, *Chem. Soc. Rev.*, 1999, **28**, 395-405

79. J. W. Lee, H. U. Kim, S. Choi, J. Yi and S. Y. Lee, *Curr. Opin. Biotechnol.*, 2011, **22**, 758-767

80. G.-Q. Chen and M. K. Patel, *Chem. Rev.*, 2012, **112**(4), 2082-2099

81. J. A. Galbis, M. de Gracia García-Martín, M. Violante de Paz and E. Galbis, *Chem. Rev.* 2016, **116**(3), 1600-1636

82. M. Yabushita, H. Kobayashi and A. Fukuoka, *Appl. Catal., B*, 2014, **145**, 1-9

83. P. C. Badger, in *Trends in new crops and new uses. Proceeding of the fifth National Symposium New Crops and New Uses: Strength in diversity* , J. Janick and A. Whipkey, ASHS Press, Alexandria, VA, 2002, 14, 17-21

84. M. J. Taherzadeh and K. Karimi, *BioResources*, 2007, **2**(3), 472-499

85. S. Brethauer and C. E. Wyman, *Bioresour. Technol.*, 2010 , **101**, 4862-4874

86. S. D. Mansfield, C. Mooney and J. N. Saddler, *Biotechnol. Prog.*, 1999, **15**, 804-816

87. A. Sørensen, M. Lübeck, P. S. Lübeck, and B. K. Ahring, *Biomolecules*, 2013, **3**(3), 612-631

88. S. Mohanram, D. Amat, J. Choudhary, A. Arora and L. Nain, *Sustainable Chem. Processes*, 2013, **1**(15), 1-12

89. H. A. Gavlighi, A. S. Meyer and J. D. Mikkelsen, *Biotechnol. Lett.*, 2013, **35**, 205-212

90. D. Klemm, B. Heublein, H.-P. Fink and A. Bohn, *Angew. Chem. Int. Ed.*, 2005, **44**, 3358-3393

91. L. H. Bock, *Ind. Eng. Chem.*, 1937, **29**(9), 985-987

92. D. G. Coffey, D. A. Bell and A. Henderson, in *Food Polysaccharides and Their Applications*, A. M. Stephen, Marcel Dekker, Inc., New York, 1995, 5, 123-153

93. D. Klemm, B. Philipp, T. Heinze, U. Heinze and W. Wagenknecht, *Comprehensive Cellulose Chemistry Volume 2 Functionalization of Cellulose*, Wiley-VCH, Weinheim, 1998

94. E. Balliana, G. Ricci, C. Pesce and E. Zendri, *Int. J. Conserv. Sci.*, 2016, **7**(1), 185-202

95. M. Christensen, H. Kutzke and F. K. Hansen, *Journal of Cultural Heritage*, 2012, **13S**, S183-S190

96. Z. Walsh, E.-R. Janeček, M. Jones and O. A. Scherman, *Stud. Conserv.*, 2016, DOI: 10.1179/2047058414Y.0000000149

97. G. Cipriani, A. Salvini, P. Baglioni and E. Bucciarelli, *J. Appl. Polym. Sci.*, 2010, **118**, 2939-2950

98. G. Cipriani, A. Salvini, M. Fioravanti, G. Di Giulio and M. Malavolti, *J. Appl. Polym. Sci.*, 2013, **127**(1), 420-431

99. R. Oliva, F. Albanese, G. Cipriani, F. Ridi, D. Giomi, M. Malavolti, L. Bernini and A. Salvini, *J. Polym. Res.*, 2014, **21**(7), 1-12

100. A. Salvini, G. Cipriani, E. Bucciarelli, M. Fioravanti and G. Di Giulio, *Gradus*, 2008, **3.2**, 43-52

101. A. Salvini, A. Papacchini, R. Oliva, G. Di Giulio, B. Perito and M. Fioravanti, *Proceedings of the 13th ICOM-CC conference on Wet Organic Archaeological Materials*, in press

102. A. D. Elbein, Y. T. Pan, I. Pastuszak and D. Carroll, *Glycobiology*, 2003, **13**(4), 17R-27R

103. T. Higashiyama and A. B. Richards, in *Sweeteners and Sugar Alternatives in Food Technology*, K. O'Donnell and M. W. Kearsley, Wiley-Blackwell, Hoboken (USA), second edition, 2012, 19, 417-431

104. K. Maruta, T. Nakada, M. Kubota, H. Chaen, T. Sugimoto, M. Kurimoto and Y. Tsujisaka, *Biosci. Biotechnol. Biochem.*, 1995, **59**(10), 1829-1834

105. N. Teramoto, N. D. Sachinvala and M. Shibata, *Molecules*, 2008, **13**, 1773-1816

106. J. Lee, E.-W. Lin, U. Y. Lau, J. L. Hedrick, E. Bat and H. D. Maynard, *Biomacromolecules*, 2013, **14**(8), 2561-2569

107. S. Nagashima, T. Shimasaki, N. Teramoto and M. Shibata, *Polym. J.*, 2014, **46**, 728-735

108. R. G. Edwards, in *Developments in Food Carbohydrate*, C. K. Lee, Applied Science Publishers, London, 1980, 5, 229-273

109. *Eur. Pat. Appl.*, 2 402 454 A1, 2012

110. G. P. Philippidis, T. K. Smith and C. E. Wyman, *Biotechnol. Bioeng.*, 1993, **41**, 846-853

111. J. E. Cadotte, F. Smith and D. Spriestersbach, *J. Am. Chem. Soc*., 1952, **74**(6), 1501-1504

112. *US Pat.* 2 606 186, 1952

113. A. Onda, T. Ochi and K. Yanagisawa, *Green Chem.*, 2008, **10**, 1033-1037

114. R. Rinaldi, R. Palkovits and F. Schüth, *Angew. Chem. Int. Ed.*, 2008, **47**, 8047-8050

115. J. Pang, A. Wang, M. Zheng and T. Zhang, *Chem. Commun.*, 2010, **46**, 6935-6937

116. P. Lanzafame, D. M. Temi, S. Perathoner, A. N. Spadaro and G. Centi, *Catal. Today*, 2012, **179**, 179-184

117. Z. Yang, R. Huang, W. Qi, L. Tong, R. Su and Z. He, *Chem. Eng. J.*, 2015, **280**, 90-98

118. L. Hu, L. Lin, Z. Wu, S. Zhou and S. Liu, *Appl. Catal., B*, 2015, **174-175**, 225-243

119. B. Hahn-Hägerdal, K. Skoog and B. Mattiasson, *Eur. J. Appl. Miocrobiol. Biotechnol.*, 1983, **17**, 344-348

120. J. A. Bootsma and B. H. Shanks, *Appl. Catal., A*, 2007, **327**, 44-51

121. L. Peña, M. Ikenberry, B. Ware, K. L. Hohn, D. Boyle, X. S. Sun and D. Wang, *Biotechnol. Bioprocess Eng.*, 2011, **16**, 1214-1222

122. M. Marzo, A. Gervasini and P. Carniti, *Carbohydr. Res.*, 2012, **347**, 23-31

123. N. Hartler and K. Hyllengren, *J. Polym. Sci.*, 1962, **56**, 425-434

124. C. T. Gi, H. Ishihara and S. Tejima, *Chem. Pharm. Bull.*, 1978, **26**(5), 1570-1575

125. S. Koto, M. Hirooka, T. Tashiro, M. Sakashita, M. Hatachi, T. Kono, M. Shimizu, N. Yoshida, S. Kurasawa, N. Sakuma, S. Sawazaki, A. Takeuchi, N. Shoya and E. Nakamura, *Carbohydr. Res.*, 2004, **339**, 2415-2424

126. S. M. Nakhla, *Stud. Conserv.*, 1986, **31**, 38-44

127. A. H. Basta, *Restaurator*, 2004, **25**, 129-140

128. R. Ploeger, C. W. McGlinchey and E. R. de la Rie, *Stud. Conserv.*, 2015, **60**(4), 217-226

129. S. H. Othman, S. A. Rashid, T. I. M. Ghazi and N. Abdullah, *J. Nanomater.*, 2010, 1-10

130. S. Karvinen and R.-J. Lamminmäki, *Solid State Sci.*, 2003, **5**, 1159-1166

131. A. Mesnage, M. A. Magied, P. Simon, N. Herlin-Boime, P. Jégou, G. Deniau and S. Palacin, *J. Mater. Sci.*, 2011, **46**, 6332-6338

132. V. Anand Ganesh, H. K. Raut, A. S. Nair and S. Ramakrishna, *J. Mater. Chem.*, 2011, **21**, 16304-16322

133. H. A. Foster, I. B. Ditta, S. Varghese and A. Steele, *Appl. Microbiol. Biotechnol.*, 2011, **90**, 1847-1868

134. I. P. Parkin and R. G. Palgrave, *J. Mater. Chem.*, 2005, **15**, 1689-1695

135. Z. Wang, G. Li, H. Peng, Z. Zhang and X. Wang, *J. Mater. Sci.*, 2005, **40**, 6433-6438

136. J. Gamage and Z. Zhang, *Int. J. Photoenergy*, 2010, **2010**, 1-11

137. M. Montazer and E. Pakdel, *Photochem. Photobiol.*, 2010, **86**, 255-260

138. A. M. Ferrari, M. Pini, P. Neri and F. Bondioli, *Coatings*, 2015, **5**, 232-245

139. M. F. La Russa, N. Rovella, M. Alvarez de Buergo, C. M. Belfiore, A. Pezzino, G. M. Crisci and S. A. Ruffolo, *Prog. Org. Coat.*, 2016, **91**, 1-8

140. A. Salvini and N. Martini, unpublished results (N. Martini, Bachelor's thesis, University of Florence, 2008)

141. National Institute of Advanced Industrial Science and Technology SDBSWeb, http://sdbs.db.aist.go.jp, accessed November 2016

142. P. P. Graczyk and M. Mikołajczyk, in *Topics in Stereochemistry*, E. L. Eliel and S. H. Wilen, John Wiley & Sons Inc., New York, NY, 1994, 159

143. C. G. Tomecko and R. Adams, *J. Am. Chem. Soc.*, 1923, **45**, 2698-2701

144. P. L. Nichols Jr., R. M. Hamilton, L. T. Smith and E. Yanovsky, *Ind. Eng. Chem.*, 1945, **37**(2), 201-202

145. M.-S. Lin and C.-S. Huang, *J. Polym. Sci., Part A: Polym. Chem.*, 1992, **30**, 2303-2312

146. H. Hu, J. You, W. Gan, J. Zhou and L. Zhang, *Polym. Chem.*, 2015, **6**, 3543-3548

147. M. Li, D. Constantinescu, L. Wang, A. Mohs and J. Gmehling, *Ind. Eng. Chem. Res.*, 2010, **49**(10), 4981-4988

148. G. Odian, in *Principles of Polymerization*, John Wiley & Sons, Inc., Hoboken, New Jersey, USA, 4th edition, 2004, 3-7c, 263-264

149. A. Salvini, L. Zucchini, unpublished results (L. Zucchini, Master thesis, University of Florence, 2013/2014)

150. H. F. Mark, *Encyclopedia of polymer science and technology, concise*, John Wiley & Sons, Inc., Hoboken, New Jersey, USA, 2007

151. D. Braun, H. Cherdron, M. Rehahn, H. Ritter and B. Voit, in *Polymer Synthesis: Theory and Practice Fundamentals, Methods, Experiments*, Springer-Verlag, Berlin Heidelberg, 5th edition, 2013, 5.1, 331-332

152. R. Oliva, A. Salvini, G. Di Giulio, L. Capozzoli, M. Fioravanti, C. Giordano and B. Perito, *J. Appl. Polym. Sci.*, 2015, **132**(23), 42047/1-42047/14

153. R. Oliva, Ph.D. thesis, University of Florence, 2014

154. K. K. Suma, S. Jacob and R. Joseph, *Mater. Sci. Eng., B*, 2010, **168**(1-3), 254-258

155. A. Salvini, M. Arcuri, unpublished results (M. Arcuri, Master's thesis, University of Florence, 2012)

156. A. Salvini, F. Sordi, unpublished results (F. Sordi, Master's thesis, University of Florence, 2013)

157. UNI ISO 483 (2005) *Plastics – Small enclosures for conditioning and testing using aqueous solutions to maintain the humidity at a constant value*

158. UNI ISO 3130 (1975) – *Wood – Determination of moisture content for physical and mechanical tests*

159. A. García Trejo, *Ecotoxicol. Environ. Saf.*, 1988, **16**(1), 25-35

160. F. Cappitelli and C. Sorlini, *Appl. Environ. Microbiol.*, 2008, **74**(3), 564-569

161. R. F. P. Nogueira and W. F. Jardim, *Journal of Chemical Education*, 1993, **70**(10), 861-862

162. S. Lakshmi, R. Renganathan and S. Fujita, *J. Photochem. Photobiol., A*, 1995, **88**, 163-167

163. C. H. Kwon, H. Shin, J. H. Kim, W. S. Choi and K. H. Yoon, *Mater. Chem. Phys.*, 2004, **86**, 78-82

164. K. Bubacz, J. Choina, D. Dolat and A. W. Morawski, *Polish J. of Environ. Stud.*, 2010, **19**(4), 685-691

165. R. Oliva, M. A. Ortenzi, A. Salvini, A. Papacchini and D. Giomi, *RCS Advances*, submitted

166. P. Tundo and M. Selva, *Acc. Chem. Res.*, 2002, **35**, 706-716

167. F. Aricò and P. Tundo, *Russ. Chem. Rev.*, 2010, **79**(6), 479-489

168. G. Poggi, R. Giorgi, N. Toccafondi, V. Katzur and P. Baglioni, *Langmuir*, 2010, **26**(24), 19084-19090